

Developing of One-Part Alkali-Activated Self-Consolidating Concrete
and Investigating its Sulfate Attack Resistance

Dima Mamoun Kanaan

A Thesis

In the Department of
Building, Civil and Environmental Engineering

Presented in Partial Fulfillment of the Requirements

For the Degree of

Doctor of Philosophy (Building, Civil and Environmental Engineering) at

Concordia University

Montreal, Quebec, Canada

September 2021

© Dima Mamoun Kanaan, 2021

CONCORDIA UNIVERSITY
SCHOOL OF GRADUATE STUDIES

This is to certify that the thesis prepared

By: **Dima Mamoun Kanaan**

Entitled: **Developing of One-Part Alkali-Activated Self-Consolidating Concrete and Investigating the Sulfate Resistance**

and submitted in partial fulfillment of the requirements for the degree of

Doctor of Philosophy (Civil Engineering)

complies with the regulations of the University and meets the accepted standards with respect to originality and quality.

Signed by the final Examining Committee:

_____	Chair
Dr. Alex De Visscher	
_____	External Examiner
Dr. Mohammed Bassuoni	
_____	Examiner to Program
Dr. Mamoun Medraj	
_____	Examiner
Dr. Biao Li	
_____	Examiner
Dr. Michelle Nokken	
_____	Thesis Supervisor
Dr. Ahmed Soliman	

Approved by _____
Dr. Mazdak Nik-Bakht Chair of Department or Graduate Program Director

September 20, 2021

Date of Defence

Dean, Dr. Mourad Debbabi

Abstract

Developing of One-Part Alkali-Activated Self-Consolidating Concrete and Investigating its Sulfate Attack Resistance

Dima Mamoun Kanaan, Ph.D.

Concordia University, 2021

Cement production is one of the major contributors to higher carbon dioxide (CO₂) emissions, leading to a higher carbon footprint. Hence, reducing cement demand will preserve natural resources and reduce CO₂ emissions associated with cement production. Moreover, the reliance on cement manifested the concern associated with the disintegration problems of the long-standing structures, indicating the handicaps of Portland cement as a binder. Nowadays, the development of cement-less sustainable concrete is gaining significant attention due to its ecological value and environmental benefits.

On the other hand, Alkali-Activated Materials (AAMs) are considered part of the future toolkit towards achieving sustainable binding systems. AAMs are likely achieved by the utilization of low-carbon footprint materials (entitled “precursors”) activated in alkaline environments (induced by “activators”). In recent research, there has been an increasing emphasis on the utilization of these advanced cementing systems in the production of concrete for particular purposes such as SCC. Therefore, the main goal of Alkali-Activated Self-Consolidating Concrete (AASCC) is to produce zero-cement SCC without sacrificing its quality and performance. One of the main challenges facing AASCC application on the industrial scale is the development of effective mineral and chemical admixtures to improve the fresh, mechanical, but most importantly, durability performances.

The durability of AASCC is a subject of controversy, especially when exposed to sulfate attacks. Furthermore, the adequacy of the standard sulfate immersion tests raises more concerns about the reported behavior. As is obvious from the research conducted by several investigators aiming for evaluating the dual aspects of AAMs potential and field-like quality. Since the resistance of AASCCs to external sulfate attack was not widely investigated as regular alkali-activated concretes (AACs). The current research work has introduced an integrated testing strategy that includes the exposure of AASCC to multiple field-like damaging factors, i.e., various cations, controlled pH, partial immersion, and wetting-drying cycles. This has helped create a fundamental knowledge of the durability of a wide range of AASCC mixtures to different external sulfate attack scenarios and capture the failure mechanisms of a wide scope of AASCC mixture designs.

Keywords: Sustainability, Alkali-Activated SCC, Sulfate Attack, Integrated Testing

Acknowledgments

First, I would like to thank Allah for all the blessings throughout this life and for letting me through all the difficulties. Sincere gratitudes and appreciations to Dr. Ahmed Soliman for his supervision, helpful discussions, recommendations, and other assistance. His guidance and advice carried me through all stages of completing my research. I would like to thank my research committee members for letting my defense be an enjoyable moment and for the brilliant comments and suggestions.

Thanks to Dr. Alexandre Arnold for recording the NMR Spectra, Ms. Galyna Shul, and Mr. Gwenaël Chamoulaud for recording the X-Ray Diffraction and Thermal Gravimetric Analysis (TGA) and particularly for helpful discussions at the Université du Québec à Montréal. Also, special thanks to Ms. Hong Guan for recording the Ion Chromatography (IC) and Inductively Coupled Plasma (ICP), Mr. Mazen Samara for recording the Scanning Electron Microscope (SEM), and for their helpful discussions at Concordia University.

Sincere thanks to the School of Graduate Studies, Concordia University (Canada) for the Ph.D. scholarship and financial support. I also would like to thank Lafarge Canada and Ciment Québec for donating the construction materials. Special thanks to Professor Adel M. Hanna at Concordia University for allowing me to use his laboratory to conduct the experimental work.

Last but not least, I would especially like to thank my parents, Dr. Mamoun Kanaan and Asswan Khalife; without you, none of this would indeed be possible. I would also like to give special thanks to my lovely family, Dr. Rola, Eng. Kenana, Eng. Mohammed and Aseel for their continuous support and understanding when undertaking my research. Your true love, support, continuous motivation, and prayers were what sustained me this far.

To My Beloved Parents; Dr. Mamoun and Asswan

To My Lovely Brother; Eng. Mohammed

To My Lovely Sisters; Dr. Rola,

Eng. Kenana and Aseel

Contributions of Authors and Dissemination

This thesis is prepared according to Concordia University regulations for a Manuscript-Based Thesis. This thesis presents experimental and theoretical work carried out solely by Dima Mamoun Kanaan. Advice and guidance were provided for the whole thesis by the academic supervisor Dr. Ahmed Soliman. During the preparation of this thesis, some of the findings were presented and submitted in the following peer-reviewed journals:

Chapter 3 was submitted to the Journal of Sustainability and Green Construction for publishing as follows;

Kanaan, D., and Soliman, A. (2021). Resistance of Alkali-Activated Materials to External Sulfate Attack: A Review of Current Standards and Future Needs. *Submitted*.

Chapter 4 was published in the ACI Materials Journal (ACI) and RIELM Association as follows;

Kanaan, D., and Soliman, A. (2021). Performance of Eco-Friendly One-Part Alkali-Activated Self-Consolidated Concrete with Multi-Activators. *ACI Materials Journal, Special Publication*, 349, 102-116.

Chapter 4 was accepted in the ACI Materials Journal (ACI) for publishing as follows;

Kanaan, D., and Soliman, A. (2021). Performance of One-Part Alkali-Activated Self-Compacted Mortar. *ACI Materials Journal (ACI)*, *Accepted*.

Chapter 5 was accepted in the Construction and Building Materials Journal (CBM) for publishing as follows;

Kanaan, D., and Soliman, A. (2021). Fresh and Mechanical Properties of One-Part Alkali-Activated Self-Consolidating Concrete. *Accepted*.

Chapter 6 was submitted to the Journal of Sustainable Cement-Based Materials for publishing as follows;

Kanaan, D., and Soliman, A. (2021). External Sulfate Attack of Ambient Cured One-Part Alkali-Activated Self-Consolidating Concrete. *In Preparation*.

Table of Contents

Chapter 1 : Introduction	1
1.1. Overview	1
1.2. Technology Presentation	2
1.3. Advances in Alkali Activators	4
1.4. Advances in Aluminosilicate Precursors.....	5
1.5. Mixing Procedure	5
1.6. Problem Statement	6
1.7. Outline and Structure of the Thesis	8
Chapter 2 : Relevant Literature Review	10
2.1. Overview	10
2.2. Fresh Properties	10
<u>2.2.1. Deformability and Flow Rate</u>	10
<u>2.2.2. Passing and stability abilities</u>	14
<u>2.2.3. Summary of Studies and Remarks</u>	16
2.3. Mechanical Properties	18
<u>2.3.1. Summary of Studies and Remarks</u>	22
2.4. Long-Term Durability Properties	24
<u>2.4.1. Summary of Studies and Remarks</u>	28
2.5. Concluding Remarks	28
Chapter 3 : Resistance of Alkali-Activated Materials to External Sulfate Attack: A Review of Current Standards and Future Needs	30
3.1. Overview	30
3.2. Chemistry and Physics Behind External Sulfate Attack	30
3.3. AAMS Deterioration	31
3.4. Effect of Exposure Conditions	32
3.5. Current Standards and Specifications for Sulfate Resistance	33
3.6. Type and Concentration of Sulfate.....	39
3.7. Specimens' Composition, Shape, and Size.....	41
3.8. PH of the Solution	43

3.9. Single Damage-Factor Tests	43
3.10. Multiple Damage-Factor Tests	44
3.11. Concluding Remarks and Recommendations.....	46
Chapter 4 : Defining Mix Design Parameters for the Production of One-Part Alkali-Activated Self-Consolidating Concrete.....	47
4.1. Overview	47
4.2. Research Significance	47
4.3. Experimental Investigation.....	47
<u>4.3.1. Phase One: Dry-Powder Activators as a Replacement</u>	<u>48</u>
<u>4.3.2. Phase Two: Dry-Powder Activators as an Addition</u>	<u>48</u>
<u>4.3.3. Materials Characterization</u>	<u>48</u>
<u>4.3.4. Mixture’s Proportions and Designations</u>	<u>50</u>
<u>4.3.5. Testing and Specimens Preparation</u>	<u>50</u>
4.4. Experimental Results and Discussion	51
<u>4.4.1. Dry-Powder Activators as a Replacement.....</u>	<u>51</u>
<u>4.4.1.1. Mini-Slump Flow</u>	<u>51</u>
<u>4.4.1.2. Compressive Strength.....</u>	<u>54</u>
<u>4.4.1.3. Early Hydration Chemistry at One Day</u>	<u>59</u>
<u>4.4.2. Dry-Powder Activators as an Addition</u>	<u>61</u>
<u>4.4.2.1. Mini-Slump Flow</u>	<u>61</u>
<u>4.4.2.2. Compressive Strength Development</u>	<u>64</u>
<u>4.4.2.3. SEM Observations.....</u>	<u>67</u>
<u>4.4.2.4. Heat of Hydration.....</u>	<u>68</u>
<u>4.4.2.5. Differential Scanning Calorimetry (DSC).....</u>	<u>74</u>
4.5. Concluding Remarks	77
Chapter 5 : Fresh and Mechanical Properties of Ambient Cured One-Part Alkali-Activated Self-Consolidating Concrete	78
5.1. Overview	78
5.2. Research Significance	79
5.3. Experimental Program.....	79
<u>5.3.1. Materials Characterization</u>	<u>79</u>
5.4. Testing Program	81
<u>5.4.1. Fresh Properties</u>	<u>81</u>

<u>5.4.1.1. Filling Ability (Unconfined Flowability)</u>	81
<u>5.4.1.2. Passing Ability</u>	82
<u>5.4.1.3. Segregation Resistance</u>	82
<u>5.4.1.4. Visual Stability Index (VSI)</u>	83
5.5. Hardened Properties	83
<u>5.5.1. Compressive Strength Development</u>	83
<u>5.5.2. Ultrasonic Pulse Velocity and Electrical Resistivity</u>	84
<u>5.5.3. Microstructural Analysis</u>	85
5.6. Results and Discussion.....	86
<u>5.6.1. Fresh Properties</u>	86
<u>5.6.1.1. Filing Ability</u>	86
<u>5.6.1.2. Passing Ability (Confined Flowability)</u>	87
<u>5.6.1.3. Segregation Resistance</u>	88
<u>5.6.1.4. Effects of Selected Activator and Dosage</u>	89
<u>5.6.1.5. Effect of Precursor Combination</u>	90
<u>5.6.2. Hardened Properties</u>	91
<u>5.6.2.1. Compressive Strength Development</u>	91
<u>5.6.2.2. Electrical Bulk Resistivity</u>	94
<u>5.6.2.3. Ultrasonic Pulse Velocity (UPV)</u>	96
<u>5.6.2.4. Capillary Sorptivity</u>	97
<u>5.6.2.4.1. Initial Rate of Absorption</u>	97
<u>5.6.2.4.2. Secondary Rate of Absorption</u>	98
<u>5.6.2.5. Permeable Pores Test</u>	99
<u>5.6.2.5.1. Early-Age Test</u>	99
<u>5.6.2.5.2. Late-Age Test</u>	100
<u>5.6.3. Microstructural Analysis</u>	100
5.7. Concluding Remarks	105
Chapter 6 : External Sulfate Attack of Ambient Cured One-Part Alkali-Activated Self-Consolidating Concrete	106
6.1. Overview	106
6.2. Research Significance	106
6.3. Experimental Program.....	107

<u>6.3.1. Materials and Mixture Proportion</u>	107
6.4. Testing Program	108
<u>6.4.1. Phase II: Single Damage-Factor</u>	108
<u>6.4.2. Phase III: Multiple Damage-Factor</u>	109
<u>6.4.3. Mass Monitoring</u>	112
<u>6.4.4. Cross-Section Variations Monitoring</u>	112
<u>6.4.5. Microstructural Observations</u>	113
6.5. Results and Discussion.....	113
<u>6.5.1. Exposure I: Controlled pH</u>	113
<u>6.5.1.1. Visual Appearance</u>	114
<u>6.5.1.2. Mass and Cross-Section Variations</u>	116
<u>6.5.1.3. Ion Chromatography</u>	122
<u>6.5.2. Exposure II: NonControlled pH</u>	123
<u>6.5.2.1. Visual Appearance</u>	123
<u>6.5.2.2. Mass and Cross-Section Variations</u>	125
<u>6.5.3. Exposure III: 5% Sulfate Solution - Controlled pH</u>	128
<u>6.5.3.1. Visual Appearance</u>	128
<u>6.5.3.2. Mass and Cross-Section Variations</u>	130
<u>6.5.3.3. Ion Chromatography</u>	133
<u>6.5.4. Exposure IV: Drying and Wetting Cycles</u>	134
<u>6.5.4.1. Visual Appearance</u>	135
<u>6.5.4.2. Mass and Cross-Section Variations</u>	137
6.6. Thermogravimetry (TGA/DTG).....	140
6.7. Proposed Deterioration Mechanisms.....	142
6.8. Concluding Remarks	144
Chapter 7 : Research Contributions and Recommendations	145
7.1. Research Contributions	145
7.2. Recommendations	146
Appendix I: Ion Chromatography Test	147
Appendix II: Mass and Cross-Section Variations	150
References	155

List of Tables

Table 1 – Fresh properties of AASCCs with garnet replacing sand [After Muttashar et al. (2018)].....	14
Table 2 – Summary of AASCCs characteristics and fresh properties reviewed in previous studies.....	17
Table 3 – Change in mechanical properties of various geopolymer composites [After Kamseu et al. (2016); Muttashar et al. (2018)]	20
Table 4 – Summary of AASCCs mechanical properties reviewed in previous studies	23
Table 5 – Changes in strength after the exposure to various sulfate environments [After Bakharev (2005)]	25
Table 6 – Mixtures characteristics and residual strength data [After Thokchom et al. (2010)].....	25
Table 7 – Mixtures identification and compressive strength loss indices [After Komljenović et al. (2013)]	26
Table 8 – Summary of the sulfate resistance tests by alkali-activated mixtures reviewed in studies	28
Table 9 – Different standards, specifications, and building codes for concrete prone to sulfate attack	34
Table 10 – Summary of AAMs resistance to external sulfate attacks reviewed in studies	41
Table 11 – Different performance requirements for concrete susceptible to sulfate attack.....	42
Table 12 – Physical and chemical compositions of source materials.....	49
Table 13 – Summary of mixture's proportions used for the designed mortars	50
Table 14 – Mixture's proportions of the different AASCC systems	80
Table 15 – EFNARC acceptance criteria for Self-Compacting Concrete	81
Table 16 – Sieve stability test in terms of SI % according to EFNARC guidelines.....	83
Table 17 – Visual stability index (VSI) rating in accordance with ASTM C1611	83
Table 18 – Interpretation of the UPV and electrical resistivity results.....	84
Table 19 – Fresh Concrete properties results for AASCC mixtures.....	86
Table 20 – Electrical resistivity test results for AASCC ternary-precursor mixtures.....	95
Table 21 – UPV results for AASCC mixtures with up to 25% activator dosage.....	96
Table 22 – Summary of mixture's proportions used for the designed AASCC mixtures.....	107
Table 23 – Ion chromatography analysis and pH after 182 days in 10% sulfate solutions of the different AASCC systems	122
Table 24 – Ion chromatography analysis and pH after 182 days in 5% sulfate solutions of the different AASCC systems	134

List of Figures

Fig. 1 – Early publications related to AAM	2
Fig. 2 – Classification of binders by calcium and aluminum contents [After Van Deventer et al. (2010)] ...	3
Fig. 3 – Dissolution of precursors together with activators [After Barbosa et al. (2000)]	4
Fig. 4 – Precipitation of hydrated aluminates [After Barbosa et al. (2000)]	4
Fig. 5 – AAMs preparation using either one-part or two-part techniques.....	6
Fig. 6 – Flow chart of the proposed research	9
Fig. 7 – Relationship between T500 and slump flow tests [Adapted from Memon et al. (2011)]	11
Fig. 8 – Relationship between T500 and slump flow tests [Adapted from Ushaa et al. (2015)].....	12
Fig. 9 – Relationship between T500 and slump flow tests [Adapted from Sashidhar et al. (2015); Shafiq et al. (2017); Patel et al. (2018)].....	13
Fig. 10 – Relationship between T500 and slump flow tests [After Manjunath et al. (2018)]	14
Fig. 11 – Relationship between J-Ring and L-Box tests [Adapted from Memon et al. (2011); Manjunath et al. (2018); Patel et al. (2018)].....	15
Fig. 12 – Effect of curing temperature (°C) and time (hours) on the compressive strength of AASCC [Adapted from Memon et al. (2011)]	19
Fig. 13 – Hardened properties of AASCC mixtures [Adapted from Manjunath et al. (2018)]	21
Fig. 14 – SEM and XRD results of a) SCC-3 b) SCC-5 and c) SCC-7 [After Manjunath et al. (2018)].....	22
Fig. 15 – Diffractograms of a) AAS and b) CEM II samples exposed to sulfate attack [Adapted from Komljenović et al. (2013)]	27
Fig. 16 – SEM micrographs and XRD pattern of mortar with 20% slag exposed to a) Na ₂ SO ₄ [Adapted from Yusuf (2015)].....	38
Fig. 17 – SEM micrographs and XRD pattern of mortar with 20% slag exposed to b) MgSO ₄ [Adapted from Yusuf (2015)].....	38
Fig. 18 – XRD patterns of source materials (a) GGBFS (b) SF, and (c) FA	49
Fig. 19 – Dry-powder activators a) MetaNa ₂ SiO ₃ b) Na ₂ CO ₃	49
Fig. 20 – (a) Geometry of a typical mini-slump cone (b) Typical mini-slump spread (c) AASCM cubic specimens	51
Fig. 21 – Mini-slump flow results of the ground and non-ground mixtures	52
Fig. 22 – Compressive strength results at 3 days for ground and non-ground blends.....	55
Fig. 23 – Compressive strength results at 7 days for ground and non-ground blends.....	56
Fig. 24 – Compressive strength results at 28 days for ground and non-ground blends.....	58
Fig. 25 – Schematic representation of the electrical double layer mechanism.....	59
Fig. 26 – Heat evolution curves at 24-h early hydration age of ground AASCC mixtures.....	60
Fig. 27 – Heat evolution curves at 24-h early hydration age of non-ground AASCC mixtures	61
Fig. 28 – Mini-slump flow results of the AASCM mixtures.....	62
Fig. 29 – Compressive strength of AASCM blends at 7 days.....	65
Fig. 30 – Compressive strength of AASCM blends at 28 days.....	67
Fig. 31 – SEM images of AASCMs a) S3-25%, b) B3-25%, c) B6-25%, d) T3-25%, and e) T6-25%.....	68
Fig. 32 – Heat evolution of AASCM blends using slag single-precursor blends a) Heat of hydration curves and b) Cumulative heat evolution curves	70
Fig. 33 – Heat evolution of AASCM blends using binary-SF blends a) Heat of hydration curves and b) Cumulative heat evolution curves	71

Fig. 34 – Heat evolution of AASCM blends using binary-FA blends a) Heat of hydration curves and b) Cumulative heat evolution curves	72
Fig. 35 – Heat evolution of AASCM blends using ternary-1 blend a) Heat of hydration curves and b) Cumulative heat evolution curves	73
Fig. 36 – Heat evolution of AASCM blends using ternary-2 blend a) Heat of hydration curves and b) Cumulative heat evolution curves	74
Fig. 37 – DSC curves of various AASCM precursor systems a) single b) binary-SF c) binary-FA d) ternary-1 e) ternary-2.....	76
Fig. 38 – Slump flow test equipment and measurements.....	81
Fig. 39 – Illustration of the L-box test.....	82
Fig. 40 – (a) Cylinder specimens and (b) A hydraulic testing.....	84
Fig. 41 – Schematic representation of the Sorptivity test procedure.....	85
Fig. 42 – Relation between a slump and slump flow rate	87
Fig. 43 – Relation between slump and L-Box blocking ratio.....	88
Fig. 44 – Relation between segregation resistance and l-box blocking ratio	89
Fig. 45 – The effect of activator dosage on the relation between a) slump flow and l-box ratio h_2/h_1 b) slump flow and SI%	90
Fig. 46 – The effect of slag content, kg/m^2 on the a) slump flow diameter, mm and b) segregation resistance SI, %	91
Fig. 47 – Compressive strength results for the AASCC single-precursor mixtures.....	92
Fig. 48 – Compressive strength results for the AASCC binary-precursor mixtures	93
Fig. 49 – Compressive strength results for the AASCC ternary-precursor mixtures	94
Fig. 50 – Bulk resistivity results for AASCC mixtures at ages a) 28 and b) 90 days	95
Fig. 51 – UPV results for all AASCC mixtures at a) 28 and b) 90 days of curing age	97
Fig. 52 – Initial rate of absorption for AASCC mixtures.....	98
Fig. 53 – Secondary rate of absorption for AASCC mixtures.....	99
Fig. 54 – Permeable pores results for AASCC mixtures.....	100
Fig. 55 – X-ray diffractograms of AASCCs with 25% silicate-carbonate activator dosage	102
Fig. 56 – ^{29}Si NMR spectra after 90 days hydration of AASCC mixtures with different precursors	103
Fig. 57 – SEM images of AASCCs using 25% activator dosage a) Single, b) Binary-1, c) Binary-2, d) Ternary-1, and e) Ternary-2	105
Fig. 58 – Phase I AASCC deterioration scheme	109
Fig. 59 – Schematic diagram of a concrete specimen exposed to a field-like multi-damaging condition adapted from (Bassuoni and Rahman, 2016).....	111
Fig. 60 – RH-T phase diagram of $Na_2SO_4 + H_2O$ system (Adapted from Doehen et al.,2002)	111
Fig. 61 – RH-T phase diagram of $MgSO_4 + H_2O$ system (Adapted from Steiger et al.,2007).....	111
Fig. 62 – AASCC single-precursor mixtures exposed to a) 10% $MgSO_4$ b) 10% Na_2SO_4 and c) 10% mixed sulfate solutions at a controlled pH environment	114
Fig. 63 – AASCC binary-1 mixtures exposed to a) 10% $MgSO_4$ b) 10% Na_2SO_4 and c) 10% mixed sulfate solutions at a controlled pH environment.....	115
Fig. 64 – AASCC binary-2 mixtures exposed to a) 10% $MgSO_4$ b) 10% Na_2SO_4 and c) 10% mixed sulfate solutions at a controlled pH environment.....	115
Fig. 65 – AASCC ternary-1 mixtures exposed to a) 10% $MgSO_4$ b) 10% Na_2SO_4 and c) 10% mixed sulfate solutions at a controlled pH environment.....	115
Fig. 66 – AASCC ternary-2 mixtures exposed to a) 10% $MgSO_4$ b) 10% Na_2SO_4 and c) 10% mixed sulfate solutions at a controlled pH environment.....	116

Fig. 67 – Time-dependent mass change of single-precursor AASCC mixtures exposed to 10% solutions at a controlled pH environment	116
Fig. 68 – Time-dependent cross-section change of single-precursor AASCC mixtures exposed to controlled pH environment.....	116
Fig. 69 – XRD spectra of AASCC single-precursor specimens exposed to sulfate attack: (a) In 10% Na ₂ SO ₄ solution; (b) In 10% MgSO ₄ solution.....	117
Fig. 70 – XRD spectra of binary-1 AASCC specimens exposed to sulfate attack: (a) In 10% Na ₂ SO ₄ solution; (b) In 10% Mixed solution ; (c) In 10% MgSO ₄ solution.....	118
Fig. 71 – Time-dependent mass change of binary-precursor AASCC mixtures exposed to 10% sulfate solutions at a controlled pH environment a) binary-1 and b) binary-2.....	119
Fig. 72 – Time-dependent cross-section change of binary-precursor AASCC mixtures exposed to 10% sulfate solutions at a controlled pH environment a) binary-1 and b) binary-2	119
Fig. 73 – XRD spectra of binary-2 AASCC specimens exposed to sulfate attack: (a) In 10% Na ₂ SO ₄ solution; (b) In 10% Mixed solution ; (c) In 10% MgSO ₄ solution.....	120
Fig. 74 – Time-dependent mass change of ternary-precursor AASCC mixtures exposed to 10% sulfate solutions at a controlled pH environment a) ternary-1 and b) ternary-2	120
Fig. 75 – Time-dependent mass change of ternary-precursor AASCC mixtures exposed to 10% sulfate solutions at a controlled pH environment a) ternary-1 and b) ternary-2	121
Fig. 76 – XRD spectra of ternary-2 AASCC specimens exposed to sulfate attack: (a) In 10% Na ₂ SO ₄ solution; (b) In 10% MgSO ₄ solution	121
Fig. 77 – AASCC single-precursor mixtures exposed to a) 10% MgSO ₄ b) 10% Na ₂ SO ₄ and c) 10% mixed sulfate solutions at a noncontrolled pH environment	123
Fig. 78 – AASCC binary-1 mixtures exposed to a) 10% MgSO ₄ b) 10% Na ₂ SO ₄ and c) 10% mixed sulfate solutions at a noncontrolled pH environment.....	124
Fig. 79 – AASCC binary-2 mixtures exposed to a) 10% MgSO ₄ b) 10% Na ₂ SO ₄ and c) 10% mixed sulfate solutions at a noncontrolled pH environment.....	124
Fig. 80 – AASCC ternary-1 mixtures exposed to a) 10% MgSO ₄ b) 10% Na ₂ SO ₄ and c) 10% mixed sulfate solutions at a noncontrolled pH environment.....	125
Fig. 81 – AASCC ternary-2 mixtures exposed to a) 10% MgSO ₄ b) 10% Na ₂ SO ₄ and c) 10% mixed sulfate solutions at a noncontrolled pH environment.....	125
Fig. 82 – Time-dependent mass change of single-precursor AASCC mixtures exposed to a noncontrolled pH environment.....	126
Fig. 83 – Time-dependent cross-section change of single-precursor AASCC mixtures exposed to a noncontrolled pH environment.....	126
Fig. 84 – Time-dependent mass change of binary-precursor AASCC mixtures exposed to 10% sulfate solutions at a noncontrolled pH environment a) binary-1 and b) binary-2.....	126
Fig. 85 – Time-dependent cross-section change of binary-precursor AASCC mixtures exposed to 10% sulfate solutions at a noncontrolled pH environment a) binary-1 and b) binary-2	127
Fig. 86 – Time-dependent mass change of ternary-precursor AASCC mixtures exposed to 10% sulfate solutions at a noncontrolled pH environment a) ternary-1 and b) ternary-2	127
Fig. 87 – Time-dependent cross-section change of ternary-precursor AASCC mixtures exposed to 10% sulfate solutions at a noncontrolled pH environment a) ternary-1 and b) ternary-2.....	128
Fig. 88 – AASCC single-precursor mixtures exposed to a) 5% MgSO ₄ b) 5% Na ₂ SO ₄ and c) 5% mixed sulfate solutions at a controlled pH environment	128
Fig. 89 – AASCC binary-1 mixtures exposed to a) 5% MgSO ₄ b) 5% Na ₂ SO ₄ and c) 5% mixed sulfate solutions at a controlled pH environment.....	129

Fig. 90 – AASCC binary-2 mixtures exposed to a) 5% MgSO ₄ b) 5% Na ₂ SO ₄ and c) 5% mixed sulfate solutions at a controlled pH environment.....	129
Fig. 91 – AASCC ternary-1 mixtures exposed to a) 5% MgSO ₄ b) 5% Na ₂ SO ₄ and c) 5% mixed sulfate solutions at a controlled pH environment.....	130
Fig. 92 – AASCC ternary-2 mixtures exposed to a) 5% MgSO ₄ b) 5% Na ₂ SO ₄ and c) 5% mixed sulfate solutions at a controlled pH environment	130
Fig. 93 – Time-dependent mass change of single-precursor AASCC mixtures exposed to 5% sulfate solutions at a controlled pH environment.....	131
Fig. 94 – Time-dependent cross-section change of single-precursor AASCC mixtures exposed to 5% sulfate solutions at a controlled pH environment	131
Fig. 95 – Time-dependent mass change of binary-precursor AASCC mixtures exposed to 5% sulfate solutions at a controlled pH environment a) binary-1 and b) binary-2.....	131
Fig. 96 – Time-dependent cross-section change of binary-precursor AASCC mixtures exposed to 5% sulfate solutions at a controlled pH environment a) binary-1 and b) binary-2	132
Fig. 97 – Time-dependent mass change of ternary-precursor AASCC mixtures exposed to 5% sulfate solutions at a controlled pH environment a) ternary-1 and b) ternary-2	132
Fig. 98 – Time-dependent cross-section change of ternary-precursor AASCC mixtures exposed to 5% sulfate solutions at a controlled pH environment a) ternary-1 and b) ternary-2.....	133
Fig. 99 – AASCC single-precursor mixtures exposed to a) 10% MgSO ₄ b) 10% Na ₂ SO ₄ , and c) 10% mixed sulfate solutions under drying and wetting cycles.....	135
Fig. 100 – AASCC binary-1 mixtures exposed to a) 10% MgSO ₄ b) 10% Na ₂ SO ₄ , and c) 10% mixed sulfate solutions under drying and wetting cycles.....	135
Fig. 101 – AASCC binary-2 mixtures exposed to a) 10% MgSO ₄ b) 10% Na ₂ SO ₄ , and c) 10% mixed sulfate solutions under drying and wetting cycles.....	136
Fig. 102 – AASCC ternary-1 mixtures exposed to a) 10% MgSO ₄ b) 10% Na ₂ SO ₄ , and c) 10% mixed sulfate solutions under drying and wetting cycles.....	136
Fig. 103 – AASCC ternary-2 mixtures exposed to a) 10% MgSO ₄ b) 10% Na ₂ SO ₄ , and c) 10% mixed sulfate solutions under drying and wetting cycles.....	137
Fig. 104 – Time-dependent mass change of single-precursor AASCC mixtures exposed to 10% sulfate solutions under drying and wetting cycles	137
Fig. 105 – Time-dependent cross-section change of single-precursor AASCC mixtures exposed to 10% sulfate solutions under drying and wetting cycles.....	137
Fig. 106 – XRD spectra of binary-1 AASCC specimens exposed to sulfate attack under drying and wetting cycles: (a) In 10% Na ₂ SO ₄ solution; (b) In 10% MgSO ₄ solution.....	138
Fig. 107 – Time-dependent mass change of binary-precursor AASCC mixtures exposed to 10% sulfate solutions under drying and wetting cycles a) binary-1 and b) binary-2	139
Fig. 108 – Time-dependent cross-section change of binary-precursor AASCC mixtures exposed to 10% sulfate solutions under drying and wetting cycles a) binary-1 and b) binary-2.....	139
Fig. 109 – Time-dependent mass change of ternary-precursor AASCC mixtures exposed to 10% sulfate solutions under drying and wetting cycles a) Ternary-1 and b) Ternary-2	140
Fig. 110 – Time-dependent cross-section change of ternary-precursor mixtures exposed to 10% sulfate solutions under drying and wetting cycles a) Ternary-1 and b) Ternary-2	140
Fig. 111 – TGA/DTG data for AASCC exposed to different sulfate solutions a) single, b) binary-1, c) binary-2, and d) ternary-2 mixtures.....	142
Fig. 112 – Proposed deterioration mechanism of AASCC cylinders in a) Na ₂ SO ₄ and b) MgSO ₄	143

List of Abbreviations

AAC	Alkali-activated Concrete
AAM	Alkali-activated Material
AAS	Alkali-activated Slag
AASCC	Alkali-activated Self-Consolidated Concrete
ACI	American Concrete Institute
ASTM	American Society for Testing and Materials
C-A-S-H	Calcium Aluminate Silicate Hydrate
C-H	Calcium Hydroxide
C-S-H	Calcium Silicate Hydrate
CO ₂	Carbon Dioxide
EFNARC	European Federation of National Associations Representing for Concrete
FA	Fly Ash
GGBFS	Ground Granulated Blast Furnace Slag
ITZ	Interfacial Transition Zone
MK	Metakaolin
$\mu\epsilon$	Microstrain
OPC	Ordinary Portland Cement
PPM	Parts Per Million
RD _{MOE}	Relative Dynamic Modulus of Elasticity
RH	Relative Humidity
SCC	Self-Consolidated Concrete
SF	Silica Fume
w/b	Water to Binder Ratio
w/cm	Water to Cementitious Material

Chapter 1 : Introduction

1.1. Overview

Cement production is one of the major contributors to increased carbon dioxide emissions. It is estimated that one ton of cement production generates an equivalent amount of carbon dioxide (CO₂) (Sadek et al., 2014). This contributes to around 5-8% of the annual global greenhouse gas emissions to the atmosphere (Najim et al., 2016). In addition, the reliance on cement manifested the concerns associated with the disintegration problems of the long-standing cementitious-based structures. This indicates the handicaps of ordinary Portland cement (OPC) as a binder. Nowadays, the development of cement-less sustainable concrete is gaining great attention due to its ecological value.

Since 1908, Alkali-Activated Materials (AAMs) were well-thought to replace OPC as a step towards sustainable development. AAMs, encompass the reaction between a solid precursor with an alkali source (activator), forming novel cementing materials similar to OPC. Solid precursor(s) are any amorphous aluminosilicate material that can be alkali-activated such as fly ash (FA) (Palomo et al., 1999; Fernández-Jiménez et al., 2005; Luukkonen et al., 2018), ground-granulated blast-furnace slag (GGBFS) (Fernández-Jiménez et al., 1999; Puertas et al., 2003), metakaolin, silica fume and rice husk (Bernal et al., 2011; Bernal et al., 2012; He et al., 2013). Alkali activators include essentially any compound with hydroxide (MOH) and silicate components (M₂O·rSiO₂), where M is either sodium (Na⁺) or potassium (K⁺). Previous studies have utilized various materials, i.e., sodium hydroxide (NaOH), sodium silicate (Na₂SiO₃), sodium carbonate (Na₂CO₃), sodium aluminate (NaAlO₂), sodium sulfate (Na₂SO₄), and potassium hydroxide (KOH), to raise the pH of mixtures by the inclusion of alkali cations and consequently to accelerate the precursor's dissolution (Luukkonen et al., 2018). Up to the present time, AASCCs were not widely investigated as ordinary self-compacted concretes (SCC) due to the limited data on their rheological, mechanical, and, most importantly, durability performance. Considering the production of alkali-activated concrete mixtures, many authors have ascribed good performance to the controlled laboratory atmosphere, materials' availability, good workmanship, and quality control (Provis, J., and Van Deventer, J., 2013). However, this is too simplistic to reflect the potential field performance.

The massive deterioration of long-standing OPC structures indicates that the current ultimate strength design procedure is no longer valid or relevant for sustainable development. This is due to the preliminary vision of a concrete evaluation strategy that is built on strength rather than its durability and deterioration. Concrete deterioration is a time-dependent process of synergetic and interrelated loading, aging, cracking, environmental conditions, and climatic changes. In other words, a complex combination of various factors and processes would outline the concrete deterioration mechanism. External sulfate attack mechanism is not fully understood among different mechanisms, which manifests the clear gap between theory, research, and practice (Roy, 1999; Mehta, 2000). Since the long-term performance of AAM, in particular, AASCC is a subject of controversy, the current work advocates the design for a holistic durability approach, in

particular external sulfate attack, intended for integrating the characteristics of AASCC with in-situ performance.

1.2. Technology Presentation

Over the past years, a growing emphasis on using no-cement concrete that best is described as alkali-activated concrete has emerged. In order to understand the scientific bases of AAMs, many researchers (**Fig. 1**) have investigated the potential of AAMs in the production of concrete over the last decades (Kuehl, 1908; Purdon, 1940; Gluchovsky, 1959; Joseph Davidovits, 1982; Malone et al., 1985; Wang et al., 1995; Roy, 1999). Since 1908, no entirely satisfactory description of AAMs has been framed. Researchers identified it by various names, i.e., inorganic polymers, alkali bonded ceramics, soil silicate, alkali ash material, mineral polymers etc. In fact, the terminology itself was a focus of disagreement.

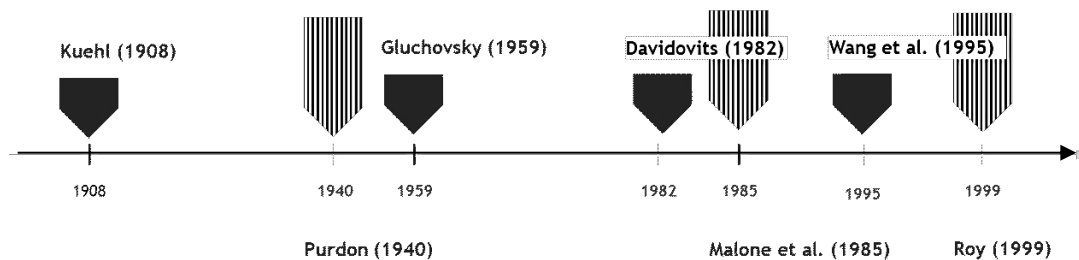


Fig. 1 – Early publications related to AAM

Lately, some authors have preferred using the “alkali-activated material” and “geopolymer” terminologies, suggesting that both are more comprehensive concepts (Provis, J., and Van Deventer, J., 2013). As noticed from recent research, AAMs are too often confused with geopolymers. A broad representation, as shown in (**Fig. 2**) suggested that geopolymer is subsumed under the AAM category as the primarily formed gel is obtained mostly by aluminosilicate sources (Van Deventer et al., 2010).

Although the geopolymer technology is contingent on very old principles, only little is known about the nature of these reactions or their products. Much of the current research, in order to better understand the chemistry behind geopolymers, have correlated the synthesis of cementitious calcium silicate hydrate (C-S-H) in conventional concrete with the production of C-(N)A-S-H and K-A-S-H in the alkali-activated concrete (Fernández-Jiménez et al., 2005; Palomo et al., 2011; Fernández-Jiménez et al., 2012; Provis, J., and Van Deventer, J., 2013). In this context, there have been dissenters to the previous views of geopolymer classification and the end-result reaction products by Davidovits (2012). The author raised a critical open question of whether the term geopolymer is an acronym for “AAM, Alkali-Alumina-Hydrate, N-A-S-H, and K-A-S-H.” In this regard and to avoid confusion, it is important to briefly clarify the differences between geopolymerization and the hardening of OPC.

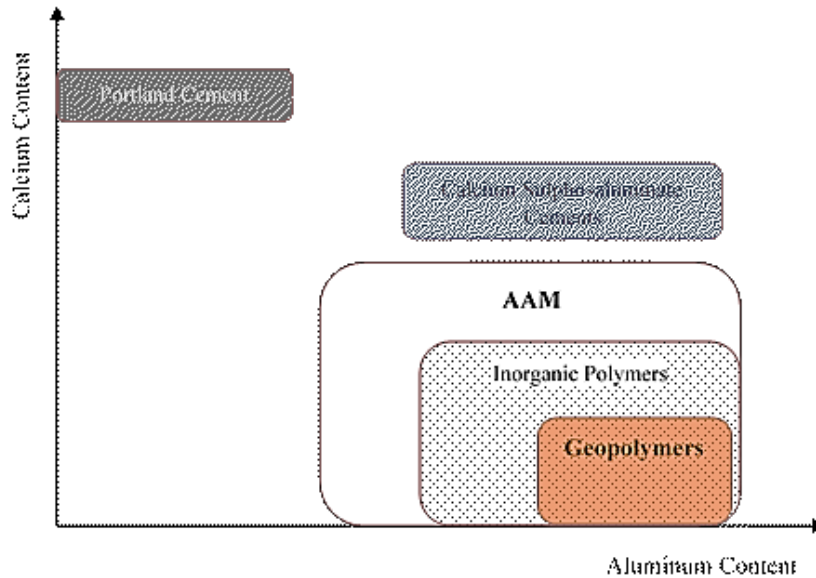
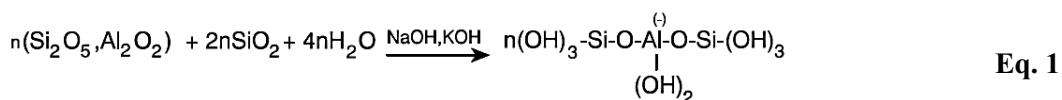
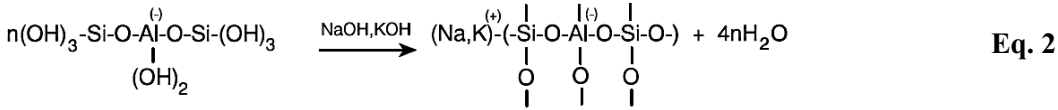


Fig. 2 – Classification of binders by calcium and aluminum contents [After Van Deventer et al. (2010)]

In conventional concrete, the main reactions associated with the cement hydration result in C-S-H and lime production, identified as $\text{Ca}(\text{OH})_2$, in addition to other products. Pozzolans are sometimes introduced to concrete mixtures to achieve higher levels of strength and durability, and shrinkage reduction. The improved performance after adding a pozzolanic material is attributed to its reaction with lime resulting in the formation of extra C-S-H strength-giving products. Although the reaction nature is different, pozzolans can also act as reagents for the synthesis of alkali-activated concretes based on interactions between the pozzolanic material and alkaline media.

In alkali-activated concrete, the dissolution of aluminosilicate sources in a strong alkaline atmosphere results in a breakdown of the polymeric Si-O-Si bonds followed by the involvement of Al atoms. The end-result aluminosilicate gels (zeolite-like) are later formed. The simplified illustration of the real structure (**Fig. 3**) shows alternating silicon and aluminum tetrahedral joined together in three directions by sharing oxygen atoms. This unstable condition where aluminum is four co-ordinated with respect to oxygen generates a negative charge imbalance; hence, cations, i.e., K^+ and Na^+ , are important to maintaining electric neutrality in the matrix. According to Davidovits (2012), the polycondensation reaction of aluminosilicate oxides with alkali polysilicates results in polymeric Si-O-Al bonds, as exhibited in **Eq. 1** and **Eq. 2**. The hardening mechanism of alkali-activated concrete consists of 1) Dissolution of precursors with the production of mobile precursors through the complex action of (OH^-) in conjunction with alkali activators, 2) Partial orientation of mobile precursors as well as the partial internal restructuring of the alkali polysilicates and 3) Precipitation of hydrated calcium silicates or aluminates as well as the regeneration of caustic solution, i.e., NaOH (Van Jaarsveld et al., 1997).





The proposed network model of Si-O-Al by Davidovits (1999) exhibits chains of SiO₄ and AlO₄ combined by oxygen bridges and does not represent calcium silicate hydrate (C-S-H) alternatives, i.e., N-A-S-H or K-A-S-H. In fact, Calcium (Ca²⁺) is known to be insoluble in water; thus, its combination with water (H) is convenient in a formula. However, if replaced by Na⁺ or K⁺ as in Sodium-Alumino-Silicate-Hydrate or Potassium-Alumino-Silicate-Hydrate, both (Na⁺, K⁺) are very soluble in water in a hydrated environment, they would be leached out. This configuration is a very simplified representation of the real structure, and it was later modified as shown in (Fig. 3 and Fig. 4) by Barbosa et al. (2000). In particular, the production of what is identified as N-A-S-H is considered the first step in the geopolymerization process (Fig. 3) to generate a 3-D polycondensate network with fixed Na in place (Fig. 4), leading to strength elaboration.

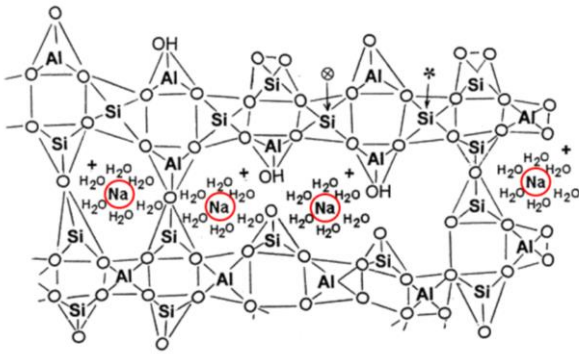


Fig. 3 – Dissolution of precursors together with activators [After Barbosa et al. (2000)]

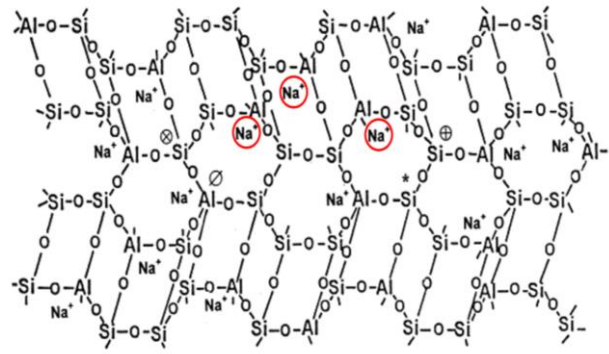


Fig. 4 – Precipitation of hydrated aluminates [After Barbosa et al. (2000)]

Both Portland cement and alkali-activated concrete possess similar characteristics, such as the resistance to water action after hardening, with a difference in the role of water during formation. In particular, water is consumed during the hydration of Portland cement to form, i.e., C-S-H gel, whereas it promotes carrying the alkali activating agents during the polymerization process without clear participation in the reactions (Škvára, 2007).

1.3. Advances in Alkali Activators

Solid alkali activators include any compound with MOH and M₂O·rSiO₂ components, where M is either Na or K, such as NaOH, Na₂SiO₃, Na₂CO₃, NaAlO₂, Na₂SO₄, KOH, red mud, maize stalk, and cob ash, etc. The modulus of water glass (SiO₂/Na₂O molar ratio) affected the alkalinity of mixtures. The reduction in modulus ratio may initiate an acidic polymerization environment, while the higher SiO₂/Na₂O ratio would produce an alkaline polymerization atmosphere (Jansson et al., 2015). On the other hand, Na₂SiO₃/NaOH ratio and NaOH molarity were believed to affect the

strength of mixtures. The utilization of Na_2SiO_3 would instigate the production of additional silica gel leading to strength improvement. Prior research conducted by Chindaprasirt et al. (2007) recommended using $\text{Na}_2\text{SiO}_3/\text{NaOH}$ ratio in the range (0.67 - 1.00) to produce high strength alkali-activated mixture, while Hardjito et al. (2005) recommended the range (0.4 - 2.5). Beyond these ranges, the reduction in strength was explained by the excessive alkali content that retarded the polymerization reaction.

The solid NaOH and aqueous Na_2SiO_3 solution are the most widely demanded chemicals in the industrial market. In the long run, the production of NaOH after the chlor-alkali process would be insufficient due to the limited chlorine (Cl_2) world market. At the same time, a high energy consumption characterizes the synthesis of alkali silicate. As a result, replacing sodium hydroxide and silicate with other sources is essential. For instance, Na_2CO_3 is a potential alternative activator to replace NaOH ; however, it can release CO_2 to the atmosphere after the precursors' calcination process (Kovtun et al., 2015). Also, NaAlO_2 is considered another alternative alkali source due to its ability to provide additional reactive aluminum (Luukkonen et al., 2018).

Although various activators have remarkable benefits on the alkali-activated concrete performance, many of these activators have some disadvantages. Some solid activators such as NaOH are corrosive, hygroscopic, and forms sodium carbonate when reacting with CO_2 . Therefore, using the appropriate personal protective equipment (PPE) is obligatory while handling corrosive alkalis (Muntesingh, 2006).

1.4. Advances in Aluminosilicate Precursors

AAMs, including those specified as geopolymers, derive their binding systems from solid precursor(s) and activator(s) reactions. The most commonly used aluminosilicate sources are similar to the used supplementary cementitious materials (SCMs) in the production of conventional concretes. Hypothetically, any material that involves a high content of silica and aluminum can be alkali-activated. For instance, both FA and GGBFS are in high demand for aluminosilicate sources in alkali-activated concretes. The use of FA (Class F) as precursor material with (low calcium content) has been demonstrated in most of the studies (Palomo et al., 1999; Fernández-Jiménez et al., 2005). On the other hand, FA (Class C) precursor is eventually less frequent due to its limited availability coupled with its high calcium content leading to the rapid setting (Luukkonen et al., 2018). GGBFS as commonly blended with FA can be utilized as the main precursor of the mixture (Fernández-Jiménez et al., 2005; Puertas et al., 2003). This can be due to its role as a calcium-rich component that can increase the early age strength of the alkali-activated concrete. Other investigations (Bernal et al., 2011; Bernal et al., 2012; He et al., 2013) have explored the use of various prime materials such as metakaolin, clay minerals, rice husk, and silica fume. Therefore, the most compelling evidence for the growth of alkali-activated systems for niche applications goes back to the existence of various by-product materials with no competition with Portland cement.

1.5. Mixing Procedure

AAMs are produced in two distinct pathways; either a dual-powder method known as “one-part mixture” or a single-powder method identified as a “two-part mixture.” The mixing procedure has a remarkable effect on the fresh and hardened properties of the alkali-activated mixture. In

particular, the mixing procedure appeared to affect concrete rheology more than its strength (Puertas et al., 2018).

In the one-part method, dry powders, including solid aluminosilicate and solid alkali sources, are mixed with aggregates, additives, fibers, and other ingredients. Thereafter, the dry mixture is combined with the mixing water with/without a calcination step (Fig. 5). Issues related to the rapid setting due to the heat generated after the dissolution of solid precursor(s) and the often-slow strength development have limited the scalability of this technique on the industrial scale. Therefore, the utilization of suitable retarding admixtures to extend the setting time and the selection of proper precursor(s) and activator(s) would be beneficial to employ the one-part method properly. On the other hand, the mainly used “two-part” method appears more likely to be compatible with precast works. The handling of chemicals (liquid activators) and curing systems can be controlled (Palomo et al., 2011; Van Deventer et al., 2012).

Recently, the one-part or “just add water” technique is considered a promising creation for the in-situ field due to the difficulty in dealing with liquid, viscous and corrosive activator(s). In contrast, the two-part method is believed to be suitable for precast applications (Puertas et al., 2003).

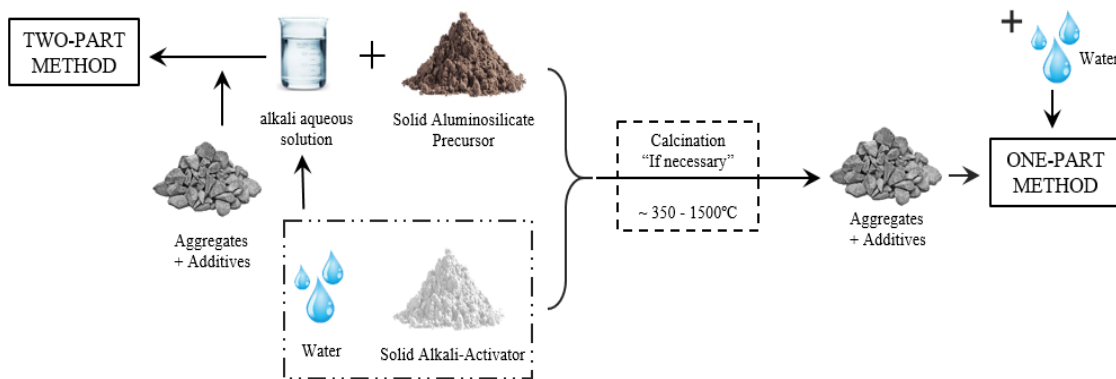


Fig. 5 – AAMs preparation using either one-part or two-part techniques

1.6. Problem Statement

Alkali-activated self-consolidating concretes (AASCC) with different binder systems have the potential to be a significant and cost-effective element of the future toolkit of eco-friendly construction materials. However, the issues associated with using corrosive alkaline solutions as activators (2-part) and their effects on the rheological behavior of the mixtures limit the system's scalability in the industry. Therefore, the production of one-part AASCCs appears to be a promising application, while the mechanical (low-early age strength) and durability characteristics remain unknown. This work aims to gain more understanding and knowledge regarding the fresh and time-dependent properties of SCCs that have been alkali-activated, which encompasses high contents of waste-based precursor materials. A further aim has been to investigate the adequacy of sulfate tests in alkali-activation of concrete to understand the underlying mechanisms that govern the mixture's deterioration. This would provide extensive global data on the functionality and overall performance of AASCC mixtures under such real and severe combined exposure circumstances.

Besides, it would contribute to the necessary shift to performance-based standards design oriented for distinctive concrete structures.

1.7. Research objectives and scope

The present work intends to advance the current level of knowledge on the potential production of one-part AASCCs and investigate their performance in sulfate-rich environments, which was not addressed in previous literature. Specific research objectives are as follows:

1. Production of various AASCC mixture designs varying in the type of binder (precursor), the combination level (single, binary, and ternary), and activator dosage.
2. Evaluation of AASCC performance using the existing immersion tests in sodium, magnesium, and a combination of both sulfates solutions (single damage factor tests) while monitoring pH and exposure time.
3. Implementation of an integrated testing approach on AASCC that considers field-like conditions, i.e., partial immersion testing, sulfate exposure (wetting), and drying in hot-arid climates (multiple damage factor tests).
4. Estimation of a precise degradation mechanism correlated with failure criteria based on the performance of AASCC mixtures in such tests.

1.8. Implications of research

This research provides a preliminary attempt to devise and formulate an investigation strategy for external sulfate attacks on AASCC mixtures. Also, it develops a systematic testing technique from the single-damage factor level (lowest) to the multiple-damage factor level (highest), which is more in line with field conditions. Interestingly, these factors have been overlooked in the current national and international standards for testing external sulfate attacks. Research contribution includes:

1. Evaluating the possible production of one-part AASCC mixtures incorporating 100% locally available industrial waste materials at different levels, i.e., single, binary and ternary.
2. Investigating the effect of activator characteristics and dosage on the fresh, hardened, and durability properties of AASCC mixtures.
3. Identifying the optimal content of activators to be used in AASCC mixtures yielding desired fresh and hardened concrete properties.
4. Proposing a comprehensive database on the durability of various AASCC mixture designs prone to sulfate solutions with different cations. As well as providing reflections of the suitability/unsuitability of different AASCCs based on fundamental mixture design parameters in highly concentrated sulfate environments.
5. Identifying different complex forms of deterioration of AASCC mixtures that may occur in service due to different combinations of binders and activators. Such degradation forms and the sulfate attack mechanisms that drove them may be used to refute the validity of current standards for estimating the durability of regular concrete structures in sulfate-rich environments.

1.7. Outline and Structure of the Thesis

The research included three experimental phases and one preliminary stage, followed by an analytical investigation for the results. The preliminary stage of the experimental program dealt with a laboratory investigation undertaken to enhance the fresh and mechanical characteristics of the AASCM mixtures. AASCC mixtures were proportioned with various contents and combinations of precursor materials activators to ensure adequate fluidity, stability, and strength. Then, mixtures with adequate performance were considered for further long-term testing to achieve the research targets. A flow chart of the research methodology is shown in **Fig. 6**.

An extensive and broad relevant literature review of available previous and recent studies that were carried out on the production of alkali-activated SCC mixtures using different precursor and activator types and dosages are summarized and presented in Chapter (2).

Chapter (3) presented a critical analysis of the adequacy of classical/advanced sulfate tests in the field of AAMs to understand the underlying mechanisms governing the mixtures' deterioration. It also raised questions about the possibility of developing novel evaluation approaches that consider the interaction between AAMs and sulfates.

Chapter (4) is divided into two main phases. Phase one focused on the collective implications of milling (mechanochemical activation) and the use of multi-activator materials replacing GGBFS on the development of eco-SCC mortar mixtures with single-, binary-, and ternary-precursor blends. For all tested mortar mixtures, the dry-powder activators replaced GGBFS by up to 25% by weight. While Phase two focused on the performance of all developed AASCC mortar mixtures, including dry-powder activators as an addition.

The results of the tested specimens are presented in Chapter (5). Fresh concrete tests (i.e., filling ability, passing ability, and segregation resistance), hardened concrete properties (i.e., compressive strength and ultrasonic pulse velocity (UPV)), and durability tests (i.e., bulk electrical conductivity test, sorptivity, and permeable pores tests) are presented and discussed in this chapter.

In Chapter 6, the performance of the AASCC mixtures is presented under single and integrated testing approaches of aggressive attacks of sodium and magnesium sulfates and when exposed to wetting and drying cycling environments.

The main research contributions and future research recommendations are presented in Chapter 7.

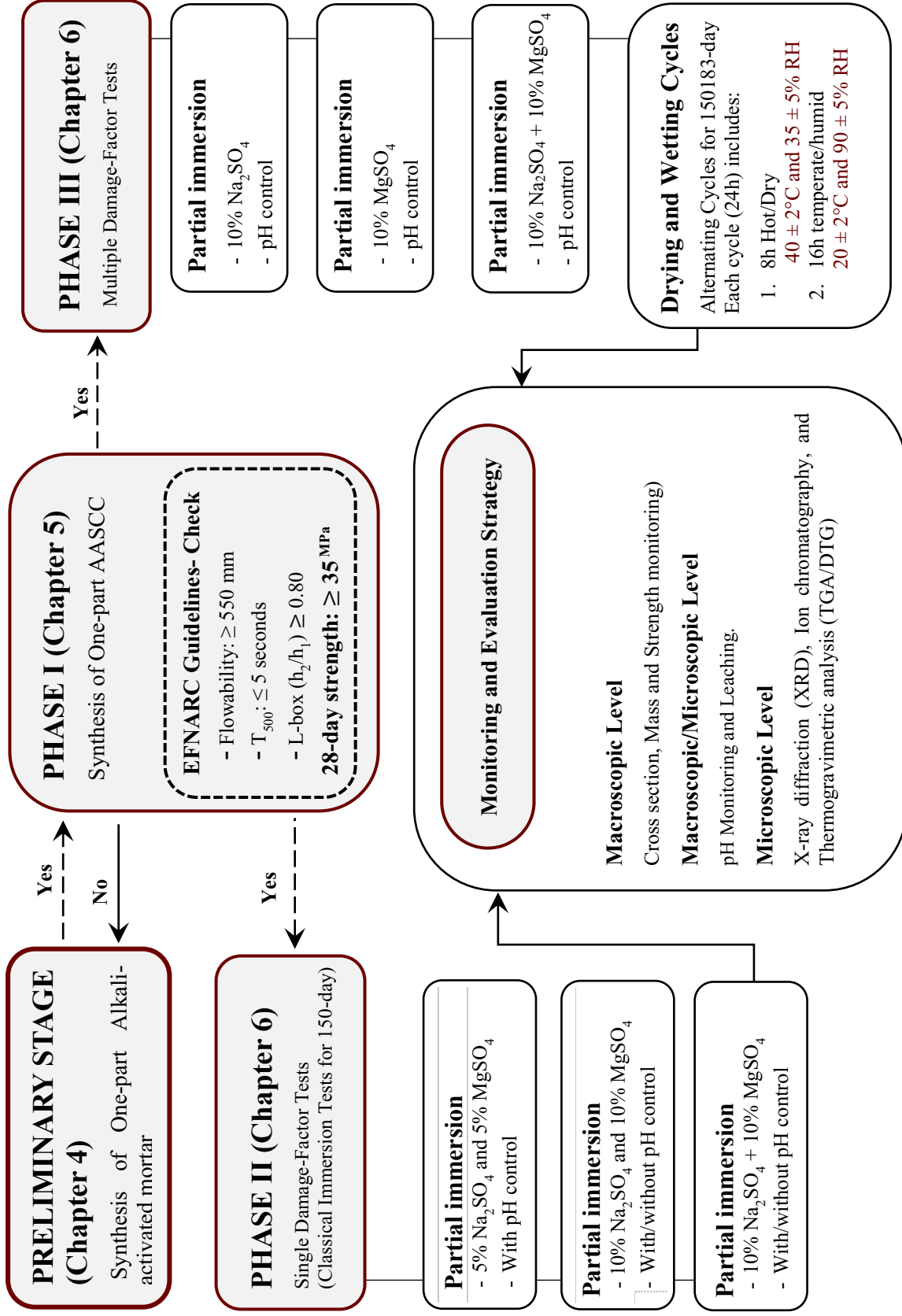


Fig. 6 – Flow chart of the proposed research

Chapter 2 : Relevant Literature Review

2.1. Overview

With the significant growth of the SCC industry over the past 30 years, customer demand has changed accordingly. The traditional criterion of concrete performance from the perspective of concrete suppliers is subsumed under its transfer and arrival to the site only, yet this view should be expanded. The end result specifications (ERS), what Bickley et al. (2006) refer to as “performance of concrete under in-situ testing,” provides another potential criterion of testing. From a practical standpoint, evaluating the in-situ SCC performance was based on direct assessment techniques, i.e., strength, representing the industrial-wide understanding of SCC, where testing for the rheology and fresh properties is marginalized. To develop technically sound performance assessment, the in-situ SCC fresh tests should be experienced and addressed to certain criteria to meet the ERS. On the other hand, an expanded framework of validity of old/new concepts and test methods should be monitored in construction sites.

2.2. Fresh Properties

Available research in alkali-activated concrete has highlighted the high priority for investigating the workability requirements of AASCC mixtures (Memon et al., 2011; Sashidhar et al., 2015; Manjunath et al., 2018; Patel et al., 2018). Fundamental parameters such as flowability, high deformability, passing ability, and proper resistance to segregation are believed to be the promoters to achieve an acceptable level of cohesion. A review of the literature revealed empirical evidence demonstrating that the use of tailored AASCCs is applicable. To the best of the author’s knowledge, the field of alkali-activation research has stressed the criticality of giving attention to the workability characteristics (i.e., slump flow, V-funnel, L-box, J-ring, and segregation).

2.2.1. Deformability and Flow Rate

Deformability is simply defined as “any change in dimension or shape” (ACI, 2013). It is also used to refer to the ability of AASCC to flow into/and fill the formwork under its weight. Indeed, slump-flow and T_{500} time tests can be used as primary indicators for flowability and flow rate of AASCC.

As a case in point, Memon et al. (2011) questioned the effect of curing time and temperature and the addition of extra water on the fresh properties of AASCC. The objective of this study was achieved by producing AASCC mixtures using FA (class F) as a sole precursor, well-graded coarse aggregates with a nominal maximum size of 14 mm in addition to fine aggregate’s fineness modulus of 2.67. A mixture of Na_2SiO_3 and 12M NaOH with a constant $\text{Na}_2\text{SiO}_3/\text{NaOH}$ ratio of 2.5 was used to prepare the alkali solutions. The mixing procedure, as mentioned in the investigation, was performed in two stages. Ten mixtures were prepared to explore the influence of curing temperature, i.e., 60-90°C, curing time, i.e., 24-96h, and extra added water, i.e., 10-20% on the performance of AASCC mixtures.

Results indicated that all of the produced AASCC mixtures showed satisfactory fresh

characteristics complying with EFNARC (2005) except for three mixtures. Although the nature of the chemical reactions of the AASCC is different from that of ordinary SCC, the results indicated that the addition of water enhanced the workability and fresh characteristics of AASCC. On the other hand, the extra added water beyond 12% (i.e., 15% and 20%) of the mixing water has resulted in bleeding and segregation of some mixtures (**Fig. 7**).

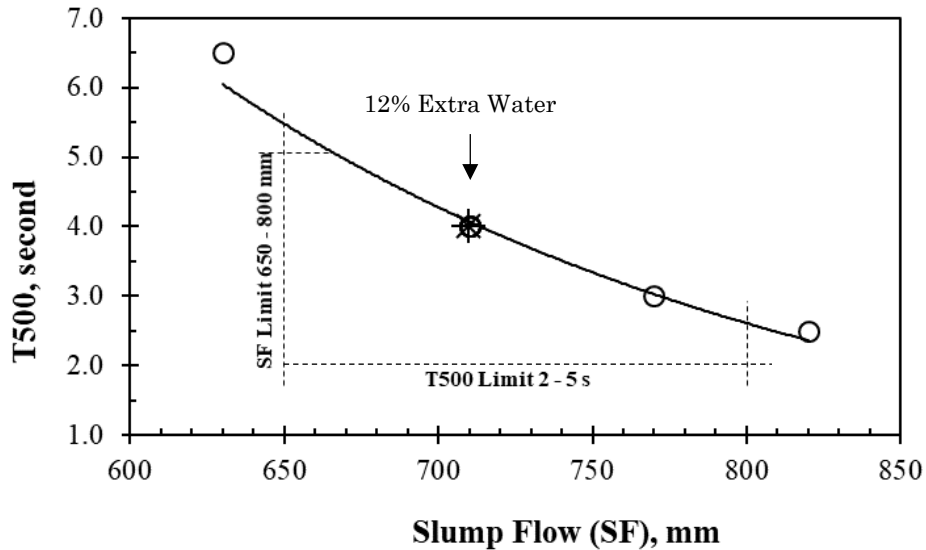


Fig. 7 – Relationship between T500 and slump flow tests [Adapted from Memon et al. (2011)]

Ushaa et al. (2015) studied the effect of using different precursors (i.e., FA, GGBFS, and SF) on the deformability of AASCC mixtures. The investigation concluded that replacing FA either with GGBFS (10%, 20%, 30%) or SF (5%, 10%, 15%) has resulted in satisfactory slump flow values ranging between 660-690 mm. Consequently, a lower dosage of superplasticizer was utilized. The T_{500} test results of AASCC mixtures ranging between 4.5-6.5 s (**Fig. 8**) were found incompatible with the EFNARC (2005) specifications due to the use of various precursors. Generally, incorporating SCMs, except for SF, in concrete mixtures may increase the workability of fresh concretes depending on their type and dosage (Thomas, 2011; Lindgård et al., 2012). Fresh concrete mixtures containing SF are usually more cohesive and less prone to segregation than concrete mixtures without SF. As a result, increasing the content of SF would alter the mixtures to become more sticky (Yogendran et al., 1987; Khayat et al., 1997). With a varying effect of each precursor, higher percentages of GGBFS generally did not affect the flow rate of AASCCs as much as SF. This can be due to the high viscous nature of mixtures prepared with SF.

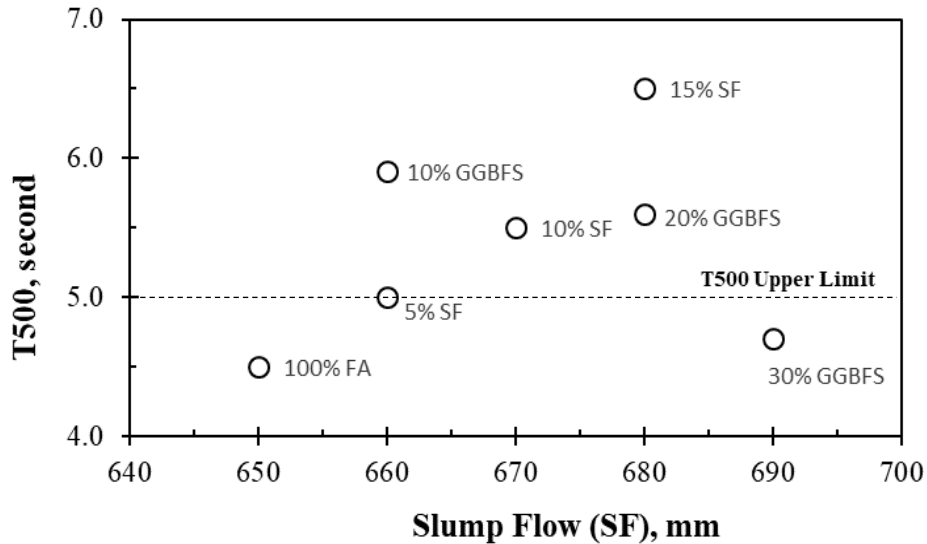


Fig. 8 – Relationship between T500 and slump flow tests [Adapted from Ushaa et al. (2015)]

Lately, Shafiq et al. (2017) viewed the potential use of ceramic waste material in the production of AASCC. The authors added some broad perspectives to the current debate on the use of alternative waste materials. The mixtures were prepared using a combination of Na_2SiO_3 and NaOH with two molarity levels, i.e., 8M and 10M. The authors concluded that the utilization of two precursors (i.e., 50% slag and 50% ceramic waste) enhanced the deformability of the produced AASCC mixtures. In particular, workability was improved as a low NaOH level (i.e., 8M) was used compared to a high NaOH level (i.e., 12M). On the other hand, a reduction in the flowability was noticed as the slag content was increasing in the AASCC. This was ascribed to the low relative density of slag that caused an increase in the paste volume.

Another study carried out by Patel et al. (2018) examined the effect of NaOH molarity and curing temperature on the workability and mechanical properties of AASCC. The investigation program consisted of two main phases. First, analyzing the performance of a reference AASCC mixture using FA as the main precursor. Second, reporting the fresh and hardened behavior of six AASCC mixtures produced by GGBFS. All mixtures were prepared using 14 mm crushed coarse aggregate, river sand as fine aggregate, and Master Glenium Sky 8784 superplasticizer with relative density 1.10 to achieve the required flowability. Authors had attributed the reduction in mixtures' flowability to the use of slag along with increasing the NaOH molarity from 8M to 14M. As declared by the authors, slag's irregular particle shape played a significant role in decreasing the fluidity relative to FA (**Fig. 9**). On the other hand, an increase in the viscosity and cohesiveness was observed as NaOH molarity increased from 8M to 14M. A similar conclusion was obtained by (Shahidhar et al., 2015; Nagaraj and Babu, 2018; Saini and Vattipalli, 2020) in other studies. However, Nagaraj and Babu (2018) demonstrated that the flowability of the mixtures improved as the sodium silicate content was increased compared with NaOH.

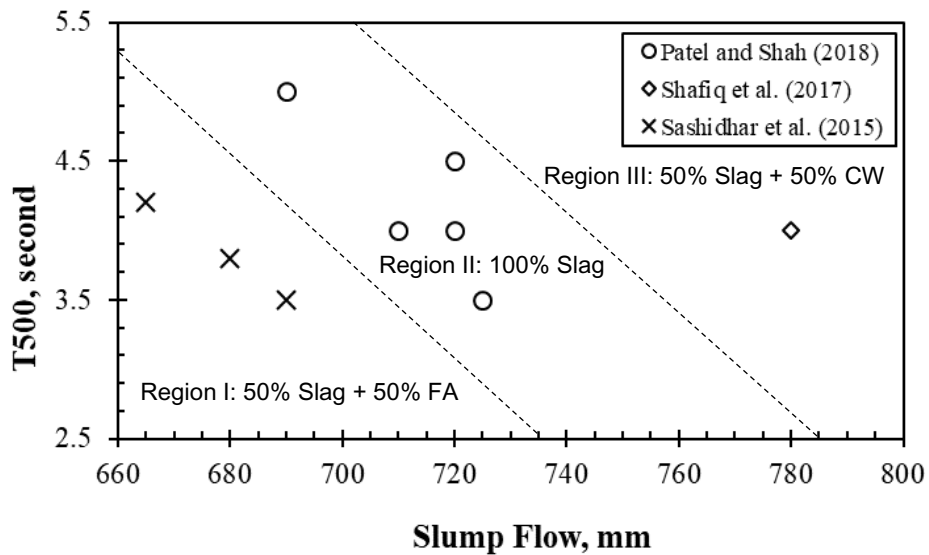


Fig. 9 – Relationship between T500 and slump flow tests [Adapted from Sashidhar et al. (2015); Shafiq et al. (2017); Patel et al. (2018)]

Recent efforts were oriented to examine the possibility of replacing natural coarse and fine aggregates with waste materials in the production of AASCC. As a case in point, Manjunath et al. (2018) conducted a specific experimental study on the production of AASCC mixtures employing GGBFS as the main precursor. Steel slag sand and electric arc furnace slag were also used as fine and coarse aggregates, respectively. The study's main objective was to create AASCC mixtures that comply with EFNARC guidelines using 100% slag. According to the study, slag content (as a binder) varied as 700 kg/m^3 , 800 kg/m^3 , and 900 kg/m^3 in the fresh concrete mixtures. The $\text{SiO}_2/\text{Na}_2\text{O}$ (i.e., 1.0) ratio was kept constant in the generated alkaline solution regardless of the change in the Na_2O percentage (i.e., 7%, 8%, and 9%). The w/b ratio of the produced concretes fluctuated between 0.47 – 0.48. According to the study, the Taguchi method was employed to optimize the number of experiments to be conducted, resulting in nine effective mixtures. The binder content, Na_2O %, and water to binder ratio were considered the main parameters affecting the potential strength of the proposed mixtures.

Results showed that all slag binder contents (i.e., 700, 800, and 900 kg/m^3) in mixtures had a satisfactory workability performance satisfying the relevant slump flow (650 - 800 mm) and T_{500} (2 - 5 s) according to EFNARC guidelines. Increasing slag content had resulted in a higher slump flow and reduction in the T_{500} values (**Fig. 10**). The excellent performance of AASCC mixtures was attributed to the high volume of slag binder that led to a reduction in the yield stresses. This, in turn, motivated AASCCs to flow like a fluid. Furthermore, the viscosity of sodium silicate as part of the alkaline solution prevented segregation and bleeding. This study has only addressed the impact of binder content (slag as a sole precursor) on the flowability characteristics of the produced AASCC. However, it did not pose questions about the influence of using other mineral admixtures, alkaline activator molarity, or even the curing regime on the aforementioned fresh properties.

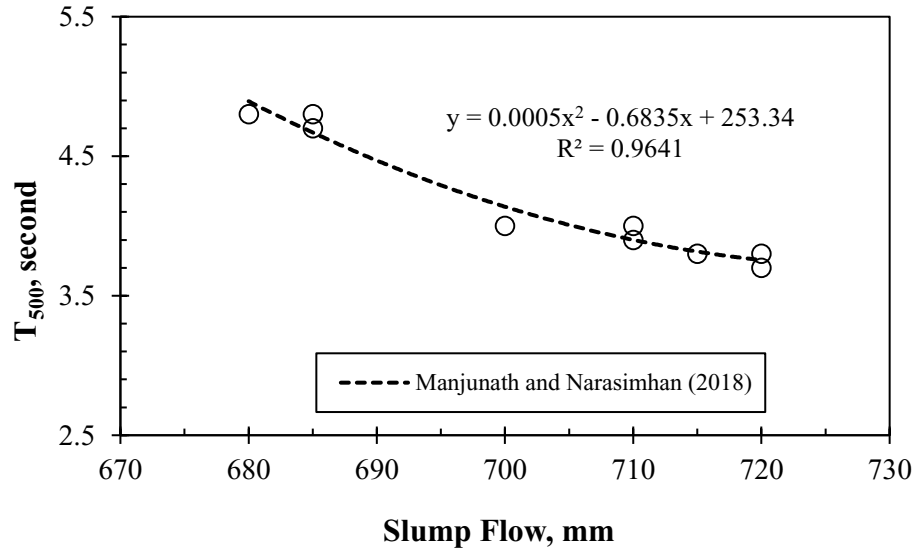


Fig. 10 – Relationship between T500 and slump flow tests [After Manjunath et al. (2018)]

A very recent study by Muttashar et al. (2018) examined the feasibility of incorporating up to 100% of spent garnet to replace river sand to achieve an enhanced AASCCs. Each mixture was produced using GGBFS as the sole precursor and a combination of alkaline NaOH and Na₂SiO₃ reagents. The solution molarity was kept constant at 8M, and the ratio of Na₂SiO₃/NaOH was 2.5. It was concluded from the fresh behavior of the AASCC (**Table 1**) that the satisfactory performance is ascribed to the shape, surface morphology, and the particle size distribution of the spent garnet that enhanced the overall fresh state performance of AASCC. Furthermore, the developed workability by 29% during replacing sand with 100% spent garnet might be attributed to the effect of fineness modulus of spent garnet, i.e., 2.05, which is much less than the specified minimum value of sand, i.e., 2.3 to ASTM C33 standard.

Table 1 – Fresh properties of AASCCs with garnet replacing sand [After Muttashar et al. (2018)]

Mix I.D.	Slump flow (mm)	T ₅₀ (s)	V-funnel (s)	L-box ratio (H ₂ /H ₁)	
TR - 0%	671	5.5	12.0	0.91	
TR - 25%	675	5.0	11.5	0.92	
TR - 50%	681	4.5	11.0	0.93	
TR - 75%	692	4.0	7.50	0.95	
TR - 100%	700	3.5	6.50	0.97	
EFNARC Guidelines	Maximum	650	2.0	6.00	0.80
	Minimum	800	5.0	12.0	1.00

2.2.2. Passing and stability abilities

Some of the criteria that are suggested by most of the investigators in a broader view were the passing ability and static stability of the produced AASCC mixtures due to the utilization of water glass “part of alkaline solution” yielding to a viscous fluid. Passing ability refers to the capacity of an SCC mixture to flow through narrow spaces and restricted openings without blocking. Several

test methods are used to measure the passing ability of SCC, such as J-Ring, L-Box, and U-Box tests. However, the potential of SCC to resist segregation and excessive bleeding is denoted as stability.

Saini and Vattipalli (2020) recently concluded that increasing the NaOH molarity from 10M to 16M decreased the passing ability of AASCC mixtures. Huseien and Shah (2020), on the other hand, illustrated that the passing and filling abilities of the AASCC mixtures increased as the slag was replaced with FA. The study also indicated that NaOH and Na_2SiO_3 couldn't activate slag-based mixtures with a reported filling ability of 560 mm. Manjunath et al. (2018) observed that increasing the slag binder content from 800 to 900 kg/m^3 had resulted in the increase of paste volume and correspondingly the passing ability. In addition, the J-Ring test result for all mixtures satisfied the EFNARC guidelines (<10 mm). Along the same line, Muttashar et al. (2018) spotted the potential of spent garnet, replacing natural sand by up to 100%, to enhance the passing ability of the produced mixtures (**Table 1**). Moreover, Memon et al. (2011) concluded that the addition of water by 10%, 15%, and 20% affected the flowability and stability of the mixtures. The addition of water by 10% placed the mixture outside the EFNARC range. Extra added water by 15% and 20% had resulted in bleeding and segregation. On the contrary, Shahidar et al. (2015) and Patel et al. (2018) have shed light on increasing the NaOH molarity $\geq 8\text{M}$ on the AASCC passing ability. Both studies linked the reduction in mixtures' passing ability and fluidity with the increase in the activator viscosity.

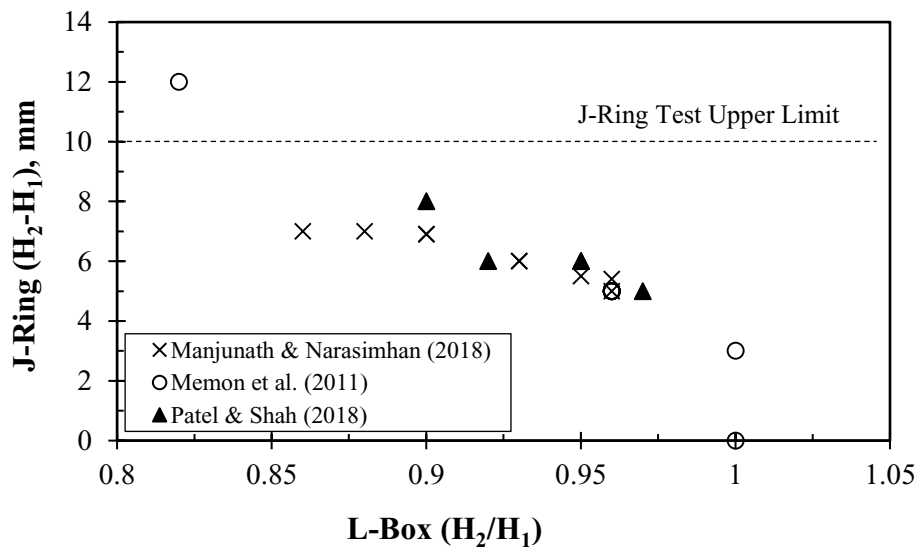


Fig. 11 – Relationship between J-Ring and L-Box tests [Adapted from Memon et al. (2011); Manjunath et al. (2018); Patel et al. (2018)]

In particular, Patel et al. (2018) noticed that as NaOH molarity was increased from 8M to (10M, 12M, and 14M), a reduction in the blocking ratio from 2% to 7% was observed (**Fig. 11**). Similarly, an increase in the J-Ring results by up to 75% was observed. This behavior is in line with the results obtained by Shahidhar et al. (2015), where the reduction in the passing ability was between 8 to 10% as the molarity increased from 10M to 12M.

2.2.3. Summary of Studies and Remarks

The rheological characteristics of AAMs are usually influenced by the type and fineness of mineral admixture(s), nature and dosage of alkali activator(s), chemical admixture(s), curing regime, and mixing procedure. Activators, in particular NaOH, have a great effect on the apparent viscosity, yield stress, and dissolution rate. However, the addition of sodium silicate largely enhances workability due to its role in improving the dissolution of the prime materials. To produce alkali-activated concrete with satisfactory workability, the molarity of NaOH should be $< 12\text{M}$. Such as conventional concrete, optimum water content is considered the most effective parameter affecting the flow of alkali-activated concrete. On the other hand, extra added water $>10\%$ over the total water (i.e., alkaline solution) of the mixture may lead to bleeding and segregation. The main findings available in the AASCC research concerning the workability requirements are summarized in **Table 2**.

Table 2 – Summary of AASCCs characteristics and fresh properties reviewed in previous studies

Reference	Precursors	Activators	Molarity	Research Parameters	EFNARC Standards	
					Filling Ability	Segregation Resistance
Huseien and Shah (2020)	FA+Slag	NaOH + Na ₂ SiO ₃	N.R.	Precursor content	✓	✓
Saini and Vattipalli (2020)	Slag+2% nano silica	NaOH + Na ₂ SiO ₃	10M,12M,16M	NaOH molarity Precursor content	✓	✓
Nagaraj and Babu (2018)	FA+Slag	NaOH + Na ₂ SiO ₃	2M–12M	NaOH molarity	✓	x
Manjunath et al. (2018)	Slag	NaOH + Na ₂ SiO ₃	N.R.	Slag waste replacing Precursor content Na ₂ O (7-9) %	✓	✓
Muttashar et al. (2018)	Slag	NaOH + Na ₂ SiO ₃	8M	Spent garnet replacing F.A.	✓	✓
Patel et al. (2018)	FA+Slag	NaOH + Na ₂ SiO ₃	8M–14M	NaOH molarity Curing temperature	✓	✓
Shafiq et al. (2017)	Slag+CW	NaOH + Na ₂ SiO ₃	8M, 12M	Precursor nature	✓	✓
Sashidhar et al. (2015)	FA+Slag	NaOH + Na ₂ SiO ₃	8M–12M	NaOH molarity Sand replacement	✓	✓
Ushaa et al. (2015)	FA+Slag+S F	NaOH + Na ₂ SiO ₃	8M–14M	Precursor nature Precursor content	x	✓
Memon et al. (2011)	FA	NaOH + Na ₂ SiO ₃	12M	Extra water Curing time Curing temperature	✓	✓
				Except for Mix 1		Except for Mixes 3,4

*F.A.: Fine Aggregates

*C.W.: Ceramic Waste

*N.R.: Not Reported

2.3. Mechanical Properties

In order to move closer towards real practices, binding precursor materials and activators are classified according to their strength-giving characteristics. This evaluation technique can be applied at early (i.e., ≤ 7 days), late (i.e., ≥ 28 days), or even both ages. Various recent studies placed primary emphasis upon studying and characterizing AASCC at both ages (Memon et al., 2011; Nuruddine et al. 2011; Demie et al., 2013; Sashidhar et al., 2015; Ushaa et al., 2015; Manjunath et al., 2018; Patel et al., 2018). In addition, the mentioned investigations utilized slag or fly ash as the main precursors. Moreover, the commercially used alkaline solution in the studies mentioned earlier consisted of $\geq 97\%$ pure NaOH flakes mixed with a sodium silicate solution.

Memon et al. (2011) studied the workability and compressive strength of AASCC produced by low-calcium fly ash (FA). It was concluded that curing temperature between 60°C to 90°C along with the additional amount of water from 10% to 20% and increasing curing period from 24h to 96h could affect the strength of AASCC mixtures. Increasing the curing period by more than 48h at a temperature above 60°C enhanced the polymerization rate significantly and gained strength (**Fig. 12**). Also, curing at 70°C recorded the highest strength (i.e., about 51 MPa). In a similar manner, the addition of an extra amount of water $\geq 12\%$ by mass of FA resulted in a significant reduction in the strength. The obtained results supported the conclusions of a previous study by the same authors Nuruddine et al. (2011). The study concluded that the compressive strength results tend to decrease as the w/b ratio increases. Furthermore, the longer the curing time, up to 96h, showed no compressive strength gain due to the completed polymerization process. The authors also recommended curing samples at 70°C using 12% extra water over the total used water for 48h curing duration, as the latter optimum conditions would enhance the compressive strength and flowability of the produced AASCC.

Another experimental study was carried out by Sashidhar et al. (2015) to examine the potential of the locally available by-product materials (i.e., FA and GGBFS) in the production of AASCC and their effects on the fresh and hardened properties. The produced mixtures, namely, M1, M2, and M3 with 8M, 10M, and 12M NaOH molarities, were prepared using FA and GGBFS with 450 kg/m^3 and a water content binder ratio of 0.4. The study concluded that the AASCC mixture with a 12M NaOH concentration level possessed the highest compressive strength value. Also, the involvement of GGBFS has motivated mixtures to attain early age strength, given that the curing process was under ambient temperature.

The particular effect of the excess content of mineral admixtures on the performance of AASCC mixtures was observed by Ushaa et al. (2015). The research reported the production of seven FA-based alkali-activated concrete mixtures replaced with 10%, 20%, and 30% by mass of GGBFS along with 5%, 10%, and 15% by mass of SF. A liquid/solid ratio value of 0.33 had been reported to have a significant effect on strength with various AAMs. On the one hand, 14-days strengths (i.e., compressive, split tensile, and flexural) were enhanced while increasing the SF content. This can be ascribed to the progressive hydration while the formation of C-S-H and the enhancement in the polymerization process leading to a compact and homogeneous matrix. Moreover, the increase in strength was even higher in the case of slag addition. Based on the experimental results, replacing FA with 30% slag was suggested by the authors to achieve an optimum performance level.

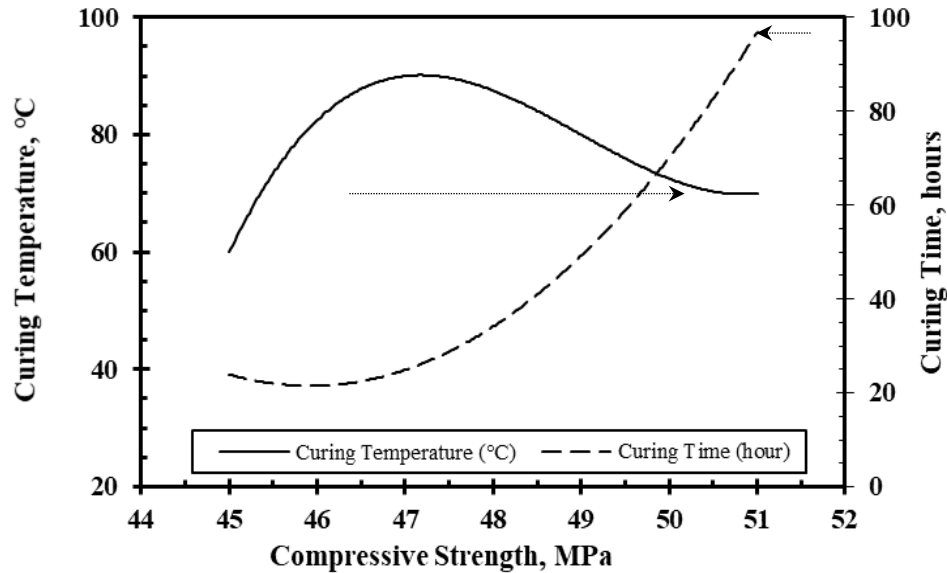



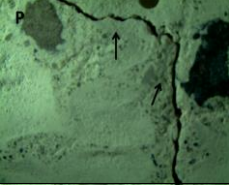
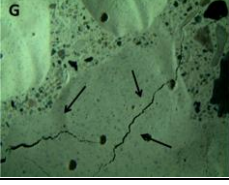
Fig. 12 – Effect of curing temperature (°C) and time (hours) on the compressive strength of AASCC
 [Adapted from Memon et al. (2011)]

Recent research work was carried out by Kamseu et al. (2016) in order to explore the structural behavior, in particular, the bi-axial four points flexural strength, of metakaolin-based AASCCs. The experimental investigation was carried out using metakaolin as a precursor, aggregates (3 mm to 9.5 mm) diameter range, river sand, and various fine materials. The three types of fines were waste materials obtained from different waste management cycles (i.e., pumice (P), recycled glass (G), and feldspar sludge (F)) from mines exploitation, a recycled glass of food containers, and nepheline syenite, respectively. The alkali-activated mixtures were prepared using 8M NaOH and (3.0) $\text{Na}_2\text{SiO}_3/\text{NaOH}$ ratios. Ten mixtures were designed, including a reference mixture and nine derived mixtures from the standard one. The mixtures were varying in the type of fines, i.e., P, G, and F, in addition to the content of added fines, i.e., 2.5%, 5%, and 7.5%. The results showed that using fine reactive materials is more efficient than using fillers to strengthen binding phases (with the remaining NaOH) into the pore solution. The formation of the previous extra bonds near the capillary pores would prevent intensive micro-cracks, leading to strength reduction. According to the authors, the variation in flexural strengths (**Table 3**) among the three fines was due to the difference in the reactivity, packing behavior, and amount of unreacted particles. Although the use of pumice and recycled glass amorphous materials had enhanced the response of AASCCs to mechanical loading, the feldspar series revealed the optimum solution for pore refinement and fracture resistance. Furthermore, the improvement in the paste matrix, in particular the interface, granted the easy transfer of stresses from aggregates to the matrix, maintaining mechanical stability.

Similar to the previous research, Muttashar et al. (2018) discussed the influence of replacing sand by up to 100% spent garnet on the mechanical characteristics of AASCCs. The research work was conducted experimentally by testing cubic and prismatic specimens in compressive and flexural strength tests. All specimens were de-molded after 24h casting and subsequently kept in the ambient laboratory environment until the testing age. The authors attributed the major reduction in the mechanical properties to the fineness and poor gradient of spent garnet particles leading to weak

densification levels. Moreover, the spent garnet replacement of 25% with natural sand exhibited the optimum performance for both workability and mechanical characteristics (**Table 3**). This can be due to the high contents of silica, alumina, and iron in the spent garnet.

Table 3 – Change in mechanical properties of various geopolymer composites [After Kamseu et al. (2016); Muttashar et al. (2018)]

Reference	Fines Types	Mix I.D.	Change in Strength, %		Micro-Cracks Propagation
			Compressive	Flexural	
Kamseu et al. (2016)	Feldspar	F1*	---	85.74	
		F2	---	126.17	
		F3	---	67.58	
Kamseu et al. (2016)	Pumice	P1*	---	8.40	
		P2	---	68.16	
		P3	---	60.94	
Kamseu et al. (2016)	Recycled Glass	G1*	---	30.47	
		G2	---	56.25	
		G3	---	48.83	
Muttashar et al. (2018)	Spent Garnet	TR1*	-2.04	-10.0	---
		TR2	-4.41	-20.0	---
		TR3	-5.50	-26.0	---
		TR4	-11.92	-34.67	---

*F (1-3): Sand Replacement by Feldspar (2.5-7.5%)

*P (1-3): Sand Replacement by Pumice (2.5-7.5%)

*G (1-3): Sand Replacement by Recycled Glass (2.5-7.5%)

*TR (1-4): Sand Replacement by Spent Garnet (25-100%)

The mechanical characteristics of AASCC mixtures produced by Manjunath et al. (2018) using 100% slag (in terms of compression and tensile tests) are illustrated in (**Fig. 13**). The high early age (i.e., 3-day) compressive and tensile strength results ranged between 55 to 70 MPa and 2.25 to 3.7 MPa, respectively. This was attributed to the early formation of C-S-H gel in an alkaline environment. Similarly, the findings of the 28-day compressive and tensile strength tests reached approximately 80 and 3.9 MPa, respectively. The prominent high performance of AASCC mixtures was confirmed in this study due to the full activation of slag, yielding to a denser microstructure.

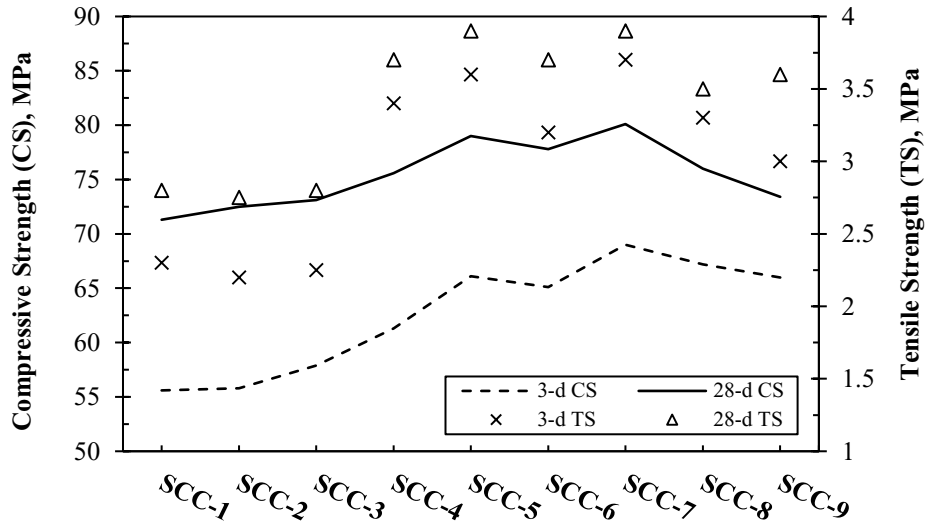


Fig. 13 – Hardened properties of AASCC mixtures [Adapted from Manjunath et al. (2018)]

At last, three mixtures with the best engineering performance were chosen for the microstructural analysis using SEM, EDS, and XRD techniques (**Fig. 14**). The XRD outcomes emphasized the activation of slag grains through the peak of C-S-H. According to the authors, the existence of the C-S-H product derives from the development of a densified layer that led to the ITZ vanishment. The author's views on the strength development are grounded on the assumption that increasing the content of the activated slag grains by alkaline solution promoted the development of C-S-H and C-A-S-H gels in the matrix, which indeed led to strength elaboration. Although this may be true, the morphology of mixtures with the highest binder content (i.e., 900 kg/m³) showed a higher portion of C-S-H gel coupled with lesser content of activated slag. In other words, alkaline solution activator quantity was insufficient to activate that higher content of slag grains.

The effect of activator molarity and curing temperature while the utilization of FA and GGBFS on the mechanical performance of AASCC were also examined by Patel et al. (2018). Results showed that increasing the molarity results in higher strength. However, 12M NaOH represents a threshold, where exceeding this value results in a reduction in strength. Increasing the molarity provides additional hydroxide ions that lower the polymerization rate (Khale et al., 2007). At ambient temperature, the 100% FA mixture failed to achieve the early age strength, while the replacement by GGBFS had resulted in 41.35 MPa compressive strength, 2.9 MPa split tensile strength, and 3.11 MPa flexural strength, respectively, after 28 days of curing. The achieved enhancement in the mechanical properties of the produced mixtures as the curing temperature was increasing, i.e., ambient, 60°C, and 70°C, was due to the fast polymerization.

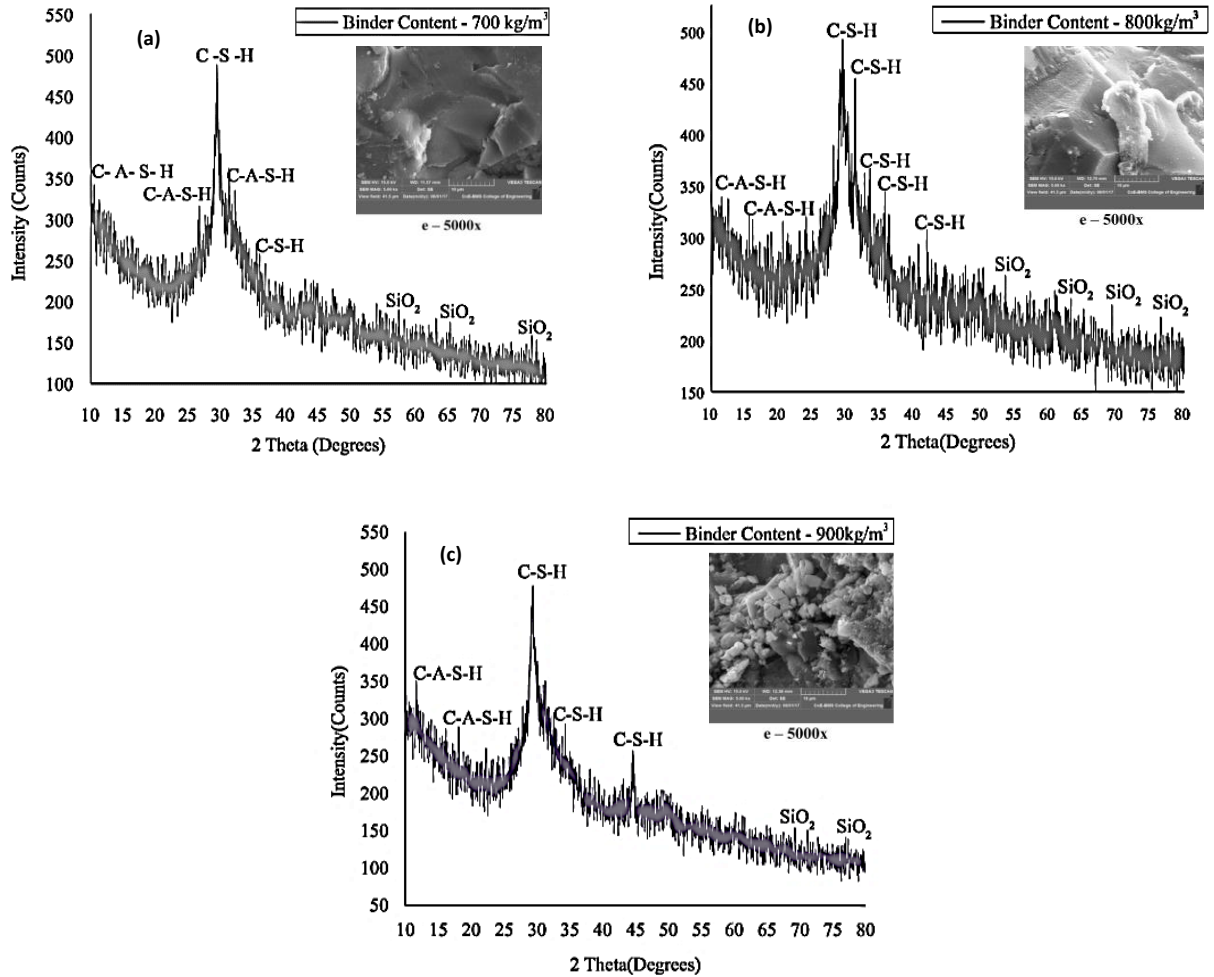


Fig. 14 – SEM and XRD results of a) SCC-3 b) SCC-5 and c) SCC-7 [After Manjunath et al. (2018)]

2.3.1. Summary of Studies and Remarks

It has been shown from the above-mentioned brief review that most of the previous studies highlighted that the utilization of various precursors in alkali-activated concretes would facilitate the formation of mineral polycondensation reactions by alkaline activation. Many current works suggested using GGBFS as the main precursor for AASCC to achieve high early-age strength due to the fast polymerization process. Achieving the optimum performance of AASCC was recorded while replacing FA by 30% GGBFS. Concerning the change in strength, it was noted that as the molarity increases (i.e., > 14M), a reduction in the strength was observed. Increasing the molarity has resulted in an additional hydroxide ions concentration that lowered the polymerization rate. Type and concentration of activators can advocate the compressive strength of alkali-activated concrete in two ways: 1) Higher dissolution rate of Si and Al and 2) Stronger Si–O bonds than Al–O bonds in the prime material. The latter bonds would dissolve rapidly in the alkali atmosphere. On the contrary, Si ions would be conserved before being involved in the dissolution process; this would promise an improvement in the mechanical properties by increasing the degree of

polymerization. The optimum molarity with the highest compressive strength value based on the earlier presented work was 12M NaOH. From the compressive strength results, as expected, the strength of AASCC developed with curing time. The 48h curing duration is considered the optimum condition where the longer the curing time up to 96h did not ensure higher compressive strength values. This is owing to the completion of the polymerization process. In fact, the rapid strength gain rate in alkali-activated concrete makes it an ideal recommendation for repairing structures. The main findings available in the AASCC research regarding the mechanical properties are summarized in **Table 4**.

Table 4 – Summary of AASCCs mechanical properties reviewed in previous studies

Reference	Research Parameters	Precursor	Age	Mechanical Properties ^a			Main Conclusions
			Days	Compressive Strength	Flexural Strength	Split Tensile Strength	
Patel et al. (2018)	NaOH molarity	FA+Slag	3	Higher	Higher	Higher	-Highest compressive strength was achieved using 12M NaOH. -Slag cured ~70°C prompted the fast geopolymerization.
	Curing temperature		28	Higher	Higher	Higher	
Muttashar et al. (2018)	Spent garnet replacing F.A.	Slag	7	Lower	Lower	Lower	-Strengths declined at all replacement stages. -Spent garnet (25%) replacement is optimum.
			28				
Manjunath et al. (2018)	Slag waste Precursor content Na ₂ O 7-9%	Slag	28	Higher	N/A	Higher	-Compressive and split tensile increased 65–80 MPa and 2–4 MPa, respectively.
Shafiq et al. (2017)	Precursor nature	Slag+CW*	28	Higher	N/A	N/A	-AASCC composed of slag and CW by 50:50 showed higher strength than 100% OPC.
Kamseu et al. (2016)	Glass waste, pumice & feldspare replacing F.A.*	Metakaolin	90	N/A	Higher	N/A	-Reduction of pore and pore size improved AASCC strengths. -Added fines resulted in pore refinement and mixtures stability.
Ushaa et al. (2015)	Precursor nature	Slag	14	Lower	Lower	Lower	Slag replacement by 30% is considered the optimum
		SF		Higher	Higher	Higher	
	Precursor content	Slag	28	Higher	Higher	Higher	
		SF		Lower	Lower	Lower	
Sashidhar et al. (2015)	NaOH molarity	FA+Slag	28	Higher	Higher	N/A	-Increase in NaOH molarity enhanced AASCC strengths. -No adverse effect was observed in mixtures with artificial sand.
	Sand replacement		56				

Table 4 – Summary of AASCCs mechanical properties reviewed in previous studies (cont.)

Reference	Research Parameters	Precursor	Age		Mechanical Properties ^a		Main Conclusions
			Day	Compressive Strength	Flexural Strength	Split Tensile Strength	
Memon et al. (2011)	Extra water	FA	2	Lower	N/A	N/A	-Strength dropped as >12% of extra water was added. -Highest strength achieved by curing for 96h and 70°C.
	Curing time		3,5	Higher			
	Curing temperature		3	Higher			

^aMechanical Properties Compared to AASCCs

*F.A.: Fine Aggregates

*N.R.: Not Reported

*C.W.: Ceramic Waste

2.4. Long-Term Durability Properties

Sulfate attack is commonly avowed as one of the most antagonistic environments to concrete structures. It generates severe deteriorations leading to a shorter service life (Najimi et al., 2011). It is frequently defined as “synthesis of complex and overlapping chemical operations and physical activities caused by deteriorative reactions between paste components and sulfate ions from external or internal sources” (Marchand et al., 2003; Najimi et al., 2011). In fact, physical sulfate attack repercussions are distinctive from those of chemical sulfate attack since it eventuates surface degradation. However, expansion and cracks are the consequences of the chemical sulfate attack due to ettringite and gypsum formation (Mehta, 2000). Hence, utilization of the generic terminology “sulfate attack” in the in-situ domain towards depicting concrete deterioration caused by sulfate ions may generate perplexity and confusion between physical and chemical attack processes that cannot be separated (Haynes et al., 1996; Suleiman, 2014). The adverse effect of sulfate on concrete structures depends on several parameters such as the quality of concrete, nature and concentration of sulfate, etc. Alkalinity in the cement pores is another key factor where any medium with a low pH value (i.e., <12.5) represents an aggressive atmosphere for the cement matrix.

Eventually, utilization of AAMs as an alternative to OPC systems may exhibit high resistance to sulfate attack. This might be due to the polycondensation of the main elemental reaction products in a 3-D network structure during the activation of aluminosilicate precursor(s), i.e., slag, FA, MK ... etc., under an alkaline atmosphere. Generally, C-A-S-H and C-S-H gels are believed to have a similar tobermorite structure (Sun et al., 2006; Provis et al., 2013). Whereas the chemical composition and structure of Na and/or K attached to Si-O-Al bonds are similar to zeolites structure (Lecomte et al., 2003). The limited degree of knowledge associated with the efficiency and durability of AAMs prone to sulfates in the concrete industry have not, to date, been addressed extensively. At the same time, most of the durability standardized test methods were established for OPC systems that may be unsuitable for AAM systems (Van Deventer et al., 2010; Van Tittelboom et al., 2009). A limited number of studies in the literature had focused on the performance of AAMs prone to sulfate environments.

The concern related to the resistance of low-calcium alkali-activated concretes to sulfate solutions was deliberated by several researchers (Bakharev, 2005; Thokchom et al., 2010). The behavior of alkali-activated FA (class-F) concretes prone to 5% Na₂SO₄, 5% MgSO₄ and 5% Na₂SO₄ + 5%

MgSO₄ for 5 months was examined by Bakharev (2005). In Na₂SO₄ solution, the compressive strengths of alkali-activated mixtures by NaOH + KOH and Na₂SiO₃ activators decreased by 65% and 18%, respectively. Furthermore, an increase in strength by 4% was noted during the utilization of NaOH only. Quite the reverse, in MgSO₄ solution, an increase in the strength was observed (**Table 5**) during the utilization of NaOH and NaOH + KOH activators by 12% and 35%, respectively, while a reduction by 24% was observed in Na₂SiO₃ activated mixture.

Table 5 – Changes in strength after the exposure to various sulfate environments [After Bakharev (2005)]

Mix I.D.	Activator	Na ₂ SO ₄ Sol.%	MgSO ₄ Sol.%	Na ₂ SO ₄ + MgSO ₄ Sol.%
OPC	---	-30	-21	-35
OPC+FA	---	-14	-4.8	-19
8FA	NaOH	+4	+12	+12
8FAK	NaOH+KOH	-65	+35	+10
8FASS	Na ₂ SiO ₃	-18	-24	-4.5

This was attributed to the migration of alkalis into solution while the exposure to Na₂SO₄. In MgSO₄ solutions, both mixtures prepared using Na₂SiO₃ and a mixture of NaOH + KOH showed migration of alkalis into sulfate solutions and diffusion of Mg²⁺ and Ca²⁺ to the subsurface areas of specimens. It was noted that the exposure to a combination of 5% Na₂SO₄ + 5% MgSO₄ resulted in the least strength changes. The best performance was observed while using NaOH activator in mixtures due to its stable cross-linked aluminosilicate polymer structure. At last, the immersion in more concentrated solutions, i.e., 5% Na₂SO₄ + 5% MgSO₄, created fewer changes in the strength of the alkali-activated specimens than immersion in less concentrated ones. A contradictory observation was found in OPC specimens where the most significant deterioration was found in concentrated solution.

Research work carried by Thokchom et al. (2010) reported the performance of alkali-activated FA (class F) mortars during the exposure to 10% MgSO₄ solution for 24 weeks. The mortar specimens were cured thermally in an oven for 48h under 85°C. The variation in the Na₂O % was found to have a significant influence on the pH value. The visual inspection results showed white anhydrite deposits (CaSO₄) on the specimen's surfaces during exposure to MgSO₄ solution, which gradually transformed from soft to hard shape with additional gain in weight. Generally, mortars produced with higher Na₂O % behaved better than those with lower alkali content (**Table 6**), with a maximum strength of 89.7%. This can be attributed to the increase in pH due to the migration of alkalis from specimens into the solution.

Table 6 – Mixtures characteristics and residual strength data [After Thokchom et al. (2010)]

Mix I.D.	Activator	Na ₂ O %	Curing temperature and Duration	Residual Compressive Strength after 24-week, %
M1	NaOH+Na ₂ SiO ₃	5.0	85°C and 48h	44.13
M2	NaOH+Na ₂ SiO ₃	6.5	85°C and 48h	78.56
M3	NaOH+Na ₂ SiO ₃	8.0	85°C and 48h	89.7

The most extensive study on the effect of external sulfate attack on the mechanical and

microstructural properties of alkali-activated slag (AAS) was made by Komljenović et al. (2013). The investigation program consisted of two main phases. First, analyzing the properties of the Portland-slag cement (CEM II/ A-S 42.5N) as the benchmark material of the produced mortars. Second, reporting the performance of the AAS during the 5% Na₂SO₄ exposure. The total water to solid ratio, including the sodium silicate activator, was 0.28. After 28 days of curing in a humid chamber at ambient temperature conditions, mortar prisms were exposed to 5% Na₂SO₄ for up to 90 days. It was observed from (Table 7) that the exposure had led to a decrease in strength of CEM II, but not of AAS samples. The compressive strength of both CEM II and AAS groups after 30 days in a sulfate-rich environment was slightly increased by 1.05 and 1.07, respectively. After 60 days of sulfate attack, AAS relative strength remained on the same level, i.e., 1.07, while in CEM II, it decreased, i.e., 0.97. CEM II relative strength continued to decrease at the end of the exposure period, i.e., 0.90, whereas AAS relative strength slightly increased, i.e., 1.11. Strength loss of 9% in the case of CEM II was ascribed to the microstructural changes. In addition, the expansion of the matrix in the aggressive sulfate environment is due to the transformation of monosulfate crystals embedded in the C-S-H to ettringite and gypsum. On the other hand, mortars prepared using AAS showed no strength loss compared to Portland-slag cement mortars. A strength gain of 11% was observed in the AAS mortar due to the high alkalinity of the sulfate medium through the continuous formation of AAS reaction products. Lastly, calcite was detected in both mortars after 28 days of curing in a humid chamber due to the carbonation process (Fig. 15).

Table 7 – Mixtures identification and compressive strength loss indices [After Komljenović et al. (2013)]

Time (Days)	Reference samples		5% Na ₂ SO ₄		Strength loss index (relative strength after sulfate attack, compared to reference samples)	
	AAS	CEM II	AAS	CEM II	AAS	CEM II
28	REF0z	REF0c	---	---	1.00 ^a	1.00 ^a
28+30	REF1z	REF1c	S-Iz	S-Ic	1.07	1.05
28+60	REF2z	REF2c	S-IIz	S-IIc	1.07	0.97
28+90	REF3z	REF3c	S-IIIz	S-IIIc	1.11	0.90

^a Initial strength – before sulfate attack (strength loss index 1.00)

These results agree with Bakharev et al. (2002), where AAS and OPC concrete were exposed to 5% Na₂SO₄ and 5% MgSO₄ solutions for 365 days. The compressive strength of the AAS group was reduced by 17% and 23%, while for OPC, the reduction was 25% and 37% after the exposure to 5% Na₂SO₄ and 5% MgSO₄, respectively. The author attributed the strength loss of AAS in MgSO₄ solution to the absence of portlandite Ca(OH)₂ that restricted the formation of protective brucite Mg(OH)₂ layer. This promoted the direct attack of Mg ions on the C-S-H structure besides the formation of M-S-H and gypsum expansive products. The destruction of C-S-H coupled with the appearance of gypsum were the main deleterious reactions affecting the resistance of AAS to MgSO₄ solution. Alkali-activated concretes, in particular high-calcium precursors, are affected by the type of cations Na and/or Mg in sulfate solutions. It was observed that AAS mixtures exposed to Na₂SO₄ solution were more resistant than MgSO₄ solution.

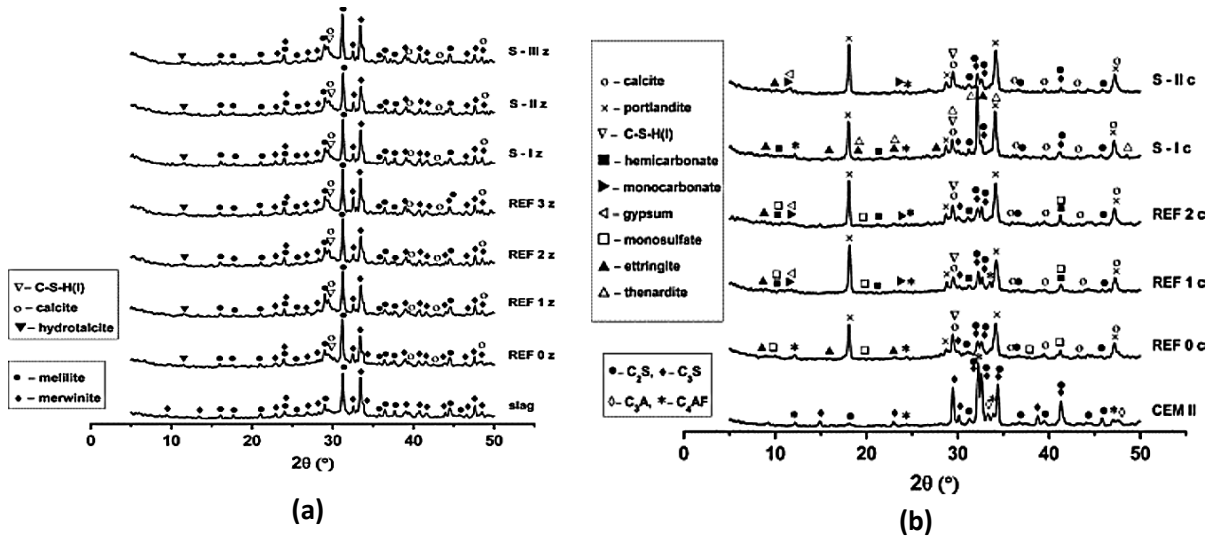
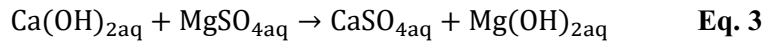


Fig. 15 – Diffractograms of a) AAS and b) CEM II samples exposed to sulfate attack [Adapted from Komljenović et al. (2013)]

An experimental study related to the influence of 5% Na₂SO₄ and 5% MgSO₄ solutions on alkali-activated slag – ultrafine palm oil fuel ash (POFA) mortars was conducted by Yusuf (2015). The experimental work was carried by testing three alkali-activated mortars with/without slag by varying the (Na₂SiO₃/NaOH) ratio between 2.5 and 1.0. Generally, the inclusion of slag up to 20% in mortars has contributed to better sulfate resistance. On the other hand, the variation in the Na₂SiO₃/NaOH ratio has resulted in a negligible strength retention difference. After 6-months of continuous immersion in Na₂SO₄ and MgSO₄ solutions, the residual strengths recorded for the slag-free mortars were 16.5% and 76.8%, respectively. The investigation attributed the severe deterioration of mortars exposed to 5% Na₂SO₄ solution to the leaching of active minerals (Ca²⁺, Mg²⁺, Na⁺), instigating the disintegration of the microstructural framework. On the other hand, better strength retention was observed in the MgSO₄ solution owing to the formation of surficial white deposits and crystallized anhydrite (CaSO₄). The results obtained from this study showed a very good agreement with previous experimental results conducted by Salami et al. (2017) in terms of the resistance to sulfate attack. The exposure to 5% Na₂SO₄ and 5% MgSO₄ solutions for 9 months confirmed that the deterioration of mortars depends on the type of cations carried by sulfate solutions.



The results of the Mithun and Narasimhan (2016) study confirmed the potential of producing alkali-activated slag concrete using copper slag (CS) as an alternative to natural river sand. The study indicated the use of an OPC-based control mixture, as a basis, for the design of five alkali-activated slag-based mixtures with CS up to 100% by volume. The alkali solution used was a mixture of liquid Na₂SiO₃ and NaOH with a SiO₂/Na₂O ratio of 1.25. The investigation concluded that the replacement of CS by natural sand has reinforced the produced OPC and alkali-activated mixtures. After 12 months of exposure to 10% Na₂SO₄ solutions, no strength deterioration was observed in conventional and alkali-activated mixtures with CS. While, in 10% MgSO₄ solutions, both groups

of mixtures suffered from a higher rate of degradation, alkali-activated mixtures being the most. This can be attributed to the absence of calcium hydroxide $\text{Ca}(\text{OH})_2$ after its reaction with MgSO_4 solutions leading to the nonstop attack of Mg ions to the C-S-H structure. The result was the formation of expansive products, i.e., M-S-H and gypsum, henceforth, alkali-activated concrete cracking.

2.4.1. Summary of Studies and Remarks

A thorough review to explore the resistance of alkali-activated concretes to the external sulfate attack has confirmed the following conclusions. The deterioration of alkali-activated mixtures depends on the type of cations, i.e., Na or Mg, carried by sulfate solutions. The previous literature indicated that various parameters might affect the resistance of alkali-activated concretes to sulfate-enriched environments, such as the mixture design, precursor and activating agent types, nature of the sulfate, and its concentration in the environment. However, it is important to bear in mind that various alkali-activated systems exhibit different degradation mechanisms in sulfate-enriched environments as a result of their different elemental and microstructural compositions. **Table 8** summarizes the characteristics of various alkali-activated mixtures and their resistance to external sulfate attack.

Table 8 – Summary of the sulfate resistance tests by alkali-activated mixtures reviewed in studies

Reference	Precursors	Activators	Sulfates	Corrosion Period	Corrosion Products	Deteriorating Environment
Bakharev et al. (2002)	Slag	NaOH + Na ₂ SiO ₃	5%Na ₂ SO ₄ 5%MgSO ₄	12-month	Gypsum	5%MgSO ₄
Bakharev et al. (2005)	FA	NaOH NaOH+KOH	5%Na ₂ SO ₄ 5%MgSO ₄ 5%(Na ₂ SO ₄ + MgSO ₄)	5-month	Precipitates	All
Thokchom et al. (2010)	FA	NaOH + Na ₂ SiO ₃	10%MgSO ₄	24-week	Anhydrite, ettringite	10% MgSO ₄
Komljenović et al. (2013)	Slag	NaOH + Na ₂ SiO ₃	5%Na ₂ SO ₄	3-month	Gypsum, Ettringite	5%Na ₂ SO ₄
Yusuf et al. (2015)	Slag+POFA	NaOH + Na ₂ SiO ₃	5%Na ₂ SO ₄ 5%MgSO ₄	6-month	Anhydrite, Brucite, Serpentine,	5%Na ₂ SO ₄
Mithun et al. (2016)	Slag	NaOH + Na ₂ SiO ₃	10%Na ₂ SO ₄ 10%MgSO ₄	12-month	Gypsum, M-S-H	10%MgSO ₄

*POFA: Palm Oil Fuel Ash

*Anhydrite: CaSO₄

*Brucite: Mg(OH)₂

*Serpentine: Mg₃Si₈O₂₀(OH)₈ 12H₂O

*Gypsum: CaSO₄ 2H₂O

2.5. Concluding Remarks

In recent years, there has been an increasing emphasis on the durability of concrete under sulfate attack environments and increasing concern about their premature failure and costly rehabilitation techniques (Skalny et al., 2002). Current knowledge indicates a gap between the laboratory research results and the actual field conditions. These conflicting forces have helped create a burgeoning interest in alternative forms of mitigating assessments.

The current assessment policies and practices coupled with the conventional classical sulfate immersion tests are in a period of rapid transformation due to the variability between the controlled laboratories and actual field conditions. Indeed, direct assessment tests, which are frequently referred to as "single damaging factor techniques," have raised doubt on their reliability and efficiency in motivating the efforts to question assessments. Deteriorated concrete structures are often due to an array of mechanisms (chemical, physical and microstructural) acting synergistically. The lack of consistent, standardized durability test procedures has guided the world to a universal shift to performance-based assessment. It is argued that the development of performance-based tests that include multi-damaging mechanisms is necessary for better modeling of the performance of concrete structures (Beushausen and Luco, 2015). Such authentic techniques derive their value primarily from effectively assessing special types of concretes such as AASCC, which encompasses high contents of various precursor materials and activators. Generally, all durability specifications and related standards were established, assuming OPC as the key binder. The inadequacy of current standards in considering the replacement of OPC by AAMs has limited its expansion in the market. Few attempts to study the resistance of alkali-activated concrete to sulfate attack were recorded. On the other hand, there is still a dearth of information on the resistance of AASCC prone to these environments.

Chapter 3 : Resistance of Alkali-Activated Materials to External Sulfate Attack: A Review of Current Standards and Future Needs

3.1. Overview

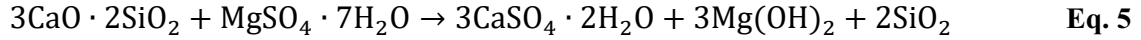
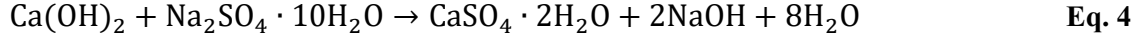
The external sulfate attack, resulting from the invasion of sulfuric ions in soils, underground, marine, or industrial wastewaters, is a significant process of deterioration of concrete in-service. Although sulfates usually damage the cement-paste matrix, their adversity depends on the types of cement (binder) used, nature and concentrations of sulfate solutions, concrete quality, and surrounding conditions. In general, cement paste pores are filled with a highly basic solution (i.e., $\text{pH} > 12.5$). Hence, any medium with a lower pH value would represent an aggressive environment for the cement matrix (Baldermann et al., 2019). Concrete exposed to sulfate attack suffers from expansion, cracking, strength loss, and eventually disintegration (Galan et al., 2019).

In recent years, there has been an increasing emphasis on the durability of concrete under sulfate attack environments and increasing concern about their premature failure and costly rehabilitation techniques (Skalny and Thaulow, 2002). The suitability of cement-based concrete standards and measures available in the literature to simulate the long-term resistance to external sulfate attacks is still controversial. On the other hand, all durability specifications and related standards were established, assuming ordinary Portland cement (OPC) as the sole binder. The inadequacy of the current standards in considering the replacement of OPC by alkali-activated Materials (AAMs) has limited its expansion in the market. Few attempts to study the resistance of AAMs to sulfate attacks were recorded (Komljenović et al., 2013). On the other hand, there is still a dearth of information on AAMs' resistance to these environments.

Therefore, this review's primary purpose is to present a critical analysis of the adequacy of classical/advanced sulfate tests in the field of alkali-activated materials to understand the underlying mechanisms governing the deterioration of those mixtures. It would also raise questions about the possibility of developing a new modeling approach that considers the interaction between AAMs and sulfates.

3.2. Chemistry and Physics Behind External Sulfate Attack

Dissolved sulfates from external sources (i.e., soil and groundwater) can migrate and react with the hydrated paste matrix leading to the formation of gypsum, ettringite, and sometimes thaumasite. These products may cause expansion, cracking, softening, and disintegration of concrete. During the reactions between sodium sulfate (Na_2SO_4) or magnesium sulfate (MgSO_4) salts with other primary mineral phases (cement clinker, carbonates, and calcium silicate hydrate (C – S – H), different reaction products are developed (Bassuoni and Nehdi, 2009; Skalny and Pierce, 1999). Ammonium sulfate, sulfuric acid, and magnesium sulfate are other forms of sulfate solutions that can decompose the cementitious matrix by inducing the decalcification of calcium silicate hydrate (C–S–H), contributing to strength loss (Cohen and Mather, 1991). Reactions between different sulfate solutions and paste matrix products are shown in the following equations.



Where (H₂O) is water, (NaOH) is sodium hydroxide, and Mg(OH)₂ is magnesium hydroxide (brucite), respectively. In addition to gypsum formation, expansion is usually associated with ettringite formation in the inner regions of the cementitious matrix with high pH, which can contribute to specimen swelling and softening of pastes (strength reduction). Furthermore, magnesium silicate hydrate (M – S – H) may be formed after the reaction between Mg(OH)₂ and aqueous silica.

According to (Skalny and Pierce, 1999; Marchand and Skalny, 2003), the consumption of calcium hydroxide (C – H) in Na₂SO₄ solutions do not result in loss of alkalinity due to the production of NaOH. However, Na₂SO₄ may cause the decalcification of C – S – H after the depletion of C – H in the cementitious matrix. On the other hand, the low solubility (0.01 g/l) of brucite, as well as the low pH (<10.5) of the pore solution due to the C – H consumption, increases the reaction rate in the MgSO₄ solution. As a result, C – S – H releases C – H to restore its pH balance, but C – H responds in a continuous cycle of reactions and reacts with MgSO₄, transforming it into gypsum and brucite.

3.3. AAMS Deterioration

The multidimensionality concerns associated with AAMs' resistance to sulfate attack (externally or internally) have led to a scientific focus to understand the decay mechanisms and consequences on AAMs structures. Various parameters such as raw source materials (nature, fineness, and mineralogy), activators (type and concentration), mixture design, curing regime, sulfate ion, and concentration, in addition to weathering conditions, are believed to affect the resistance to sulfate attack. Alkali-activated materials can be classified into two categories according to their main elemental reaction products; high-calcium and low-calcium AAMs systems. For example, alkali-activated slag (AAS) belongs to the high-calcium CaO – Al₂O₃ – SiO₂ – H₂O (C – A – S – H in cement notation) gel class in addition to the formation of secondary phases. In contrast, alkali-activated low-calcium fly ash (class F) (AAFA) or metakaolin (AAMK) generates gels classified as Na₂O – Al₂O₃ – SiO₂ – H₂O (N – A – S – H in cement notation). It is important to note that the activator's selection dramatically affects the chemistry of high and low calcium systems (Myers et al., 2016; Taylor et al., 2010; Yang et al., 2014). For example, in the AAS system, the crystalline phase of the hydrotalcite gel type is produced with either NaOH or water glass (Wang and Scrivener, 1995) while calcium carbonate is formed in Na₂CO₃ activated systems (Park et al., 2020).

The most dominant theme of sulfate attack that leads to expansion and cracking in high-calcium AAMs is the ettringite and gypsum precipitation (Gonzalez and Irassar, 1997; Santhanam et al., 2003; Tian and Cohen, 2000; Neville, 2004). A source of aluminum (Al) and calcium is needed after penetration of sulfates to react and form calcium sulfoaluminate (C₆AS₃H₃₂) and gypsum (CaSO₄ · 2H₂O) (Nijland and Larbi, 2010). Even though alkali-activated systems are incredibly

resistant to sulfate attack, given the presence of hydrotalcite gels, absence of portlandite, and tightly bound aluminum in the C – (A) – S – H, N – A – S – H, and N – (C) – A – S – H (Komljenović et al., 2018). El-Sayed et al. (2011) reported better durability and higher resistance to ettringite formation in AAS mixtures activated with NaOH + Na₂SiO₃ than with NaOH; in a 5% MgSO₄ solution for 180 days. Similar conclusions were drawn by Puertas et al. (2002), who detected traces of ettringite in NaOH-activated FA/slag mortars compared with NaOH + Na₂SiO₃ mixed solution in Na₂SO₄ solutions. On the other hand, Ismail et al. (2013) found that FA/slag mixtures activated by Na₂SiO₃ deteriorated severely when immersed in 5% MgSO₄ solution than in 5% Na₂SO₄ due to gypsum formation and C – S – H decomposition. Also, since Al was assumed to participate in N – A – S – H gels' structure, ettringite was not detected. Similar findings by Saavedra et al. (2016) in FA/slag (80/20) concrete mixtures, reporting gypsum formation and the hostility of MgSO₄ solutions.

On the other hand, low-calcium AAMs systems typically demonstrate adequate sulfate resistance due to the development of a more robust structure (Zhang et al., 2017). An extensive study by Bakharev (2005) reported the resistance of AAFA concretes to 5% Na₂SO₄, 5% MgSO₄ and 5% Na₂SO₄ + 5% MgSO₄ for 5 months using either NaOH + KOH, NaOH, or Na₂SiO₃ activators. It was concluded that the AAMs compressive strengths using NaOH + KOH and Na₂SiO₃ activators decreased by 65% and 18%, respectively, in Na₂SO₄ solution, but increased by 4% using NaOH. Conversely, in the MgSO₄ solution, an increase in the strength was observed during the utilization of NaOH and NaOH + KOH activators by 12% and 35%, respectively, while a reduction by 24% using Na₂SiO₃ activator. This was attributed to the migration of alkalis into solution while the exposure to Na₂SO₄.

In MgSO₄ solutions, both mixtures prepared using Na₂SiO₃ and a mixture of NaOH + KOH showed the migration of alkalis into sulfate solutions and diffusion of Mg²⁺ and Ca²⁺ to the subsurface areas of specimens. It was noted that exposure to 5% Na₂SO₄ + 5% MgSO₄ resulted in the least strength changes compared to cement-based specimens. Thokchom et al. (2010) reported the performance of AAFA mortars exposed to 10% MgSO₄ solution for 24 weeks. The variation in Na₂O % was found to have a significant influence on the pH value, causing the migration of more alkalis from specimens into the MgSO₄ solution. Mortars produced with higher Na₂O % behaved better than those with lower alkali content.

These controversial findings are attributed to the various assessment criteria and evaluation methods associated with the microstructural changes during sulfate attacks. Unifying assessment criteria and evaluation methods would help in identifying the deterioration process and understand its related damaging products.

3.4. Effect of Exposure Conditions

The results obtained from existing standards and specifications are difficult to compare, as different testing systems and procedures can be applied. Most research was conducted with ASTM C1012 (sulfate immersion test). Tests carried out in research labs vary concerning sulfate solution concentration, type of cation, pH, exposure time, sample size, in addition to mixtures' composition. In addition to the varied global standards and specifications, these factors are believed to alter the

attack mechanism. The following subdivisions will address the main factors that may lead to OPC or alkaline-activated concrete degradation.

3.5. Current Standards and Specifications for Sulfate Resistance

Building materials must meet the minimum standards outlined in building codes to pre-qualify concrete mixtures in different exposures along with standard test methods (Hooton, 2008). Therefore, specifications should be evolved on an ad hoc basis to develop and add new testing techniques or set new specification limits for various commercially available binders. However, standards are widely criticized for not being responsive to new research findings and lagging behind recent materials technology and construction practices. A summary of the primary current and former standards and specifications for concretes prone to sulfate attack is presented in the following subdivisions.

ASTM C 452 standard, which was developed in 1946 and initially published in 1960, was the first standardized test in North America for assessing the sulfate resistance of conventional concrete material. Throughout this standard, concrete resistance to sulfate attack is evaluated by measuring the expansion of mortar bars produced from ordinary cement and extra gypsum blend, making a total SO_3 content of 7% by mass of cement. Before mortar bars are made, gypsum should be added to Portland cement; hence, the transport properties do not control the attack rate. This technique would accelerate the experiment by reducing the time for sulfate ingress to mixtures. Cast mortar bars are then stored in water at 23°C , and expansion is measured for up to 14 days. Specifications such as ASTM C452 and ASTM C150, along with ACI 318, indicated that the sulfate-resisting Portland cement (Type V) expansion limit is 0.04% at 14 days (**Table 9**).

It should be noted that the ASTM C 452 technique is unsuitable for testing blended cement or blends of Portland cement with pozzolans or slags (ASTM C 1012). The main aim of using blended cement in concrete is to reduce the diffusion of external aggressive constituents such as sulfate solutions. Following ASTM C 452, sulfate reactions start immediately due to an admixed gypsum that does not reflect the role of blended cement in slowing the diffusion of external sulfate solutions. These blended systems' nature depends on consumed calcium hydroxide to provide resistance and reduce permeability, thus requiring hydration before sulfate exposure.

ASTM C 1038, published in 1985, is similar to ASTM C 452, except that no additional gypsum is added. However, the test only applies to a Portland cement binder. This test method determines how a mortar bar is expanded when stored in water containing sodium sulfate. The expansion limit of 0.02% is the criterion of the ASTM C 1038 and Canadian CAN3- A5-M83 standards in 14 days of water immersion. Since this standard may be designed to set minimum concrete requirements exposed to an externally aggressive environment, the 14-day expansion limit was decreased to half compared to ASTM C 452. Hypothetically, this could be due to slow concrete deterioration after exposure to external sulfate substances and, as a result, a potential decrease in the expansion (owing to volume change). After 14 days of continuous immersion in sulfate solutions, the results of the ASTM C 1038 method would be achieved; but the sulfate attack mechanism would no longer represent the conditions in the field realistically. Therefore, a new approach was needed for field-like testing conditions using ordinary or blended cement; thus, ASTM C1012 was published.

Table 9 – Different standards, specifications, and building codes for concrete prone to sulfate attack

Standard	Class of Exposure	Category	Concentration of Sulfates as SO_4^{2-}		Max. w/cm	Min. strength (MPa)	Cementitious Material
			Dissolved in Water (ppm)	Water Soluble in Soil (% by mass)			
ACI 318 (2014)	S0	Negligible	< 150	<0.10	N/A	17	N/A
	S1	Moderate	≥ 150 and < 1500	≥ 0.10 and < 0.20	0.50	28	Type II or equivalent [§]
	S2	Severe	≥ 1500 and $\leq 10,000$	≥ 0.20 and ≤ 2.00	0.45	31	Type V or equivalent [§]
	S3	V. Severe	> 10,000	> 2.00	0.40	31	Type V plus pozzolan/slag cement
CSA A23.1 (2014)	S-1	V. Severe	> 10,000	>2.00	0.40	35 ^b	HS or HSb
	S-2	Severe	1500-10,000	0.60-2.00	0.45	32 ^b	HS
	S-3	Moderate	150-1500	0.20-0.60	0.50	30 ^b	MS, MSb
NBR 12655 (2015)	I	Low	0-150	<0.10	0.60	20	SR
	II	Moderate	150-1500	≥ 0.10 and < 0.20	0.50	35	SR
	III & IV	Severe & V. Severe	> 1500	≥ 0.20	0.45	40	SR
EN 206-1:2013	XA1	Mild	≥ 200 and ≤ 600	≥ 0.20 and ≤ 0.30	0.55	30	High SRPC CEM III/B
	XA2	Moderate	> 600 and ≤ 3000	≥ 0.30 and ≤ 1.20	0.5	30	High SRPC CEM III/B
	XA3	V. Severe	> 3000 and ≤ 6000	> 1.20 and ≤ 2.40	0.45	35	High SRPC CEM III/B
IS 456 (2000)	I	Mild	< 300	< 0.2	0.55	20	OPC or OPC/slag or OPC/pozzolan cement
	II	Moderate	300-1200	0.2-0.5	0.50	25	OPC or OPC/slag or OPC/pozzolan cement or SRPC
	III	Severe	1200-2500	0.5-1.0	0.45	30	OPC/slag or OPC/pozzolan or SRPC
	IV	V. Severe	2500-5000	1.0-2.0	0.45	35	SRPC
	V	Extreme	> 5000	> 2.0	0.40	40	SRPC
AS 3972	A2	Mild	<1000	<0.50	0.55	25	GP, GB
	B1	Moderate	1000-3000	0.50-1.0	0.55	32	GP, GB
	B2	Moderate	3000-10,000	1.0-2.0	0.50	40	SR
	C1 & C2	Severe & V. Severe	>10,000	>2.0	0.45	≥ 50	SR

*N/A: Not Applicable (no special requirement)

*MS: Moderate sulfate-resistant hydraulic cement (CSA A3001-03); former designation Type 20

*HSb: High sulfate-resistant blended hydraulic cement (CSA A3001-03); former designation Type 50

*a : SO_4^{2-} in mg/kg

*GB: General purpose blended cement

[§] For Class 1 exposure, equivalents are (ASTM C150 Type III, ASTM C595 Type IS(MS), Type IP(MS), Type IS-A(MS), or Type IP-A(MS); ASTM C1157 Type MS or any blend meeting requirements). For Class 2 exposure, equivalents are (ASTM C150 Type III or ASTM C1157 Type HS or any blend meeting requirements). For Class 3 exposure ASTM C150 Type V or ASTM C1157 Type HS with pozzolan, slag, or any other blend meeting requirements)

*b: Compressive strength at 56-day

*MSb: Moderate sulfate-resistant blended hydraulic cement (CSA A3001-03); former designation Type 20

*SRPC: Sulfate-resisting cement

*GP: General-purpose cement

*SR: Sulfate-resisting cement

ASTM C 1012 was established by the ASTM C01.29 sulfate resistance subcommittee based on an understanding of the ASTM C452 boundaries. The committee started the formulation of a new performance test that would apply to Portland cement in addition to Portland cement blends. As a result, the ASTM C1012 mortar bar test was established, standardized, and published in 1984. In this test, during the mixing process, the addition of sulfate to the mortar is prevented. However, after the mortar has reached a specific strength, mortar specimens are immersed in a high concentration of sodium sulfate solution (5.0% Na₂SO₄ at 23 °C). Then, the change in length (expansion) is measured. Given the high variation over many years, the subcommittee established a minimum strength requirement of 20 MPa before immersion, regardless of the cement material used, in addition to solution molarity of 0.352 Na₂SO₄.

To meet the ASTM C1012 test procedure, ACI 201.2R Guide to Durable Concrete has established four classes of sulfate exposure and their corresponding prescriptive measures. These limits are still used in North American specifications such as ACI 318 and CSA A23.1 for blended cement (ASTM C 595, C 1157, C 989, and C 1240 and CSA A3001). The expansion limits rely on the severity of desired exposure conditions. The test criterion requires a maximum expansion limit of 0.10% for 6 months of exposure to moderate sulfate (S1) environment while maximum limits of 0.05% and 0.10% for severe sulfate exposure environment (S2) at 6 and 12 months, respectively. For exposure to an extremely severe sulfate environment, the standard permits up to 0.10% expansion after 18 months of exposure. ASTM C 1012 has rapidly become the only critical performance test for cementitious systems and concretes exposed to sulfate-rich environments (Hooton and Day, 2000). It represented the field exposure conditions more closely than the ASTM C452, specifically when sulfates penetrate the mortar before hydration products react. However, the only disadvantage can be that the test is too slow to be accelerated, as it takes an average of 6 months before important test outcomes are achieved.

Other international standard codes are quite similar in their testing procedures and conditions; however, their evaluation techniques and failure criteria may differ (Bakharev et al., 2002; Pan et al., 2003; Mithun and Narasimhan, 2016). For example, CSA A 3004-C8 was adapted from ASTM C1012 to evaluate blended cement mortar bars' expansion due to external sulfate attack through two procedures. Procedure A is the same as in ASTM C1012, where mortar bars are exposed to 5% Na₂SO₄ solution at 23 °C, to determine the resistance to the ettringite form of sulfate attack. Procedure B is the same as Procedure A, but the storage conditions are different. In Procedure B, mortar bars are stored at 5 °C in the same sulfate solution to trace the potential of sulfate thaumasite attack, as outlined in the 13th edition of CSA A3004-C8. However, Procedure B was withdrawn in the 5th update of the 2013 version. As its findings in compliance with CSA protocol A3004-C8 have not contributed to the concrete resistance of sulfate. Furthermore, Procedure A expansion limits are appropriate for showing good concrete resistance to sulfate attack (CSA-Group, 2018).

CSA A3004-C8 also outlines the abridged prescriptive requirements for concretes under different exposure classes besides the limiting values such as the maximum w/cm ratio, minimum compressive strength, the age at test. It should be noted that, instead of the regular 28-day strength, the Canadian standard specified 56-day compressive strength for certain exposure groups due to the potential use of blends of Portland-cement (**Table 9**).

The Australian Standard AS 2350 was developed and derived from ASTM C1012 to determine the potential of different cement types in a rich-sulfate environment. Test results demonstrated that the ASTM mortar bars (25 x 25 x (285) or 160 mm) displayed minimal expansion relative to the German bars (10 x 40 x 160 mm) using different cement types. It also showed that after 16 weeks of immersion in a 5% Na₂SO₄ solution, it is possible to distinguish between the various cement types. Hence, it adopted and updated ASTM C452 and C1012 test methods to establish a more reliable and rapid test protocol. Based on these results, using the adjusted mortar bar (15 x 40 x 160 mm) that cured for 7 days is the most convenient and practical measure for sulfate attack specified in AS 2350. According to AS 3972, the maximum expansion criterion for sulfate-resistant cement (Type SR) should be below 900 µε at 16 weeks (0.09%). However, this criterion is not appropriate for different types of SR cement, whether Portland or blended cement.

EN 206-1 (BSI, 2013) identifies several sulfate exposure classes and specifies some concrete characteristics to be used accordingly (**Table 9**). However, in the European specifications, there is no equivalent standard to ASTM C1012 for determining the sulfate resistance of Portland or blended cement (EN 197-1, 2000). Therefore, an amendment to EN 197-1 (2000) was adopted in 2006 by proposing seven cement types, CEM I cement with (C₃A ≤ 5%), slag cement (CEM III B/C) and pozzolan cement (CEM IV A/B) with low (C₃A ≤ 9%) for concretes functioning in sulfate environments (Hooton, 2008). It should be noted that exposure classifications in EN 206-1 are considered for use in the South African National Standard SANS 10100-2 in a revised format to fit South Africa's conditions.

The Indian IS 456 (2000) code, first published in 1953 and entitled "Practice Code for Plain and Reinforced Concrete for General Construction," is considered as a convenient benchmark for durability-related parameters. In terms of sulfate attack, excessive amounts of water-soluble sulfate (SO₃) in most cement, and some aggregates may cause concrete to expand and deteriorate. Hence, the overall SO₃ quantity in concrete mixtures, as specified in IS 456, shall not exceed 4% by mass of cement. However, concrete mixtures containing IS 6909-compliant super-sulfated cement shall not apply the 4% limit. According to the sulfate concentration severity, three exposure conditions were qualitatively defined for external sulfate attack, such as mild, moderate, and severe. However, the 4th revision of IS 456 standard was adopted and developed to include detailed durability factors. Two environmental exposure conditions, i.e., very severe and extreme exposure conditions, have been added, as shown in **Table 9**. The guideline also includes recommendations for concrete mixtures prone to sulfate attacks, such as the type of cement used, the minimum cement content, and the maximum water/cement ratio.

Two Brazilian committees developed NBR 13583; CB/CE-18 to determine the dimensional variation of cement mortar bars exposed to sodium sulfate solution. The test method includes preparing mortar bars (25 x 25 x 285 mm) for length change measurements. This is followed by a curing procedure, 48-h (first stage) in a humid chamber, then 12 days (second stage) in a lime-saturated water solution before the exposure to sodium sulfate solution. After 14, 28, and 42 days, the mortar bars' resulting expansion should be determined. NBR 13583 is believed to be a comparative analysis standard since it does not specify the maximum expansion limit to which the composition may or may not be considered resistant to sulfate attack. On the other hand, the Technical Brazilian Standard Association, ABNT-NBR 12655 (2015), suggested four aggressive

exposure environments (**Table 9**) in addition to the minimum in-service concrete requirements to be met before sulfate exposure.

The Chinese GB 749 standard, adapted in 1954 from the H114-54 Soviet Union standard, measures concrete resistance to sulfate attacks from the relative flexural strength of mortar prisms. Strength tests are performed on mortar bars (10 mm square-section x 30 mm) that are immersed in a Na_2SO_4 solution or any field-like environment, in addition to mortar bars immersed in plain water for comparison. It should be noted that GB 749 is considered a simple evaluation criterion technique. One explanation can be that this approach does not reveal the concentration of sulfate solution. In other words, the effect of sulfate concentration, i.e., high and low (SO_4^{2-}) on the mechanism of attack is not taken into consideration (Li and Zhang, 2012).

Later, the GB 2420 test method was developed based on the GB 749 limitations, but a change in the prism length dimension of $10 \times 10 \times 60$ mm was made before the full immersion in a 3% Na_2SO_4 solution. The pH level of sulfate solutions should be maintained at 7.0 for exposure periods of 28 days and up to 6 months by titrating at 1N H_2SO_4 . Since GB 2420 is intended to be an accelerated test to investigate different cement types, the experiment should be performed concurrently with the GB 749 test to provide more reliable results. Mortar bars with a relative flexural strength of ≤ 0.80 at the age of 6 months are classified as low sulfate resistance. GB 2420 may eventually reflect the cement's ability to withstand gypsum crystallization, but this method does not reveal the potential to resist sulfate completely.

The evaluation of sulfate attacks in Germany follows the old German method, DIN 1164:1958, derived from the Wittekindt method. The method involves the exposure of 10 mm x 40 mm x 160 mm cement mortar prisms, with defined masses of cement, fine and coarse sand plus w/c ratio, to a high concentration of Na_2SO_4 solution renewed monthly. The concentrated solution used in the original Wittekindt method was 0.15 mole Na_2SO_4 or 14,400 mg/l SO_4^{2-} (Locher, 2013). The SO_4^{2-} concentration is 2.4 times higher than the upper limits of the XA3 exposure class to chemical attack, which is by far the most aggressive class than those set by current European standards (EN 206-1:2013). It is worth noting that these limitations are proposed for aqueous solutions only and not for soils without freeze-thaw scenarios. On the other hand, the renewal of solutions to preserve the concentration of SO_4^{2-} ; to allow the attack to continue is another crucial issue mentioned in the Wittekindt method. This can be because, in reality, the origin of SO_4^{2-} is continuously renewed, depending on the fresh supply of sulfate ions at either a lower or higher rate.

In conclusion, sulfate attack is a well-known problem leading to concrete structures deterioration. However, much of the current debate revolves around the lack of consensus on the variables governing the attack mechanisms in international standards and specifications. These include, as illustrated in the previous sections, the concentration of solutions, test conditions, sample size, testing periods, insensitivity of the measurement tools to the progression of sulfate attack, and unpredictable relationship to field degradation mechanisms (Clifton et al., 1999). This also led to an inconclusive debate on whether the current standards and specifications can cope with the variation in the new commercially available binders. In general, blended cement types were found inefficient as their performance depends on the physical and chemical characteristics of source materials, the type of Portland cement used in the blend, and the dosage. On the other hand, the severity of the sulfate attack can be limited to some extent by a combination of compositional

control and permeability control. According to Mehta (1992), for the development of sulfate-resistant concrete, monitoring the permeability (w/cm) is considerably more important than controlling the chemistry of cementitious binders. The findings of the Hearn and Young (1999) investigation support the claim that achieving good resistance to sulfate attacks with different cations is linked to the use of low w/cm (< 0.40). It has to be noted that the role of w/cm was addressed in all of the specifications and building codes listed in Table 9, where all specifications endorse the use of a low w/cm value (< 0.45) for severe attack conditions.

Research worldwide focuses on the use of other robust, sustainable, and greener binders, promoting higher durability capacity for structures vulnerable to aggressive environments. Among those binders, AAMs system is a promising alternative for OPC. However, due to their different reaction properties and microstructures relative to OPC, the attack mechanisms and evaluation techniques should differ. Existing standards and test methods were questioned for their authenticity and reliability relevant to alkali-activated concrete resistance to sulfate attack.

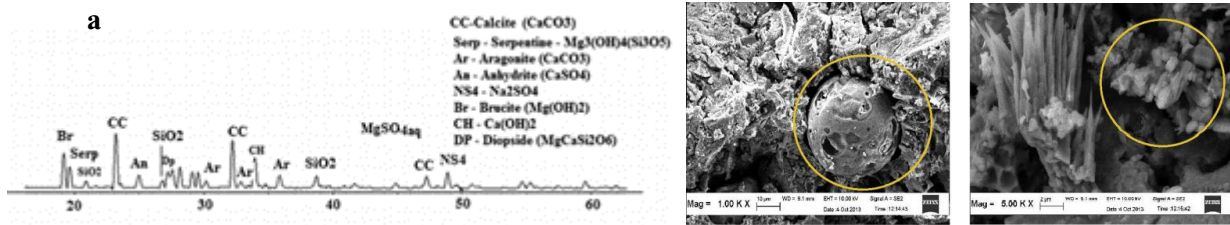


Fig. 16 – SEM micrographs and XRD pattern of mortar with 20% slag exposed to a) Na_2SO_4 [Adapted from Yusuf (2015)]

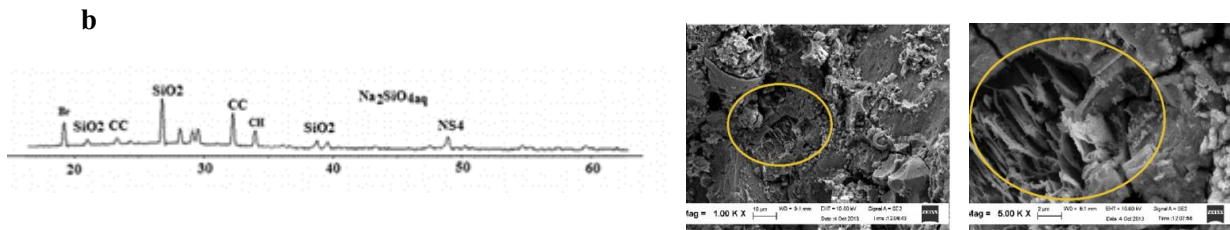


Fig. 17 – SEM micrographs and XRD pattern of mortar with 20% slag exposed to b) MgSO_4 [Adapted from Yusuf (2015)]

The exposure to Na_2SO_4 appear to be favorable for AAMs structural evolution and system densification, which corresponds to Na_2SO_4 's defined function as an activator (Shi et al., 2006). Under existing test protocols, exposure of AAMs to Na_2SO_4 solutions generally do not promote material expansion or cracking, as the former deterioration mechanisms are linked to the formation of secondary ettringite and gypsum products. On the other hand, leaching of Ca^{2+} , Na^+ , and Mg^{2+} from active minerals was reported to instigate the disintegration of microstructural frameworks (Yusuf, 2015; Salami et al., 2017; Aragón et al., 2020), as shown in Fig. 16 and Fig. 17. In contrast, MgSO_4 attack can lead to decalcification of C – A – S – H gels, in addition to gypsum and MgOH_2 formation (Yusuf, 2015; Aragón et al., 2020).

3.6. Type and Concentration of Sulfate

Since ASTM standards have been proposed as methods for investigating the sulfate resistance of cement-based materials, their reliabilities were questioned and criticized for a long time. ASTM C1012, for example, is widely believed to overlook important field performance parameters for concrete structures exposed to sulfate attacks (Skalny and Pierce, 1999; Hooton and Day, 2000; Hooton, 2008; Bassuoni and Nehdi, 2009). A closer look at the standard reveals that the sulfate attack mechanisms are pertinent to the composition of sulfate solution but more to the SO_4^{2-} ion. Thus, ASTM C 1012 does not cover solutions other than Na_2SO_4 ; also, it marginalizes other sulfate solutions such as MgSO_4 that are available for simulating environmental exposure conditions in the field. However, the mechanism of attack and the manifestation of damage varies depending on the cation that accompanies sulfate ions, such as Ca^{2+} , Na^+ , Mg^{2+} , and Fe^{3+} . For example, Na_2SO_4 solution attacks tricalcium aluminum (C_3A) and calcium hydroxide ($\text{C} - \text{H}$) and forms ettringite and gypsum reaction products that result in severe cracking due to expansive stresses generated. On the other hand, all cement reaction products, even $\text{C} - \text{S} - \text{H}$, are attacked when the attacking solution is MgSO_4 . To the best of found knowledge, the maximum expansion of Portland cement mortar was reported after the exposure to MgSO_4 (Xu et al., 1998). In such circumstances, a dense brucite layer forming on the surface makes the surface degradation imperceptible until the late period of attack, while a decrease in strength starts very early.

Sulfate Resisting Portland Cement (SRPC) is a blended cement designed to promote the quality of concrete that is vulnerable to sulfate attacks. However, the SRPC did little to combat the attack against MgSO_4 . For instance, replacing cement with 70% of blast-furnace slag mortar did not last long in the MgSO_4 solution, and similarly, the partial replacement with silica fume (SF) was found to be detrimental (Frearson and Higgins, 1995; Yeginobali and Dilek, 1995). Concretes containing supplementary cementitious materials (SCM) such as SF are beneficial in their resistance to Na_2SO_4 only but are particularly susceptible to MgSO_4 attacks (Locher, 1966; Bonen, 1993). As a case on point, Giergiczny (1997) reported a significant decrease in strength and a substantial amount of gypsum in mortars with 10% SF after a year of exposure to 0.123 mole/L MgSO_4 solution. This significantly confirms that the $\text{C} - \text{S} - \text{H}$ decalcification and brucite growth ($\text{Mg}(\text{OH})_2$) are critical degradation processes during the MgSO_4 attack. The use of Na_2SO_4 and MgSO_4 sulfate solutions are widespread, as these salts can produce a high SO_4^{2-} environment due to their high solubilities. Prior research has suggested using solutions containing both sulfate types in equimolar quantities or in proportions that simulate the field condition (Mehta et al., 1979; Mehta, 1992; Bonen, 1997). When MgSO_4 is used in a procedure similar to ASTM C1012, it should be noted that vigorous stirring of the solutions is often necessary to prevent the growth of brucite, which slows down the rate of damage (Hooton and Day, 2000).

On the other hand, ammonium sulfate has been used occasionally in some studies. However, this salt has been shown to damage concrete more than Na_2SO_4 (Eglinton, 1998). In particular, cement containing SF performed worse than cement with low- C_3A in ammonium sulfate solutions (Bate, 1984). As different sulfate solutions cause divergent types of damage, a proper parameter must be used to define the damage. For instance, expansion indicates a stronger Na_2SO_4 attack, while strength loss is a more suitable predictor of the MgSO_4 attack to cement-based materials. Therefore, using one single parameter such as expansion may not be sufficient to define damage

(Santhanam et al., 2002; Beltrame et al., 2020). The ASTM C 1012 standard does not cover those measures.

There is a consensus that the test method ASTM C 1012 accelerates the attacking mechanism for submerged samples in a high concentration of sulfate solution. The most frequently used solution concentration is 5% Na_2SO_4 (0.35 mole/L) and 5% MgSO_4 (0.41 mole/L). It should be noted that the maximum concentration of sulfate dissolved in water is $\geq 1\%$ among all standards, while water-soluble in the soil is $\geq 2\%$. To conduct an accelerated test, the use of "natural" concentration values of sulfate ions in the solution appears not acceptable. Therefore, higher concentrations of sulfate in solutions would enable the attack to develop faster (Costa et al., 2018). Only a few research works in literature illustrate the use of a very high concentration sulfate solution, i.e., 10% Na_2SO_4 . The two main arguments put forward are that the deterioration mechanism may be quite different from the chemical attack to be simulated due to the high sulfate concentration that may be close to or above the solubility level. For example, Yu et al. (2013) measured the sulfate profile of immersed mortar samples in Na_2SO_4 solutions. The authors observed that the sulfate penetration depth is independent of the sulfate concentration and sample size. Highly concentrated sulfate solutions, however, would promote gypsum formation (Bellmann et al., 2006; Lothenbach et al., 2010). However, 10% of MgSO_4 solutions are used for accelerated experiments (Hooton and Wafa, 1994) without any signs of salt crystallization.

Since, in most cases, AAMs do not contain portlandite but mostly C – S – H, and because of aluminum's vital presence in C – A – S – H and hydrotalcite gels, this form of binding material could be highly resistant to sulfate attack (Komljenović et al., 2013; Rodríguez et al., 2008; Heikal et al., 2014). Therefore, to predict its performance in rich sulfate environments, the synergistic effect of different sulfate concentrations and types should be considered to simulate field conditions. **Table 10** summarizes the resistance of AAMs to external sulfate attacks, reviewed in previous studies.

Alkali-activated concretes, in particular, high-calcium precursors, are affected by the type of cation Na or Mg in sulfate solutions. Komljenović et al. (2013) investigated the resistance of alkali-activated slag (AAS) mortars to immersion in a 5% Na_2SO_4 solution. It was reported that after 90 days of immersion, AAS mortars showed no mass loss and an 11% increase in strength. This could be due to the continuous formation of AAS reaction products due to the sulfate medium's high alkalinity. These results are in agreement with Bakharev et al. (2002), where AAS mixtures exposed to 5% Na_2SO_4 showed more resistance than to 5% MgSO_4 solutions after 365 days (**Table 10**), which was also observed by Beltrame et al. (2020). The author attributed the strength loss of AAS in MgSO_4 solution to the absence of portlandite $\text{Ca}(\text{OH})_2$ that allows the formation of a protective brucite $\text{Mg}(\text{OH})_2$ layer. This promoted the direct attack of Mg ions on the C – S – H structure besides the formation of M – S – H and gypsum expansive products.

Yusuf (2015) and Salami et al. (2017) investigated the resistance of AAS-ultrafine palm oil fuel ash (POFA) mortars to 5% Na_2SO_4 and 5% MgSO_4 solutions. In Yusuf (2015), the inclusion of slag up to 20% in mortars has contributed to better sulfate resistance. The variation in the $\text{Na}_2\text{SiO}_3/\text{NaOH}$ ratio has resulted in a negligible strength retention difference. The residual strengths for the slag free mortars were 16.5% (in Na_2SO_4) and 76.8% (in MgSO_4) after 6-months, respectively. The investigation attributed the severe deterioration of mortars exposed to 5%

Na₂SO₄ solution to the leaching of active minerals (Ca²⁺, Mg²⁺, Na⁺) instigating the disintegration of the microstructural framework. However, better strength retention was observed in MgSO₄ solution owing to the formation of surficial white deposits and crystallized anhydrite (CaSO₄). Similar results were obtained by Salami et al. (2017) in terms of the resistance to sulfate attack. The exposure to 5% Na₂SO₄ and 5% MgSO₄ solutions for 9 months confirmed that the deterioration of mortars depends on the type of cations carried by sulfate solutions. Mithun and Narasimhan (2016) have studied the resistance of AAS concrete using copper slag (CS) as an alternative to natural river sand with up to 100% by volume. It was concluded that the replacement of CS by natural sand had reinforced the produced alkali-activated mixtures. After 12 months of exposure to 10% Na₂SO₄ solutions, no strength deterioration was observed in AAS with CS. Contrary, in 10% MgSO₄ solutions, mixtures suffered from a higher rate of degradation due to the constant attack of Mg ions to the C – S – H structure, forming M – S – H and gypsum.

Table 10 – Summary of AAMs resistance to external sulfate attacks reviewed in studies

Reference	Precursor	Activator	Sulfates	Ageing Protocol		
				Corrosion Period	Corrosion Products	Deteriorating Environment
Bakharev et al. (2002)	Slag	NaOH + Na ₂ SiO ₃	5%Na ₂ SO ₄ 5%MgSO ₄	12-month	Gypsum	5%MgSO ₄
Bakharev et al. (2005)	FA	NaOH NaOH+K OH	5%Na ₂ SO ₄ 5%MgSO ₄ 5%(Na ₂ SO ₄ + MgSO ₄)	5-month	Precipitates	5%Na ₂ SO ₄ 5%MgSO ₄
Thokchom et al. (2010)	FA	NaOH + Na ₂ SiO ₃	10%MgSO ₄	24-week	Anhydrite, ettringite	10% MgSO ₄
Komljenović et al. (2013)	Slag	NaOH + Na ₂ SiO ₃	5%Na ₂ SO ₄	3-month	Gypsum, Ettringite	5%Na ₂ SO ₄
Yusuf et al. (2015)	Slag+POF A	NaOH + Na ₂ SiO ₃	5%Na ₂ SO ₄ 5%MgSO ₄	6-month	Anhydrite, Brucite, Serpentine	5%Na ₂ SO ₄
Mithun et al. (2016)	Slag	NaOH + Na ₂ SiO ₃	10%Na ₂ SO ₄ 10%MgSO ₄	12-month	Gypsum, M-S-H	10%MgSO ₄
Aragón et al. (2020)	Slag+NVP	NaOH + Na ₂ SiO ₃	5%Na ₂ SO ₄ 5%MgSO ₄	730-day	Gypsum, Brucite	5%MgSO ₄

*POFA: Palm Oil Fuel Ash

*Brucite: Mg(OH)₂

*Gypsum: CaSO₄ 2H₂O

*Anhydrite: CaSO₄

*Serpentine: Mg₃Si₂O₇(OH)₂ · 3H₂O

*NVP: Natural Volcanic Pozzolan

3.7. Specimens' Composition, Shape, and Size

The primary assessment for the sulfate attack test is the length change of the mortar prisms, although the size of prisms differs. ASTM C 1012 and most other standards specified the composition of mortar prisms, i.e., sand to cement ratio of 2.75:1 and w/c of 0.485. Higher w/cm ratios of ≥ 0.50 and the higher sand-to-cement ratio of 3 or 4 were also used in other experiments. However, the higher w/cm used in specimens contributes to greater total porosity and permeability, promoting the ingress of sulfate and quick deterioration. The cement-rich samples showed better workability, higher expansion, and higher capillary pores content per unit volume of mortar at a

constant w/cm ratio. However, paste or mortar prisms would affect the process of deterioration by eliminating the physical effect of the inferential-transition zone (ITZ) between the hydrated cement paste and aggregates (Skalny and Pierce, 1999; Cohen and Mather 1991; Hooton and Day, 2000). The presence of ITZ may have an impact on the resistance of concrete mixtures to sulfate attack as it is richer in C-H and characterized by its higher porosity.

Various studies have demonstrated the significant effect of samples' composition, geometry, and scale on the concrete resistance to sulfate attack. According to the assessment's main objective, samples' geometry and composition might vary beside the acceleration needed for the test. Various research methods, such as lean mortar bar tests with different cross-sectional sizes, have been commonly used. Indeed, inconsistencies are associated with the samples' structure in the wide-ranging test protocols and international standards (**Table 11**). For example, the cross-section of specimens in various codes ranges from 25 x 25 mm in ASTM methods to 10 x 10 mm in GB methods, 15 x 40 mm in AS methods, and 10 x 40 mm in DIN 1164 (German-Wittekindt flat prism technique). These inconsistencies have affected the proper simulation of field-like conditions. **Table 9** and **Table 11** provide a summary of the main test methods, along with their requirements.

Table 11 – Different performance requirements for concrete susceptible to sulfate attack

Standard	Class of Exposure	Performance requirements – Maximum expansion (%)						Sample size
		At 14 days	At 112 days	At 3 months	At 6 months	At 12 months	At 18 months	
ACI 318 (2014)	S-0				---	---	---	25 × 25 × 285
	S-1				0.10	---	---	
	S-2	---	---	---	0.05	0.10	---	
	S-3				---	---	0.10	
ASTM C452	---	0.04	---	---	---	---	---	25 × 25 × (285) or 160
ASTM C1038	---	0.04	---	---	---	---	---	25 × 25 × 285
ASTM C1012	---	---	---	---	0.05	0.1	---	25 × 25 × 285
AS 2350-14	---	---	0.09	---	---	---	---	15 × 40 × 160
CSA A3004-C8	S-1				0.05	0.10	0.10 [§]	25 x 25 x 285
	S-2	---	---	---	0.05	0.10	0.10 [§]	
	S-3				0.10	0.10	0.10 [§]	
DIN 1164:1985	---	---	---	≤ 0.50 ^a	---	---	---	10 × 40 × 160
GB 2420 & 749	---	---	---	---	≤ 0.08 ^{**}	---	---	10 × 10 × 60
IS 12330-1988	---	≤ 0.045	---	---	---	---	---	25 × 25 × 250
NBR 13583	---	---	---	---	---	---	---	25 × 25 × 285

^{*} For high sulfate resistance (HSRPC) cement type

^{**} Relative flexural strength

^a Expansion difference ($\Delta\epsilon$)

[§] Maximum expansion when tested using CSA A3004-C8 Procedure B at 5°C, %

Unlike square-section prisms (i.e., 10 x 10 mm or 25 x 25 mm), flat-section mortars of 10 x40 mm or 15 x 40 mm have shown earlier and higher expansion values than their counterparts. Recent research appears to validate the view that when the size of mortar prisms increased, expansion began to be delayed (Yu et al., 2013; Planel et al., 2006; Ferraris et al., 2005). Yu et al., for example, pointed out in 2013 the occurrence of expansive forces when sulfates penetrate the mixtures, which are hindered by the core. The use of flat prisms would, therefore, help to overcome the constraining effect of the core. In which sulfate components can penetrate the inside of the

specimen in less time and produce more consistent outcomes. However, the reported expansion values would be much lower with thicker specimens. Also, the attack would disintegrate the surface of the specimen due to opposed expansion between layers. Concerning the behavior of AAMs in the sulfate environment, Beltrame et al. (2020) suggested that the use of 10 x 60 mm prismatic paste samples increased the expansion rate.

3.8. PH of the Solution

The average pH of 1.8 million soil samples collected from different locations in North America was ≤ 6.0 (Fixen, 2002), while the average pH of seawater was around 8.0 (Skalny et al., 2002). Some sulfate attack experimental systems allow for pH monitoring to better simulate conditions in the field, i.e., groundwater or seawater, besides accelerating the test procedure. (Wang, 1994). For example, by constant sulfuric acid titration (H_2SO_4), Mehta (1975) suggested a preliminary immersion test with a low Na_2SO_4 solution pH value of 6.2. Brown (1981) followed the same method and found that monitoring the pH has significantly accelerated the rate of sulfate attack by increasing the consumption of sulfate ions simultaneously as the leaching of hydration products. This accelerated the onset of mortar expansion due to the formation of ettringite products. Cao et al. (1997), on the other hand, demonstrated that lowering the pH of sulfate solutions ($pH \approx 3$) had a significant impact on the resistance of FA (class F) + silica fume and slag blended systems due to C – S – H decalcification. Fernandez-Altable (2009) and Chabreliie (2010) noted that maintaining a constant pH of sulfate solutions had delayed the expansion and prevented leaching. The pH of the initial Na_2SO_4 bathing solution in the ASTM C 1012 ranges between (6.0-8.0). Whereas after immersion of specimens, the pH value increases gradually to ≥ 12.0 due to the leaching of alkalis from concrete to the surrounding solution. It should be noted that the pH of the sulfate solution is not controlled in the commonly used standard. Therefore, the used ASTM standard is not a fully valid indication of the field condition, and if used to predict field performance, discrepancies may arise.

Varying performance is reported for AAMs, ranging from superior to weak when exposed to aggressive sulfate environments. This can be due to the wide-ranging mixture formulation starting from the precursor and activator selection to the dosage used and the curing condition ending with the test protocol used. In general, using an appropriate high alkaline activator in AAMs would increase the system's pH and protect it from sulfate attacks. Also, the use of carbonate anion, for example, accompanying the activator, may decrease the risk for decalcification, thereby increasing the solubilization of silica and alumina (Abora et al., 2014). Questioning the binder's composition and the microstructure of AAC would indeed detect its deterioration mechanism in terms of the total matrix porosity and alkali leaching to the sulfate solution (Van Eijk and Brouwers, 1998). Therefore, monitoring the pH of the sulfate solution and conducting leaching tests would help track the amount of leachable elements and increase these materials' credibility.

3.9. Single Damage-Factor Tests

Different test methods are used to study the external sulfate attack mechanisms and effects, such as ASTM C1012 "Standard Test Method for Length Change of Hydraulic-Cement Mortars Exposed to a Sulfate Solution." This international ASTM C1012 test procedure has frequently been used but criticized due to its limitation (orientation-expansion effect). In 1997, Taylor pointed

to the fact that laboratory studies focus on expansion and specimen cracking, but experiences in the field indicate a higher loss of adhesion and strength as a predominant sign of deterioration. Moreover, most of the existing standardized durability testing methods have mainly been developed to test Portland cement systems' long-term durability performance. On the other hand, the use of a single damaging technique, as seen in ASTM C1012, would affect the general understanding of attack mechanisms. This is very important as the transport mechanism in partially exposed concrete structures does not appear to cause the same distress as in entirely exposed concrete components. Diffusion (as an exposure method addressed in ASTM C1012) is the primary transport mechanism that causes a higher deterioration rate under saturated conditions. Diffusion is also known to be slower than other mechanisms, as an aqueous ionic transport mechanism, and is not apparent until a thermal or concentration gradient is generated. Therefore, the "sulfate-related deterioration rate defies the expectations of the relevant models," as stated by Santhanam et al. (2002).

The lower portion may be saturated with seawater or groundwater in partially exposed sulfate structures, while the upper portion remains at ambient temperature and humidity conditions. The deterioration usually happens when the sulfates are drawn into the concrete, permeated upwards, and then evaporated upon reaching the surface (wicking action). As a result, various types of degradation, i.e., leaching, microcracking, paste and permeability characteristics alteration, efflorescence, and surface scaling, may present. The degradation can be accelerated through the transfer of larger amounts of sulfates throughout the matrix. For example, Boyd and Mindess (2004) have partially exposed concrete cylinders to a 5% Na₂SO₄ solution. The authors concluded that while scaling implies significant damage, the internal damage caused by sulfate attacks may be considerably more severe. To date, this physical form of sulfate attack is not evident when testing a fully saturated specimen, the standard method of exposure. In addition, there is no standard test available for the partially immersed concrete in sulfate solutions. The absence of standardized testing and evaluation criteria for AAMs represents one of the main barriers facing its spread as no reliable long-term durability data are available. Similar to OPC, the intake of sulfate is much slower if it depends on pure diffusion only, but the use of consecutive damaging mechanisms, such as loading/unloading, wetting/drying, and freeze/thaw cycles, allows for the uptake of more aggressive substances that accelerate the rate of deterioration. Thus, integrated testing methods are essential to predict AAM's different damage mechanisms better while being exposed to sulfate attacks.

3.10. Multiple Damage-Factor Tests

Field concrete undergoes wetting and drying cycles due to fluctuations in water levels caused by flooding, rainwater runoff, tides, and the cyclic migration of sulfate-containing groundwater through capillarity into the above-ground portion of structures. Such activities induce sulfate salts' crystallization under the concrete surface layer leading to cracking, scaling, and delamination. These complicated deterioration mechanisms cannot be predicted or captured by the current testing approaches (i.e., continuous immersion exposure). Besides, standard immersion tests have frequently presented different performances relative to the observed ones in real-field cases (Mittermayr et al., 2013). This might be due to the techniques applied and indoor test procedures in current standard tests such as ASTM C1012 that overlook the critical field conditions. Therefore,

a mandatory shift to performance-based specifications for concretes demands elaborating a performance-based evaluation policy that better depicts field conditions.

The question of whether wetting-drying cycles and the underlying mechanisms of this form of damage are physical or chemical is still controversial among researchers. For example, Kalousek et al. (1972) have investigated the length change of concrete cylinders exposed to Na_2SO_4 solutions by 2.1% in a 20-year long-term research program. Specimens were subjected to wetting-drying cycles to accelerate the test. The specimens were immersed in sulfate solutions for 16h at room temperature in each cycle, then air-dried for 8h at 54 °C. After one year in wetting-drying exposures, it was found that eight years of continuous immersion exposure caused comparable damage to concrete specimens under wetting-drying. On the other hand, de Almeida (1991) proposed immersing samples in 16% Na_2SO_4 solutions for 2h (wetting) followed by drying at 105°C for 10 to 15h. It was concluded that specimens failed under physical rather than chemical action. Nehdi and Hayek (2005) carried out a study in which mortar cylinders were partially immersed in 10% sodium and 10% magnesium sulfate solutions and exposed to 32-95% constant or cyclic relative humidity (RH) for up to 151h. In their extensive study, they found a thick efflorescence layer on the surface of partially immersed specimens in 10% Na_2SO_4 solution only, particularly with cyclic RH. The study of Sahmaran et al. (2007) reported the resistance of mortar samples to a 5% sulfate solution accompanied by wetting-drying cycles. Each cycle consisted of the exposure at room temperature for 6 days, followed by drying for 1 day at 100°C. The wetting-drying exposure was observed to be more aggressive than continuous immersion exposure and has contributed to the complete disintegration of the samples within 17 weeks due to repeated hydration and evaporation of sulfate salts. Similarly, Haynes et al. (2008) conducted an experiment on partially immersed concrete cylinders in (5% Na_2SO_4) and exposed to various temperatures and RH. It was concluded that samples disintegrated after the exposure to cycles between 20°C with 82% RH and 40°C with 31% RH in two-week intervals. On the other hand, Loser and Leemann (2015) introduced a new accelerated sulfate resistance test to Swiss norms. Four cycles of drying and immersion were applied to concrete mixtures throughout different protocols in an oven at 50 or 40°C. To increase expansion during further immersion, the change from drying for 2 days and immersion for 5 days (Protocol 1) to 5 days drying and 2 days immersion (Protocol 2) was applied. The Na_2SO_4 concentration has to be doubled (protocol 3) and the MgSO_4 is used instead of Na_2SO_4 in protocol 4. Using a mixed solution of $\text{Na}_2\text{SO}_4 + \text{MgSO}_4$ (protocol 5). In protocols 6 and 7, drying was extended to 12 days at 50°C and 40°C, respectively. It was concluded that the use of Protocol 2 should lead to higher ingress of sulfate in addition to the prolongation of the drying step up to 12 days. However, the use of protocols 3, 4, and 5 did not increase specimen expansion.

More research is still needed on sulfate attack assessments, including wetting-drying cycles. A number of researchers (Puertas et al., 2003; Slavik et al., 2008; Zhang et al., 2010) reported that wetting and drying cycles had no significant adverse impact on AAMs' performance. Some micro-cracks have been introduced due to changes in temperature and/or humidity conditions (Puertas et al., 2003; Häkkinen, 1993). However, several questions remain unanswered at present, such as the real mechanisms of deterioration after these cycles (e.g., the dry/wet cycles, acceleration of mass transport or leaching of calcium and alkalis), the degree and time of drying that can simulate the real field conditions. Variations in these parameters remain a challenging task for researchers and standardization agencies. Furthermore, similar to partial immersion exposure tests, there is no

standard test available for concrete exposed to drying and wetting cycles. The performance of alkali-activated concrete in various exposure environments simulating field-like conditions needs to be addressed. This procedure would provide an adequate understanding of the mechanisms of deterioration of AAMs in the evaporation zones, resembling partially buried concrete elements, to develop reliable data on their durability.

3.11. Concluding Remarks and Recommendations

This chapter presents a critical review of the compatibility of current OPC-related aging protocols with AAMs' resistance to external sulfate attacks. The following conclusions can be drawn based on the results and discussion:

1. The resistance of AAMs using a high volume of waste materials that have been alkaline activated using a wide range of activators requires a high level of effort to be spent on the relevant standards for recognizing decay and deterioration mechanisms binders. Further validation is needed in laboratory and field studies to determine the concrete mixtures' overall permeability to control AAMs' transport properties.
2. Sulfate attack tests for assessing AAMs' sulfate resistance are based on test methods for conventional OPC concrete mixtures, despite their different reactions' mechanisms and microstructures. Therefore, selecting the correct test conditions and techniques would allow the accurate assessment of AAMs' performance under different aggressive conditions and the generation of service life models to help understand AAM's resistance to specific decay processes.
3. Particular attention should be paid to cation accompanying salt and its concentration in sulfate-rich environments while analyzing AAMs structures' resistance. This would alter AAMs' deterioration mechanism, leading to the decay of these binders when exposed to aggressive environments.
4. Monitoring mechanisms for mass loss, strength loss, leaching of active minerals, and matrix cracking due to chemical attacks are recommended to help determine the degradation mechanisms of AAMs exposed to external sulfate attacks.
5. Developing holistic assessment techniques to detect sulfate attacks' synergistic effects, single to multiple damage mechanisms, under accelerated real-field conditions to determine potential durability is needed.

Chapter 4 : Defining Mix Design Parameters for the Production of One-Part Alkali-Activated Self-Consolidating Concrete

4.1. Overview

The successful development of SCC mainly depends on its high flowability without the tendency for segregation. A common practice that promoted the development of SCC includes incorporating high powder content, less water to powder ratio, and new generations of efficient admixtures (Shi et al., 2015). However, cement is continuing to be an essential ingredient to make concrete, although too many environmental problems are associated with the process of its production (Mehta, 1999). Hence, the shift to utilize entirely greener material that completely replaces cement in concrete, i.e., alkali-activated materials (AAM), would directly contribute to positive environmental impacts. Up to the present time, Alkali Activated SCC (AASCC) was not widely investigated as ordinary SCC owing to the limited data on its rheological, mechanical, and durability performance under high alkaline environments.

Many studies have highlighted the importance of developing “just add water” AAMs using GGBFS, mainly with low CO₂ emissions. However, little research has been reported on the effectiveness of grinding GGBFS together with an alkali activator (Wang et al., 1994). For example, Pu et al., 1988 demonstrated that grinding Na₂CO₃ with slag produces the highest strength. Yang and Song (2009) demonstrated that increasing the fineness of GGBFS material resulted in a higher compressive strength value. Therefore, in this chapter, the results for mechanochemical activation of GGBFS with a dry-powder activator are discussed through the results of the fresh and hardened properties of alkali-activated self-compacted mortar mixtures under ambient curing conditions.

4.2. Research Significance

The literature has demonstrated the need for a basic understanding of the ideal technique to enhance the reactivity of the precursor materials without affecting the production of a highly flowable mortar mixture. Thus, the collective effects of milling (mechanochemical activation), the replacement of multi-activator materials with GGBFS, or their addition to binder systems were the focus of this chapter in the production of eco-SCC mortar mixtures.

4.3. Experimental Investigation

The chapter consisted of two experimental phases. Phase one: AASCM mixtures were evaluated while replacing slag with multi-activator materials to determine its effect on the fresh and mechanical properties. Phase two: evaluate the performance of fresh and hardened mortar mixtures incorporating the multi-activator materials as an addition to the total binder system.

4.3.1. Phase One: Dry-Powder Activators as a Replacement

In this phase, AASCM mixtures were tested for fresh and mechanical properties using the collective activation process by milling and multi-activator materials. Two dry-powder activator types, namely sodium metasilicate ($\text{MetaNa}_2\text{SiO}_3$) and sodium carbonate (Na_2CO_3), were used to activate single, binary, and ternary binder combinations. GGBFS was replaced with the two dry-powder activators with up to 25% by weight. The mini-slump flow test was used to determine the flowability of the produced AASCM mixtures. While, isothermal calorimetric analysis was used to determine the heat flow. The compressive strength development for all developed AASCM mixtures was evaluated as per the ASTM C109.

4.3.2. Phase Two: Dry-Powder Activators as an Addition

This phase focused on using the two dry-powder activators as an addition to the total binder content (16%, 20%, and 25% by mass) in various AASCM mixtures. Three AASCM mixtures were investigated with a different binder precursor system and content (single, binary, and ternary). The effect of dry-powder addition on mortar mixtures was evaluated through performing several tests that determined the fresh and hardened properties. Fresh mortar was evaluated by measuring the mini-slump flow as per the EFNARC specification. Also, the isothermal calorimetric analysis was evaluated by measuring the heat of hydration for 72h. Hardened concrete in terms of compressive strength development was measured with age at 7 and 28 days. Three cube specimens with dimensions 50 mm were tested at each age. A scanning electron microscope (SEM) equipped with energy dispersive spectroscopy (EDS) was used to determine the morphology and main mixtures composition of the mortar mixtures in addition to the differential scanning calorimetry (DSC) tests.

Initially, the activators and binders were mixed for approximately 30s before adding the fine aggregates. All solid materials (i.e., binder, activator, and sand) were mixed for an additional 1 min. Then, water was added to the mixture, and all the ingredients were mixed for around 2 min until having a homogenous mixture.

4.3.3. Materials Characterization

Ground granulated blast furnace slag (GGBFS), fly ash (Class F), and silica fume (SF) with different weight percentages were used to produce the AASCM precursor blends. **Table 12** shows the chemical and physical properties of all used precursors. The frequently used moduli in determining GGBFS's reactivity is related to its main oxides. Hence, it was considered high reactivity modulus according to Germany's (≥ 1.0) and Japanese standards (≥ 1.4). The XRD patterns for the unreacted three precursor materials are shown in **Fig. 18**. It can be seen that slag is mainly amorphous, without significant crystalline phases, and shows a peak hump between 2θ of 25° and 35° (**Fig. 18a**). The ultra-fine SF shows an amorphous state pattern as well (**Fig. 18b**). The unreacted FA includes crystalline phases such as quartz (SiO_2), mullite ($\text{Al}_6\text{Si}_2\text{O}_{13}$), and anorthic (CaSi_2O_5) with a broad, amorphous hump; between 2θ of 15° and 35° (**Fig. 18c**).

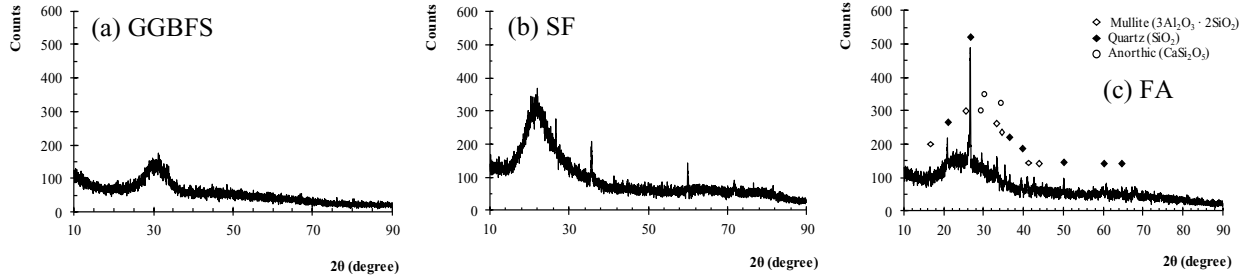


Fig. 18 – XRD patterns of source materials (a) GGBFS (b) SF, and (c) FA

Table 12 – Physical and chemical compositions of source materials

Oxide (%)	GGBFS	FA	SF
SiO ₂	36.5	48.9	94.0
CaO	37.6	3.8	0.4
Al ₂ O ₃	10.2	23.3	0.1
Fe ₂ O ₃	0.5	14.9	0.1
MgO	11.8	0.7	0.4
K ₂ O	0.4	1.7	0.9
SO ₃	3.1	0.2	1.3
Na ₂ O	0.8	0.6	0.1
TiO ₂	1.0	—*	0.3

* not measured items.

For all AASCM mixtures, a combination of two dry-powder activators (**Fig. 19**) was used to activate the precursors, namely, anhydrous sodium metasilicate (Na₂SiO₃) and Sodium carbonate (Na₂CO₃). The PQ Corporation's MetaNa₂SiO₃ (CAS 6834-92-0) with 50.5% Na₂O:46.2% SiO₂ and a density of 1.09 g/cm³ was used. Also, Fisher Chemicals Na₂CO₃ powder (CAS 497-19-8) with ≥ 99.5% purity and a density of 2.53 g/cm³. Natural siliceous sand with a fineness modulus of 2.5, a specific gravity value of 2.68, and water absorption of 1.5% was used. In phase one, GGBFS and Na₂CO₃ dry-powder activator material were milled for 3.5 to 4-hr. The specific surface area of the non-ground mixture and ground mixture was 515 m²/kg and 550 m²/kg, respectively. Also, boric acid with ≥ 99.5% purity level was used as a retarder.



Fig. 19 – Dry-powder activators a) MetaNa₂SiO₃ b) Na₂CO₃

4.3.4. Mixture's Proportions and Designations

A total of fifteen mortar mixtures were designed and cast. The mixtures were divided into three groups: single-, binary-, and ternary-precursor groups. The single 100% GGBFS mixtures are designated as S1, S2, and S3. Two binary mortar groups were tested: i) mixtures with 90% GGBFS and 10% SF, which had the designated codes B1, B2, or B3; and ii) mixtures with 70% GGBFS and 30% FA, with designated codes B4, B5, or B6. Also, two ternary mortar groups were tested: i) ternary-1 mixtures with 60% GGBFS, 33% FA, and 7% SF, which had the designated codes T1, T2, and T3; and ii) ternary-2 mixtures with 50% GGBFS, 45% FA and 5% SF, with designated codes T4, T5, and T6. The main variation between mixtures in the same group is the activator's content (i.e., 16, 20, and 25%). The mixtures' identification used was M-xx, where M is the mixture group (S, B, or T), and xx is the MetaNa₂SiO₃ + Na₂CO₃ activators %. For example, S2-20% represents the mixture with single GGBFS precursor material and 10% MetaNa₂SiO₃ + 10% Na₂CO₃ activators.

For phase one, the main varying parameter in all tested mortar mixtures was the activator's content as GGBFS replacement. Boric acid was added to all AASCC mixtures to retard the effect of the alkaline activation process with about 4%. GGBFS, the primary source material, was grounded with Na₂CO₃ before adding MetaNa₂SiO₃ and boric acid to mortar mixtures. A summary of the mixture's proportions used for the designed mortars is presented in **Table 13**.

Table 13 – Summary of mixture's proportions used for the designed mortars

Mixture ID	Binder Description		Activator Description		w/b
	Type	%	MetaNa ₂ SiO ₃ %	Na ₂ CO ₃ %	
S1-16%			8	8	
S2-20%	GGBFS	100	10	10	0.4
S3-25%			12.5	12.5	
B1-16%			8	8	
B2-20%	GGBFS:SF	90:10	10	10	0.4
B3-25%			12.5	12.5	
B4-16%			8	8	
B5-20%	GGBFS:FA	70:30	10	10	0.4
B6-25%			12.5	12.5	
T1-16%			8	8	
T2-20%	GGBFS:FA:SF	60:33:7	10	10	0.4
T3-25%			12.5	12.5	
T4-16%			8	8	
T5-20%	GGBFS:FA:SF	50:45:5	10	10	0.4
T6-25%			12.5	12.5	

4.3.5. Testing and Specimens Preparation

According to the EFNARC (European Federation of National Associations Representing for Concrete) specifications, the workability for various mixtures was assessed by performing a mini-slump flow cone test. Immediately after mixing, a cylindrical frustum was filled with mortar. The

spread diameter (d_m) was recorded after lifting the cone vertically (without jolting), allowing the mortar mixture to flow freely. All mixtures were designed to satisfy the flow properties requirement set by EFNARC guidelines for the SCC mortar mixture (i.e., d_m within the range of 250 ± 10 mm or $(9.84 \pm 0.39$ in.)). Compressive strength development was evaluated according to ASTM C 109. Cubic specimens [50-mm or (2-in.)] were tested for each AASCM mixture at 7 and 28 days. Specimens were cast, kept in molds for 24-hr, and then de-molded and sealed under ambient laboratory conditions until the testing age (**Fig. 20b**).

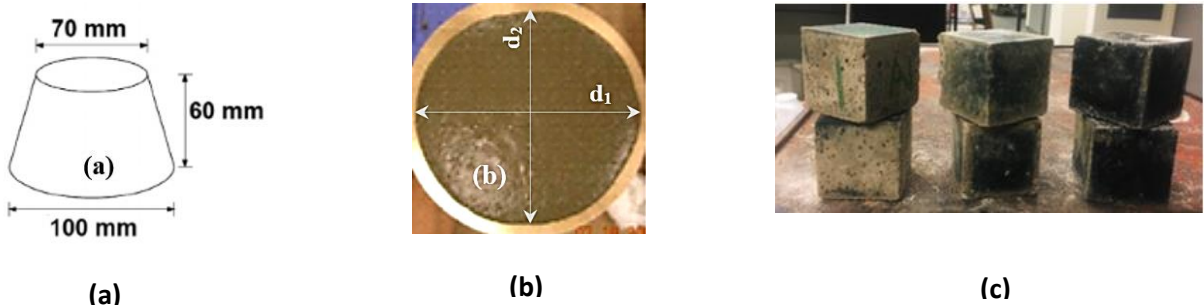


Fig. 20 – (a) Geometry of a typical mini-slump cone (b) Typical mini-slump spread (c) AASCM cubic specimens

The heat evolution of AASCMs was measured using an isothermal conduction calorimeter at a constant temperature of 23°C for 24h (phase one) and 72 h (phase two). Samples were mixed externally and then loaded into the isothermal calorimeter following ASTM C 1679. The estimated time between the powder's instant activation and loading the paste into the calorimeter was about 1 min. It should be mentioned that the first initial peak may not be wholly captured. The heat evolution and cumulative heat released were then recorded, normalized by the dry binder's mass (g). Different hydration products' formation was evaluated using a TA instrument by conducting differential scanning calorimetry analysis (DSC). After 28 days of curing age, the ground powder samples were heated up to 600 °C at a rate of 5 °C /min with air as the carrier gas. Collected data and curves were analyzed using TA Instruments thermal analysis software.

4.4. Experimental Results and Discussion

4.4.1. Dry-Powder Activators as a Replacement

4.4.1.1. Mini-Slump Flow

In the absence of effective chemical admixtures to enhance the flowability of one-part AASCC mixtures, the selection of the proper precursor material is a must. For instance, Fly ash (FA) can improve the functionality and flowability of mixtures, mainly due to its spherical shape or “ball bearing” effect. Moreover, silica fume addition was reported to enhance the workability of alkali-activated mixtures conversely to conventional cementitious mixtures (Talling, 1989; Gifford and Gillott, 1997; Collins and Sanjayan, 1999). The results of the mini-slump flow test for the ground and non-ground mixtures are presented in **Fig. 21**. The shaded area shows the range of spread flow values recommended by the EFNARC-2005 guidelines. The process of milling (particle comminution) has promoted the development of flowable mixtures due to the increased extent of the interface surface area by exposing new surfaces and changing the surface charge.

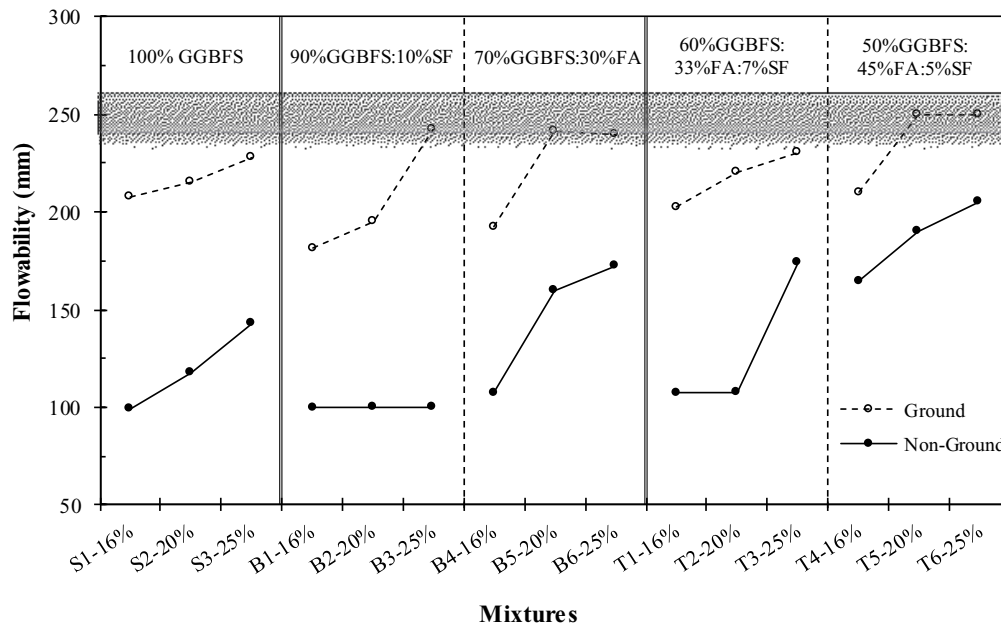


Fig. 21 – Mini-slump flow results of the ground and non-ground mixtures

Generally speaking, zeta potential is a crucial indicator of the forces between particles of the electrical double layer. Such forces are important in determining the suspended particle flocculation or dispersion and thus have a direct relationship to yield stress. Thus, flowability depends on the binder's particle size, morphology, bulk density, and zeta potential. On the other hand, using Na_2CO_3 and $\text{MetaNa}_2\text{SiO}_3$ activators in AASCC mortar mixtures results in consistent yield stress affecting the rheology of the mortar. In Na_2CO_3 -activated GGBFS, it is often stated that the increase in the concentration of CO_3^{2-} anion is responsible for slow reactions, which reduce the yield stress (Shi and Day, 1995). In the $\text{MetaNa}_2\text{SiO}_3$ -activated systems, lower yield stress was also observed due to the deflocculation behavior of alkali silicates in different suspension mediums. Consequently, the surface adsorption of silicate particles enhances repulsive forces on the particle surfaces (Fernández-Jiménez et al., 1999).

a) Single-precursor. All 100% GGBFS mixtures showed lower flowability out of the recommended range by EFNARC-2005 guidelines. Moreover, increasing the activator content resulted in a higher flowability. For instance, increasing the activator dosage from 16% to 25% resulted in about a 43% increase in the achieved flowability. Grinding GGBFS and activator seems to enhance mixtures flowability significantly. The increase in flowability as a result of grinding was in the range of 55% up to 115%. For instance, flowability ground mixtures with 16% activator were around 210 mm (8.3 in.) compared with 100 mm (3.9 in.) for non-ground mixtures. However, the flowability for the ground mixture was still lower than the suggested range by EFNARC-2005 guidelines. It should be noted that increasing the activator's dosage from 16% to 25% only marginally benefits ground mixtures. The inter-grinding of GGBFS and sodium carbonate (Na_2CO_3), so-called mechanochemical activation, lead to a higher degree of fineness. Consequently, the binder had a higher specific surface area and substantial surface energy due to more acting faces, which led to higher dissolution rates of precursor solids. The increase in the pH

due to the higher dissolution adversely affected the calcium solubility. This explains the improvement in flow characteristics due to grinding (i.e., mechanochemical activation process) along with minor effects for the increase of activator content.

b) Binary-precursor. For non-ground binary mixtures, adding SF as a 10% replacement for GGBFS seems to counteract the effect of increasing the activator content as all mixtures did not self-flow. It should be noted that GGBFS, due to the silanol groups on SiO_2 surfaces spread in alkaline solution, initially tends to have a profoundly negative surface charge. With continuous interactions between GGBFS particles and alkaline solution, alkaline cations, i.e., calcium (Ca^{2+}), continued to be released into the pore solution and adsorbed to the GGBFS surface that is negatively charged. Therefore, the GGBFS surface might become either less negative or overall positively charged; in the equilibrium state, according to the amount of Ca^{2+} cations. During the rapid reactions between Ca^{2+} cations, SiO_2 on the GGBFS surface, and SF particles, initial calcium–silicate–hydrate (C–S–H) might be formed. With the pH progression due to higher activator's concentration, the dissolution rate increased, affecting the flowability of the mortar mixtures. Moreover, the use of SF in concrete significantly increases the demand for water due to its small particles and high reactivity. In other words, the high silica content in GGBFS/SF blend increased the negative zeta potentials. Once water is added, GGBFS/SF system was then be shielded by a tightly bound shell of water-oriented molecules (HO–H) and adsorbed ions (Barhoum et al., 2018). Hence, the mixture's rheological properties and flowability of binary-blends with SF were affected.

A different trend was found for ground mixtures. The flowability for ground mixtures with SF had increased as the activator content increased. SF had resulted in a lower flowability compared to 100% GGBFS mixtures at low activator dosage. However, at 25% activator content, SF seems to significantly enhance the flowability to meet EFNARC-2005 guidelines. The mechanochemical activation; grinding process increases not only the material's surface area but also the active centers, edges, and solid projections. These altered centers of GGBFS were in a higher energy condition than their regular structure, resulting in higher reactivity and dissolution rates (Yuan, 2017). Therefore, increasing the activator content along with inter-grinding and GGBFS replacement by 10% SF was essential for the early dissolution rate of solid particles under high pH levels. Moreover, the milling process allowed some particles to be amorphized, and consequently, the hydraulic activity could be increased in addition to the flowability.

Conversely to SF, flowability for both ground and non-ground binary mixtures with FA replacing 30% GGBFS had significantly increased. For instance, binary mixtures (B5-20%) with 20% activator exhibited about 30% and 11% increase in flowability of non-ground and ground binder compared to single mixtures (i.e., 100% GGBFS), respectively. In addition to GGBFS partial substitution with 30% FA, the increase in GGBFS fineness induced by the mechanochemical activation has shifted mortar mixtures to the SCC mortar criteria presented in the EFNARC-2005 guidelines. Although the impact of grinding on mixture flowability was more apparent in the SF group than in the FA category; higher levels of deformability were achieved by FA set of mortar mixtures. This can be attributed to precursor materials' chemical composition, physical properties, and morphology.

On the other hand, the self-flow values of non-ground binary-precursor mixtures with 30% FA, had increased as activator content increased. For instance, increasing the activator content from 16% to 20% increased the flowability with about 60%. For ground mixtures, steady growth of around 25% in slump flow can be observed as the activator content increased from 16 to 20%. This indicates that activators' content of about 20 to 25% is optimum to achieve higher levels of flowability that meets the EFNARC-2005 guidelines. The release of hydroxide (OH^-) after the contact between GGBFS and water causes the increase of pH, which has a strong positive impact on the activator's efficiency (Shi et al., 2003).

c) Ternary-precursor. The effect of mechanochemical activation on the slump flow values of the two ternary mortar sets was generally obvious in the T1 group (>30%) than that of the T2 mortar group (<30%). This can be attributed to the higher GGBFS+ Na_2CO_3 milled content in T1 mortars' group. Thus, due to the defects initiated by plastic deformations and shear impacts into the inter-ground sample, free energy in the amorphous phases would increase (Kashani et al., 2014).

For both T1 and T2, the flowability had increased by increasing the concentration of the activators along with the commutation of particles and source material ratio. In the first set of non-ground ternary mortar mixtures (with 60% GGBFS, 33% FA and 7% SF); increasing the activator's content from 16 to 20% showed no substantial change in the self-flow spread value (107.5 mm or 4.2 in.), yet using 25% resulted in an increase in the slump flow value of 174 mm. On the other hand, as the amount of FA increased to 45% while GGBFS and SF decreased to 50% and 5% in the second set of ternary mortar mixtures, respectively; slump flow values increased by 15% and 24%. On the other hand, as the amount of FA precursor in ternary ground mortar combinations grew from 33% to 45%, slump flow value also increased by 19% with a 25% activator level. Along with the effect of precursor materials, the flowability of mixtures also depends on the nature, concentration, and modulus of the activators used in terms of their alkalinity potential. This implies that the ternary sets of mortar mixtures containing higher amounts of silica and alumina more than calcium oxide maintain better flowability values as their solubility at higher pH values increases (Tanada et al., 2003).

4.4.1.2. Compressive Strength

The mechanochemical activation technique, in which GGBFS was milled with dry- Na_2CO_3 activator, was found affecting the strength development of dry-powder AASCC mortars. With the incorporation of Na_2CO_3 into the GGBFS structure, aluminosilicate bonds were interrupted, which resulted in improved properties such as increased strength and fine microstructure. The average values of compressive strength (**Fig. 22 to Fig. 23**) vary widely at an early and late age for one-part AASCC mortar mixtures due to the inter-grinding process and different precursors used. Mixtures composed of finely ground GGBFS+ Na_2CO_3 promoted higher strength results, specifically at an early age than non-ground mixtures. The reaction between milled blends and water increased the pH value through the hydration process, which motivates the dissolution of source materials and subsequent formation of early reaction products. The dissolution and reactions of solid precursors should begin with a high pH in most AAM systems, but this does not necessarily result in a faster or more complicated reaction. A higher activator dose thus increases the pH without controlling the reaction rate, as seen in section 4.4.1.3, using the findings of the heat flow curves to provide further insight. Also, when characterizing the alkaline activity of

various activators, the influence of accompanying anions on the activator has a more significant impact than pH due to variations in reaction chemistry (Shi and Day, 1995). As a result, the higher early reaction rate and the mechanical properties of slag mortars triggered by specific activators are $\text{Na}_2\text{SiO}_3 > \text{Na}_2\text{CO}_3 > \text{sodium sulfate } (\text{Na}_2\text{SO}_4) > \text{NaOH}$ (Wang et al., 1994; Fernández-Jiménez et al., 1999). Mechanochemical activation, on the other hand, has proven to be an effective method for improving adsorption by exposing new surfaces where early Si-rich products are formed rapidly on GGBFS particles.

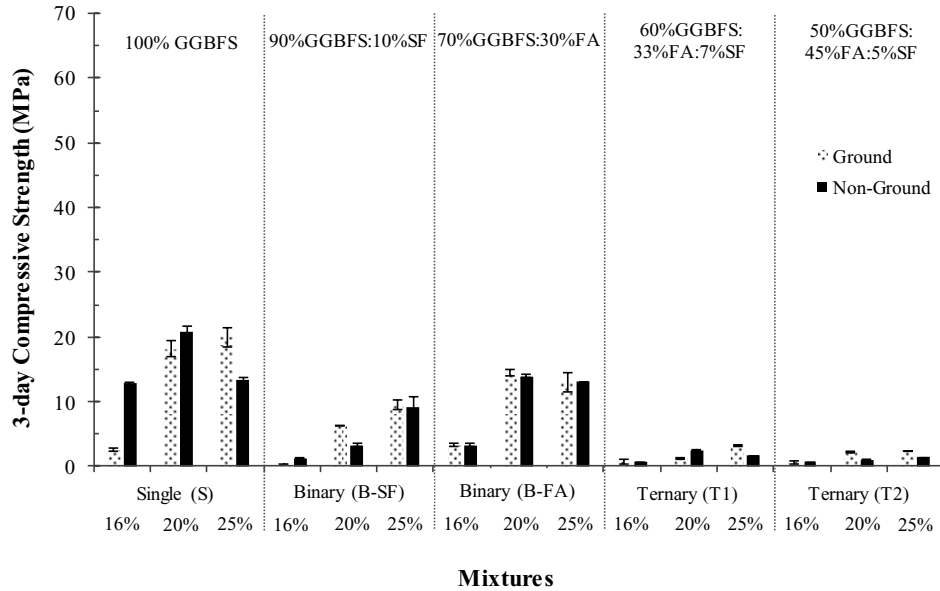


Fig. 22 – Compressive strength results at 3 days for ground and non-ground blends

a) Single-precursor. At the age of 3 days, 100% GGBFS mixtures achieved the highest measured compressive strength values among the other combinations with 20.8 MPa (3016.8 psi) and 20 MPa (2900.8 psi) for non-ground and ground blends, respectively. Similarly, a moderate to high compressive strength values of over 25 MPa (3625.9 psi) developed at 7 days of age for non-ground and ground AASCCs, i.e. 27.6 MPa (4003 psi) and 39.7 MPa (5757.9 psi), respectively. The optimum activator dose was 25% for ground mixtures, whereas 20% for non-ground mixtures. There has been strong evidence of the activator percentage impact in addition to the mechanochemical activation technique on the strength growth of ground and non-ground single-precursor mixtures at an early age. The inter-grinding technique, which generates close contact between GGBFS and Na_2CO_3 particles, stimulated early-age hydration through nucleation and late-age hydration through a partially solid-state mechanism (Dave, 1981; Tanada et al., 2003).

Also, during the initial reaction period, anionic components of alkaline activators react with dissolved Ca^{2+} from GGBFS to form Ca-rich products, which tend to increase with the increase in activators content (Sobolev et al., 2006). For instance, a strength growth of $\sim 98.5\%$ was noted, with a 25% activator share for ground mixtures aged between 3 and 7 days. In non-ground

mixtures, the strength had also increased by 30% among 3 and 7 days only with 20% of activator dose. With the increase in activator content, the strength gain was 700% (ground blends) and up to 63% in the non-ground mixtures at 3 days. Whereas an increase of 61% (ground) and 46% for non-ground on 7 days. The effect of increasing the fineness of GGBFS on strength development confirms previous findings in the literature (Wang and Scrivener, 1995; Hubler et al., 2011).

A different trend was observed at the age of 28 days. The highest strength was found using a 20% activator dose that was optimal for both ground (50.2 MPa or 7280.9 psi) and non-ground (42.1 MPa or 6106.1 psi) single-precursor mixtures compared to activated ones with 16 and 25% activator dose. Higher $\text{MetaNa}_2\text{SiO}_3$ content on GGBFS+ Na_2CO_3 suspension may cause more silica to be adsorbed or precipitated on the GGBFS particle surfaces and thus increase negative zeta potential values. As a result, a higher concentration of silicates relative to the availability of Ca^{2+} may be the reason of strength reduction (Shi and Day, 1995). This outcome was similar to the results obtained previously in the literature (Shi and Day, 1996). It was found that $\text{NaO}\cdot\text{SiO}_2$ and Na_2CO_3 are the most effective activator for $\text{CaO}\text{--}\text{SiO}_2$ and $\text{CaO}\text{--}\text{MgO}\text{--}\text{SiO}_2$ (single), $\text{CaO}\text{--}\text{Al}_2\text{O}_3\text{--}\text{SiO}_2$ (binary and ternary) systems.

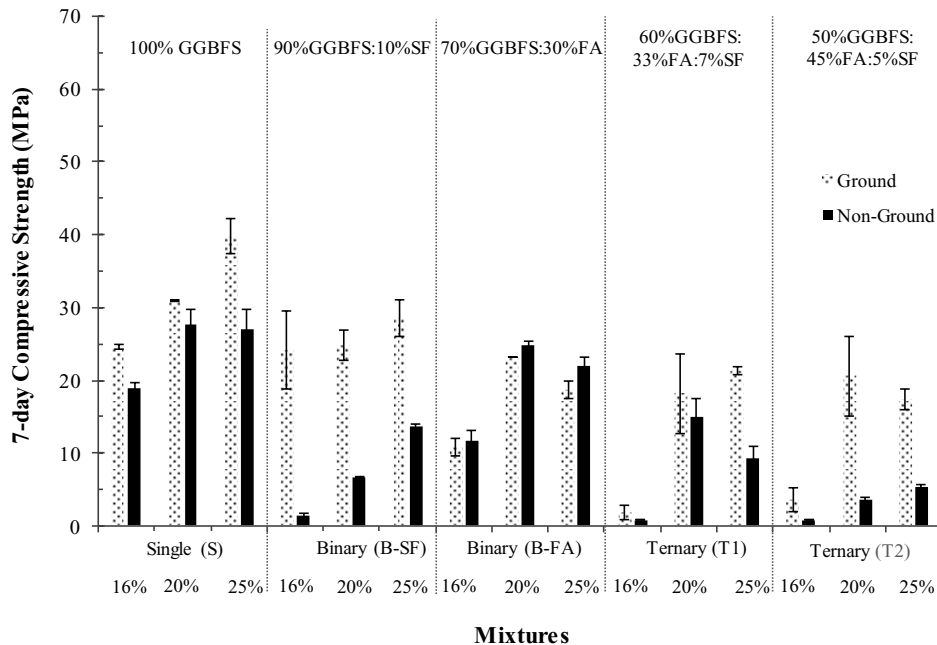


Fig. 23 – Compressive strength results at 7 days for ground and non-ground blends

b) Binary-precursor. In the binary blends with pozzolanic materials such as FA and SF, the mechanochemical activation effect was insignificant at 3 days owing to the dilution effect. Compared with 100% of GGBFS blends, the strength gain of the binary mixtures replacing GGBFS by either 30%FA or 10%SF is slow at an early age. For both ground and non-ground binary mixtures, the highest strength values of 14.5 MPa (2103 psi) and 13.9 MPa (2016 psi) were achieved using a 30% FA and 20% activator ratio. On the other hand, for ground and non-ground

10% SF mixtures, increasing the activator ratio by up to 25% resulted in similar strength values of 9.5 MPa (1377.9 psi) and 9.3 MPa (1348.9 psi), respectively.

For example, at the age of 7 days, the increase in activator content by up to 20% increased the compressive strength values by 23.2 MPa (3364.9 psi) and 24.9 MPa (3611.4 psi) for ground and non-ground binary mixtures by 30% FA, respectively. On the other hand, SF replacement showed a distinct trend where the use of 25% activator dose resulted in a 201% increase in strength for ground mixtures compared to a 47% increase in strength for non-ground binary blends confirming previous findings in the literature (Andersson and Gram, 1987). The dilution and inter-grinding of GGBFS and Na_2CO_3 in binary blends change the ionic and anionic concentration of solid activators in the mixtures. This reduces the pH in the pore solution while the quantities of alkali in mixtures are fixed. As a result, reduced pH would significantly slow the development of strength at an early age. Besides, the lower activation capability of the Na_2CO_3 activator, due to its lower pH potential, played a vital role.

The sensitivity of strength development to activator content is significantly reduced if GGBFS+ Na_2CO_3 were inter-ground together. For SF mixtures, the highest 28 days' strength was achieved using a 25% activator dose at 35.5 MPa (5148.8 psi) for non-ground blends while 40.3 MPa (5845 psi) for ground mixtures with 20% activator dose. On the other hand, replacing GGBFS with 30% FA at 28 days has resulted in a strength gain value of 44.8 MPa or 6497.7 psi (ground) and 45.8 MPa or 6642.7 psi (non-ground) using 20% activator, while further activator dose reduced strength. This indicates that the inclusion of 20% activator dosage is the optimum to achieve higher strength values, regardless of the grinding process and additional activator dose in binary mixtures with 30% FA. This can be because the apparent activation energy decreases as the dosage of the activator increases (Shi et al., 2003). Generally speaking, the hydraulic reactivity of GGBFS without grinding, in addition to the optimum activator ratio used, has always provided an adequate strength in comparison with ground ones. These findings are consistent with the outcomes found in the literature (Wang and Pu, 1991; Krivenko, 1992; Wang and Scrivener, 1995).

c) Ternary-precursor. The difference in anionic components released by precursors and activators significantly impacts strength development at an early age (Tanada et al., 2003). The strength gain for ground and non-ground T1 and T2 ternary blends was very low, < 3.5 MPa (507.6 psi) at 3 days of age. The inter-grinding effect at 3 days of age was not yet clear whether it contributed to this strength reduction or not. Conversely, increasing the activator percentage in mixtures reported a gradual strength development for both ground and non-ground T1 and T2.

At 7 days of age for ground T1 and T2 ternary mixtures, comparable values of 21.4 MPa and 20.6 MPa using 25% and 20% activator content were recorded. This indicates the role of mechanochemical activation in the development of strength. On the other hand, replacing the ground ternary blend with a non-ground ternary blend containing a higher amount of pozzolans resulted in a significant drop in strength, especially at an early age. For instance, T1 and T2 non-ground blends achieved 14.9 MPa (2161.1 psi) and 5.5 MPa (797.7 psi) using 20% and 25% activator content. It should be noted that the reaction rate of this non-ground ternary combination was slow at ambient temperature making the samples wet and difficult to de-mold after one day of age, although, with time, the hydration progresses to 28 days (**Fig. 24**) and has reasonable strength. T1 scored a higher strength gain value compared to T2 due to the presence of 10% more GGBFS

in its structure. Besides alkaline activators, strength in ternary-precursor systems may be accelerated by adding calcium-rich materials such as GGBFS.

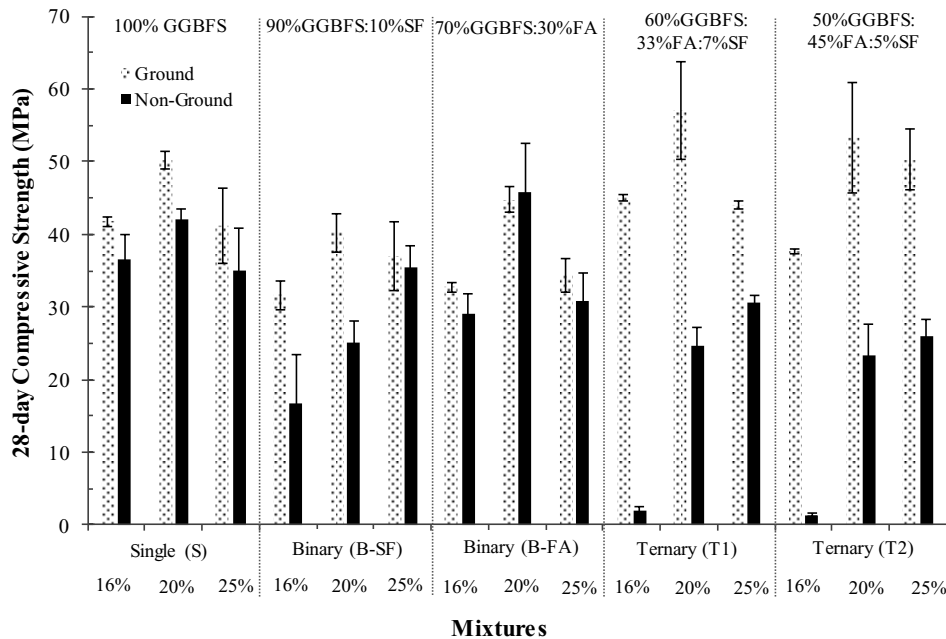


Fig. 24 – Compressive strength results at 28 days for ground and non-ground blends

Fig. 24 shows the compressive strength values at 28 days of age for ground and non-ground GGBFS with Na_2CO_3 mixtures. At 28 days of age, the two best-performing mixtures are ground T1 and T2 with a 20% activator ratio at 57.1 MPa (8281.7 psi) and 53.3 MPa (7730.5 psi), respectively. This can be ascribed to the various source materials' chemical composition, leading to different strength-giving products using the selected activators. Furthermore, because of Al-O bonds' low bonding energy compared to Si-O bonds, the presence of Al increases the dissolution (Shi et al., 2003). It can be concluded that activator dose has a significant impact on the strength development of non-ground mixtures, and in all cases, the optimal dosage is between 20% to 25% of GGBFS mass. In this study, the effect of anhydrous $\text{MetaNa}_2\text{SiO}_3$ ($M_s \sim 1.0$) was like the effect of water glass solution in terms of strength-giving characteristics. This can be attributed to the formation of primary C-S-H products or polymerization of silicate anions, promoting a less porous framework in line with the “optimum modulus phenomena” (Cheng et al., 1992).

Further Discussion. The zeta potential of the AASCM mixtures seems to be affected by the alkalinity of the solution and milling process. The suspended solid particles' surface is electrically charged on contact with an aqueous medium due to chemical reactions. The resulting surface potential of particles allows counter ions to be attracted, ions opposite to the surface in charge. On the other hand, at the liquid/solid interface, the ionized particles are shielded with a thin liquid layer that makes it work as an integral whole. Thus, the electrokinetic potential is influenced by the discrepancy between the shells' external surface and liquid as a whole. Depending on the zeta

potential phenomenon, ionization, ion adsorption, and ion dissolution are important factors for the surface charge of particles and surrounding ions. Further ion adsorption occurs in the Stern layer resulting in either the Stern (**Fig. 25**) or the diffuse double layer.

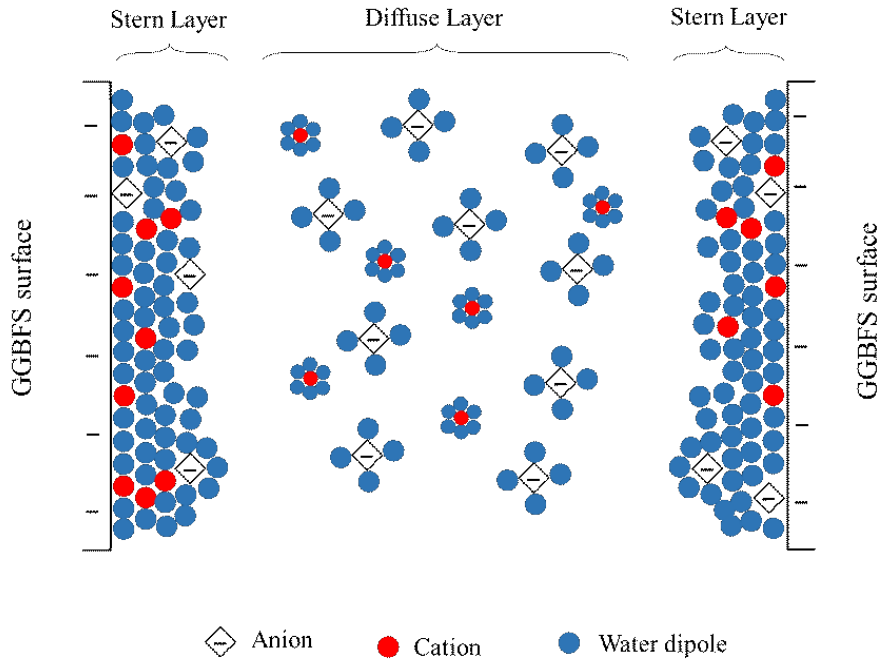


Fig. 25 – Schematic representation of the electrical double layer mechanism

While both positive and negative ions may be found in the Stern layer, counter ions' adsorption seems quite likely. In AAM's suspensions, the mechanisms associated with the formation of surface charge are complex. The equilibrium between these sites and the water depends on the pH of the activator being used. In AAM suspension medium (high pH), negative silanol groups predominate on the surface of siliceous precursor materials, i.e., GGBFS, SF, FA. The anions and cations are adsorbed in the Stern layer, depending on the surface charge. It must be acknowledged that the milling process has increased the extent of the surface area of the interface by exposing new surfaces and adjusting the surface charge. This increased the negative zeta potential, which does not allow further cation adsorption and hinders initial hydration product formation. Thus, it increases the repulsive forces on the surfaces of the particles.

4.4.1.3. Early Hydration Chemistry at One Day

Fig. 26 and **Fig. 27** present the heat of hydration curves for the ground and non-ground SCC-activated mortar mixtures using Na_2CO_3 and $\text{MetaNa}_2\text{SiO}_3$. The heat evolution curves of ground AASCC mixtures can be divided into three periods; (I) initial (pre-induction) period, (II) induction period, and (III) acceleration (post-induction) period, which is obvious in single-precursor mixtures. It can be observed that the system becomes exothermic immediately after mixing. At about 10 minutes, an exothermic peak reaches a maximum for all combinations, indicating the formation of hydration products. The peak during the pre-induction period is generally attributed

to the rapid dissolution of GGBFS under the effect of OH^- and the hydrolysis of silicate anions (Pu et al., 1988; Shi and Li, 1989; Douglas et al., 1991; Cheng et al., 1992; Huanhai et al., 1993; Tanada et al., 2003). Wang and Scrivener (1995) had declared that the activation reaction of the GGBFS is characterized by heat absorption due to the formation of silica gel and OH^- anions. However, due to the lag in heat transfer in mortar samples, the endothermic peak cannot be recognized via the regular calorimeter and is assumed to overlap with the main exothermic peak. Thus, one exothermic peak is demonstrated in **Fig. 26** and **Fig. 27**.

The combination of the two dry-powder activators, i.e., Na_2CO_3 and $\text{MetaNa}_2\text{SiO}_3$, has changed mortar mixtures' heat evolution characteristics. With activator percentages of 20% and 25%, the induction period ended after 12-h for single mixtures and more than 24-h for all other mixtures. The results are in good agreement with Shi and Day (1996). Grinding had accelerated the hydration peak at the end of the induction period, especially for single-precursor mixtures. The finer the GGBFS grains resulted in a shortened time to reach the second peak compared to the coarser ones. This can be attributed to the high specific surface area of the ground GGBFS providing additional surface provided for the nucleation and development of hydration products (Shi et al., 2003).

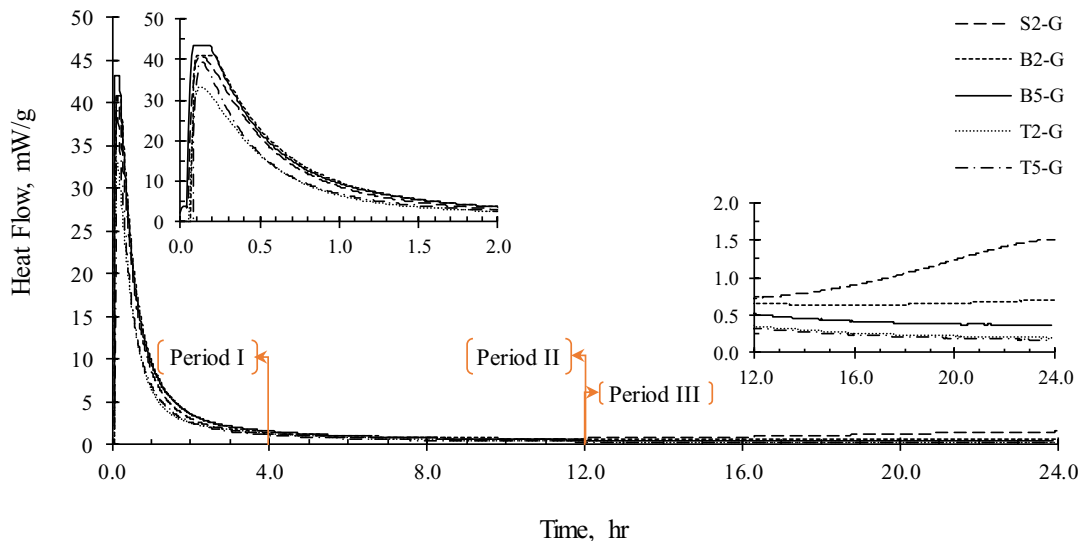


Fig. 26 – Heat evolution curves at 24-h early hydration age of ground AASCC mixtures

For the non-ground mixtures, the heat evolution curves (**Fig. 27**) indicate a higher degree of hydration with increased silica content in < 1 -h. The first exothermic peaks appeared promptly with binary precursors SF or FA with GGBFS during the initial 4-h pre-induction period, followed by single and ternary mixtures. This was followed by a very long induction period that extended to more than 24-h. This can be due to the effect of alkaline activators on activated GGBFS, SF, and FA. The system with Na_2CO_3 and $\text{MetaNa}_2\text{SiO}_3$ has a relatively lower pH value, so the dissolution of silica and alumina in the system would be expected to take a longer time. These

findings indicate that the concentration of SiO_2 significantly impacts the degree of hydration and reaction kinetics of activated slag systems.

The rapid increase in heat flow is frequently comparable to the early development in the mechanical properties of AASCC mixtures with $\text{MetaNa}_2\text{SiO}_3 + \text{Na}_2\text{CO}_3$. The dissolution of GGBFS (as the primary precursor) particles into the solution and the formation of reaction products on both the GGBFS surface and in liquid regions causes changes in yield stress of these systems. The long induction period correlates to the expected workability retention. Combining the heat evolution of AASCC mixtures with compressive strength results show that ground-activated systems exhibit higher cumulative heat of reaction. This indicates that the strength development of AASCC depends not only on the type and dosage of the used dry-powder activators but also on the type and fineness of the main precursor material. The finely ground GGBFS affected the degree of hydration, while the activator type and dosage affected the microstructural development and hydration product compositions (Shi et al., 2003).

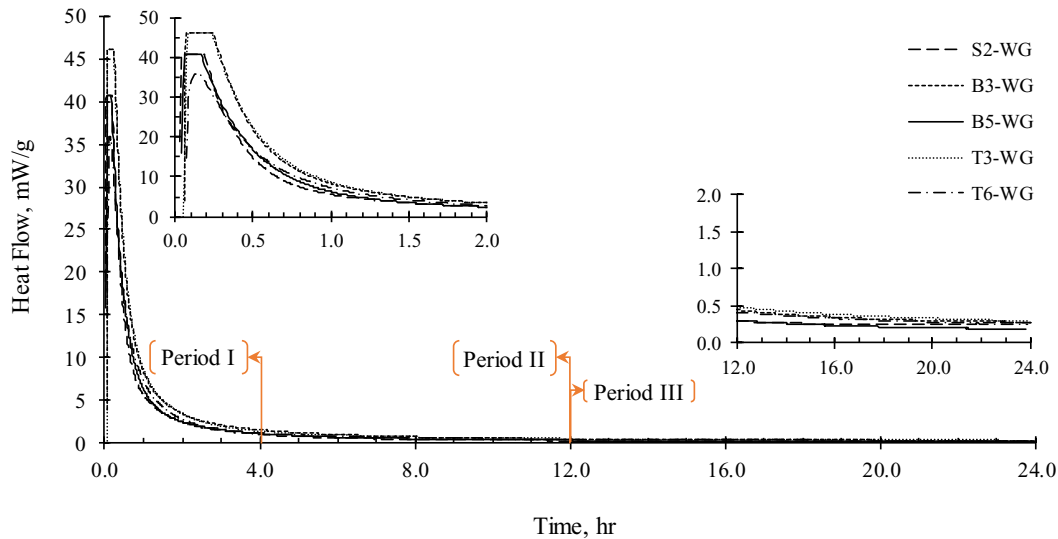


Fig. 27 – Heat evolution curves at 24-h early hydration age of non-ground AASCC mixtures

4.4.2. Dry-Powder Activators as an Addition

4.4.2.1. Mini-Slump Flow

Mortar properties in the SCC are predominant as the coarse aggregate content of the highly flowable mixtures is lower than that of normal concrete. Testing the properties of mortars is an intrinsic aspect of AASCM mixture design processes; therefore, it is useful to know the properties of mortars. The flow characteristics of AASCMs were determined by the composition, morphology, and content of precursors, type of activator, initial pH in the environment, and zeta potential. As the pH increases by increasing the activator content, a reversal of the surface

precursor charge occurs, thereby positively influencing the zeta potential and consequently AASCM workability to a certain level (Barhoun et al., 2018; Kashani et al., 2014). The mini-slump flow test results are presented in Fig. 28.

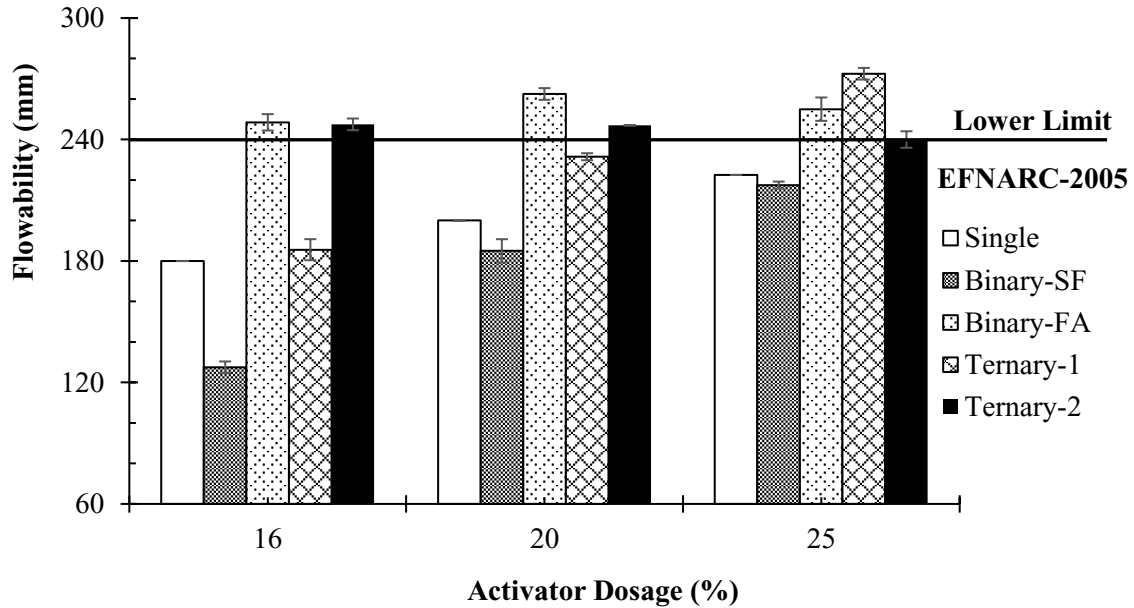


Fig. 28 – Mini-slump flow results of the AASCM mixtures

Precursor combination effect. The flow of fresh mortars requires low yield stress and sufficient plastic viscosity levels to prevent the mixture from segregating during the flow. Using proper chemical admixtures would therefore ensure that the rheology of SCC mixtures is stabilized. However, the lack of effective chemical admixtures to enhance the flowability of one-part AASCM mixtures entails proper precursor materials. For this purpose, two precursor materials, FA and SF, have partially replaced slag in mixtures with different dosages. Due to its spherical shape or "ball bearing" effect, FA can enhance the functionality and flowability of mixtures. While the addition of SF has been reported to improve the workability of alkali-activated mixtures, in contrast to its performance in conventional concrete mixtures (Talling, 1989; Gifford and Gillott, 1997; Collins and Sanjayan, 1999).

Slag/SF systems resulted in a lower flowability than 100% slag mixtures, specifically at low activator dosage. SF in concrete significantly increases the demand for water due to its small particles and high reactivity. In other words, the high silica content in the slag/SF blend increased the negative zeta potentials. After adding water, a tightly bound shell of water-oriented molecules (HO-H) and adsorbed ions shielded the slag/SF (Tanada et al., 2003). The rheological properties and flowability of binary blends (slag/SF) have been adversely affected. Conversely to SF, the flowability of binary mixtures with FA replacing slag had significantly increased compared to slag and slag/SF mixtures. The partial substitution of slag with 30% FA has shifted mortar mixtures to the SCC mortar criteria presented in the EFNARC guidelines. This can be due to the spherically

shaped FA particles acting as miniature ball bearings, providing a lubricant effect (Yang and Tan, 2005).

The spherical shape of the FA particles in both ternary mixtures lubricates the well-proportioned mixture, making it easier to self-flow. However, the higher concentrations of silica and alumina in the second set than calcium oxide instigate an impermeable coating of aluminosilicate layers on the surfaces of slag grains, which inhibits further reactions as the activator content increases (Huanhai et al., 1993). The mechanism governing the formation of an aluminosilicate gel depends on the mixture's chemical composition and the selected precursor. As it would typically be the case in FA/slag systems, the presence of Ca^{2+} could significantly alter the system's chemistry and improve the colloidal interactions between grains (Favier et al., 2013).

Activator content effect. The use of Na_2CO_3 and $\text{MetaNa}_2\text{SiO}_3$ activators in AASCM mixtures resulted in consistent yield stress affecting the rheology of the mortar. For Na_2CO_3 activated slag, it is often stated that increasing the concentration of CO_3^{2-} anion is responsible for slow reactions due to its lower pH potential, which reduces the yield stress (Yuan, 2017). In the $\text{MetaNa}_2\text{SiO}_3$ activated systems, lower yield stress was also observed due to alkali silicates' deflocculating behavior in different suspension mediums. Consequently, the surface adsorption of silicate particles enhances repulsive forces on the particle surfaces (Kashani et al., 2014). Although increasing the activator content resulted in higher flowability levels, all single mixtures showed lower flowability outside of the EFNARC range. High activator dosage from 16% to 25% resulted in about 11% and 25% increase in the achieved flowability. The alkali hydration process of the slag systems starts with the dissolution of slag bonds such as Ca–O, Mg–O, Si–O–Si, Al–O–Al, and Al–O–Si. Slag grain surfaces were then coated with Si–Al layers, which led to the formation of initial hydration products (Faimon, 1996). As a result, and with a high activator dosage, Si^{2+} increases the pore solution while the calcium level gradually decreases due to the formation and precipitation of initial hydration products (Song and Jennings, 1999). This explains the improvement of the flow due to the high activator content despite the precursor's predominant effect (i.e., slag) type.

For binary-precursor mixtures, replacing slag with 10% SF seems to counteract the effect of increasing the activator dosage, as not all mixtures were self-flowed. It should be noted that slag, due to the silanol groups on SiO_2 surfaces spread in alkaline solution initially tends to have a profoundly negative surface charge. With continuous interactions between slag particles in the alkaline atmosphere, alkaline cations i.e. Ca^{2+} , continued to be released into the pore solution and adsorbed to the slag surface that was negatively charged. Therefore, the slag surface might become either less negative or overall positively charged; in the equilibrium state, according to the amount of Ca^{2+} cations. During the rapid reactions between Ca^{2+} cations, SiO_2 on the slag surface and SF particles; initial silica-rich products might be formed. With the pH progression due to higher activator dosage, the dissolution rate of precursors increased. On the other hand, the flowability for binary-FA mixtures had increased as the activator content increased. The increase in flowability as the activator dosage increased from 16 to 20% was 9.78 – 10.33 in. [248.5 – 262.5 mm]. A plateau was then reached in the flow as the activator content increased from 20 to 25%. This can be due to the release of hydroxide (OH^-) after contact between water and slag, resulting in a high pH, which is quite satisfactory for the activator's efficiency (Shi et al., 2003).

For both ternary-precursor groups, the flowability increased by increasing the activators' dosage and precursor ratios. It should be noted that the increase in the activator content dominated the self-flow of the two ternary sets and was generally noticeable in the first ternary group (increase > 45%) compared to a decrease of up to 3% in the second set. In addition to the effect of precursor composition, the flowability of mixtures depends on the activators' nature, concentration, modulus, and alkalinity potential (Huanhai et al., 1993). A well-proportioned AASCM mixture (i.e., second ternary set) displays satisfactory fresh properties compared to the first set using the same activator dosage, except for a 25% dosage.

4.4.2.2. Compressive Strength Development

In terms of their initial pH value and accompanying anion, the selectivity of the appropriate alkaline activators was found to affect the strength development of the one-part AASCM mixtures. With the incorporation of silicate ions from $\text{MetaNa}_2\text{SiO}_3$, an initial C-S-H was formed, accelerating the setting time of mixtures and improving the hardened properties. On the other hand, carbonate ions from Na_2CO_3 have an opposite effect that contributes to a slowdown in the hydration process (Yuan, 2017). The combination of both alkaline activators has enhanced the fresh and mechanical characteristics of AASCM mixtures. Results for compressive strength for different tested mixtures are shown in **Fig. 29** and **Fig. 30**. Mixtures composed of high activator contents promoted higher strength, specifically at an early age compared to later ages. This could be due to a higher amount of dissolved Si^{2+} and Ca^{2+} that contribute to more hydrated gels.

Increasing the activator dosage provides a higher alkalinity environment appropriate for the hydration process, driving the dissolution of precursors and the subsequent formation of early reaction products (Ouyang et al., 2020). The dissolution and reactions of precursors should begin with a high pH in most AAM systems, but this does not necessarily result in a faster or more complicated reaction. The effect of the accompanying anions to activators, on the other hand, has a more profound impact than the activator's initial pH (Shi and Day, 1995). It is therefore assumed that activators in the order $\text{Na}_2\text{SiO}_3 > \text{Na}_2\text{CO}_3 > \text{sodium sulfate } (\text{Na}_2\text{SO}_4) > \text{NaOH}$ trigger the initial dissolution of precursors and thus improve the mechanical properties of slag-based mortars (Wang et al., 1994; Li et al., 2019). This is in good agreement with the heat flow curves findings in the following section.

Early-age strength. The compressive strength of different precursor systems and various activator dosages after 7 days is shown in **Fig. 29**. It can be seen that a moderate compressive strength of 22.4 MPa (3248.8 psi) was achieved using a 16% activator dosage, while the strength gain was 51.3% for 20% dosage and up to 71% in the 25% dosage, respectively. There has been strong evidence of the activator dosage impact on the strength growth of single mixtures at an early age, with the optimum activator dosage of 25% for all mixtures. It is important to note that the initial pH of the dry-powder activators plays a crucial role in the initial dissolution of slag, which tends to increase while increasing the activator's content (Li et al., 2019). Hence, during the initial reaction period, the anionic components of alkaline activators, i.e., SiO_3 and CO_3^{2-} react with dissolved Ca^{2+} from slag to form Ca-rich products as the major hydration products (Shi and Day, 1995; Wang et al., 1994).

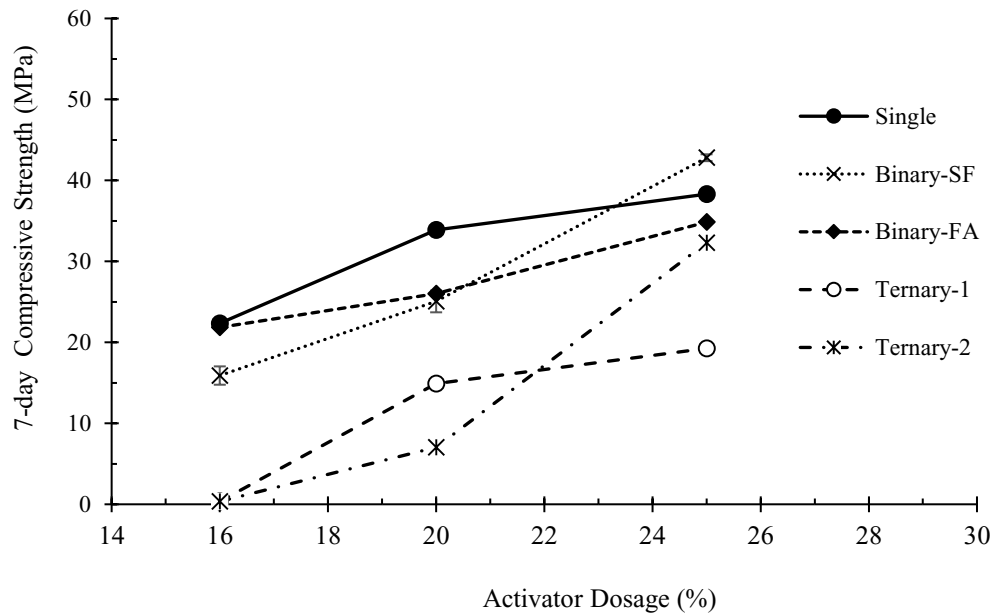


Fig. 29 – Compressive strength of AASCM blends at 7 days

For the binary-precursor blends with pozzolanic materials such as FA and SF, increasing the activators' dosage up to 20% was insignificant at 7 days owing to the dilution effect. Compared with 100% slag blends, the strength gain of the binary mixtures with 30% FA or 10%SF was generally slow at an early age. This can be due to the lower reactive rate of the pozzolanic materials at room temperature (Bui et al., 2018). For both 30% FA and 10%SF binary mixtures, the highest strength values of 34.85 MPa (5054.56 psi) and 42.8 MPa (6207.6 psi) were achieved at 7 days (37% and 63% increase) using up to 25% activator ratio, respectively. It should be noted that the use of FA or SF materials has modified the particle size distribution of binary activated systems, resulting in a reduction in the initial porosity of the matrix, besides improved fresh and hardened properties. On the other hand, the relatively higher activator content had led to the dissolution of Ca – O, Si – O, and Al – O bonds, instigating the formation of different hydration products (Bin et al., 1992).

The increase in the activator dosage for both ternary-1 and ternary-2 sets was reflected in a modest increase in strength. Although the effect of pH progression in ternary blends was generally not evident at an early age, the difference in anionic components released by precursors and activators is believed to impact strength development (Wang et al., 1994). A sharp increase in compressive strength values of 19.3 MPa (2799.2 psi) and 32.3 MPa (4684.7 psi) for ternary-1 and ternary-2 mixtures was observed at 7 days age, with 25% dosage. Ternary-2 scored a higher strength gain value compared to ternary-1 due to the presence of 10% more pozzolana. For ternary-1 blends, the degree of hydration was assumed quite high due to the consumption of SiO₂ and Ca²⁺ in the system, leading to higher pH values that decreased over time, resulting in a modest increase in strength at 7 days. Thus, it can be concluded that the high alkalinity (pH value) was the main factor affecting the late age strength, whereas the silicate concentration only affects the early hydration.

Late-age strength. A different trend was observed at the age of 28 days. The highest strength was found using a 20% dosage for single mixtures (44.8 MPa or 6497.7 psi) compared to activated ones with 16% and 25% dosage. This indicates that the inclusion of 20% dosage was the optimum to achieve later higher strength values, regardless of additional shares in 100% slag mixtures. The effect of increasing the activator dosage on the strength development of slag precursor confirms the previous findings in the literature (Wang et al., 1994; Bin et al., 1992). Higher $\text{MetaNa}_2\text{SiO}_3$ and Na_2CO_3 content in mixtures may cause more SiO_3 and CO_3^{2-} to be adsorbed, reacted, and precipitated on the slag particle surfaces. As a result, a higher silicate concentration relative to the availability of Ca^{2+} hindered the reactions and caused a reduction in strength at late ages (Shi and Day, 1995). This is in line with the heat evolution results, as discussed in the following section. The first (dissolution) peak was often followed by a period of induction during which soluble concentrations of calcium, alumina, and silica rise to a threshold value. The dormant period was shortened by using a higher activator content indicating a rapid precipitate formation on the slag grain surface, which negatively affected further reactions and high strength at a late age. This outcome was similar to the results obtained previously in the literature (Sun and Vollpracht, 2018; Krivenko, 1994). Therefore, activators' apparent activation energy decreased as the activator's dosage increased (Shi et al., 2003). It should be noted that $\text{NaO}\cdot\text{SiO}_2$ and Na_2CO_3 were the most effective activators for $\text{CaO}-\text{SiO}_2$ and $\text{CaO}-\text{MgO}-\text{SiO}_2$ (single), $\text{CaO}-\text{Al}_2\text{O}_3-\text{SiO}_2$ (binary and ternary) systems (Shi et al., 2003). Generally, the hydraulic reactivity of slag mixtures, in addition to the optimum activator ratio used, has always provided an adequate strength in comparison with other systems.

The sensitivity of strength development to activator contents was significantly increased with the slag replacement by 10% SF and 30% FA in binary mixtures (**Fig. 30**). The 28 days' strength for SF binary mixtures using a 25% activator dosage was around 56.3 MPa (8165.6 psi) compared to 34.6 MPa (5018.3 psi) and 41.2 MPa (5975.6 psi) for 16% and 20% dosages, respectively. By replacing slag with 10% SF, the hydration process was significantly improved by developing a well-defined and compact matrix. On the other hand, replacing slag with 30% FA, at 28 days, had resulted in the highest strength gain value of 32 MPa (4641.21 psi), 48.95 MPa (7099.6 psi), and 58.35 MPa (8462.9 psi) using 16%, 20%, and 25% dosages, respectively. This indicates that the inclusion of a 25% dosage was optimum to achieve higher strength values, regardless of the type of binary material. For 30% FA binary blends, the activators began to react with slag causing the formation and precipitation of $\text{CaO}-\text{Al}_2\text{O}_3-\text{SiO}_2-\text{H}_2\text{O}$ (C-A-S-H in cement notation) layers; hence, the pH was likely to increase in the mixture. This instigated the dissolution of FA, causing the formation of $\text{Na}_2\text{O}-\text{Al}_2\text{O}_3-\text{SiO}_2-\text{H}_2\text{O}$ (N-A-S-H in cement notation), leading to a denser and less porous matrix than slag-based mixtures. It can be concluded that the development of early-age strength was associated with the reaction of slag, while ultimate strength gains were due to the contribution of the FA (Collins and Sanjayan, 2000; Ismail et al., 2014).

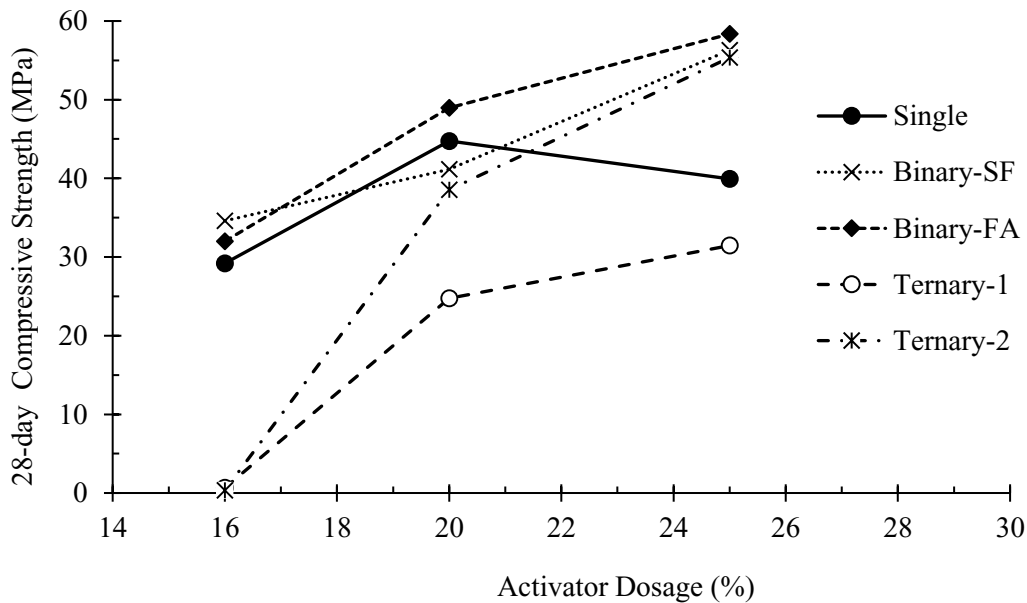


Fig. 30 – Compressive strength of AASCM blends at 28 days

The 28 days compressive strength results for AASCM ternary-1 mixtures were significantly lower than that of the ternary-2 (**Fig. 30**). This is attributed to the high pozzolanic content in the ternary-2 structure that increased the homogeneity of the hardened matrix at a late age (Long et al., 2019). The two best-performing ternary mixtures were T3 and T6, with a 25% dosage at 31.45 MPa (4561.4 psi) and 55.35 MPa (8027.8 psi), respectively. This can be ascribed to the various precursors' chemical compositions, leading to different strength-giving products. Furthermore, Al–O bonds have low bonding energy than the Si–O bonds, Al increases the dissolution (Shi et al., 2003). It can be concluded that the activator dosage had a significant impact on the strength development of ternary mixtures, and in all cases, the optimal dosage was 25%. This can be attributed to the formation of primary C-A-S-H and N-A-S-H products and polymerization of silicate anions, promoting the less porous framework in line with the "optimum modulus phenomena" (Shi and Li, 1989).

4.4.2.3. SEM Observations

SEM images of AASCM mixtures activated with 25% activator dosage after 28 days of curing are presented in **Fig. 31 (a-e)**. After 28 days of hydration, the activator dosage still significantly affected the compressive strength. The highest compressive strength values of 58.4 and 56.3, and 55.4 MPa (8470.2, 8165.6, and 8035.1 psi) were recorded in the binary blends of slag/FA, slag/SF, and ternary-2 group, respectively. The additional quantity of silica and alumina provided by FA and SF substitutes had a profound effect on the formation of hydration products leading to the strength development. The BSE images confirmed that the major hydration product in all mixtures was (N,C)-A-S-H. Single-precursor (**Fig. 31a**) sample exhibits a homogeneous matrix around slag particles with many platy crystals. Angular particles belong to partially reacted anhydrous slag, which was surrounded by reaction products. Similar crystals have been observed in binary-

precursor slag/SF blends up to 5 μm thick. The slag/FA blend (**Fig. 31c**) exhibited a homogeneous paste matrix with some unreacted FA-shaped phases. This may be an indicator of a high-strength reaction product at this combination level. The BSE images did not clearly observe the platy precipitates (c) and (d) for ternary blends. Some pores and cracks, on the other hand, were present even after 28 days of curing. EDS analysis was carried out to determine the microstructural phases.

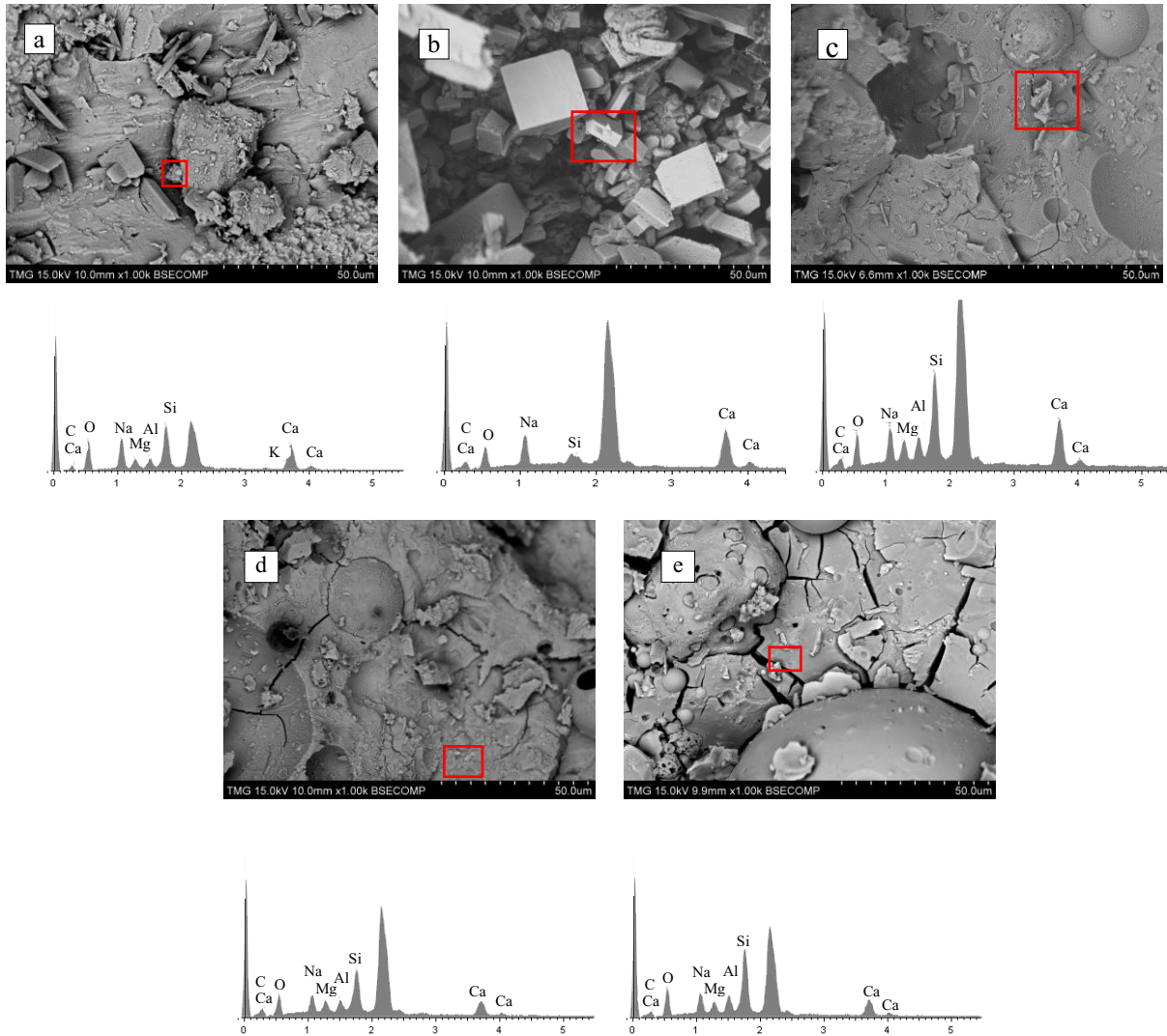


Fig. 31 – SEM images of AASCMs a) S3-25%, b) B3-25%, c) B6-25%, d) T3-25%, and e) T6-25%

4.4.2.4. Heat of Hydration

The polymerization reactions, patterns, and phases of AASCM systems are interpreted in heat flow and cumulative heat evolution curves. The early hydration of the AASCM systems can be divided into four periods based on the heat evolution curves: i) pre-induction period (initial dissolution), ii) induction period, iii) post-induction period (acceleration/deacceleration), and iv) stable period (diffusion). For all AASCM blends, two exothermic calorimetric peaks were observed 1) an initial

peak with significant heat flow and 2) a secondary peak with relatively low intensity at around 12 to 65 h. The obtained calorimetric data are in good agreement with the heat evolution findings in the literature (Brough et al., 2000; Chithiraputhiran and Neithalath, 2013; Deir et al., 2014; Zhang et al., 2016). After a few minutes of mixing, the pre-induction stage corresponds to the initial dissolution and wetting of the precursor materials. Initial calcium silicate hydrates (C-S-H) were then formed due to the initial hydration as well as the reactions between silicate (SiO_3) and carbonate (CO_3^{2-}) groups of activators with Ca^{2+} , Si^{2+} , and Al^{3+} ions of precursor materials.

The magnitude of the peaks of the pre-induction stage depends on the initial pH value, activator content, type, and accompanied anion, such as SiO_3 and CO_3^{2-} . Whereas the second exothermic peak of the post-induction stage mainly depends on the precursor materials' chemical composition (Zhang et al., 2016). The reactions were then suppressed by forming new reaction products that grew rapidly, coating the unreacted precursors' grains and causing the so-called (induction) stage. It was found that the induction period was slightly shortened as the activator content increased, leading to a higher initial pH value of the systems. In the post-induction period, the alkalis penetrated the formed layers around unreacted grains due to the continuous supply from the activators to the systems and reactivated the reactions (Sun and Vollpracht, 2018).

Single-precursor combination. The heat of hydration curves for the slag AASCM mixtures in the first 72 h is presented in **Fig. 32a**. Calorimetric curves showed two main thermal peaks; the first peaks occurred within 5 min due to slag particles' initial dissolution coupled with the massive formation of the first reaction products (i.e., C-S-H). The heat of the hydration curves then dropped to an induction period that lasted for a few hours. It can be attributed to the precipitation of the initial hydration products on the surfaces of unreacted slag particles that inhibited the reactions. Several hours later, the second exothermic peaks appeared mainly due to the interactions between slag components and alkalis provided by the activators, resulting in the formation of secondary hydrates and other complicated products (Criado et al., 2018). As mentioned earlier, increasing the activator dosage (pH) resulted in a shorter time to reach the second peak. Moreover, an increase in activators' content of 20% and 25% resulted in a significant increase in peak magnitude between 25%-50% compared to mixtures with a 16% activator dosage.

Cumulative heat evolution curves showed more heat evolution as the activator content increases in mixtures (**Fig. 32b**). The sharp increase in the curve corresponded to the first interaction between slag particles, water, and activators. Then, under the polarisation effect of OH^- , the Si-O, Al-O, and Ca-O bonds eventually break (Royak et al., 1978; Teoreanu, 1991). As the reactions proceed after the initial dissolution cycle, a relatively modest increase in the heat was observed during the induction period associated with precipitation of formed layers on the unreacted slags' grains, preventing further reactions. The continuous supply of alkalis from activators and dissolved Ca^{2+} and Si^{2+} ions from the slag advanced the reactions. Moreover, alkalis and ions concentrations increased in systems that may exceed C-S-H saturation, resulting in continuous nucleation, growth, and precipitation of C-S-H (Criado et al., 2018). Therefore, all mixtures exhibited a significant heat increase throughout 12 to 20 h in the post-induction stage.

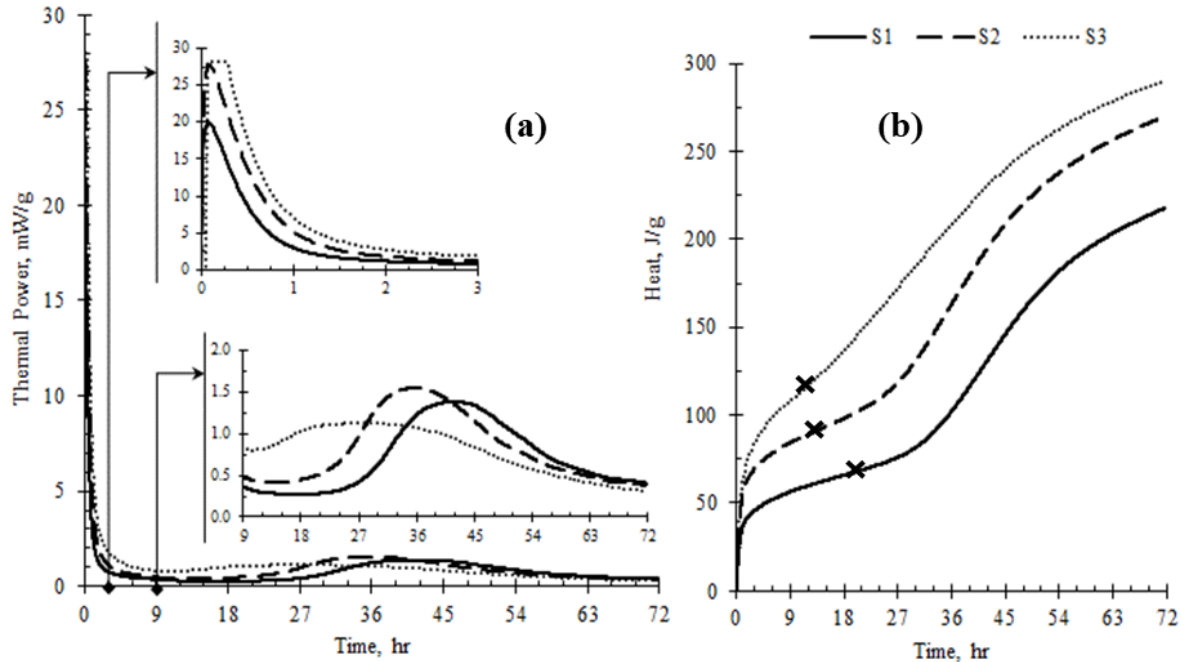


Fig. 32 – Heat evolution of AASCM blends using slag single-precursor blends a) Heat of hydration curves and b) Cumulative heat evolution curves

With pH progression due to higher activator's dosage, the curves of single mixtures with 20% and 25% dosage converge to approximately the same degree of hydration (with a difference of < 1%) near the end of the test period. Compared to S1-16%, S2-20%, and S3-25% exhibited > 20% increase in the cumulative heat evolved. This can be attributed to the apparent activation energy of the activators, which decreased as the dosage increased. Thus, an inverse relationship between the content of activators and total heat evolution was revealed and reflected in early-age compressive strength findings.

Binary-SF combination. The 10% replacement of slag with SF has altered the hydration mechanism starting from the initial dissolution stage. Compared with single blends (**Fig. 32**), this substitution has affected the initial peaks' magnitude, increasing the heat flow at a high slag content. The results also indicated that 10% SF appeared to counteract increasing the activator content. There was no noticeable effect on the peaks' magnitude as the activator content increased by up to 20%.

The activation with $\leq 20\%$ activator content has reduced, but the high activator level of 25% has increased, the evolved heat of hydration to some extent. This can be attributed to the initial systems' pH and the different chemical and physical effects of SF on heat evolution. During the pre-induction phase, SF underwent rapid dissolution (within a few minutes) along with having alkalis and Ca^{2+} ions rapidly released from the activator and slag, respectively. This has reduced the Ca^{2+} content in the solution, the formation of initial hydration products, and low- Ca^{2+} silica-rich layers, leading to increased heat (Gebregziabihier et al., 2015). The gel-like layers then started to coat SF particles, due to their comparatively small size, tended to agglomerate around unreacted slag grains (Gebregziabihier et al., 2015). The available water in the system may also become enclosed in the

gel-like layers and low-pH system, preventing further reactions and delaying the hydration (Gebregziabihier et al., 2015). The dissolution rate increased by increasing the activator content, and the induction time shortened. Thus, the hydration continued to accelerate, as noticed in B2-20% and B3-25% mixtures. As the hydration process continued, the reaction rate decreased gradually due to the continuous accumulation of hydration products. Then, with continued water consumption in reactions, layers of hydration products grew and thickened rapidly, covering slag grains, resulting in long diffusion processes that gradually slowed down hydration (Zuo et al., 2019). It should be noted that, after a relatively long induction of ~ 51 h, the low activator level in B1-16% did not show any distinct acceleration/deceleration stages.

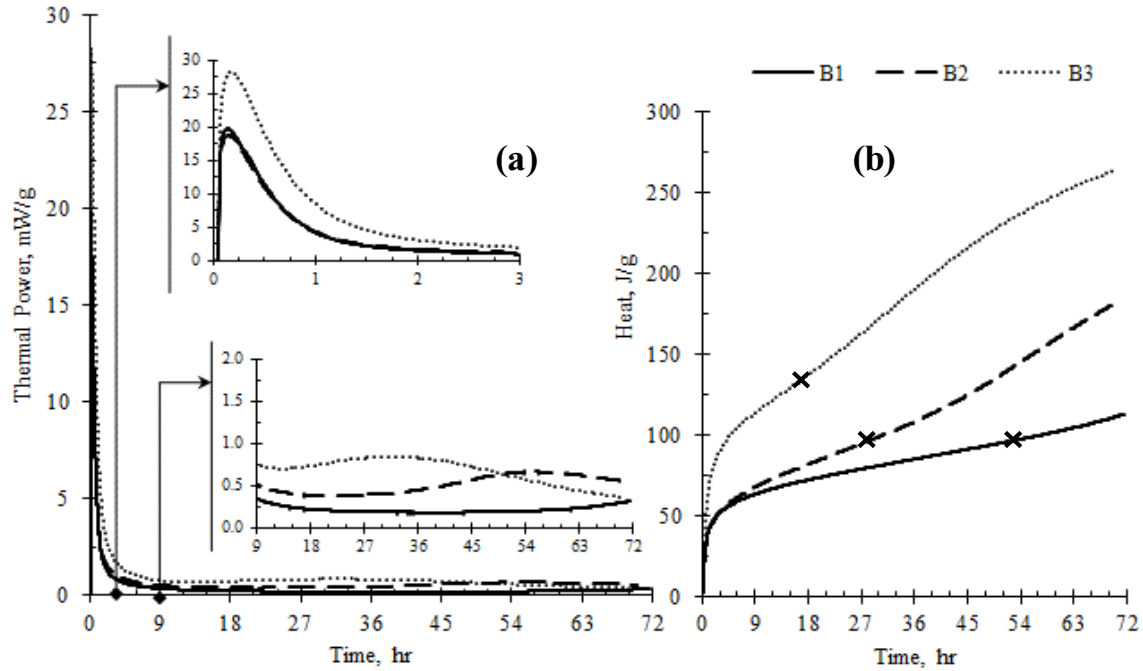


Fig. 33 – Heat evolution of AASCM blends using binary-SF blends a) Heat of hydration curves and b) Cumulative heat evolution curves

Fig. 33 (a and b) shows the cumulative heat evolution of the binary-SF blends. Using 16%, 20%, and 25% activator dosages resulted in a cumulative heat of 112, 179.8, and 253.2 (J/g), respectively. Given that the activator content would increase the pH, no significant difference in cumulative heat was observed in B1 (low-pH) and B2 (high-pH) mixtures during the 4 h pre-induction stages. The low SiO_2 content, which was consumed rapidly during the initial stage in the B1-16% mixture, resulted in a rapid increase in pH value (close to B2-20%) characterized by similar peak times and magnitudes. In later stages, the availability of SiO_2 in B2-20% has accelerated the hydration process. It is noteworthy that increasing the dosage increased the heat release with about 61% to 126% using 20% to 25% compared to 16% dosage, respectively. This indicates the contribution of SF particles to the activation of slag grains compared to single mixtures.

Binary-FA combination. The effect of increasing the activators' content on the heat evolution curves was generally apparent in the FA/slag group than that of the SF/slag. This can be due to the

differences in chemical and physical characteristics between both materials. The FA (Class F) was commonly characterized by its relatively low reactivity, resulting in a mild reaction and slightly lower heat evolution at ambient temperature. Standard calorimetric curve phases were identified; however, the duration of each stage was shorter as the pH increased (**Fig. 34a**). The dissolution peaks' magnitude reached 10.8, 18.2, and 28.8 (mW/g) within 14, 11, and 5 min, in B4-16%, B5-20%, and B6-25% mixtures, respectively. This increased the liberated heat by 41% and 63% using 20% and 25% compared to 16% dosage. The reaction process with a high activator content was accelerated significantly, suggesting the dissolution of Ca-O, Si-O, and Al-O bonds in FA/slag due to the high alkalinity. A prolonged dormant phase followed while the activator dosage decreased. This can be attributed to the dissolution of slag (mainly weaker Ca-O bonds) and activators, resulting in the formation and precipitation of initial hydration products on the FA particles, which acted as nucleation sites (Gao et al., 2015). The second heat evolution peak appears at around 34 h in the B4-16%.

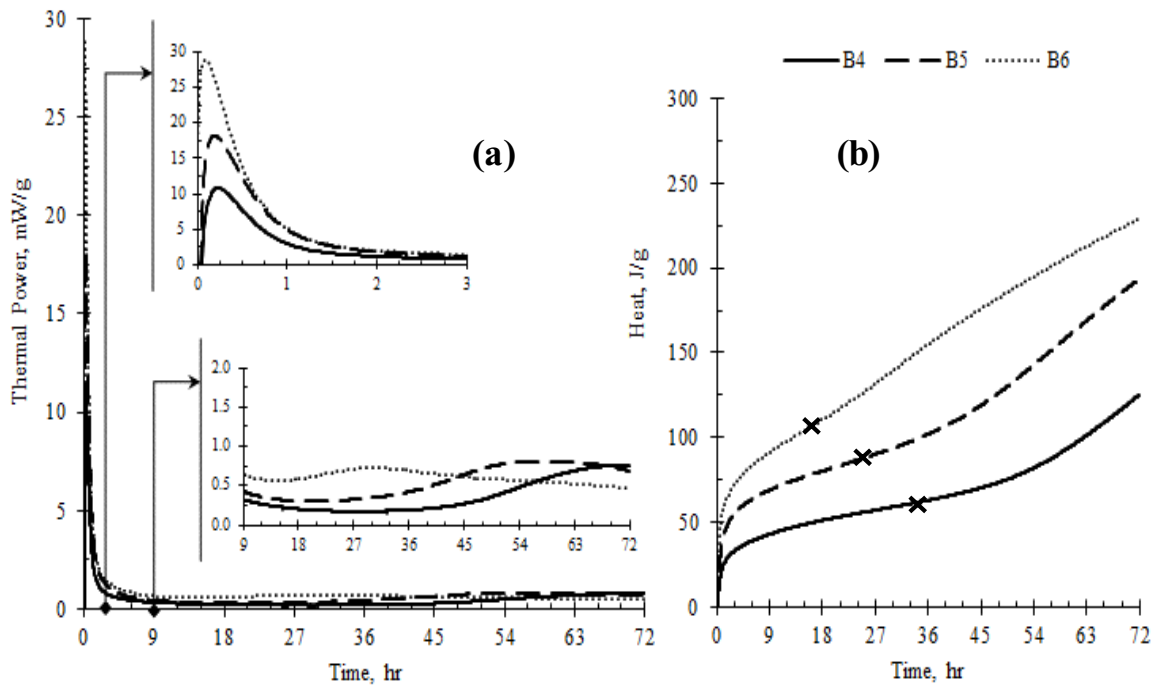


Fig. 34 – Heat evolution of AASCM blends using binary-FA blends a) Heat of hydration curves and b) Cumulative heat evolution curves

Fig. 34b shows the cumulative heat of hydration of FA/slag mixtures. Results indicated that the presence of 16% and 20% of the activator dosage increased the total heat evolution of 124.3 and 185.7 (J/g) during the first 72 h of hydration, respectively. Under high alkalinity conditions, slag possessed a higher degree of reactivity than FA under ambient temperature (Qiu et al., 2019). Hence, the high slag content resulted in a higher total heat release. This can be ascribed to the apparent activation energy of slag that decreased with the system's pH increase (Li et al., 2019). The activation energy for B4-16%, B5-20%, and B6-25% was 19.1, 18.4, and 17.1 (kJ/mol), respectively. The contact between FA/slag, activators, and water initially induces precursor materials' dissolution under a high alkaline atmosphere. The high activator dosage instigated the

formation of an aluminosilicate impermeable shell that coated slag and FA (Ionescu, 1999). This physical barrier was the justification for the low system activating energy, which to some point, surpassed further reactions. However, as the system's reactions proceeded, this thin layer dissolved or broke, leading to strength development (Bijen, 1996; Roy, 1999; Altan and Erdoğan, 2012).

Ternary-precursor combination. Heat flow curves for ternary blends were relatively different from single and binary mixtures. Maximum heat flow values were affected by the activators' initial pH. For example, the reported heat flow (**Fig. 35a**) was 12.8, 17.9, and 26.7 (mW/g) for T1-16%, T2-20%, and T3-25%. While for ternary-2 mixtures, the dissolution peaks with activator content of up to 20% were < 15 mW/g within 15 min, while 25.6 mW/g (within 10.8 min) using 25% dosage. After initiation of hydration, a very long dormant period was observed in all ternary mixtures with 16% and 20% dosages and approximately 24.04 h to 26.05 h in T3-25% and T6-25%, respectively. Following this very long induction period, the acceleration period began only in T3-25% (0.47 mW/g) and T6-25% (0.49 mW/g), in which hydration continued. The complete absence of an induction period indicated the rapid formation of precipitates on precursors' surface, which inhibited further reactions (Ionescu, 1999).

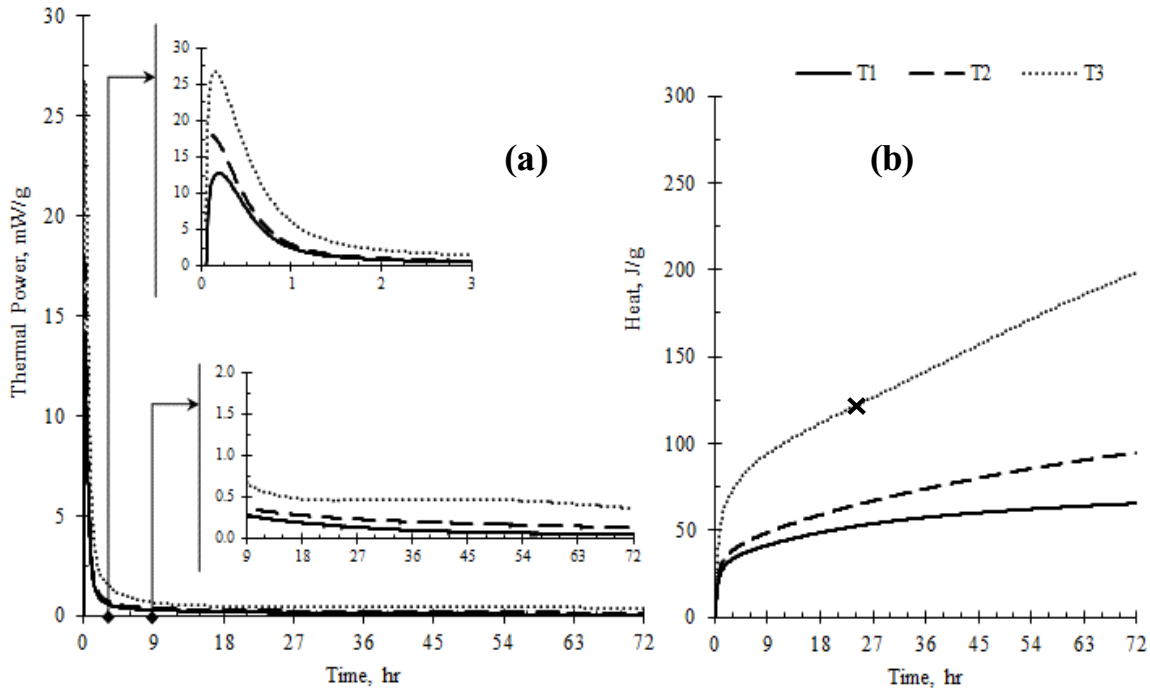


Fig. 35 – Heat evolution of AASCM blends using ternary-1 blend a) Heat of hydration curves and b) Cumulative heat evolution curves

The cumulative heat evolution of all ternary mixtures is shown in **Fig. 35b** and **Fig. 36b**. It is believed that the hydration process of ternary mixtures activated with up to 20% dosage may be divided into two stages (initial dissolution and induction); however, with an additional post-induction stage when using a 25% dosage. The sharp increase in the heat curves correlates to the initial wetting and dissolution of precursors and dry activators after water addition. This was followed by a relatively moderate increase, associated with a very long induction period after the initial stage. The concentration of dissolved ion species increased over this long period and reached

a threshold for the onset of the following reactions (Sun and Vollpracht, 2018). The higher activator content has shortened dormant periods and accelerated early reactions. The continuous dissolution of the ternary system increased the concentrations of ion species in the pore solution, surpassing the concentrations of saturation of hydration products formed. This contributes to the polymerization and condensation of the phases of hydration products, which is explained by the delayed nucleation theory (Huanhai et al., 1993; Shi et al., 2003).

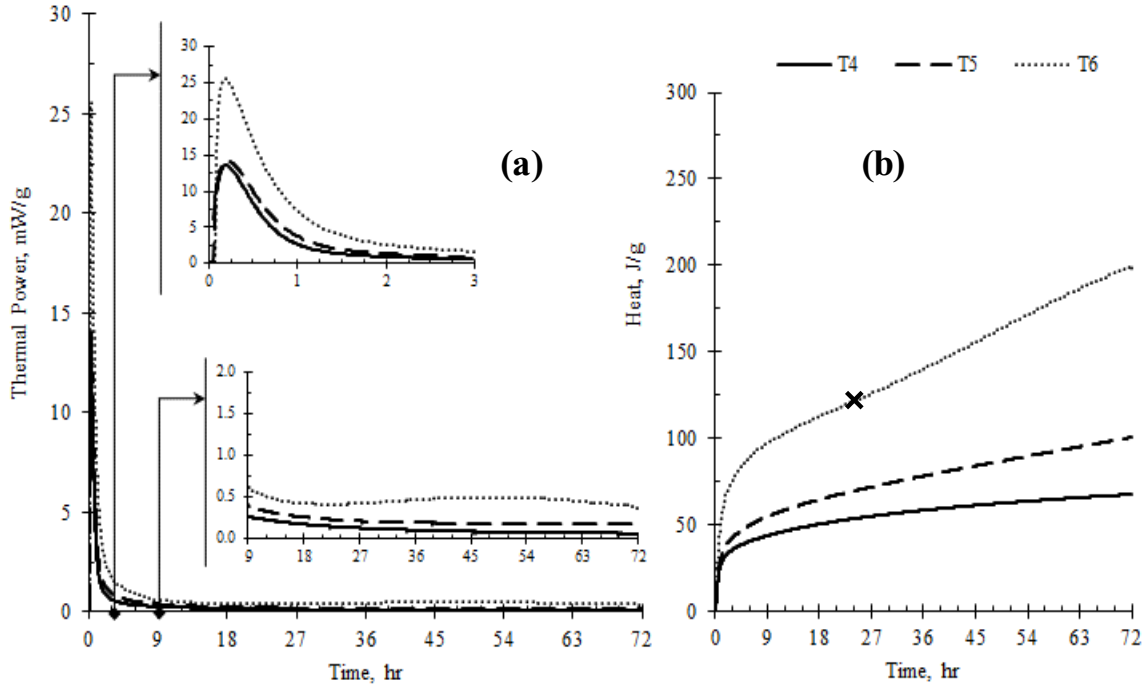


Fig. 36 – Heat evolution of AASCM blends using ternary-2 blend a) Heat of hydration curves and b) Cumulative heat evolution curves

Cumulative heat values were relatively similar in ternary blends (51.9 and 53 J/g) in T1 and T4 using 16% and (109.7 and 109.5 J/g) in T3 and T6 using 25% dosage, respectively. The development of early hydration products was associated with the dissolution of slag, followed by the subsequent formation of hydration products after the contribution of pozzolans, FA, and SF. In ternary-1 mixtures, the relatively high content of Ca^{2+} and Si^{2+} resulted in the infilling and accretion of hydration products on unreacted particles. With free water consumption, hydration products (layers) grew and thickened, mostly causing the full consumption of Ca^{2+} , hindering further reactions, affecting early and late age strength (Gao et al., 2015). Ternary-2 blends exhibited the release of mostly Al^{3+} and Si^{2+} species resulting in the formation of N-A-S-H gel with low bound water compared with C-A-S-H (Duxson et al., 2007; Djobo et al., 2016). Thus, the pore solution conserved water facilitates less porous matrix formation, resulting in better strength.

4.4.2.5. Differential Scanning Calorimetry (DSC)

After the interaction between the precursors and the dry-powder activators with the water, the AASCM mixture's hydration began immediately and was almost completed around 28 days. In a

highly alkaline medium, the formation of C – (N) – A – S – H contributes to the strength of the alkali-activated binders (Bernal et al., 2013). Changes in AAMs' weight after heating mixtures provide information on pore structures' different reaction mechanisms and distinctive characteristics. The DSC patterns of AASCM mixtures with different precursor systems are shown in **Fig. 37**. It can be seen that there was one main heat absorption peak in all mixtures apart from one main exothermic peak in only ternary mixtures.

The endothermic peaks are located between 105°C and 135°C, corresponding to the release of physically bound water together with the dehydration of C-S-H and C-(N)-A-S-H hydration products (Shi et al., 2020). Among all systems, a single slag mixture (i.e., S3-25%) exhibited the highest weight loss in the temperature range of 110-135 °C. In binary-precursor blends of 10% SF and 30% FA, the incremental yet significant mass loss within the 108-127 °C range was associated with releasing the molecular water in the material's pore structure (Shi et al., 2020). In the first ternary set with slag replaced by 33% FA and 7% SF (T3-25% activator dosage), the mass loss occurs predominantly below 110 °C. Similar to the T3 ternary specimen case, the dehydration of binding gel products in T6-25% occurred at the same spot. The exothermic peaks in T3 and T6 were at the position of 412.4 and 418.2 °C. This can be due to the further crystallization or transformation of the corresponding silica-rich gels in mixtures (Bernal et al., 2013).

There was a substantial mass loss in all mixtures before 200 °C, mainly because of the loss of physically bound water in the reaction products. The highest evaporable water content of around 32.3% and 27.3% was recorded in T6 and T3 ternary mixtures with a 25% activator dosage, respectively. This was followed by 19.1% and 18% evaporable water content loss in binary mixtures B3-25% with 10% SF and B6-25% with 30% FA, respectively. Finally, in the single S3 mixture with a 25% activator dosage, there was a slight but detectable evaporable water content of around 14.4%. This indicates that the reaction products are mainly amorphous gels with bound water. Also, the higher the silica content of precursor materials can function as a nucleation site and provide an additional source of reactive silica to help the matrix bind more water.

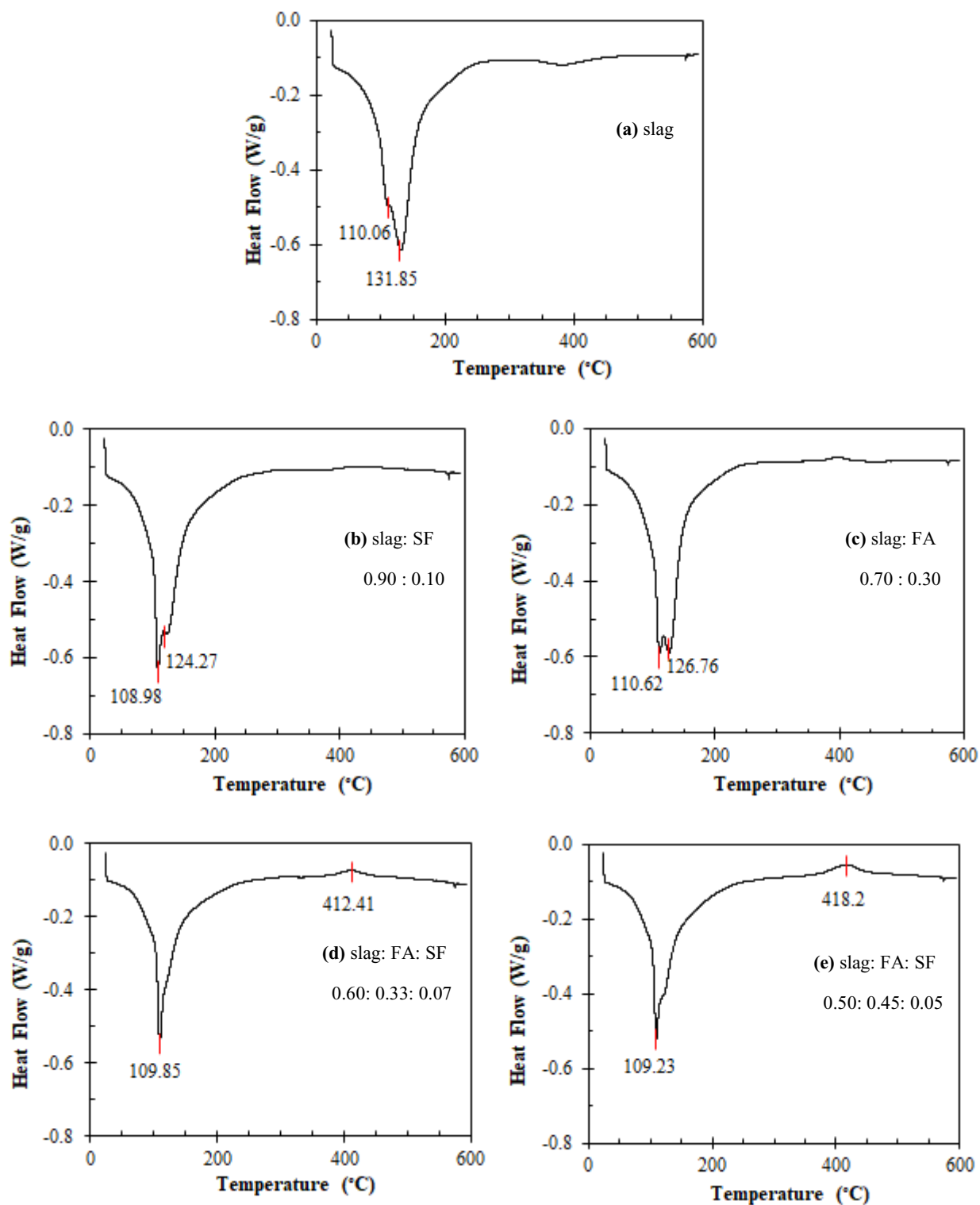


Fig. 37 – DSC curves of various AASCM precursor systems a) single b) binary-SF c) binary-FA d) ternary-1 e) ternary-2

4.5. Concluding Remarks

This chapter aimed to investigate the potential production of dry-powder Alkali-activated SCC mortar mixtures. In addition, it focused on identifying the effect of type and fineness of source materials in addition to the nature and concentration of dry-powder activators. The following conclusions can be drawn from the results of this study:

1. In the absence of a clear methodology for the design of AASCM mixtures, the proper selection of precursor materials, proportions, activator type, and dosage plays a decisive role in the efficient development of AASCM mixtures.
2. The combination of 20% to 25% of Na_2CO_3 and $\text{MetaNa}_2\text{SiO}_3$ activator is considered the optimum to achieve the highest workability and strength values.
3. The workability of AASCC mixtures increased as the percentage of the alkali activator increased by up to 25% in the mortar mixtures due to Na_2CO_3 slow reaction and Na_2SiO_3 deflocculation behavior.
4. Combinations of Na_2CO_3 and $\text{MetaNa}_2\text{SiO}_3$ have accelerated the hardening and strength development of dry-powder AASCC mixtures composing single, binary, or ternary precursor materials extent of their promising behavior for in-situ applications and without elevated heat curing.
5. To overcome the problems associated with the low early age strength, source materials and dry-powder activators should go under a milling process to increase the amorphousness of the particles, enhance the dissolution and reactivity of AASCC mixtures.
6. Calorimetric analysis has shown that generally, there is an almost instantaneous reaction after adding water corresponds to the initial dissolution and wetting of precursor materials. The magnitude of the pre-induction stage peaks depends on the initial pH value, the activator content, the type, and the accompanying anion. Whereas the second exothermic peak of the post-induction stage mainly depends on the precursor materials' chemical composition and the mechanochemical activation process.
7. For the addition group, the highest compressive strength values were achieved using a 25% activator dosage for all AASCM mixtures, except for single-precursor mixtures where up to 20% was appropriate for gels formation. On the other hand, the highest compressive strength was reported in binary mixtures of more than 55 MPa after 28 days compared to ternary and single combinations.

Chapter 5 : Fresh and Mechanical Properties of Ambient Cured One-Part Alkali-Activated Self-Consolidating Concrete

5.1. Overview

Self-consolidating concrete (SCC) is very distinct from conventional concrete. A low yield stress value is required to ensure a minimum flow resistance without aggregates' segregation and excessive bleeding (Ling et al., 2018). The design for SCC systems is sophisticated as it is directly correlated with the binder nature, liquid to powder ratio, and used admixtures (Heikal et al., 2013; Shunsuke and Kazuo, 1999). Furthermore, combining cement with one or more mineral materials is a must to achieve a high powder content. Therefore, SCC requires a comprehensive understanding of its various components and their impacts on the fresh, mechanical, and durability characteristics (Khayat and Hadriche, 2000). Recently, alkali-activated materials (AAMs) were proposed as an alternative binder for ordinary Portland cement (OPC), meeting sustainability and eco-friendly criteria. A wide range of precursors and activators had been used in AAMs productions. In contrast to OPC systems, AAMs demonstrated higher mechanical properties and resistance to aggressive environments (Bernal et al., 2014b; Walkley et al., 2016; Palacios and Puertas, 2004).

Alkali-activated self-consolidating concrete (AASCC) is not widely accepted as cement-based SCC due to the limited data on its rheological and mechanical performance. Many questions have been raised about the main factors influencing the performance of AASCC. The total binder content and type, activator type, dosage, and molar ratio, in addition to admixture type and dosage, were identified as dominating factors (Santana et al., 2020; He et al., 2020). For example, Manjunath and Narasimhan (2018) showed that AASCC mixtures satisfying mechanical and workability requirements by EFNARC guidelines could be produced a high slag content (around 900 kg/m³). Recent studies (Shafiq et al., 2017; Ushaa et al., 2015; Sashidhar et al., 2015; Huseien and Shah, 2020) have shown that the fluidity level of fly ash (FA) based AASCC mixtures decreases as the percentage of ground-granulated blast-furnace slag (GGBFS) substitutes increased. This was attributed to the angular morphology and faster reactivity of GGBFS in a highly alkaline environment. On the other hand, Huseien and Shah (2020) observed that AASCC mixtures' workability improved when GGBFS was replaced by 40%, 50%, and 60% FA. Slag and ceramic waste were also used to produce AASCC; however, flowability decreased as slag content increased (Shafiq et al., 2017).

Moreover, it was reported that the viscosity of the used activator and pH would have a major role. For instance, the high viscosity of sodium silicate activators was found to reduce bleeding and segregation for AASCC (Huseien and Shah, 2020). Also, increasing sodium hydroxide (NaOH) content in the activator solution had an adverse effect on AASCC flowability (Shafiq et al., 2017). Moreover, the high alkaline activator was found to adversely affect the effectiveness of the superplasticizer (SP) (Palacios and Puertas, 2004; Bakharev et al., 2000, Santana et al., 2020). Nematollahi and Sanjayan (2015) have indicated that the different SPs' effect on the workability and strength of the FA-based mixtures mainly depends on the type of activator and SP. For

example, Naphthalene-based SP was an effective type when using an 8 M NaOH solution, whereas modified Polycarboxylate-based SP was the most effective type when a multi-compound activator was used. Moreover, Demie et al. (2013) showed that the FA-based AASCC compressive strength and microstructure characteristics had changed as the SP dosages increased up to 7%. Moreover, adding low SP dosages resulted in a loose and porous interfacial transition zone (ITZ) and consequently reduced compressive strength and vice versa.

5.2. Research Significance

AASCC combines the benefits of both self-consolidating concrete (SCC) and sustainable development. In light of earlier studies' results, the present chapter aimed to examine the potential production of one-part AASCCs mixtures against the backdrop of identical OPC mortar characteristics. Also, it is intended to explore the effects of the nature, concentration, and combination of various source materials and dry-powder activators on AASCC fresh and hardened properties cured under ambient curing conditions. Concrete mixtures were developed by incorporating different dosages of dry-powder activators. The influences of activator dosage and binder composition on the fresh (slump flow, L-box passing ability, and segregation index) and mechanical properties were critically assessed in terms of experimental findings.

5.3. Experimental Program

5.3.1. Materials Characterization

Ground granulated blast furnace slag (GGBFS) was used as the main precursor to produce single, binary, and ternary AASCC. Fly ash Class-F (FA) and silica fumes (SF) were added with different weight percentages as a replacement for GGBFS. For all AASCC mixtures, a combination of two dry-powder activators was used to activate the source materials, namely, anhydrous sodium metasilicate (Na_2SiO_3) and sodium carbonate (Na_2CO_3). The used Na_2SiO_3 had a molar ratio of 1.0 and a density of 1.09 g/cm^3 . The Na_2CO_3 powder had $\geq 99.5\%$ purity and a density of 2.53 g/cm^3 . Natural siliceous sand with a fineness modulus of 2.5, a specific gravity value of 2.68, and water absorption of 1.5% was used. Furthermore, coarse aggregate with a maximum nominal size of 19mm, a specific gravity value of 2.71, and water absorption of 0.4% was used. Their volumetric contents were set to 60% and 40%, respectively.

5.3.2. Sample Preparation

This study used various combination levels of precursor materials (i.e., single, binary, and ternary) to produce different AASCC systems. The total binder content was kept constant at 525 kg/m^3 , providing a relatively high fine content (paste volume of $381\text{--}448 \text{ l/m}^3$), complying with the SCC design guidelines (EFNARC, 2005). For all mixtures, the dry-powder activator was added at three levels (i.e., 16, 20, and 25% by mass of the precursor material). The levels were chosen based on several trial-and-error tests until reaching those levels that provide sufficient alkalinity without efflorescence. The water-to-binder (w/b) ratio was fixed at 0.40 by the mass of the binder. Detailed information on the proportions for all mixtures is presented in **Table 14**. Before adding water to the mixtures, all solid materials (i.e., aggregates, binders, and activators) were initially mixed for

about 1 min. Then, water was added to the mixture, and all the ingredients were mixed for around 3 min until having a homogenous mixture.

5.3.3. Mixtures Designations

The AASCC mixtures were divided into three groups: single-precursor, binary-precursor, and ternary-precursor groups. The single-precursor mixtures with 100% slag are designated as (S) mixtures. Two binary-precursor concrete groups were tested: i) mixtures with 90% slag and 10% SF, with a designated code (B1); and ii) mixtures with 70% slag and 30% FA with a designated code (B2). Two ternary concrete groups were tested: i) mixtures with 60% slag, 33% FA, and 7% SF with a designated code (T1); and ii) mixtures with 50% slag, 45% FA, and 5% SF, with a designated code (T2).

The main varying parameter between concrete mixtures in the same group is the activator's content (i.e., 16, 20, and 25%). The activator was prepared by mixing an equal percentage of the two powder activators (i.e., sodium Metasilicate (Na_2SiO_3) and sodium carbonate (Na_2CO_3)). Therefore, the mixtures' identification used is M-xx, where M is the mixture group (S, B, or T), and xx is the $\text{MetaNa}_2\text{SiO}_3 + \text{Na}_2\text{CO}_3$ activators %. For example, S2-20% represents the mixture with single slag precursor material and 10% $\text{MetaNa}_2\text{SiO}_3 + 10\%$ Na_2CO_3 activators.

Table 14 – Mixture's proportions of the different AASCC systems

Class	Mixture I.D.	Slag, kg/m ³	FA, kg/m ³	SF, kg/m ³	Sand, kg/m ³	CA, kg/m ³	Paste vol., L/m ³
Single	S-16	525	0	0	661	830	438
	S-20	525	0	0	654	830	441
	S-25	525	0	0	646	830	444
Binary-1	B1-16	472.5	0	52.5	652	835	440
	B1-20	472.5	0	52.5	652	830	442
	B1-25	472.5	0	52.5	652	825	443
Binary-2	B2-16	367.5	157.5	0	641	845	440
	B2-20	367.5	157.5	0	637	845	442
	B2-25	367.5	157.5	0	637	840	443
Ternary-1	T1-16	315	173	37	629	845	445
	T1-20	315	173	37	625	845	446
	T1-25	315	173	37	625	840	448
Ternary-2	T2-16	289	210	26	629	845	445
	T2-20	289	210	26	625	845	446
	T2-25	289	210	26	624	840	448

Note: SF = silica fume, FA = Fly Ash, and CA = coarse aggregate

5.4. Testing Program

A total of fifteen AASCC mixtures were prepared with various contents of precursors (GGBFS, FA, and SF) and activator concentrations ($\text{MetaNa}_2\text{SiO}_3$ and Na_2CO_3) based on the preliminary results of mortar mixtures found in Chapter 3. For the 15 mixtures, the total binder content was kept constant at 525 kg/m^3 , providing a relatively high volume of fine content (paste volume of $381\text{--}448 \text{ l/m}^3$), complying with the SCC design guidelines (EFNARC, 2002). The water-to-binder ratio (w/b) was fixed at 0.40 for all mixtures (**Table 14**). The rheological attributes were evaluated based on EFNARC (2002) guidelines shown in **Table 15**. Also, a visual inspection was used as a secondary quality control measure to ensure no segregation and no bleeding for the tested mixtures. The hardened characteristics, including compressive strength, ultrasonic pulse velocity (UPV), bulk electrical conductivity test, sorptivity, and permeable pores tests of the produced mixtures, were assessed at different ages. At last, any mixture that maintains the ability to meet the fundamental fresh and hardened requirements were considered for further durability assessments under an external sulfate attack condition.

Table 15 – EFNARC acceptance criteria for Self-Compacting Concrete

Property	Test Method	Unit	EFNARC Range of Values	
			Minimum	Maximum
Filling Ability	Slump flow	mm	650	850
	T_{500}	sec.	2	5
Passing Ability	L-box	(H_2/H_1) ratio	0.8	1.0
Segregation Resistance	Stability test	%	0	15

5.4.1. Fresh Properties

5.4.1.1. Filling Ability (Unconfined Flowability)

The slump flow test was used to measure the horizontal free flow of the SCC mixtures. AASCC mixtures were poured into a standard slump cone without consolidation. The mean diameter of the concrete spread (measured in two perpendicular directions) and the time needed for the concrete to spread 500 mm (T_{500}) were measured at the end of a slump test (**Fig. 38**).

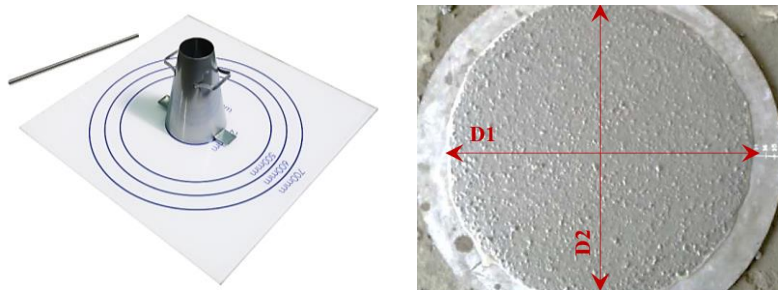


Fig. 38 – Slump flow test equipment and measurements

The EFNARC (2005) Guidelines proposed a classification of the concrete's slump flow values; SF1 ranges from 550 mm to 650 mm, SF2 from 660 to 750 mm, and SF3 from 760 to 850 mm. At >850 mm, the concrete might segregate, and at <500 mm, it may be difficult for the concrete to flow in a highly congested reinforcement. It was reported by the ACI-237 that the longer the time (i.e., $T_{500} \geq 5s$) needed by the mixture to spread, the higher the viscosity level of the mixture.

5.4.1.2. Passing Ability

According to EFNARC guidelines, the L-box test would evaluate SCC mixtures' self-leveling characteristics in terms of their passing ability through vertical reinforcement bars. The L-box test consists of an 'L' shape rectangular-section box separated by a moveable gate (Fig. 39), in front of which (3x the maximum aggregate size) vertical reinforcement bars. Both the EFNARC guidelines and the ACI Committee 237 had specified the minimum h_2/h_1 ratio to be 0.8 following Eq. 7 and Eq. 8. The nearer this ratio to 1.0, the better the flow potential of the mixture.

$$h_1 = 600 - H_1 \quad \text{Eq. 7}$$

$$h_2 = 150 - H_2 \quad \text{Eq. 8}$$

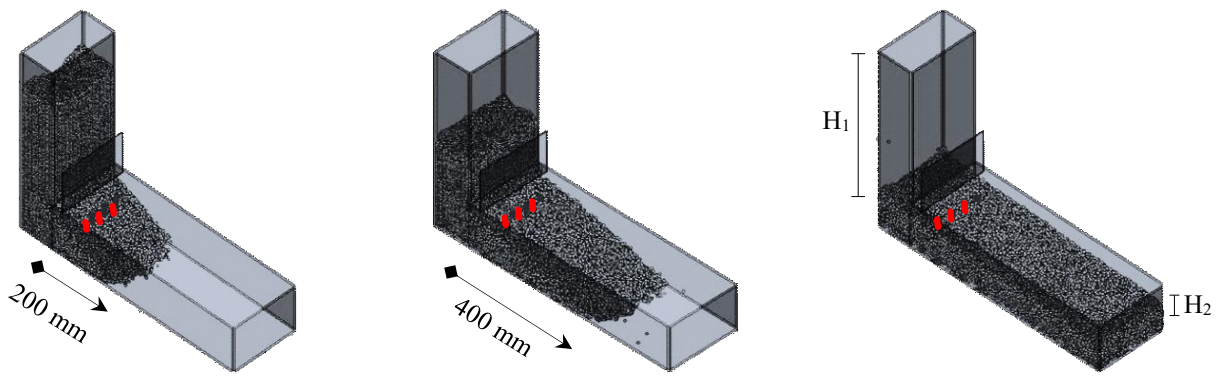


Fig. 39 – Illustration of the L-box test

5.4.1.3. Segregation Resistance

The GTM screen stability test was conducted according to EFNARC 2005 specifications to evaluate AASCC mixtures' stability and segregation resistance. For the GTM technique, 2-L fresh concrete is poured over a 5-mm mesh, and determining the mortar's mass passing through the mesh after 5 min. The passing mortar ratio relative to the original concrete sample (Eq. 9) is identified as the segregation index (SI). For concrete to be stable, the SI value must be less than 5% as shown in Table 16 (EFNARC, 2005). However, the 5% index limit is believed too sensitive, and a threshold of 10% seems more representative.

$$SI = \frac{\text{Mortar volume passing 4.75 mm mesh}}{\text{Total concrete volume (2L)}} \quad \text{Eq. 9}$$

Table 16 – Sieve stability test in terms of SI % according to EFNARC guidelines

Segregation Index (SI), %	Criteria
< 5	Too cohesive or viscous mixture.
5 – 15	The optimum amount of resistance to segregation.
15 – 30	Likely to be susceptible to segregation.
> 30	Likely to be susceptible to severe segregation.

5.4.1.4. Visual Stability Index (VSI)

The VSI, as per ASTM C1611, is a technique for evaluating the relative stability of SCC mixtures based on the specific visual properties of their flow spread. To distinguish the texture and homogeneity of various AASCC mixtures, the slump flow was qualitatively ranked according to a set criterion provided in **Table 17**. AASCC mixtures were assigned stable and suitable for the intended practice if the VSI rating is 0 or 1.

Table 17 – Visual stability index (VSI) rating in accordance with ASTM C1611

Rating	VSI value	Criteria
0	Highly stable	No evidence of segregation in slump flow patty, mixer drum, or wheelbarrow
1	Stable	No mortar halo in slump flow patty, but some slight bleeding on the surface of the concrete in mixer drum or wheelbarrow
2	Unstable	Slight mortar halo (< 10 mm) in slump flow patty and a noticeable layer of mortar on the surface of testing concrete in mixer drum and wheelbarrow
3	Highly unstable	Clearly segregating by evidence of massive mortar halo (> 10 mm) and a thick layer of mortar or bleed water on the surface of testing concrete in mixer drum or wheelbarrow

On the other hand, a VSI rating of 2 or 3 indicates the potential of the mixture to segregate. The VSI is considered a static stability index when it is examined in a wheelbarrow or even a concrete mixer at rest time (static condition). However, it can be viewed as a part of the dynamic stability of SCC, knowing that concrete can show some non-uniform texture during the transport of fresh concrete.

5.5. Hardened Properties

5.5.1. Compressive Strength Development

The mechanical properties in terms of the compressive strength of concrete mixtures were evaluated following ASTM-C39 (Standard Test Method for Compressive Strength of Cylindrical Concrete Specimens). For each concrete mixture, cylindrical specimens with dimensions of 100 mm x 200mm were cast (**Fig. 40**). After casting, cylinders were covered with a plastic lid to prevent water loss. The specimens were de-moulded after 24h and cured at the ambient laboratory conditions until the testing age. At each testing ages 3, 7, 28, and 90 days at least two specimens were tested.

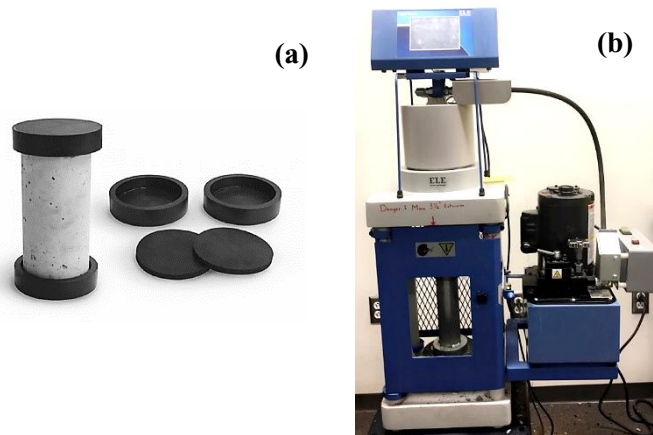


Fig. 40 – (a) Cylinder specimens and (b) A hydraulic testing

5.5.2. Ultrasonic Pulse Velocity and Electrical Resistivity

Ultrasonic pulse velocity (UPV) measurements are used to evaluate the concrete homogeneity, presence of (cracks, voids, or imperfections), and changes in properties over time. The UPV test results' interpretation is based on the quality of the concrete samples tested in terms of the occurrence or absence of inner cracks and flaws, using the values given in **Table 18**. Electrical resistivity was measured following the ASTM C1760. Higher electrical resistivity values indicate high concrete quality with low corrosion potential, according to ACI 222R. Direct measurement of UPV and electrical resistivity were conducted on cylinders with dimensions 100 x 200 mm at ages of 28 and 90 days.

Table 18 – Interpretation of the UPV and electrical resistivity results

IS:13311-part 1-1992		ACI-222R	
Pulse Velocity (m/s)	Concrete Quality	Resistivity (kΩ.cm)	Corrosion Protection
Above 4.5	Excellent	Above 20	Very High
3.5 to 4.5	Good	10 to 20	High
3.0 to 3.5	Medium	5.0 to 10	Moderate to Low
Below 3.0	Doubtful	Below 5.0	Low

5.5.3. Permeable Pores and Sorptivity

The permeable pores test was performed following ASTM C642 to assess the concrete microstructure development. According to ASTM C1585, the water sorptivity test measures the waterfront's mobility rate in capillary suction through concrete mixtures. Both tests were performed to evaluate concrete water permeability as an indirect indicator for other aggressive environments. For each AASCC mixture, three disc specimens with a diameter of 100 mm and a height of 50 mm were used. Permeable pores and sorptivity tests were conducted at 28 and 90 days of age.

According to the ASTM C642 standard, the water absorption and volume of permeable pores in concrete mixtures were measured. The test specimens were oven-dried at a temperature of 110 °C for about 24h. Specimens after that cooled in a desiccator, and the oven-dry mass was recorded. After that, a specimen was immersed in a water container at an ambient temperature of the laboratory. After immersion for 48h, specimens were surface dried and weighed. The saturated specimen was immersed in water and allowed for about 5h boiling. After cooling, SSD mass was measured, and the mass of the specimen underwater was measured. The volume of permeable pores was calculated in **Eq. 10**, where A is the oven-dried mass in the air (g); C is the surface-dry mass in the air after immersion and boiling (g) ; D is the suspended specimen mass in water after immersion and boiling (g).

$$\text{Volume of permeable pores} = \frac{C-A}{C-D} \times 100 \quad \text{Eq. 10}$$

For the sorptivity test, the disc samples were pre-conditioned in an oven at 110 ± 5 °C for about 24h before the measurements of capillary sorption were carried out. After that, specimens were removed from the oven to cool down then the disc side was sealed with vinyl tape. In a plastic container, support was placed in the bottom and water-filled the bowl to about 5 mm above the support, as seen in **Fig. 41**. Electronic balance with an accuracy of 0.001 g was used to measure the mass change of the specimens with time. Mass was measured at intervals of 1, 2, 5, 9, 15, 20, 30, and 60 minutes up to 7 days from the first contact of the samples with water. The calculated capillary suction depth versus the square root of time was used to estimate the initial and secondary sorptivity index.

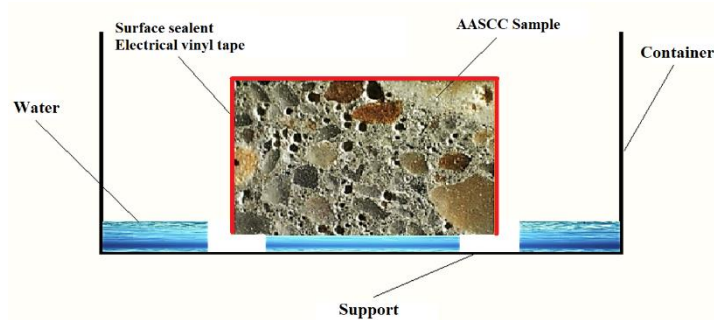


Fig. 41 – Schematic representation of the Sorptivity test procedure

5.5.3. Microstructural Analysis

X-ray diffraction (XRD) was conducted using a Bruker D8 Advance diffractometer (Cu K α radiation, 1.5406 Å) with an imaging plate detector to collect data from $10^\circ < 2\theta \leq 90^\circ$. Also, solid-state ^{29}Si MAS nuclear magnetic resonance (NMR) spectra were collected on a Bruker, Avance III HD 400 MHz spectrometer with a high-power ^1H decoupling. The spectra were obtained at a spinning speed of 10 kHz and with a delay of 5 s. Representative samples from selected specimens were crushed, ground, and sieved. Powder samples $< 75 \mu\text{m}$. Were used in both XRD and ^{29}Si NMR. Scanning electron microscopy (SEM) analysis was conducted on small chunks from selected specimens using a Hitachi S-3400N SEM at 15.0 kV accelerating voltage. This was

coupled with energy dispersive X-ray analysis (EDX) using a JEOL 35-cf spectrophotometer for elemental mapping and spot analysis.

5.6. Results and Discussion

5.6.1. Fresh Properties

5.6.1.1. Filling Ability

In terms of unconfined flowability, the slump flow and T_{500} test results for all AASCC mixtures are reported in **Table 19**. For all tested mixtures, increasing the activator dosages increased the slump. For AASCC single-precursor mixtures, S-25% was the only mixture that met the EFNARC-requirements (i.e., > 550 mm). Increasing the activator dosage from 16% to 20% had resulted in a considerable increase in slump flow from 30 mm to 510 mm for single-precursor mixtures; however, it was still below the SF1 class. The continuous dissolution of slag particles instigated the silicate and carbonate anions in the medium to be adsorbed on the slag surfaces as Ca^{2+} cations shield the slag silanol groups. This could lead to strong electric double layer repulsive forces between slag particles and particle separation, resulting in yield stress reduction. These results are in good agreement with (Kashani et al., 2014).

Table 19 – Fresh Concrete properties results for AASCC mixtures

Mixture I.D.	Slump flow diameter, mm	Slump flow rate (T_{500}), s	L-box ratio, h_2/h_1	Segregation Index (SI %)
S-16%	30.00	---	0.55	0.00
S-20%	510.00	4.60	0.65	2.00
S-25%	690.00	2.02	0.85	5.00
B1-16%	443.00	13.60	0.55	2.00
B1-20%	448.00	8.82	0.55	7.00
B1-25%	583.00	3.05	0.75	7.00
B2-16%	698.00	2.44	0.88	15.00
B2-20%	795.00	1.41	0.94	17.00
B2-25%	833.00	1.13	1.00	27.00
T1-16%	718.00	2.66	0.88	8.00
T1-20%	768.00	2.10	0.90	17.00
T1-25%	828.00	1.45	0.98	25.00
T2-16%	705.00	2.63	0.85	20.00
T2-20%	798.00	1.84	0.95	28.00
T2-25%	830.00	1.10	0.99	30.00

A similar trend was observed in binary-precursor mixtures while replacing slag with 10% SF. For example, in the B1 group, the addition of 16, 20, and 25% activator dosage increased the slump flow values from 443 mm to 448 mm and 583mm, respectively. In the B1 group, replacing slag with 10% SF resulted in higher negative values for zeta potential and elevated the pH to a higher level. Cations such as Ca^{2+} were released during slag dissolution, where it is more prone to adsorb on slag particles' silanol groups, resulting in attraction forces. It also caused the rapid formation of C-A-S-H gels and some electrostatic bonding, which led to substantial changes in the fresh

properties. Conversely, B2 binary-precursor mixtures with 30% FA replacing slag showed higher slump flow diameter values. For example, increasing the activator dosage from 16% to 25% resulted in a 19% increase in the achieved flowability (> 800 mm). All ternary-precursor mixtures in both groups had the best overall performance following the 550 to 850 mm flow range in EFNARC-guidelines with lower-viscosity levels. The filling capacity of these AASCCs remains high (i.e. > 700 mm) beside the low viscosity levels (i.e. $T_{500} < 3.0$ s). Moreover, for T1 and T2 mixtures increasing the activator from 16% to 25% resulted in about 15% and 18% increase in the flowability, respectively.

Overall, binary and ternary mixtures incorporating $\geq 30\%$ FA and using the lowest activator dosage were within the second class (SF2) as per the EFNARC classification. Concrete mixtures in the SF2 class are suitable for many applications with excellent surface finishing and controlled segregation resistance. However, it can be concluded that replacing slag with 10% SF at the highest activator dosage in B1 mixtures decreased the slump flow values and shifted the mixture to the slump flow SF1 class (**Fig. 42**). In the case of highly congested concrete reinforced structures, using a B1 mixture is critical. Conversely, as the FA ratio increased by up to 50% along with a 20% activator dosage, the mixtures tended to achieve the slump flow class SF3. This means better surface finishing characteristics would be obtained from a set of mixtures containing less slag, but it would be harder to overcome the segregation, as explained later.

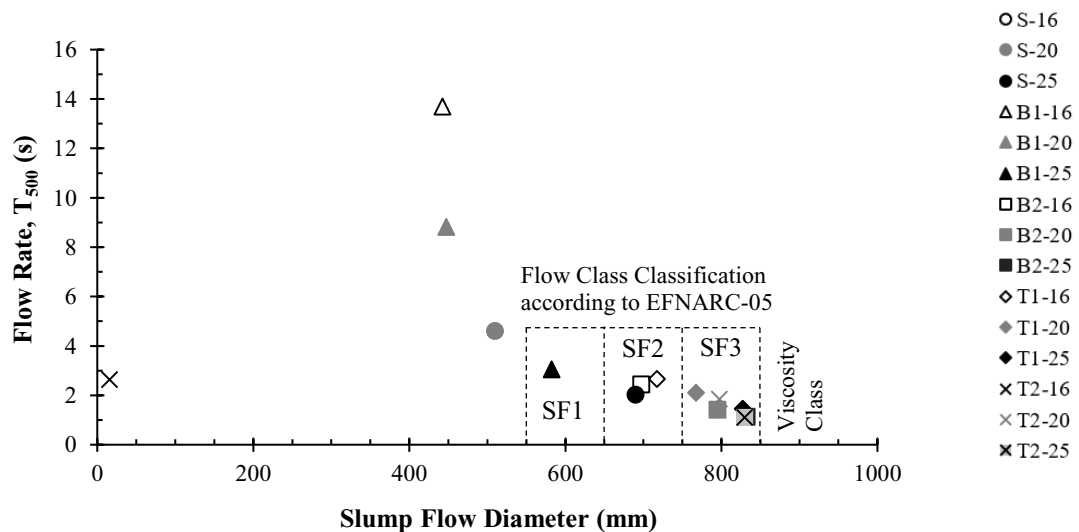


Fig. 42 – Relation between a slump and slump flow rate

5.6.1.2. Passing Ability (Confined Flowability)

Generally, all AASCC mixtures prepared with a high dry-powder activator dosage (i.e., 25%) exhibited better passing ability than those made with lower contents (**Table 19**). For AASCC single-precursor mixtures, changing the activator dosages from 16% and 20% did not change the L-box test result (≤ 0.65), while 85% was achieved with 25% activator dosage.

Mixtures B1-16% and B1-20% showed a noticeable blocking at an L-box ratio of 0.55. However, B1-25% reported better performance, with a 36% increase in the measured blocking ratio. The

second set of binary mixtures showed a better passing ability value as 30% FA is used. The blocking ratio of the B2 mixtures set ranged from 0.88 to 1.00 as the activator dosage increased, meeting EFNARC guidelines (i.e., blocking ratio between 0.80 and 1.00). All ternary-precursor mixtures exhibited similarly blocking ratios > 0.85 (Fig. 43), which are greater than the EFNARC guidelines for concrete mixtures vulnerable to blocking around reinforcement bars (i.e., < 0.8). Thus, ternary-precursor mixtures showed excellent flowabilities and deficient viscosity levels, suitable for congested reinforcement structures. This is consistent with prior slump flow results (Fig. 42), which showed that increasing the activator dosage reduced plastic viscosity and yield stress, improving the rheological properties.

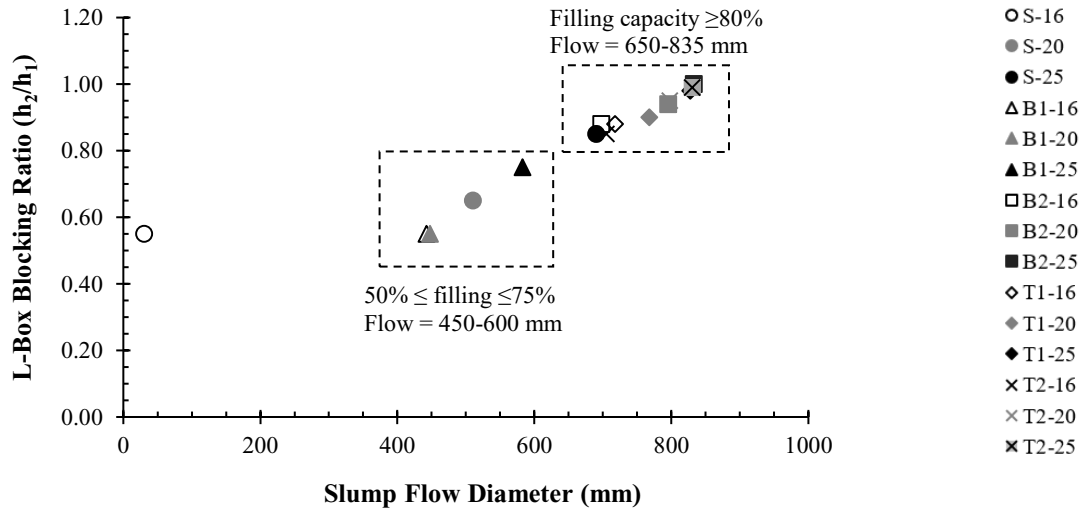


Fig. 43 – Relation between slump and L-Box blocking ratio

5.6.1.3. Segregation Resistance

Table 19 presents the segregation resistance test results for all AASCC mixtures. Results were visually examined and ranked by the segregation index (SI%) in Fig. 44. Test results of various mixtures showed three zones; resistant, tend to segregate, and severely segregated AASCC mixtures, divided by lines reflecting the suggested values. Generally, all mixtures exhibited good passing ability with a segregation potential as the activator dosage increases. However, an exception was observed in single-slag mixtures with 16% and 20% activator dosages and binary B1 (slag-SF) mixtures. For instance, the segregation potential increased marginally by about 5% as the activators' dosages increased in the single-precursor mixtures. However, all B1 binary-precursor mixtures were found viscous. The SI was about 7% even when the activator dosage increased from 20% to 25%.

On the contrary, B2 mixtures containing 367.5 kg/m^3 of FA replacing slag tended to be segregated SI~15 to 30%. For example, the B2-16% mixture resulted in $\text{SI} = 15\%$, which is less than 12% provided by B2-20%. However, B2-25% reported a higher segregation potential, with about an 80% increase in the measured stability ratio compared to B2-16%. Adequate segregation resistance is achieved as SI is below 15% as per the EFNARC guidelines. For the two sets of ternary-precursor mixtures, most of the mixtures exhibited a high potential for segregation. The

segregation resistance increased by 212.5% as the activator dosage increased to 25% in T1-AASCC, while it increased by 50% in T2-AASCC mixtures.

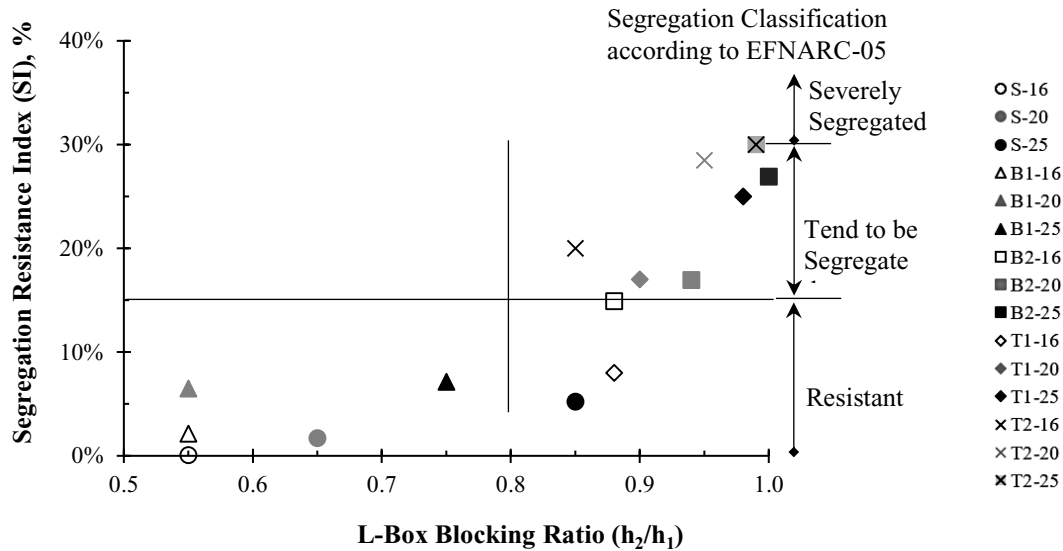


Fig. 44 – Relation between segregation resistance and l-box blocking ratio

Overall, mixtures designed with binary and ternary precursor mixtures and higher activator dosages tend to have higher segregation potentials when slump flows are greater than 700 mm. Thus, there is a clear relationship between resistance to segregation and activator dosage compared to precursor combination effects. Increasing the activator dosages (carbonate/silicate) had a positive effect on reaction kinetics retardation. The inclusion of sodium metasilicate had raised the magnitude of zeta potential and lowered the yield stress of the AASCC by increasing the double layer repulsive forces, in addition to the carbonate ions effect. It is important to note that such visual observations are insufficient but remain suitable to estimate the AASCC stability visually. This test was coupled with slump flow and l-box tests in the following sections.

5.6.1.4. Effects of Selected Activator and Dosage

The type and dosage of alkaline activators and their combination fundamentally affect the fresh characteristics of AASCC mixtures. When the activator dosage increased from 16% to 25%, the slump flow diameter and the passing ability increased synchronously for all AASCC mixtures Fig. 45 (a). This can be ascribed to the retardation in the reaction kinetics as the fraction of sodium carbonate/silicate activators increased (Bernal et al., 2015). The activator's efficiency and pH value significantly affect the initial dissolution of source materials and the prolonged condensation reactions (Lothenbach and Gruskovnjak, 2007; Shi and Day, 1996). The most commonly used activators for the alkali activation process are sodium hydroxide and sodium silicate (water glass) due to their high alkalinity potential (Yan et al., 2021). While sodium carbonate (Na_2CO_3) yields a lower early-age strength due to its lower pH potential. Therefore, the activation with Na_2CO_3 would delay the formation of early age strength-gaining products (Atiş et al., 2009). This can be due to the fast reactions between the dissolved calcium ions (Ca^{2+}) from slag with sodium and carbonate (CO_3^{2-}) ions from the activator before the formation of C-(N)A-S-H gels (Bernal et al., 2015). Thus, delayed initial reactions would affect the mixtures' workability results.

On the other hand, the use of synthetic silica chemicals such as anhydrous sodium metasilicate (Na_2SiO_3) resulted in better workability and high strength values for slag and FA one-part mixtures as reported previously (Nematollahi et al., 2015). This is attributed to the anhydrous metasilicate particles being not fully dissolved, which significantly reduces the yield stress at early ages, improving workability (Landrou et al., 2016). Hence, the combination of sodium metasilicate and Na_2CO_3 is recommended to enhance AASCC workability. The relationship between the slump flow diameter and the segregation resistance index derived from the different AASCC mixtures using up to 25% dry-powder activators is shown in **Fig. 45b**. There are easy ways to prevent segregation and maintain the homogeneity of OPC-SCC mixtures without the use of chemical admixtures, according to the EFNARC guidelines. For example, increasing the fine material's content, decreasing the coarse aggregate content, and lowering the water-to-powder ratio (w/b) (Okamura and Ouchi, 2003). The addition of activator powder over a constant binder content in AASCC mixtures was expected to influence the plastic viscosity and consequently mixture segregation resistance. However, the current study's values indicated an inversely proportional relationship between the amount of dry-powder activator and the segregation resistance percentage, more precisely in binary and ternary-precursor mixtures with FA. The higher the water-to-binder ratio due to FA's low reactivity and activator dosage, the higher the segregation potential.

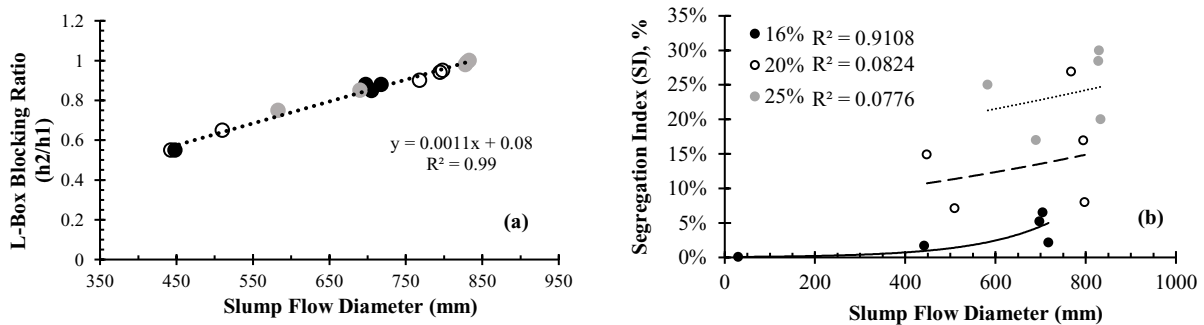


Fig. 45 – The effect of activator dosage on the relation between a) slump flow and l-box ratio h_2/h_1 b) slump flow and SI%

5.6.1.5. Effect of Precursor Combination

The lack of effective chemical admixtures to enhance the flowability of one-part AASCC mixtures necessitates proper precursor materials to ensure that the rheology of SCC mixtures is stabilized. In binary and ternary systems, slag replacement with different SF or FA ratios can adjust the particle size distribution of the binder materials. The systems' initial porosity would also be adjusted and reduced, improving the fresh concrete's workability. **Fig. 46 (a and b)** shows the effect of replacing slag with SF and FA in different binary and ternary systems on the slump flow and segregation resistance within the first hour from the time of mixing. AASCC mixtures containing slag $>400 \text{ kg/m}^3$ and activated with $>20\%$ activator dosages achieved satisfactory values in the EFNARC-2005 guidelines. On the other hand, the use of binary and ternary precursor blends in AASCCs showed significantly better workability than slag-precursor mixtures with an activator dosage of at least 16%. However, binary and ternary precursor blends tended to segregate

due to their particle size, morphology, and bulk density variations compared with slag-based mixtures. Generally, the spherical morphology of FA is preferable for achieving higher workability and lower water content mixtures (Bernal et al., 2014b).

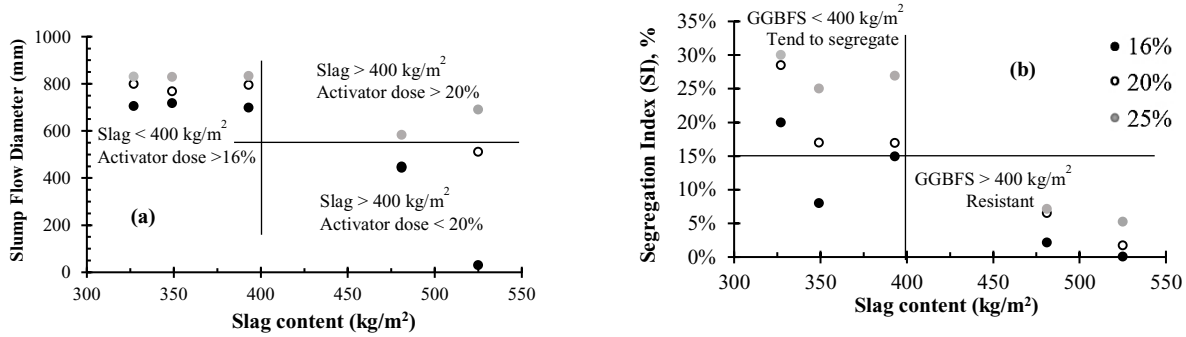


Fig. 46 – The effect of slag content, kg/m² on the a) slump flow diameter, mm and b) segregation resistance SI, %

5.6.2. Hardened Properties

5.6.2.1. Compressive Strength Development

The compressive strength results of single-precursor AASCC mixtures are shown in **Fig. 47**. At ages 3 and 7 days, mixture S-25% exhibited the highest compressive strength values (i.e., 26.5 MPa (3843.5 psi) and 35 MPa (5076.32 psi), respectively). Increasing the activator dosage from 16% to 25% resulted in about 121% increase in the strength value. This can be attributed to the fact that alkali-activated slag mixtures' strength progression is speedy due to the spontaneous reaction at the very early hydration stage. As the activator dosage increases, the pore solution retains higher Si²⁺ and Na⁺ concentrations, accelerating the C-S-H precipitation process (Gebregziabihier et al., 2015; Gruskovnjak et al., 2006). A similar trend was obtained at age 28 days due to the continued microstructural growth contributing to strength development. A mixture achieved the highest 90-day strength with a 25% activator dose of approximately 46.3 MPa (6715.25 psi) compared to S-20% (26 MPa or 3770.9 psi) and a 16% activator dose (22 MPa or 3190.8 psi), respectively. The high activator dosage is responsible for the high pH, silicate, and carbonate ions in the system resulting in continuous reactions with Ca²⁺ ions from the slag leading to precipitation of C-A-S-H. These results are in good agreement with (Fernández-Jiménez and Puertas, 2003), where the main factor affecting the alkali-activated slag mixture's mechanical characteristics is the type of anion accompanying the activators after the high pH value. This would lead to the formation of stable hydration products.

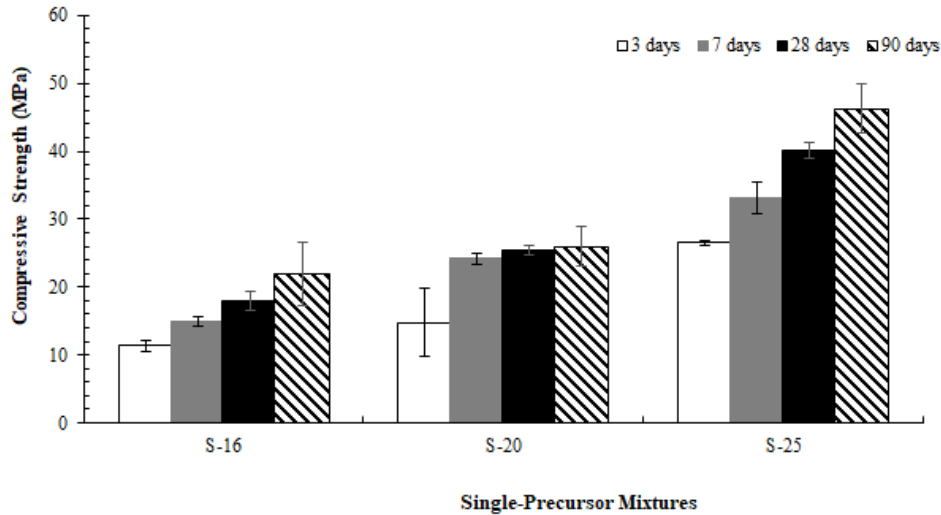


Fig. 47 – Compressive strength results for the AASCC single-precursor mixtures

Fig. 48 shows the compressive strength values for the binary-precursor mixtures. Similar to the single-precursor mixtures, the highest strength was achieved at the highest activator dosage regardless of the combination of the binary precursor. For instance, at age 3 days, the B1-16% mixture achieved around 6 MPa (870.2 psi), while a sharp increase in strength to 24.4 MPa (3538.9 psi) and 24.7 MPa (3582.4 psi) as the activator dosage increased to 20% and 25%, respectively. After 7 days, B1-25% achieved the highest strength at 36 MPa or 5221.4 psi (i.e., almost double that of B1-16%). At 28 days, both the B1-16% and B1-20% revealed almost similar strength values (i.e., around 33 MPa or 4786.3 psi) while S-25% exhibited 49.5 MPa (7179.34 psi). It is noteworthy that the mechanical performance of AASCC binary mixtures was improved by replacing slag with SF. This is in line with the previous studies (Kim and Kang, 2020; Alanazi et al., 2019; Cheah et al., 2019; Gülşan et al., 2019; Ramezani pour and Moeini, 2018), which ascribed to SF micro-filling and nucleation effects, leading to a dense matrix.

As for the B2-mixtures set using 30% FA, the increase in strength was gradual as the activator dosage increased at different ages. Similar to the B1-mixtures set, the higher the activator dosage, the higher the compressive strength regardless of age. This confirms that the optimum activator dosage for obtaining the highest compressive strength was 25%. Moreover, at this optimum activator dosage, the single-precursor blend of AASCC achieved the highest strength than B2-25%. This indicated that the difference in chemical composition between slag and FA significantly affected the alkali-activation mechanisms. Also, the high reaction rate of slag-based mixtures due to their nature than to the crystalline pozzolanic nature of FA-based mixtures. According to Ismail et al. (2014), the first cycle of hydration (slag dissolution) releases Ca^{2+} , which is then absorbed into the N-A-S-H type gel formed by FA activation, resulting in a hybrid C-(N)A-S-H gel. During the second cycle of the reaction process, FA was partially dissolved and participated (Puertas et al., 2000).

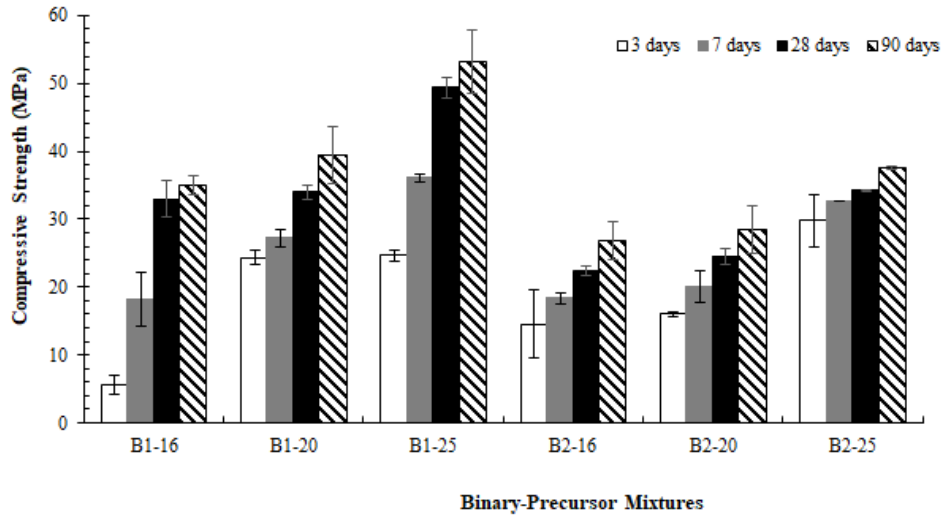


Fig. 48 – Compressive strength results for the AASCC binary-precursor mixtures

The strength development behavior of the two ternary AASCC sets is shown in Fig. 49. All ternary AASCC mixtures demonstrated almost similar strength gain of an average of 81%. In addition, higher activator dosage is evident to possess higher mechanical properties. It was found that the high strength gain of 7 to 28 days instead of 28 to 90 days implies that the reaction rate and intensity are mainly rapid due to the system's high pH (Ding et al., 2016). After 28 days, the strength gained by T1-AASCC mixtures with activator dosage of 16% was (21.9 MPa or 3176.3 psi), 20% (23.5 MPa or 3408.4 psi), and 25% (44.8 MPa or 6497.7 psi), respectively. Similarly, the highest compressive strength value for T2-AASCC mixtures at 28 days was reported using 25% with 39.3 MPa (5699.9 psi). The T1-AASCC mixtures incorporating slag with about 60%, 33% FA, and 7% SF acquired higher late age strength values than in T2-AASCC mixtures after 90 days of age. For instance, the compressive strength values of 50.5 MPa (7324.4 psi) and 42.5 MPa (6164.1 psi), respectively, were achieved by the tested T1-25% and T2-25% specimens.

The lower strength gain in the T2 set than in the T1 set could be due to slag replacement by up to 50% FA and 5% SF, resulting in fewer strength-giving products. It is important to note that alkali-activated concrete's mechanical performance depends on the system's pH value that controls the hydration process. Early production of strength-giving products is driven by rapid reactions at a high pH value > 11.5, which is impossible below pH 9.5 (Song et al., 1999). The higher the activator dosage in a mixture contributed to a higher pH value, which resulted in improved hydration activation capacity and satisfactory mechanical properties (Fernández-Jiménez and Puertas, 2003; Song et al., 2000). On the other hand, several studies confirmed the slower setting rate of the FA compared with slag (Nath et al., 2015; Kumar et al., 2010; Vijai et al., 2010; Sugama et al., 2005). This may be due to the pure slag's high pH value (11.5) relative to pure FA, which was 8.5 (Song et al., 1999). As FA content increased in the AASCC matrix, lower CaO content and higher SiO₂ and Al₂O₃ concentrations resulted in a slower hydration cycle (Huseien and Shah, 2020).

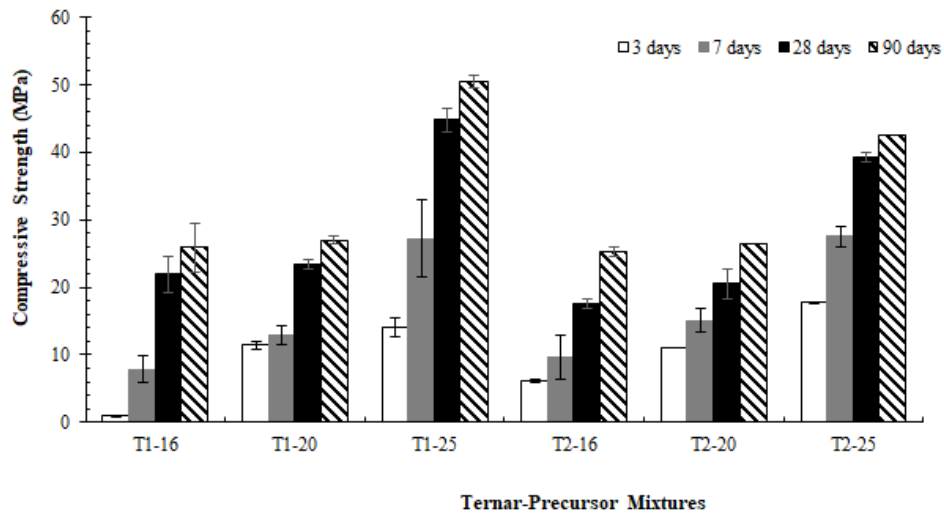


Fig. 49 – Compressive strength results for the AASCC ternary-precursor mixtures

5.6.2.2. Electrical Bulk Resistivity

The electrical resistivity results of AASCC mixtures are shown in **Table 20**. Although, all single-precursor mixtures exhibited high electrical resistivity values, indicating a very high level of corrosion resistance at ages 28 and 90 days. The electrical resistivity is significantly decreased as the dosage of activators increases. For example, S-20% and S-25% achieved resistivity values of 12.5% and 20.3% lower than S-16% at age 28 days. A similar trend was observed after 90 days.

On the other hand, substituting slag with up to 10% SF substantially improved the resistivity of the B1-mixtures. Incorporating 16, 20, and 25% activator dosage in B1 mixtures resulted in a “very high” resistivity level of 44.61, 43.48, and 28.53 k Ω .cm after 28 days of curing, respectively. The resistivity values continued to increase tremendously with time after 28 days, showing about 43%, 30%, 28% increase for mixtures with 16%, 20%, and 25% activator dosage at 90 days. On the other hand, B2-mixtures incorporating 30% FA replacing slag resulted in a “very high” corrosion protection level at age 28 and 90 days. When observing each mixture separately, B2-mixtures exhibited a substantial increase in the resistivity values with (60.84, 57.40, 41.75 k Ω .cm) in B2-16%, B2-20%, and B2-25% after 28 days and, (73.67, 64.21, 58.48 k Ω .cm) at 90 days of age, respectively. This may be attributed to the densified microstructure of B2-mixtures due to slag replacement and the formation of a significant amount of reaction products (Li et al., 2010). Therefore, this reduces the potential for corrosion due to low pore connectivity and migration of ions.

For ternary-precursor mixtures, all mixtures exhibited substantial corrosion resistance at ages 28 and 90 days. For example, mixtures T1-16%, T1-20%, and T1-25% resulted in resistivity values of 13, 21.23, and 26.39 k Ω .cm at 28 days of age, achieving “very high” corrosion protection, respectively. On the other hand, T2-mixtures of up to 45% FA and 5% SF replacing slag attained “very high” corrosion resistance at all ages, except for the T2-16% at 28 days of age belonging to the “high” category. At 90 days of age, the resistivity values tended to increase tremendously. The increase in resistivity values is 51%, 30.3%, and 46% at 90 days than those at age 28 day.

Table 20 – Electrical resistivity test results for AASCC ternary-precursor mixtures

Mixture I.D.	Electrical Resistivity, kΩ.cm		Corrosion Protection
	28 days	90 days	
S-16%	71.10	108.56	Very High
S-20%	62.27	87.50	Very High
S-25%	56.70	76.37	Very High
B1-16%	44.61	63.74	Very High
B1-20%	43.48	56.35	Very High
B1-25%	28.53	36.59	Very High
B2-16%	60.84	73.67	Very High
B2-20%	57.40	64.21	Very High
B2-25%	41.75	58.48	Very High
T1-16%	13.00	25.51	High to Very High
T1-20%	21.23	38.69	Very High
T1-25%	26.39	42.16	Very High
T2-16%	17.65	26.64	High to Very High
T2-20%	22.67	29.54	Very High
T2-25%	26.35	38.37	Very High

According to ACI 222R, the corrosion properties were analyzed based on the bulk electrical resistivity performance, as shown in **Fig. 50**. The electrical resistivity of AASCC mixtures was found to depend on the resistivity of the pore solution. For all AASCC mixtures (i.e., single, binary and ternary), the higher the activator dosage, the lower the pore solution resistivity was observed. This can be due to the pore solutions' highly ionic nature and conductivity as the activator dosage increased, contributing to lower resistivity results (Ma et al., 2016). On the other hand, the precursor combination plays an enormous role in the overall electrical resistivity results. For instance, single and binary precursor mixtures resulted in higher corrosion protection levels than ternary-precursor blends, which were highly ionic and conductive. This is in good agreement with results reported by (Rodríguez et al., 2008; and Ma et al., 2016).

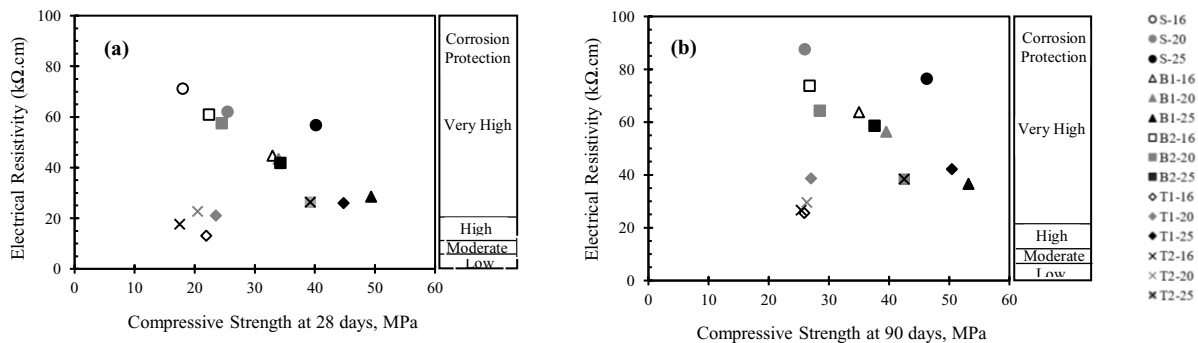


Fig. 50 – Bulk resistivity results for AASCC mixtures at ages a) 28 and b) 90 days

5.6.2.3. Ultrasonic Pulse Velocity (UPV)

The findings of the non-destructive UPV testing of AASCC mixtures using multi-precursor and activator combinations are shown in **Table 21**. For AASCC single-precursor mixtures, the measured UPV values ranged from 3000 to 3500 m/s for S-16% and S-20%, meeting medium quality classification. However, the UPV result significantly increased as the activator dosage increased to 25%, indicating the high homogeneity for the S-25% mixture.

Table 21 – UPV results for AASCC mixtures with up to 25% activator dosage

Mixture I.D.	UPV, m/s		AASCC Quality
	28 days	90 days	
S-16%	3225	3275	Medium
S-20%	3294	3316	Medium
S-25%	3824	3944	Good
B1-16%	3696	3796	Good
B1-20%	3710	3860	Good
B1-25%	4098	4262	Good
B2-16%	3484	3714	Medium to Good
B2-20%	3521	3721	Good
B2-25%	3883	4133	Good
T1-16%	3590	3659	Good
T1-20%	3677	3686	Good
T1-25%	4016	4041	Good
T2-16%	3446	3582	Medium to Good
T2-20%	3472	3594	Medium to Good
T2-25%	3846	3981	Good

UPV is affected by changes in the hardened AASCC matrix due to the activator dosage and the slag replacement ratio. This is better described by considering the results of the two binary-precursor sets and the single-precursor set results. The UPV findings in the B1-AASCC with up to 25% activator dosage were relatively high at 28 and 90 days. For example, B1 mixtures activated at 16%, 20%, and 25% achieved 3696, 3710, and 4098 m/s at 28 days, respectively, with UPV gain of about 3-4% at 90 days. Replacing slag with 30% FA in B2-mixtures led to a decrease in UPV from 3484 to 3521 to 3883 m/s, respectively, at 28 days as the activator dosage increased 16% to 25% compared with single and B1 mixtures. However, all the measured B2-mixtures displayed UPV readings between 3714 and 4133 m/s after 90 days of age. Results for T1- mixtures showed good quality classifications at ages 28 and 90 days. On the contrary, T2- mixtures followed a decreasing trend as the slag replacement was 50%. At 28 days of age, the UPV values for T2-mixtures were 3446 m/s and 3472 m/s for 16% and 20% activator dosages. The increase in UPV findings was substantial at 90 days than at 28 days of age, as the quality of AASCC was shifted from medium to good using 16% and 20% activator dosages. T2-AASCC, on the other hand, with a 25% activator dosage, reported a UPV value of 3846 m/s after 28 days, with just a 4% increase at 90 days.

Fig. 51 (a and b) presented the relationship between UPV and compressive strength findings for AASCC mixtures with single, binary, and ternary precursor blends at 28 and 90 days. The results presented for all AASCCs showed that, regardless of curing age, the compressive strength and UPV findings increased gradually with an increase in the activator dosage of up to 25%. This can be attributed to the higher activator dosage, which accelerates the hydration process of AASCC mixtures, leading to the production of significant quantities of hydration products, leading to a higher strength (Pasupathy et al., 2017). The effect of ageing on the time-dependant microstructural growth of the AASCC mixtures has increased the UPV and, accordingly, strength values. The UPV test depends on the AASCC mixtures' density. A precursor material of higher density enables the ultrasonic wave to pass through the matrix very quickly, yet a denser material implies a higher velocity (Wardhono et al., 2015). Therefore, the UPV values were significantly affected by the high FA ratio substituting slag due to the higher porosity level. This coincides with the findings of (Huseien et al., 2021), where slag was replaced with up to 70% FA. It was concluded that the higher the FA level in mixtures, the lower the measured density and the corresponding UPV values.

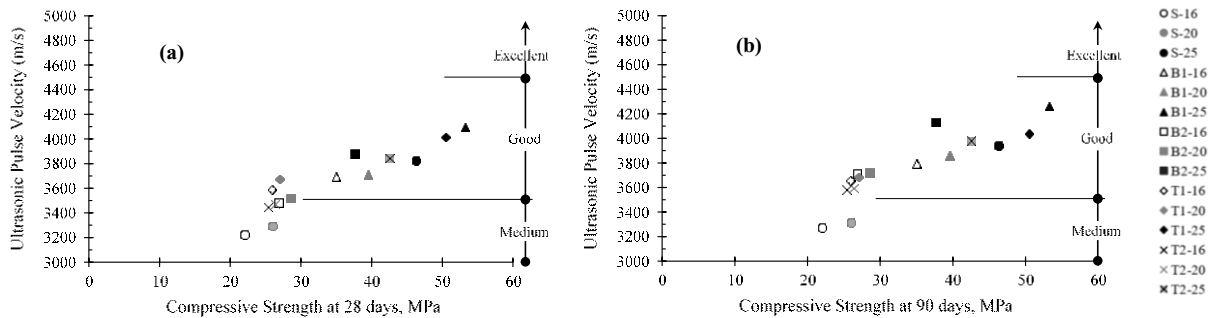


Fig. 51 – UPV results for all AASCC mixtures at a) 28 and b) 90 days of curing age

5.6.2.4. Capillary Sorptivity

Under capillary suction, the water sorptivity test is often used to measure the extent of water flow through concrete. The lower water sorptivity index, which reflects the microstructural properties of concrete and curing efficiency, is related to concrete durability. Based on the type of concrete and curing protocol, specimen maturity level may directly impact the test results. Thus, testing before 28 days after casting is not recommended.

5.6.2.4.1. Initial Rate of Absorption

Fig. 52 shows the initial absorption rates for all AASCC-precursor combinations activated with about 25% activator dosage at ages 28 and 90 days. In general, the single-precursor S-25% mixture shows the highest initial absorption rate among all precursor combinations. While the early absorption rate decreased as SF and FA replaced slag in binary and ternary mixtures relative to single-precursor mixtures at both ages. For example, binary mixtures B1 and B2 with 25% activator dosage exhibited the lowest initial absorption rate of 0.05 and 0.08 mm/mm^{1/2} at 28 days, respectively. Ternary mixtures also displayed the second-best performance with 0.09 mm/mm^{1/2}

and $0.015 \text{ mm/mm}^{1/2}$ at ages 28 and 90 days, respectively. According to Provis (2018), the nature of activators, rather than the chemical composition of precursor materials, plays a significant role in developing porosity. In addition, while increasing the activator modulus and decreasing the water content, the rate of water uptake in alkali-activated systems decreased (Glasser, 2001).

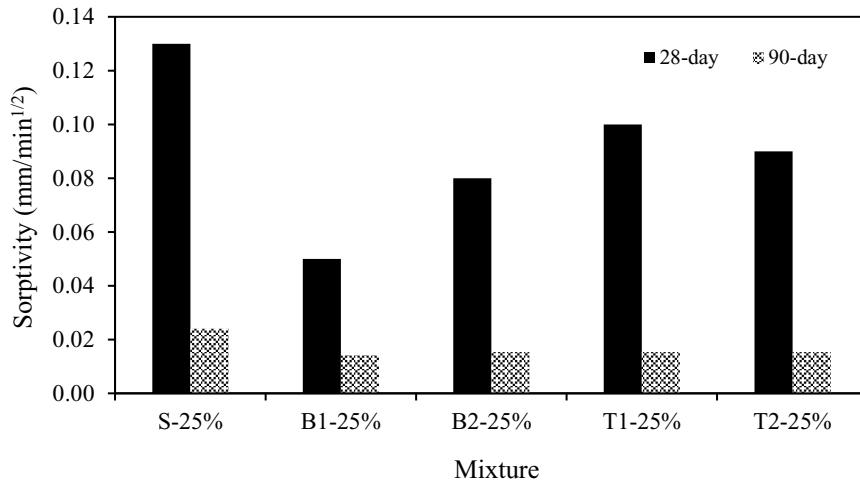


Fig. 52 – Initial rate of absorption for AASCC mixtures

5.6.2.4.2. Secondary Rate of Absorption

The second absorption rate for all AASCC mixtures at age 28 and 90 days is presented in **Fig. 53**. Except in SF and FA's binary mixtures, the general trend of using different precursor combinations on the secondary absorption rate values is indeed not apparent. However, as mixtures continue to develop with age, their secondary absorption rate decreases. For example, at age 28 days, the lowest secondary absorption rate was obtained in binary mixtures B1-25% and B2-25% with 0.015 and $0.037 \text{ mm/mm}^{1/2}$, respectively. This is followed by single-precursor and ternary-precursor mixtures i.e., S-25% ($0.052 \text{ mm/mm}^{1/2}$), T2-25% ($0.052 \text{ mm/mm}^{1/2}$) and T1-25% ($0.054 \text{ mm/mm}^{1/2}$), respectively.

For all AASCC mixtures, the percentage changes within the secondary absorption rate from 28 to 90 days were calculated. Generally, capillary sorptivity decreased with the degree of maturity and development of the curing age, which is compatible with the findings of (Glasser, 2001). The single-precursor exhibited a 96% reduction compared to all other AASCC mixtures. The ternary-precursor mixtures yielded a reduction level of 88% compared with the single-precursor blend. Binary-precursor blends of FA experienced an almost similar reduction of 82%, while SF replacing slag mixture resulted in a 65% reduction. Generally, capillary pores in AASCC mixtures have been observed to be refined and tortuous, contributing to a comparatively low level of capillary sorptivity. This observation is consistent with prior research, displaying a dense pore structure in mainly AAMs (Bernal et al., 2011; Bernal et al., 2010; Adam et al., 2009).

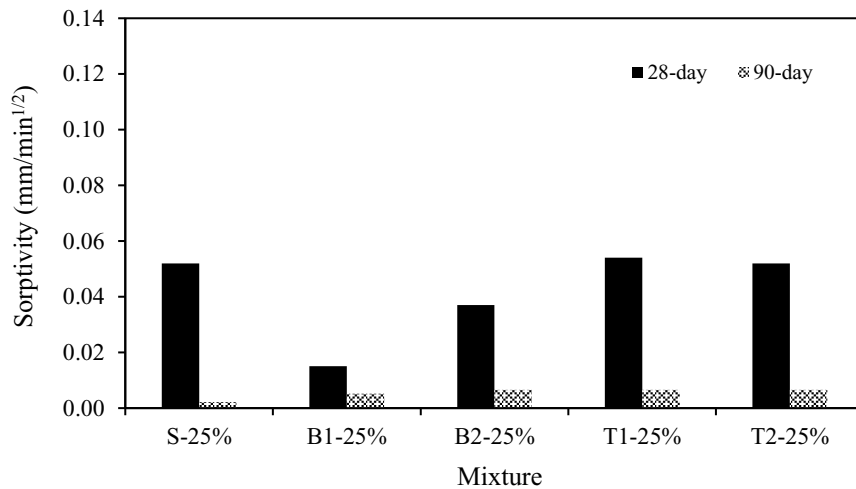


Fig. 53 – Secondary rate of absorption for AASCC mixtures

5.6.2.5. Permeable Pores Test

Standard porosity and water absorption measurement techniques are currently used to evaluate alkali-activated concrete mixtures' durability performance. The strong effect of the reaction products and the different binding gels may govern the transport mechanisms. Hence, the following sub-sections present the permeable voids volume results for all AASCC mixtures using the standard ASTM C642 test for 28 and 90 days specimens' age.

5.6.2.5.1. Early-Age Test

Permeable pore percentages for all AASCC mixtures with different precursor mixtures are shown in Fig. 54 after 28 days of age. Generally, all AASCC mixtures had an overall average of 23% permeable pores at an early age. When using 100% slag precursor material and 25% activator dosage, the single-precursor mixture experienced 19% permeable pores. Since 10% SF was used to replace slag in binary-precursor blends, the volume of permeable pores was the lowest of the five mixtures at 17%. When ternary- and binary-precursor mixtures with a $\geq 30\%$ FA than single-precursor blend, the volume of permeable pores showed a tendency to increase. The mixtures B2-25% and T1-25%, for example, exhibited about 21% and 23% of permeable pores, respectively. The volume of permeable pores in AASCC mixtures with higher slag content, single- and binary-precursor slag/SF mixtures, is lower than in binary- and ternary-precursor mixtures with FA. This can be attributed to the presence of C–A–S–H gel types that dominate the microstructure of slag/FA systems, which is denser than the aluminosilicate gels (Ismail et al., 2014). The C–A–S–H type of gel has a better pore-filling ability than the aluminosilicate gel due to the presence of more bound water due to Ca^{2+} in C–A–S–H. The results obtained are consistent with the previous studies (Provis et al., 2012; Ismail et al., 2013). Permeable pore volume increased when FA replaced slag in AASCC mixtures above 30% due to the gel type's nature that promotes different pore structure and porosity systems.

5.6.2.5.2. Late-Age Test

Fig. 54 represents the ratio of permeable pores in all AASCC mixtures at a late age, ranging from 13% to 18%. Using the optimal activator dosage of 25%, the volume of voids in single and binary-precursor with SF mixtures decreased at 90 days. In a single-precursor mixture, for example, the volume of pores was 13.6%. With 472.5 kg/m^3 (10%), partial replacement of slag by SF in a binary mixture resulted in about 14% permeable pores volume, yet increased to about 17% in B2-25%. The average permeable pores volume increased by up to 17% in both ternary-precursor mixtures when slag was substituted with FA and SF in T1 (315 kg/m^3) and T2 (289 kg/m^3). With the evolution of curing time up to 90 days, the volume of permeable voids values of AASCC mixtures decreased, mainly in samples with higher slag content. These results are consistent with previous findings in several studies (Collins and Sanjayan, 2010; Bernal et al., 2012), which found that porosity decreased over time as curing continued due to a greater extent of reaction.

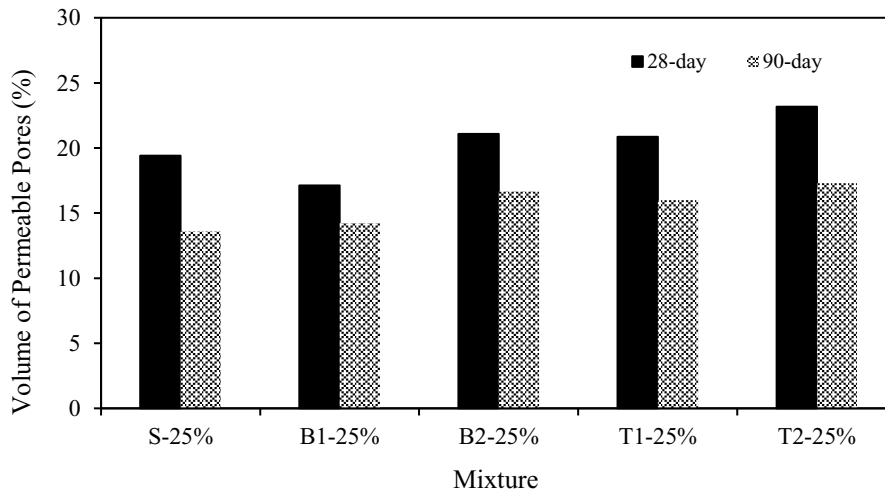


Fig. 54 – Permeable pores results for AASCC mixtures

5.6.3. Microstructural Analysis

The effect of multi-precursor combinations on the structural development of silicate-carbonate-activated AASCC mixtures was investigated in this section. At 90 days of age, the nature and composition of the reaction products produced were determined using X-ray diffraction (XRD), ^{29}Si nuclear magnetic resonance (NMR) spectroscopy, and scanning electron microscopy (SEM).

Fig. 55 shows the x-ray diffraction of AASCC concrete mixtures with single, binary and ternary-precursor blends. The predominant crystalline phases present in all AASCC mixtures after 90 days of curing age were quartz (SiO_2): (powder diffraction file (PDF) 00-005-0490) and calcium carbonate (CaCO_3): calcite (PDF 00-005-0586). In calcium-rich systems activated with sodium carbonate, calcite was commonly detected due to a reaction between dissolved carbonate ions present in the pore solution and calcium ions due to slag dissolution (Bernal et al., 2015). Also, it contains a series of minority crystalline phases such as prehnite (PDF 00-007-0333), scolecite (PDF 00-011-0171), paragonite (PDF 00-002-0243), riversideite (PDF 00-002-0600), merwinite

(PDF 01-074-0382), sodalite (PDF 00-041-0009) and calcite, magnesian (PDF 01-089-1304). In addition to nanocrystalline mineral consisting of a calcium magnesium silicate, hydrated calcium aluminum silicate [C-A-S-H], hydrated calcium silicates [C-S-H], and sodium aluminosilicate hydrate [N-A-S-H] gels were found in all AASCC mixtures with various precursor blends. The calcium consumption by carbonate ions, which forms carbonates, has been coupled to the formation of zeolites in sodium carbonate-activated slag binders. This may be due to the pore solution being saturated with silicon and aluminum species, resulting in aluminosilicate zeolite-type products (Bernal et al., 2015).

In a single-precursor mixture, slag was activated with silicate-carbonate activators; the halo was recorded between 25-35° in 2θ. The sharp peaks in the AASCC-slag indicate a higher crystallinity level due to the presence of quartz: (SiO₂ PDF 00-005-0490), calcite: (CaCO₃ PDF 00-005-0586) and calcite, magnesian ([Mg_{0.03} Ca_{0.97}]-CO₃ PDF 01-089-1304). While the intensities of merwinite (PDF 01-074-0382), sodalite (Na₈(AlSiO₄)₆(OH)₂·4H₂O PDF 00-041-0009), scolecite (CaAl₂Si₃O₁₀·3H₂O PDF 00-011-0171), prehnite (PDF 00-007-0333 Ca₂Al₂Si₃O₁₀(OH)₂), paragonite (3Al₂O₃·Na₂O₆SiO₂·2H₂O PDF 00-002-0243) and riversideite (2CaSiO₃·3H₂O PDF 00-002-0600) are weak. These peaks were identified in all samples regardless of the precursor nature and combination used while using the silicate-carbonate activators as reported by (Bernal et al., 2015). The diffraction pattern changed after the replacement of slag in binary- and ternary-precursor blends. In binary-precursor mixtures with 10% SF and 30% FA replacing slag, the diffused broad humps were in the range of 20-40° in 2θ compared to single-precursor mixtures. In the x-ray diffractogram of binary mixtures, the same peaks were observed in addition to higher intensities of merwinite (PDF 01-074-0382), scolecite (CaAl₂Si₃O₁₀·3H₂O PDF 00-011-0171), and riversideite (2CaSiO₃·3H₂O PDF 00-002-0600) in slag/SF mixture, yet sodalite (PDF 00-041-0009) in slag/FA mixture. On the other hand, Margarite (CaAl₂(Si₂Al₂)O₁₀(OH)₂ PDF 00-018-0276) was identified in ternary-precursor mixtures only compared with the single- and binary-precursor blends. When using silicate-carbonate activators under strongly alkaline conditions, the addition of sodium metasilicate induces the formation of sodalite-type zeolites (PDF 00-041-0009) rather than zeolite (Chen et al., 2010).

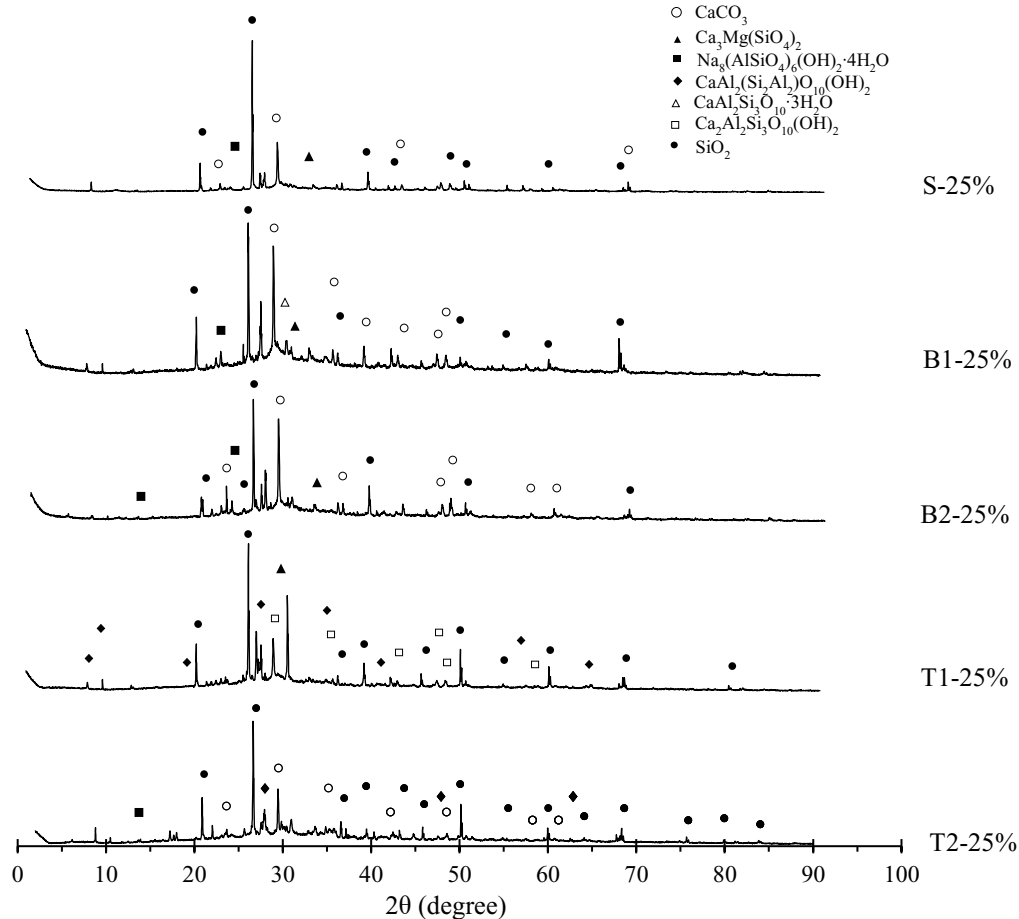


Fig. 55 – X-ray diffractograms of AASCCs with 25% silicate-carbonate activator dosage

In ^{29}Si MAS NMR resonances, the presence of Q^0 monomers, Q^1 dimers, and Q^2 bridging groups can be seen, and their compositions vary depending on the activator composition and curing condition (Peng et al., 2015). The ^{29}Si MAS NMR spectra of the AASCC systems containing both high calcium C-A-S-H and low calcium aluminosilicate products C-(N)A-S-H and activated with silicate-carbonate activators are shown in **Fig. 56**. Together with XRD and SEM, the presence of Q^1 to Q^3 silicon units determined by ^{29}Si NMR confirms the existence of two distinct types of reaction products in the blended systems. The dissolved Ca^{2+} and Al^{3+} groups affect the mixture of C-S-H gel, and its composition gradually changes into C-A-S-H and C-(N)A-S-H gels, respectively, as the structural shifts of Si are detected. (Garcia et al., 2013). After 90 days of age, high-intensity peaks centered between -80 to -84 ppm were assigned to Q^1 and Q^2 (1A1) for all AASCC mixtures with single, binary, and ternary-precursors blends. Resonance at -97.1 ppm was observed in AASCC single-precursor mixture, corresponding to Q^2 site, while -90 ppm for the other AASCC precursor blends consistent with the formation of an Al-substituted C-S-H type (C-(N)A-S-H) gel structure (Bernal et al., 2014; Le Saoût et al., 2011). This is due to the presence of multi-dry-powder activators with high activator dosage, which successfully promote the formation of strength-giving products. In single-precursor and binary-precursor blends with 10% SF and 30% FA mixtures, resonances of -107.6, -105.5, and -107 ppm were detected as the reaction progressed. However, peaks at -100 ppm and -101 ppm were observed for ternary-blends with a higher amount

of Al-substituted. These intensities are appointed to Q^3 (1Al) and Q^3 species in the spectra, which could overlap. This is in line with the authors' recent structural model and analysis of ^{29}Si MAS NMR findings (Bernal et al., 2014; Myers et al., 2013), which found a strongly cross-linked and densified C-(N)A-S-H gel type in these systems. Previous analyses of sodium silicate-activated and sodium carbonate-activated slag binders (Bernal et al., 2016) have indeed attributed this band to a Q^3 (1Al) component.

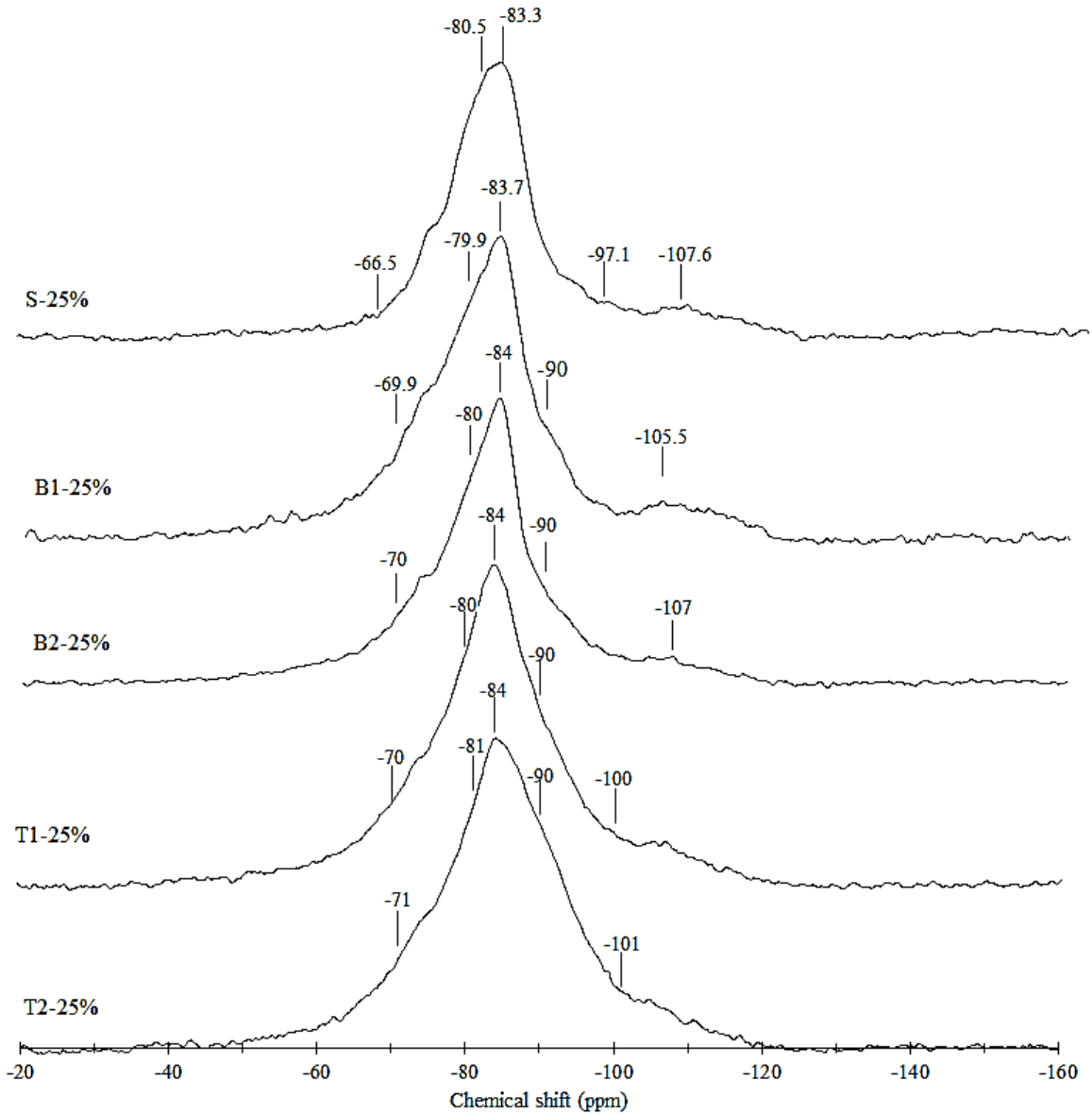
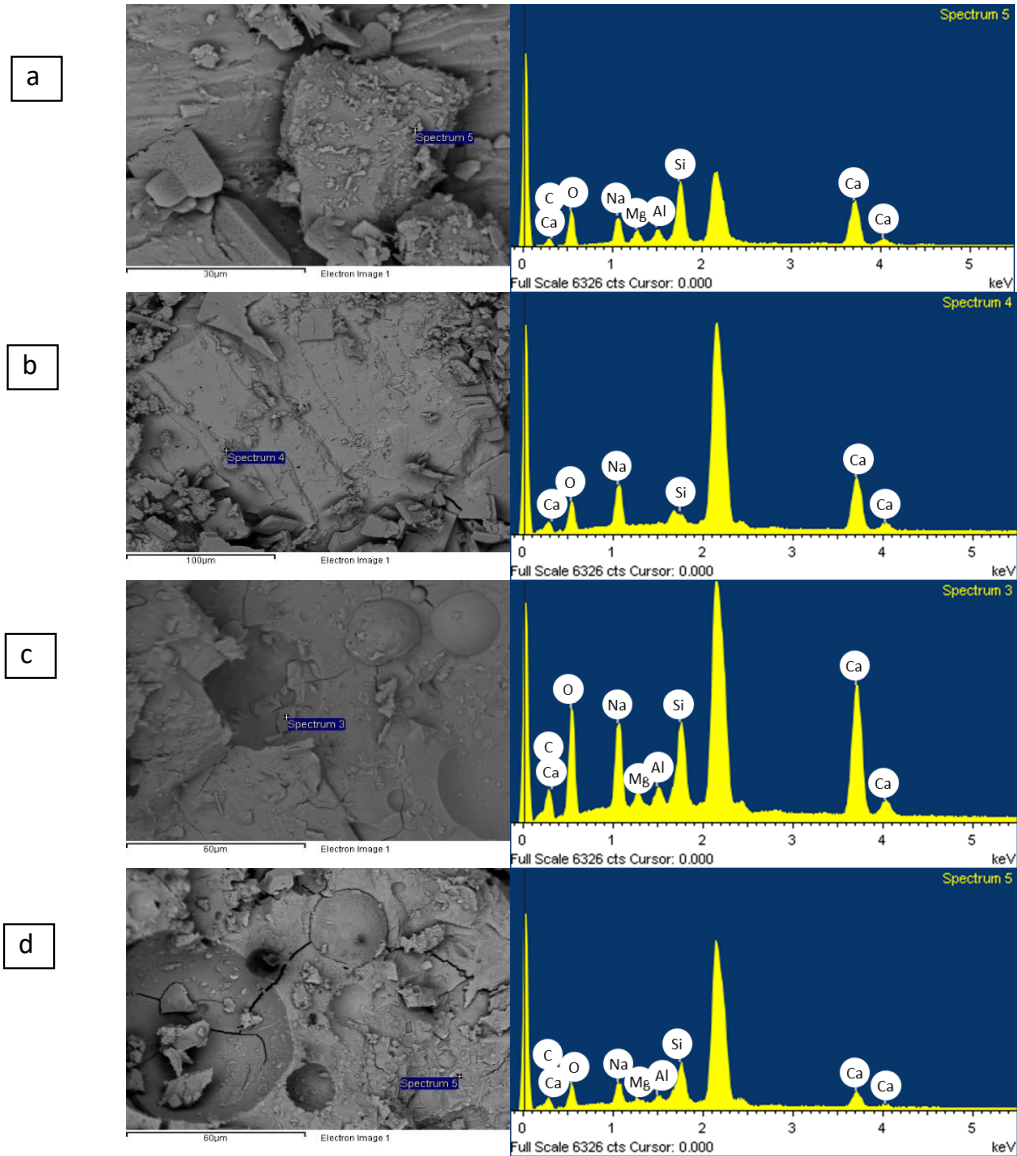


Fig. 56 – ^{29}Si NMR spectra after 90 days hydration of AASCC mixtures with different precursors

SEM images of single, binary, and ternary AASCC mixtures activated with 25% dry-powder activator dosage after 90 days of curing are presented in **Fig. 57 (a-e)**. It can be seen that all AASCC mixtures exhibited a homogeneous and highly tortuous structure. The additional quantity of silica and alumina provided by FA and SF substitutes in binary and ternary mixtures profoundly affected the formation of hydration products, leading to the strength's development. The BSE images confirmed that the major hydration product in all mixtures was C-(N)A-S-H. The SEM study was supported by the results of the XRD and ^{29}Si NMR. The densified microstructure and refined pore network were provided by the presence of prehnite (PDF 00-007-0333), scolecite (PDF 00-011-0171), riversideite (PDF 00-002-0600), and sodalite (PDF 00-041-0009).



e

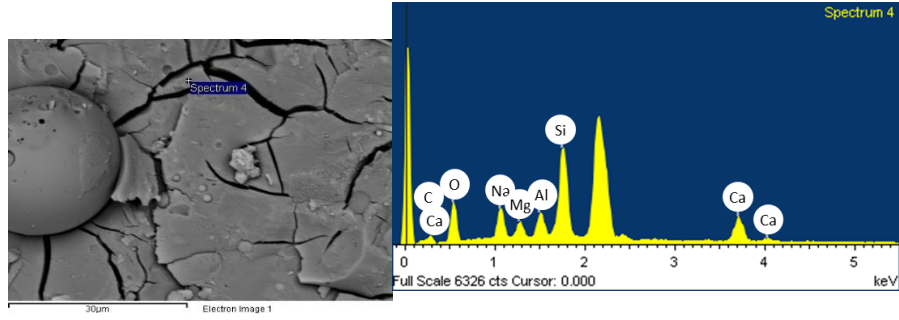


Fig. 57 – SEM images of AASCCs using 25% activator dosage a) Single, b) Binary-1, c) Binary-2, d) Ternary-1, and e) Ternary-2

5.7. Concluding Remarks

In this chapter, multi precursor and activator materials were successfully used to develop one-part 'just add water' AASCC mixtures. This step is significant for the adoption of low-carbon binders that are best suited for in-situ applications. The following conclusions can be drawn from the present experimental data and analysis:

1. The proper selection of precursor materials, proportions, activator type, and dosage plays a decisive role in the efficient development of AASCC mixtures in the absence of a distinct methodology.
2. The higher fraction of sodium carbonate/silicate activators in all systems, single, binary and ternary, contributed to the delayed reaction kinetics due to their nature. The combination of 20% to 25% activator dosage is recommended to achieve satisfactory fresh and mechanical properties.
3. Slag replacement with different SF or FA class-F ratios can adjust the particle size distribution of the total binder material and improve the fresh concrete characteristics in binary and ternary systems.
4. For all AASCC mixtures, a 25% activator dosage resulted in the highest compressive strength and UPV values, particularly in binary-SF and ternary-1 mixtures of more than 50 MPa after 90 days than other combinations.
5. The formation of different reaction products and binding gels, i.e., C-(N)A-S-H, strongly influences the different transport mechanisms, such as capillary sorptivity, permeable pores, and bulk electrical resistivity.

Chapter 6 : External Sulfate Attack of Ambient Cured One-Part Alkali-Activated Self-Consolidating Concrete

6.1. Overview

The external sulfate attack, resulting from the invasion of sulfuric ions in soils, underground, marine, or industrial wastewaters, is a significant process of deterioration of concrete in-service. Although sulfates usually damage the cement-paste matrix, its adversity depends on the types of cement (binder) used, nature and concentrations of sulfate solutions, concrete quality, and surrounding conditions. In general, cement paste pores are filled with a highly basic solution (i.e., $\text{pH} > 12.5$). Hence, any medium with a lower pH value would represent an aggressive environment for the cement matrix. Concrete exposed to sulfate attack suffers from expansion, cracking, strength loss, and eventually disintegration.

Different test methods are used to study the external sulfate attack mechanisms and effects, such as ASTM C1012 "Standard Test Method for Length Change of Hydraulic-Cement Mortars Exposed to a Sulfate Solution." This international ASTM C1012 test procedure has frequently been used but criticized due to its limitation (orientation-expansion effect). In 1997, Taylor pointed to the fact that laboratory studies focus on expansion and specimen crackage, but experiences in the field indicate a higher loss of adhesion and strength as a predominant sign of-deterioration. Moreover, most of the existing standardized durability testing methods have especially been developed to test the long-term durability performance of Portland cement systems. The absence of standardized testing and evaluation criteria for AAMs represents one of the main barriers facing its spread as no reliable long-term durability data are available. Different testing methods are thus essential to better predict the AAM's different damage mechanisms while being exposed to sulfate attacks (i.e., partial immersion exposure tests).

Thus, this chapter was dedicated to investigating the chemical and physio-chemical degradation mechanisms (physical or chemical) of AASCCs partially exposed to aggressive aqueous solutions. This is very important as the transport mechanism in partially exposed concrete structures does not appear to cause the same distress as in entirely exposed concrete components. Diffusion (as an exposure method) is the main transport mechanism that causes a higher deterioration rate under saturated conditions. Diffusion is also known to be slow in comparison to other mechanisms, as an aqueous ionic transport mechanism, and is not apparent until a thermal or concentration gradient is generated. Therefore, the "sulfate-related deterioration rate defies the expectations of the relevant models," as stated by (Santhanam et al., 2002).

6.2. Research Significance

The mechanism of sulfate attack on alkali-activated concrete, particularly AASCC, is complex and contradictory. This could be due to the wide range of precursor and activator materials used in the production of AASCC mixtures, which has called into question the reliability and validity of

existing evaluation procedures and practices. This chapter presents a systematic research effort on AASCC mixtures prone to various sulfate attack scenarios that are thought necessary to establish a proposed criterion. This would result in a better understanding of the sulfate attack mechanism as well as the development of more reliable assessment tools for predicting AASCC performance and service life.

6.3. Experimental Program

6.3.1. Materials and Mixture Proportion

Ground granulated blast furnace slag (GGBFS) was used as the main precursor to produce single, binary, and ternary AASCC. Fly ash Class-F (FA) and silica fumes (SF) were added with different ratios replacing GGBFS. Two dry-powder activators, $\text{MetaNa}_2\text{SiO}_3$ and Na_2CO_3 with a 1:1 ratio, were mutually utilized to activate the AASCC mixtures. Five AASCC concrete mixtures with different precursor blends and compositions but the same activator dosage (25%) were prepared, as indicated in **Table 22**. The S-25 designation refers to a single-precursor 100% GGBFS AASCC combination activated with 25% dosage. Both binary AASCC groups used 90% GGBFS and 10% SF (designated code B1) or 70% GGBFS and 30% FA (designated code B2). The AASCC ternary mixtures contained 60% GGBFS, 33% FA, and 7% SF (code T1) or 50% GGBFS, 45% FA, and 5% SF (code T2).

Table 22 – Summary of mixture’s proportions used for the designed AASCC mixtures

Mixture I.D.	Slag, kg/m ³	FA, kg/m ³	SF, kg/m ³	Sand, kg/m ³	CA, kg/m ³
S-25	525	0	0	646	830
B1-25	472.5	0	52.5	652	825
B2-25	367.5	157.5	0	637	840
T1-25	315	173	37	625	840
T2-25	289	210	26	624	840

Along with ASTM C1012, samples were continuously exposed to aggressive solutions of sodium sulfate (Na_2SO_4) and magnesium sulfate (MgSO_4). The selection of the different cations (Na^+ and Mg^{2+}) accompanying SO_4^{2-} shows not only different attacking and damage mechanisms but also different solubility. Although sodium is not an aggressive component, it has a significant impact on the solubilization of cement species and the pH of the pore solution. The effect of magnesium sulfate is far more significant than either sodium or calcium sulfates. Magnesium and sodium solubilities are 35.7g and 28.1g in 100g water at 25 °C, respectively, Rebel et al. (2005). These values are significantly higher than that of calcium (i.e., 0.205g in 100 g water at 25 °C). The sulfate salts used in assessing the sulfate resistance of AASCC concrete mixtures were Na_2SO_4 (CAS Number 7757-82-6) and MgSO_4 (CAS Number 7487-88-9) of percentage purity > 99%. Each solution was prepared by dissolving 100 g of the solutes in 1-L tap water to obtain (10%) of the sulfate solution.

6.4. Testing Program

Based on Phase I: Synthesis of AASCC, mixtures with optimum performance were considered for further assessment in this chapter. These mixtures were selected based on their ability to balance the restricted fresh characteristics, strength gain, and expected durability performance. Mixtures were tested for their resistance to external sulfate attack. The effect of precursor content was evaluated at the macroscopic level using visual inspection, mass, and cross-section changes. While x-ray diffraction, ion chromatography, and thermogravimetric analysis (TGA/DTG) tests were used on a microscopic level. The assessment process is divided into two parts: single-damage-factor tests and multi-damage-factor tests.

6.4.1. Phase II: Single Damage-Factor

In partially exposed sulfate structures, the lower portion may be saturated with seawater or groundwater, while the upper portion remains at ambient temperature and humidity conditions. The deterioration usually happens when the sulfates are drawn into the concrete, permeated upwards, and then evaporated upon reaching the surface (wicking action). As a result, various types of degradation, i.e., leaching, microcracking, paste and permeability characteristics alteration, efflorescence, and surface scaling, may present. The degradation can be accelerated through the transfer of larger amounts of sulfates throughout the matrix (Exposure I scenario of the current work). For example, Boyd and Mindess (2004) have partially exposed concrete cylinders to a 5% Na₂SO₄ solution. The authors concluded that while scaling implies significant damage, the internal damage caused by sulfate attacks may be considerably more severe. To date, this physical form of sulfate attack is not evident when testing a fully saturated specimen, the standard method of exposure. In addition, there is no standard test available for the partially immersed concrete in sulfate solutions.

In the context of accelerated degradation tests, a step to simulate harsh field conditions, AASCCs were partially exposed to 10% Na₂SO₄ and 10% MgSO₄ in addition to a mixed solution of 10% Na₂SO₄ + 10% MgSO₄ in laboratory conditions. The attack intensity is well known to be mainly dependent on the pH of aggressive solutions. Attempting to control pH is a simulation of field conditions in which concrete is exposed to an environment that usually contains mobile sulfate. Therefore, the effect of monitoring the pH of the solution on the leaching mechanisms of the AASCC mixtures was evaluated. On the other hand, the resistance of AASCC mixtures to 5% Na₂SO₄ and 5% MgSO₄ was evaluated for comparative purposes. The initial pH value for sulfate solutions was kept in the range of 6.0–8.0, as recommended by the ASTM C1012 standard. The exposure to the sulfate solutions lasted for 6 months (26 weeks) under ambient laboratory conditions. For specimens in controlled pH environments, the pH was maintained at the range of 6.0–8.0 by titration with dilute sulfuric acid solutions at constant time intervals. To guarantee a homogenous distribution of the solutions, regular stirring was accompanied by adding a pH regulator (i.e., sulfuric acid solutions).

Furthermore, sulfate solutions were replenished every 4 weeks with fresh ones. The importance of monitoring the pH of the sulfate solutions, although not specified in ASTM C1012 standard, is associated with the real field conditions in which concrete would be exposed to a continual supply of sulfate ions (Skalny and Pierce, 1999; Mehta, 1992). Mixtures were evaluated based on their

visual appearance, changes in mass, cross-section variation, and pH values of the sulfate solutions for 183 days at the end of each 30 days. The concrete deterioration scheme proposed for Phase II is shown in **Fig. 58**. Following this scheme; mixtures were divided into six groups as follows:

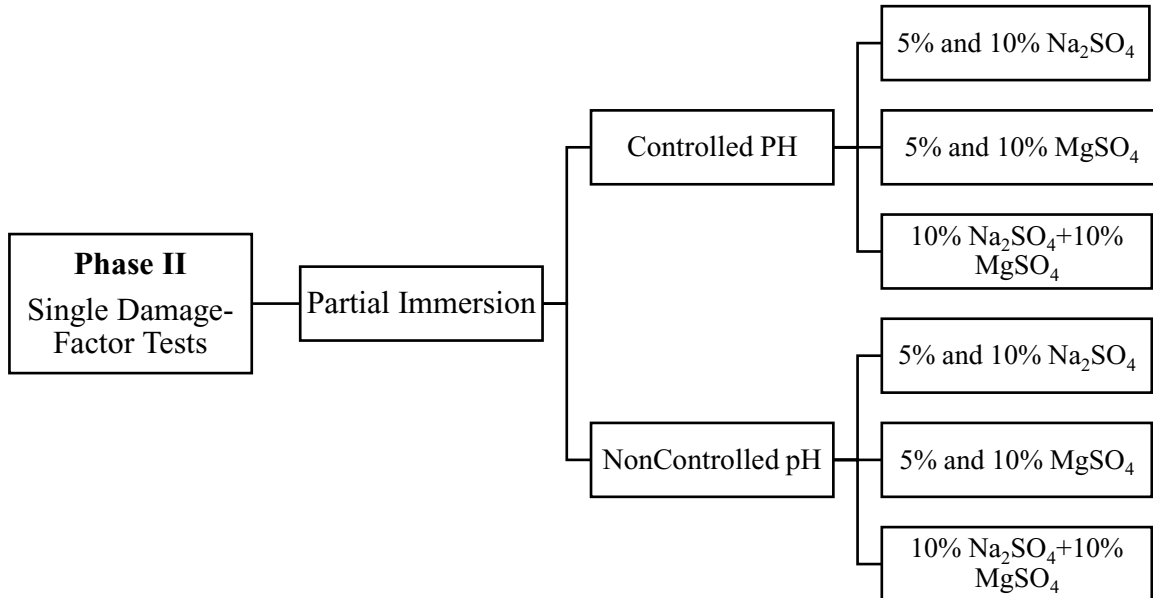


Fig. 58 – Phase I AASCC deterioration scheme

6.4.2. Phase III: Multiple Damage-Factor

Field concretes undergo wetting and drying cycles due to fluctuations in water levels caused by flooding, rainwater runoff, tides, and the cyclic migration of sulfate-containing groundwater through capillarity into the above-ground portion of structures. Such activities induce the crystallization of sulfate salts under the concrete surface layer leading to cracking, scaling, and delamination. Current testing approaches cannot predict or capture these complicated deterioration mechanisms (i.e., continuous immersion exposure). Besides, standard immersion tests have frequently presented different performances relative to the observed ones in real-field cases. This might be due to the applied techniques and indoor test procedures in current standard tests, such as ASTM-C1012 (2004), that overlook the critical field conditions. Therefore, a mandatory shift to performance-based specifications for concretes demands the elaboration of a performance-based evaluation policy that better depicts field conditions.

The question of whether wetting-drying cycles and the underlying mechanisms of this form of damage are physical or chemical is still controversial among researchers. For example, Kalousek et al. (1972) have investigated the length change of concrete cylinders exposed to Na_2SO_4 solutions by 2.1% in a 20-year long-term research program. Specimens were subjected to wetting-drying cycles to accelerate the test. In each cycle, the specimens were immersed in sulfate solutions for 16h at room temperature, then air-dried for 8h at 54 °C. After one year in wetting-drying exposures, it was found that eight years of continuous immersion exposure caused comparable damage to concrete specimens under wetting-drying. De Almeida (1991) proposed immersing samples in 16% Na_2SO_4 solutions for 2h (wetting) followed by drying at 105°C for 10 to 15h. It was concluded

that specimens failed under physical rather than chemical action. Nehdi and Hayek (2005) carried out a study in which mortar cylinders were partially immersed in 10% sodium and 10% magnesium sulfate solutions and exposed to 32-95% constant or cyclic relative humidity (RH) for up to 151h. Their extensive study found a thick efflorescence layer on the surface of partially immersed specimens in 10% Na₂SO₄ solution only, particularly with cyclic RH. The study of Sahmaran et al. (2007) reported the resistance of mortar samples to 5% sulfate solution accompanied with wetting-drying cycles. Each cycle consisted of the exposure at room temperature for 6 days, followed by drying for 1 day at 100°C. The wetting-drying exposure was observed to be more aggressive compared to continuous immersion exposure and has contributed to the complete disintegration of the samples within 17 weeks due to repeated hydration and evaporation of sulfate salts. Similarly, Haynes et al. (2008) experimented on partially immersed concrete cylinders in (5% Na₂SO₄) and exposed them to various temperatures and RH. It was concluded that samples disintegrated after the exposure to cycles between 20°C with 82% RH and 40°C with 31% RH in two-week intervals.

More research is still needed on sulfate attack assessments, including wetting-drying cycles. Several questions remain unanswered, such as the real mechanisms of deterioration after these cycles and the degree and time of drying that can simulate the real field conditions. Variations in these parameters remain a challenging task for researchers and standardization agencies. Furthermore, similar to partial immersion exposure tests, there is no standard test available for concrete exposed to drying and wetting cycles. Also, the performance of alkali-activated concrete in various exposure environments simulating field-like conditions needs to be addressed. This phase would provide an adequate understanding of the mechanisms of deterioration of AASCC mixtures in the evaporation zones, resembling partially buried concrete elements, to develop reliable data on their durability. Mixtures in Phase III were evaluated while the exposure to different sulfate attack environments was considered with other concurrent damage mechanisms (i.e., cyclic environmental conditions).

After the curing process of AASCC mixtures, concrete cylinders were kept in ambient laboratory conditions (i.e., the temperature of $23 \pm 2^\circ\text{C}$ and relative humidity (RH) 50%) for 48h to remove the excess moisture from surfaces. This technique would guarantee sufficiently dry samples for a uniform basis of analogy. After that, their preliminary physio-mechanical characteristics were recorded before the exposure to sulfate occurs. Specimens were partially immersed in highly-concentrated solutions of (10%) sodium sulfate and (10%) magnesium sulfate solutions to evaluate the resistance AASCCs to combined effects of external sulfate attack with other ongoing deteriorating mechanisms (i.e., cyclic environmental conditions). **Fig. 59** illustrates the technique used to resemble the performance of concretes exposed to external sulfate attack as performed by (Bassuoni and Rahman, 2016). The exposed part of the specimens, up to one-third of the total height of the cylinder, was fully immersed and sealed to minimize the evaporation of solutions and ensure that solutions were lost only by the cylinder's uptake. This phase investigated the capability of holistic testing techniques in capturing the AASCC deterioration mechanisms within a reasonable testing duration. Therefore, sulfate solutions with a very high concentration were used to accelerate the deterioration process.

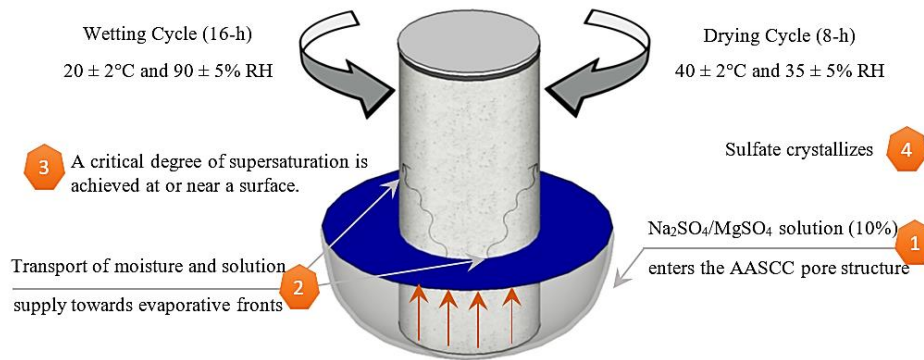


Fig. 59 – Schematic diagram of a concrete specimen exposed to a field-like multi-damaging condition adapted from (Bassuoni and Rahman, 2016)

The effect of interacting deterioration parameters, partial immersion in sulfate solutions under cyclic environmental conditions could depict the seasonal variations of atmospheric temperature (T) and relative humidity (RH) found in many geographic locations, i.e., southern parts of the United States. These unfavorable exposure conditions, an exposed portion of specimens to cycles of varied ambient temperature and RH, resembled a repeated crystallization deliquescence and hydration-dehydration processes that can cause rapid decay of AASCC mixtures. The repetitive crystal growth of sodium and magnesium sulfates from anhydrous to hydrous states was associated with a significant volume increase due to phase changes. Based on the stability phase diagram of Na_2SO_4 solution shown in (Fig. 60), the direct precipitation of thenardite (above $\sim 32.4^\circ\text{C}$) and the rapid crystallization of mirabilite after thenardite dissolution causes a higher deterioration level in porous mixtures than mirabilite crystallization only (Doehen et al., 2002). On the other hand, Fig. 61 depicts the RH-T stability diagram of the MgSO_4 system from 0 to 80°C and up to 100% RH. Based on the available thermodynamic data and close to room ambient temperature, the crystalline phase of MgSO_4 (epsomite) would be stable. However, under dry conditions, epsomite would tend to dehydrate to form a monohydrate kieserite phase.

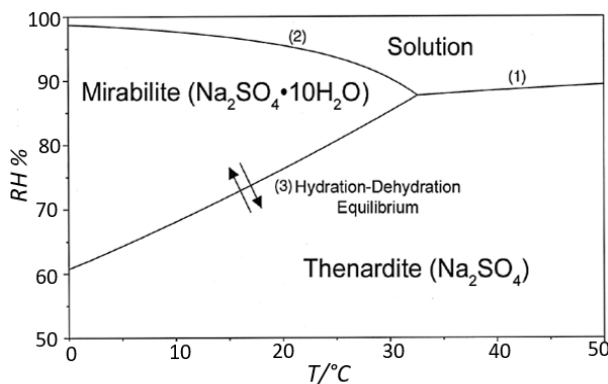


Fig. 60 – RH-T phase diagram of $\text{Na}_2\text{SO}_4 + \text{H}_2\text{O}$ system (Adapted from Doehen et al., 2002)

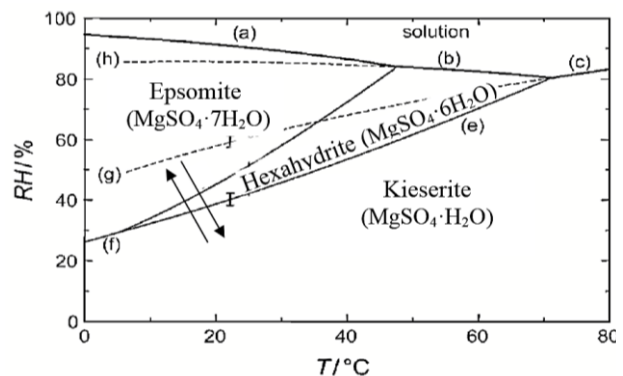


Fig. 61 – RH-T phase diagram of $\text{MgSO}_4 + \text{H}_2\text{O}$ system (Adapted from Steiger et al., 2007)

In this study, cylindrical specimens were subjected to alternating temperature and humidity cycles for 183 days incessantly. Each cycle (24h) includes two consecutive stages; an 8h of the hot/dry stage ($40 \pm 2^\circ\text{C}$ and $35 \pm 5\%$ RH) followed by a 16h temperate/humid stage ($20 \pm 2^\circ\text{C}$ and $90 \pm 5\%$ RH). The loss in the sulfate solutions due to the continuous uptake, mainly during the dehydrating (drying) cycles, were frequently refilled up to one-third of the cylinder's height. Moreover, sulfate solutions were renewed every 30 cycles (days).

A conceptual framework is presented that considers four main visible deteriorating phenomena by external sulfate attack, i.e., spalling, delamination, cracking, and loss of cohesion (mass and strength loss). All of these phenomena are the consequences of the chemical interactions between external sulfate sources and concretes. These complex physicochemical processes were monitored at two levels; macroscopic and integrated microscopic.

6.4.3. Mass Monitoring

To study the performance of AASCC mixtures in sulfate environments, samples were partially immersed in sulfate solutions after a 90-day curing age. The masses of the samples were recorded monthly for 183 days. For mass change measurements, samples were weighed before the exposure to sulfate solutions at age 90-days and were taken as initial masses (M_i). After a specified time interval, specimens were removed from the sulfate solutions and were brushed using a nylon brush to remove the attached debris. Under ambient laboratory conditions, samples were left to dry for 30 min before visual inspection, and measurements of masses were then recorded. The change in weight (MC %) was calculated using the following equation (Eq. 11);

$$\text{MC (\%)} = \frac{M_i - M_j}{M_i} \times 100 \quad \text{Eq. 11}$$

Where M_i (in grams) is the average weight of two cylindrical samples; and M_j (in grams) is the average weight of two cylindrical samples exposed to sulfate solutions.

6.4.4. Cross-Section Variations Monitoring

During the sulfate attack, cross-sectional variations of samples can be monitored by certain geometrical parameters such as sample volume, longitudinal expansion, and lateral variations of transverse sections (radius). The longitudinal expansion is the most commonly questioned geometrical parameter under the ASTM C1012 standard. Expansion and swelling of cement-based materials under sulfate attack are frequently associated with the formation of ettringite and gypsum due to crystal growth pressure (Santhanam et al., 2002). Gypsum and ettringite formation require a calcium source that can be supplied from the leaching of portlandite and C-S-H. Portlandite leaching and progressive C-S-H decalcification lead to softened cement matrix and reduced strength. The formation of (usually expansive) calcium sulfate-containing degradation products is related to Portland cement behavior. Expansion, however, does not capture certain-degradation-induced changes, while volume and sample monitoring for the radius enables the evaluation of leaching activities and geometrical variations accordingly. The extent of leaching of elements is affected by the pH level, binder microstructure, permeability, and porosity of the material considered. The behavior of various AASCC mixture systems under sulfate attack is associated

with the existence of C-S-H and C-A-S-H hydrotalcite gel; the former phase could be highly resistant to sulfate attack.

The cylindrical samples' longitudinal and volume variations were directly evaluated from experimental data where the proposed lateral vs. longitudinal deformation pattern corresponds to the deformation path. This allows various binder materials to be classified according to the magnitude of the deformation in concrete mixtures. The lateral deformation is more sensitive to sulfate attacks than longitudinal expansion, making this approach useful in testing low expansion materials (i.e., AAMs). **Equation 12** refers to the relative variation in the cross-sectional radius derived from the relative variation of the elongation x and the relative variation in volume z monitored during the test.

$$y = \sqrt{\frac{1+z}{1+x}} - 1 \quad \text{Eq. 12}$$

Where $x = \frac{\Delta L}{L_i}$, $y = \frac{\Delta R}{R_i}$ and $z = \frac{\Delta V}{V_i}$ with V_i initial global volume, L_i initial sample length, and R_i initial radius of a cross-section.

6.4.5. Microstructural Observations

After the visual inspection of test specimens, their degradation mechanisms were analyzed using X-ray diffraction (XRD), ICP-OES (Inductively coupled plasma-optical emission spectrometry), ion chromatography, and differential scanning calorimetry (DSC) at a heating rate of 10 °C/min. XRD measurements were performed on powder samples, passing #200 sieve (75 μm), extracted from the superficial surfaces of the exposed samples (0-15 mm) after each exposure interval. For further medium analysis with the ICP and ion chromatography, the solutions pH measurements and ion concentrations, i.e., Ca^{2+} , Na^+ , SO_4^{2-} and Mg^{+2} , were performed after the immersion of AASCC specimens.

6.5. Results and Discussion

6.5.1. Exposure I: Controlled pH

Sulfate penetration is often governed by diffusion through the pore structure and is consequently slow in the early stages of exposure. While exposed to a 10% sulfate solution in step 1, gypsum precipitation and ettringite production may reduce and offset the sulfate concentration in the pore solution. The presence of microcracks after a period of exposure raises the sulfate concentration in the pore solution in step 2 because sulfates can pass through the open cracks unhindered. For AASCC cylinders partially exposed to different concentrations of sulfate solutions, it was discovered that the crystallization pressure does not increase proportionally with the supersaturation of the pore solution. On one hand, changes in solution concentration due to the dual interactions between the paste and sulfate solutions may affect the crystallization pressure less in the Exposure I (high supersaturation) scenario than in the Exposure III (low supersaturation) environment. On the other hand, due to kinetic effects, the lower the concentration of sulfates in

solutions, the slower the formation of expansive products, such as ettringite, resulting in lower crystallization pressure (Chatterji, 2005; Scherer, 2004).

Effect of sulfate concentration. Considering different exposure scenarios, the difference in crystallization pressure in AASCC cylinders may have different causes. Using 10% sulfate solutions (Exposure I) and 5% solutions (Exposure III), the sulfate concentrations inside the cylinders were expected to be similar despite the considerable variation in sulfate concentration between the container solution and specimens. However, the higher stress could be due to a higher sulfate concentration (Exposure I), promoting cylinder supersaturation.

6.5.1.1. Visual Appearance

Single-precursor mixtures. The Malhotra et al. (1988) rating system was used to assess the visual situation of each concrete cylinder after six months of partial immersion in sulfate solutions. The visual examination of AASCC single-precursor mixtures revealed no signs of deterioration at the specimens' surface in the 10%Na₂SO₄ (**Fig. 62b**) 10%Na₂SO₄ + 10%MgSO₄ mixed solutions (**Fig. 62c**) in a controlled pH environment. An exception was observed when the concrete cylinders were exposed to a 10% MgSO₄ solution. The exposed areas were cracked, and surface delamination was observed (**Fig. 62a**).

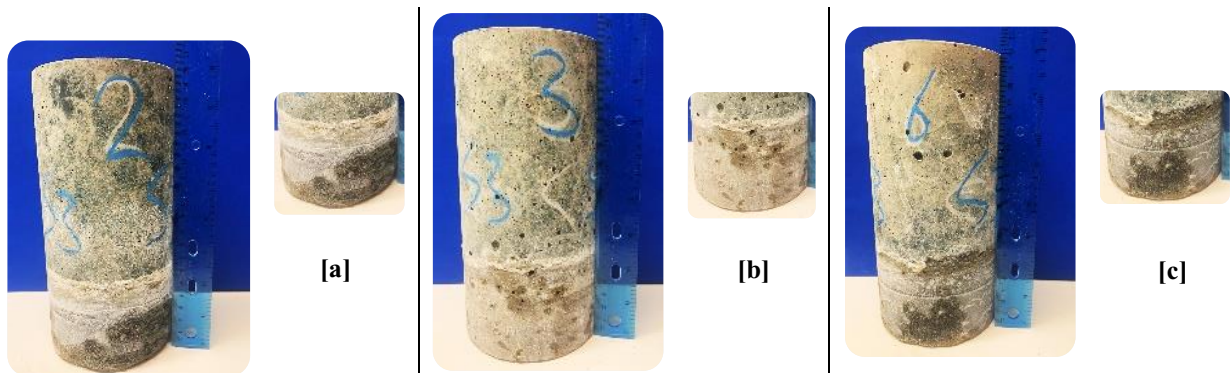


Fig. 62 – AASCC single-precursor mixtures exposed to a) 10% MgSO₄ b) 10% Na₂SO₄ and c) 10% mixed sulfate solutions at a controlled pH environment

Binary-precursor mixtures. The samples of binary-1 mixtures using 10% SF replacing slag and subjected to 10% sulfate solutions showed that magnesium sulfate greatly affected the properties of the concretes. The AASCC binary-1 mixture showed an expansion and cracking after exposure to 10% MgSO₄. The exposed area of the concrete mixture also suffered a massive loss (**Fig. 63a**). Samples in mixed solutions exhibited a significant surface spalling above the exposed area to sulfate solution (**Fig. 63c**). While in Na₂SO₄ solution (**Fig. 63b**), cracking along the length of the sample was more pronounced. For binary-2 mixtures using 30% FA replacing slag, no visible signs of deterioration (**Fig. 64**) were detected after exposure to different sulfate solutions after 6 months. However, cracks were noticeable in the surface of specimens exposed to 10% MgSO₄ (**Fig. 64a**) and 10% mixed sulfate (**Fig. 64c**) solutions.

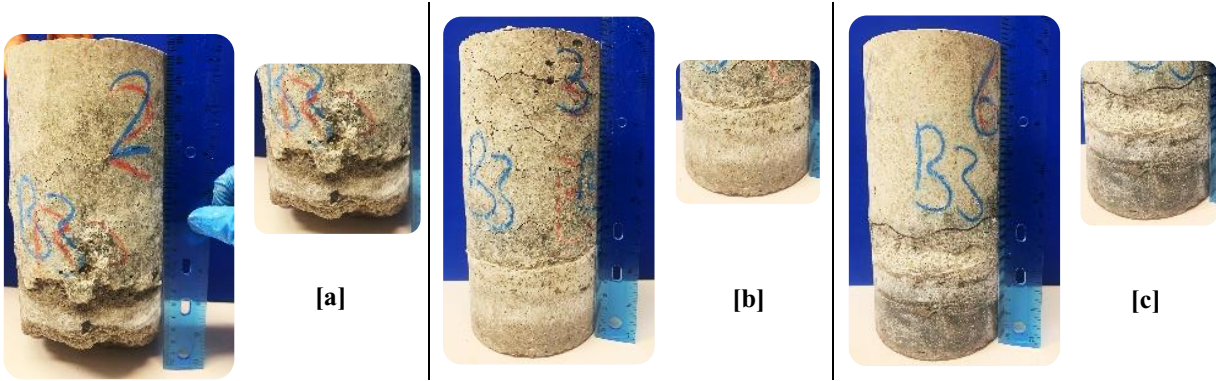


Fig. 63 – AASCC binary-1 mixtures exposed to a) 10% $MgSO_4$ b) 10% Na_2SO_4 and c) 10% mixed sulfate solutions at a controlled pH environment

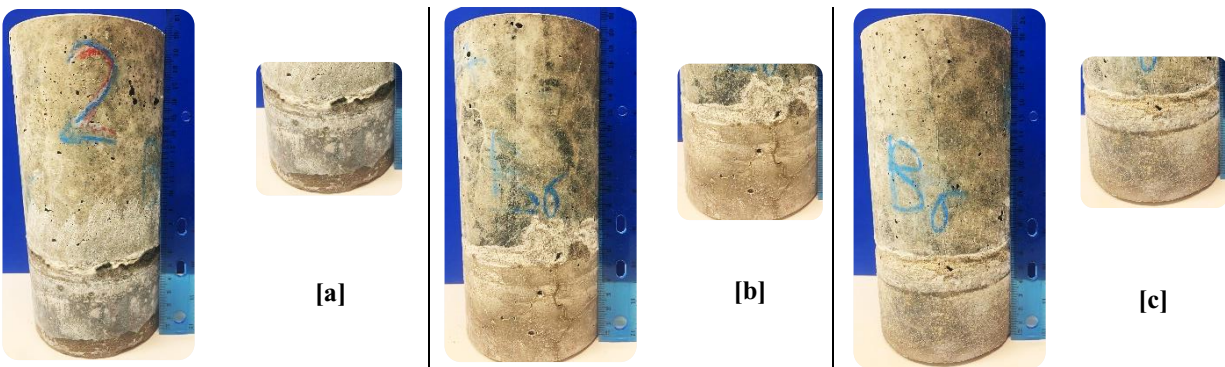


Fig. 64 – AASCC binary-2 mixtures exposed to a) 10% $MgSO_4$ b) 10% Na_2SO_4 and c) 10% mixed sulfate solutions at a controlled pH environment

Ternary-precursor mixtures. No visible signs emerged of deterioration while exposing the ternary mixtures to different sulfate solutions in a controlled pH environment. However, the ternary-1 set of mixtures yielded a greater surface scaling at the exposed area in the 10% $MgSO_4$ (**Fig. 65a**) than in 10% Na_2SO_4 (**Fig. 65b**) sulfate solution, but the substantial loss was more significant in the former.

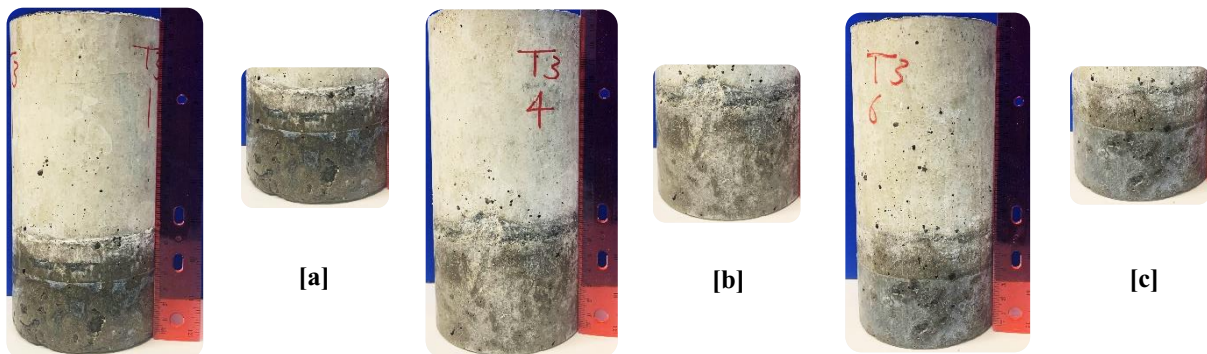


Fig. 65 – AASCC ternary-1 mixtures exposed to a) 10% $MgSO_4$ b) 10% Na_2SO_4 and c) 10% mixed sulfate solutions at a controlled pH environment

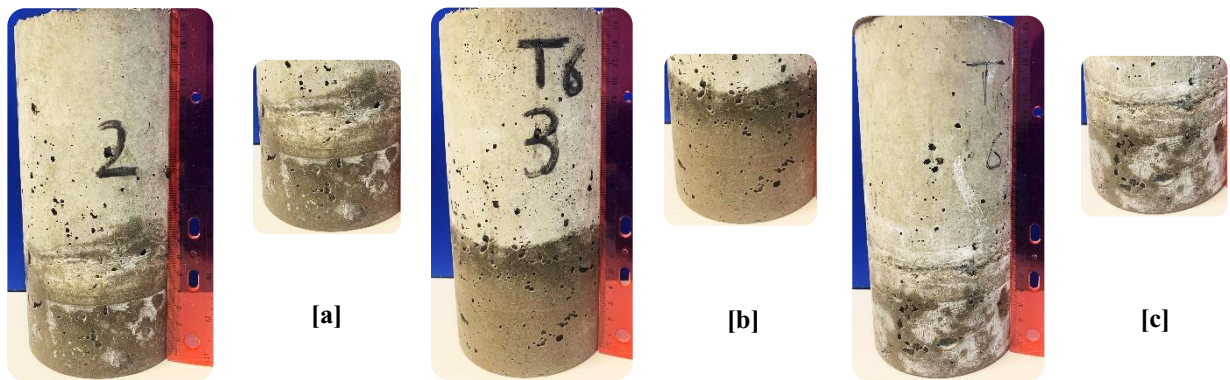


Fig. 66 – AASCC ternary-2 mixtures exposed to a) 10% MgSO_4 b) 10% Na_2SO_4 and c) 10% mixed sulfate solutions at a controlled pH environment

6.5.1.2. Mass and Cross-Section Variations

Single-precursor mixtures. Fig. 67 shows the mass variation of single-precursor AASCC cylinders after the partial immersion in 10% MgSO_4 , 10% Na_2SO_4 , and 10% mixed controlled pH sulfate solutions. While Fig. 68 shows the cross-section variation of these specimens after the partial immersion for 182 days. When exposed to a 10% MgSO_4 , 10% mixed, and 10% Na_2SO_4 sulfate solutions, the cross-section decrease (0.5%, 1%, and 1.4%) was negligible, while the mass remained to decrease but below 1%, probably due to alkalis and calcium leaching.

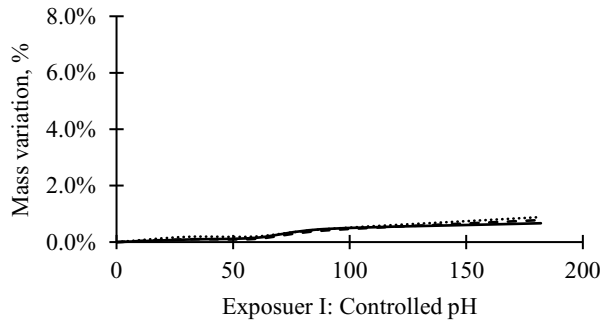


Fig. 67 – Time-dependent mass change of single-precursor AASCC mixtures exposed to 10% solutions at a controlled pH environment

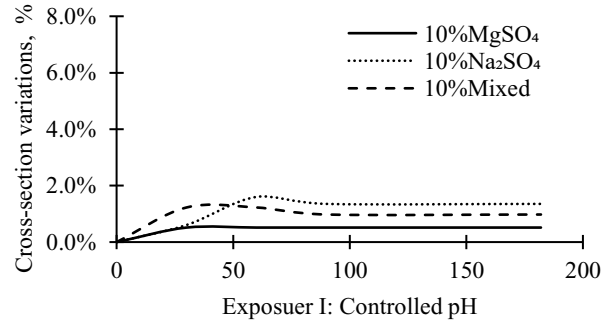


Fig. 68 – Time-dependent cross-section change of single-precursor AASCC mixtures exposed to controlled pH environment

The absence of significant damage in AASCC single-precursor specimens using 100% slag in the 10% sulfate solutions suggests the scarce formation of expansive products such as ettringite and gypsum. The presence of aluminum in C-A-S-H and hydrotalcite gels, combined with the absence of portlandite, can result in high resistance to sulfate attack in single-precursor mixtures containing 100% slag (Komljenović et al., 2013). The XRD analysis suggests that the supply of calcium and/or aluminum in single-precursor mixtures is insufficient to allow ettringite formation, as

shown in **Fig. 69**. However, traces of gypsum were detected in the samples exposed to 10% MgSO_4 solutions.

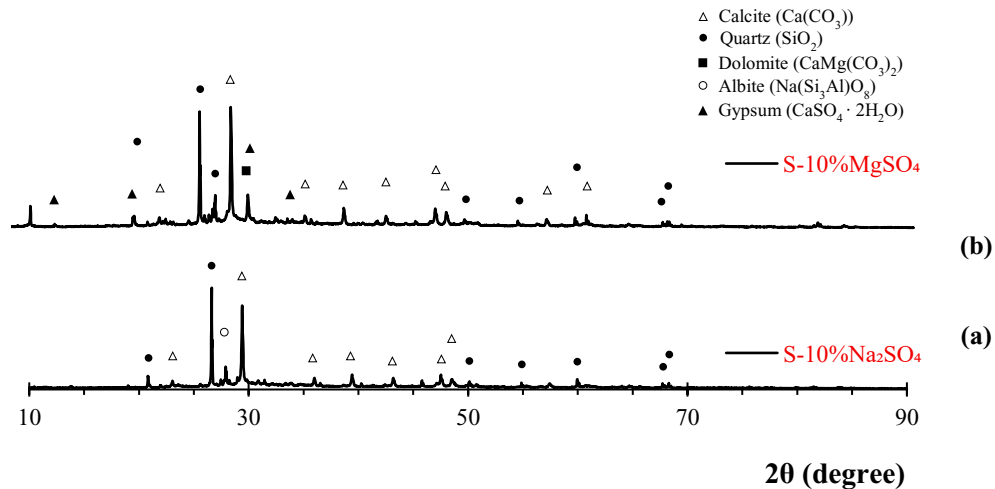


Fig. 69 – XRD spectra of AASCC single-precursor specimens exposed to sulfate attack: (a) In 10% Na_2SO_4 solution; (b) In 10% MgSO_4 solution

Binary-precursor mixtures. The mass and cross-section variations of binary-precursor specimens after six months of partial immersion in 10% different sulfate solutions were presented in **Fig. 71** and **Fig. 72 (a and b)**. It can be observed that the results in binary mixtures vary depending on the precursor type used, either SF in binary-1 or FA in binary-2. In the controlled 10% MgSO_4 solution, the binary-1 AASCC mixture made with 10% SF replacing slag yielded a maximum mass and cross-section loss of about 6.6% and 11.5%, respectively. This expected behavior can be attributed to the two-way ion diffusion between MgSO_4 sulfate solution and mixtures. The high concentrations of Ca, Mg, and Na in the binary-1 AASCC mixture have been observed in ion chromatography results in **Table 23**, resembling the sulfate resistance performance of the binary-1 mixture.

In the AASCC binary-1 mixtures with 10% SF substituting slag, XRD analysis revealed various degradation products in different sulfate solutions (**Fig. 70**). Gypsum was the predominant expansive product present in MgSO_4 solution samples after 6 months of immersion. It is important to note that gypsum formation can result in softening and a loss of mass and strength over time. However, a trace of ettringite was found in samples subjected to Na_2SO_4 solution due to the interactions between sulfate ions and AASCC paste components. Likewise, ettringite was present in the samples exposed to a 10% MgSO_4 + 10% Na_2SO_4 mixed solution, and a significant amount of thenardite precipitates was identified. The damage above the solution level can be explained through the salt crystallization pressure theory. A supersaturated solution can create salt crystals, which exert pressure on the concrete pore walls, potentially damaging the matrix (Thaulow and Sahu, 2004).

Overall, the average pore diameter of a material determines its permeability, which influences the ion exchange rate after exposure to a sulfate environment. Therefore, increasing the densification

level of the forming pore structure appears to enhance the performance of concrete exposed to aggressive environments. According to the sorptivity and volume of permeable pores results in Chapter 5, the positive substitution of slag with SF in binary-1 mixtures reduced their durability when exposed to external sulfate environments. This could be related to an increase in the small-diameter pores percentage in binary-1 mixtures and an increase in capillary suction. As a result, the specimen's upper surface area for evaporation increased, making the cylinder more vulnerable to physical attack.

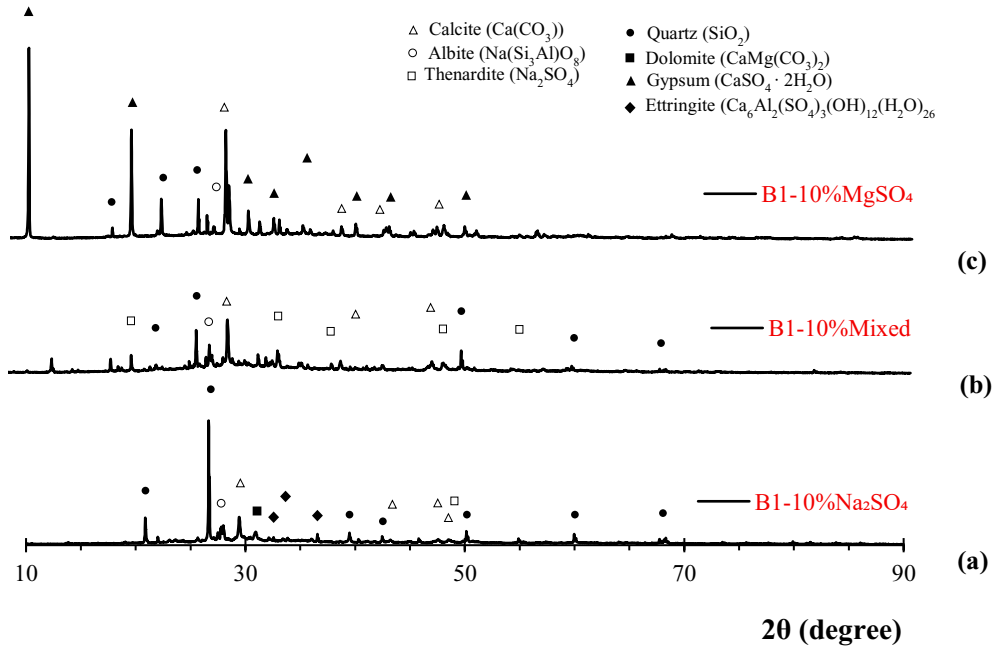


Fig. 70 – XRD spectra of binary-1 AASCC specimens exposed to sulfate attack: (a) In 10% Na_2SO_4 solution; (b) In 10% Mixed solution ; (c) In 10% MgSO_4 solution

The binary-2 mixture made with 30% FA, on the other hand, had a mass and cross-section loss that was about 86% lower than the binary-1 mixture. When exposed to 10% Na_2SO_4 and mixed sulfate solutions, the mass loss was limited to 1% in binary-1 and 1.5% in binary-2 mixtures. For both binary sets, the minimal mass and cross-section variation was observed in 10% Na_2SO_4 due to the C-(N)-A-S-H gel changes leading to the formation of microcracks within the binary network structure. However, the MgSO_4 attack mechanism can cause decalcification of calcium-containing systems such as C-(N)-A-S-H gels with high calcium content. This can lead to the formation of gypsum ($\text{CaSO}_4 \cdot 2\text{H}_2\text{O}$) gels that lack cementing properties (Ismail et al., 2013; Yusuf, 2015; Elyamany et al., 2018; Valencia-Saavedra et al., 2018).

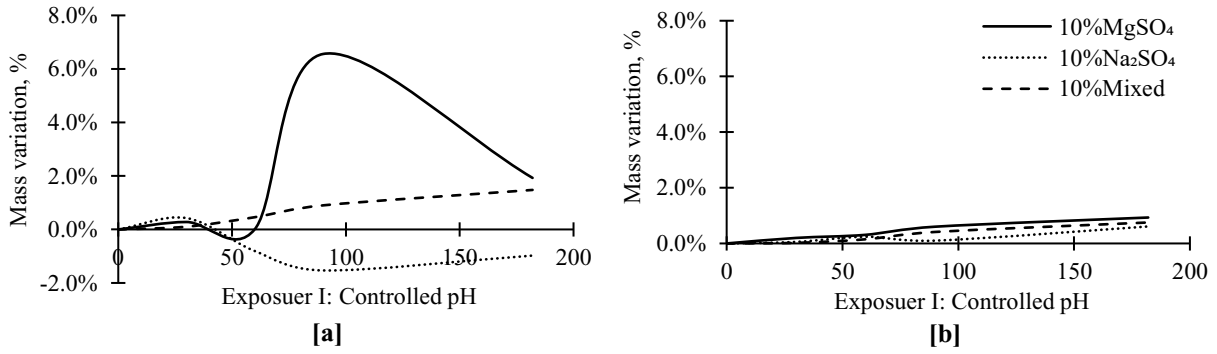


Fig. 71 – Time-dependent mass change of binary-precursor AASCC mixtures exposed to 10% sulfate solutions at a controlled pH environment a) binary-1 and b) binary-2

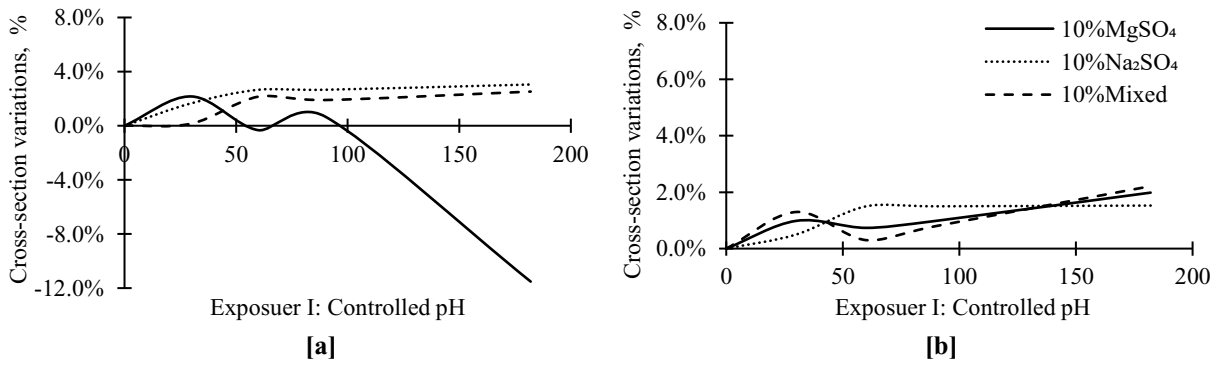


Fig. 72 – Time-dependent cross-section change of binary-precursor AASCC mixtures exposed to 10% sulfate solutions at a controlled pH environment a) binary-1 and b) binary-2

The only main component responsible for sulfate attack identified in the degraded sections above the solution level in all AASCC samples was gypsum (**Fig. 73**). However, there was evidence of physical sulfate attack damage in the form of surface scaling above the solution level, notably in the samples subjected to 10% mixed solution. Thus, chemical sulfate attack resulting from dual interactions between sulfate solutions and samples is more likely to be the dominating mechanism.

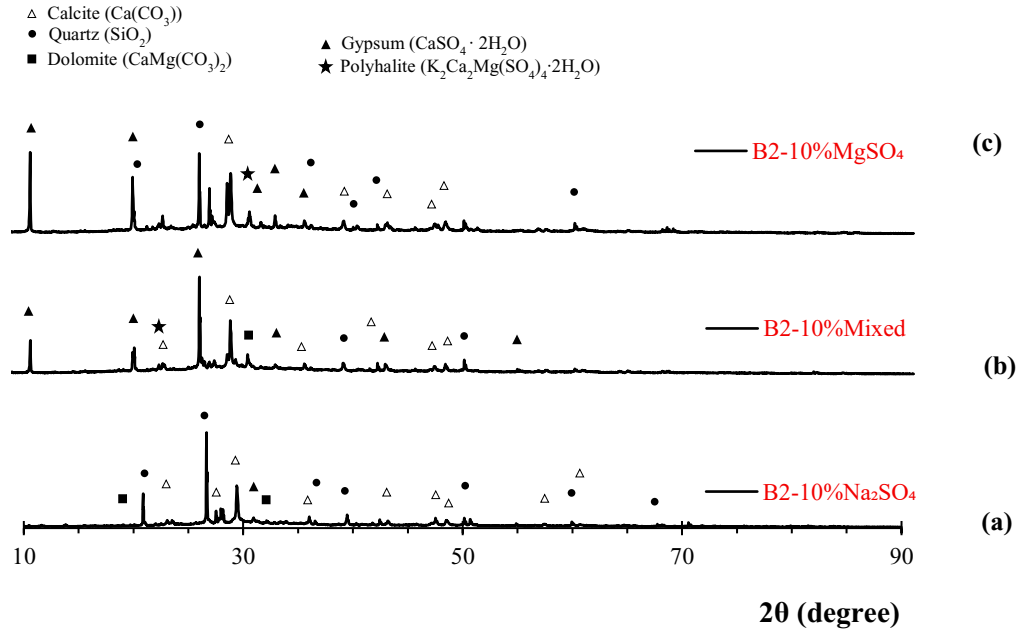


Fig. 73 – XRD spectra of binary-2 AASCC specimens exposed to sulfate attack: (a) In 10% Na₂SO₄ solution; (b) In 10% Mixed solution ; (c) In 10% MgSO₄ solution

Ternary-precursor mixtures. The mass and cross-section variations of the ternary-precursor mixtures were almost identical. Both sets lost about 2.3% of their mass but remained constant until the end of the testing period (**Fig. 74**). At the same time, ternary-1 specimens resulted in about 2% and 4% cross-section loss in 10% MgSO₄ + 10% Na₂SO₄ and 10% Na₂SO₄ solutions, respectively. The mass loss in ternary blends can be attributed to the occurrence of C-A-S-H gels in calcium-rich mixtures due to the inclusion of Al₂O₃ in their structure, which resembles the sulfate attack mechanism in OPC mixtures. Incorporating low or free-calcium precursors, on the other hand, increased the ion exchange reactions between the various sulfate solutions and the ternary-precursor matrix. However, due to the high competition between carbonate and sulfate ions, extensive ettringite formation may be overlooked and kept under control when a sodium carbonate activator is used.

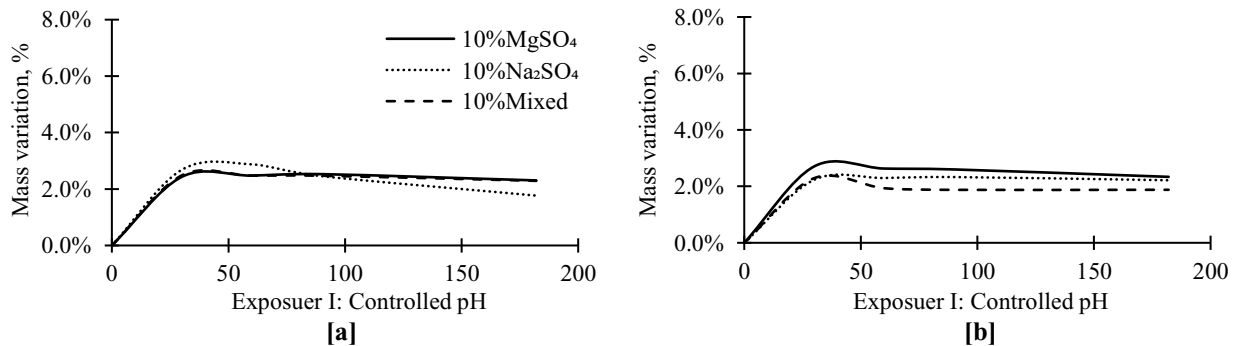


Fig. 74 – Time-dependent mass change of ternary-precursor AASCC mixtures exposed to 10% sulfate solutions at a controlled pH environment a) ternary-1 and b) ternary-2

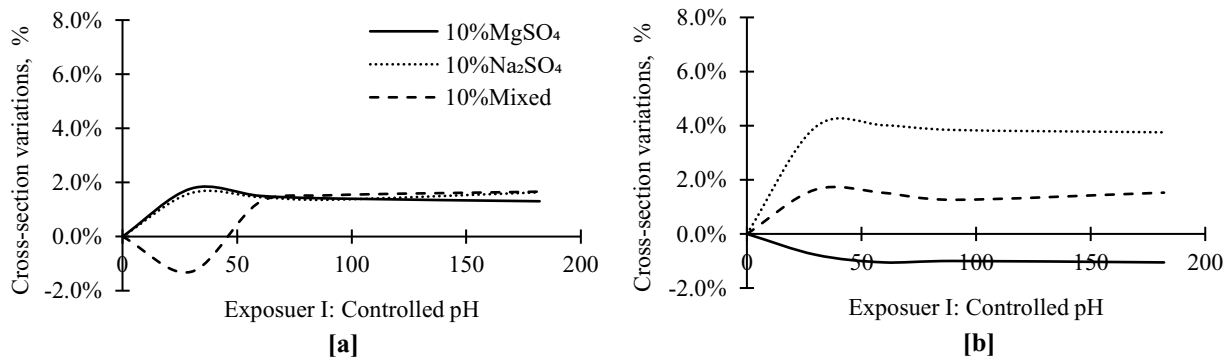


Fig. 75 – Time-dependent mass change of ternary-precursor AASCC mixtures exposed to 10% sulfate solutions at a controlled pH environment a) ternary-1 and b) ternary-2

XRD spectroscopy (**Fig. 76**) verified the structural changes in ternary-precursor blends, revealing thenardite in the damaged regions of samples exposed to a 10% Na_2SO_4 solution; however, gypsum was formed in specimens immersed in a 10% MgSO_4 solution. Overall, the formation of expansive gypsum and ettringite crystals is associated with exposure to external sources of sulfate attack. These crystals can colonize and accumulate in the concrete mixture's pores. Once filled, these crystals can cause significant volumetric strain, leading to microcracking and concrete deterioration. Thus, crystallization of sulfates in macroscopic pores and cracks is preferred. This is related to the formation of large-size expansive crystals, such as ettringite, which cannot exert a high crystallization pressure and thus are unlikely to be the source of the destruction. Since small crystals are prone to dissolution due to their unstable state, they are in equilibrium with higher concentrations of sulfates.

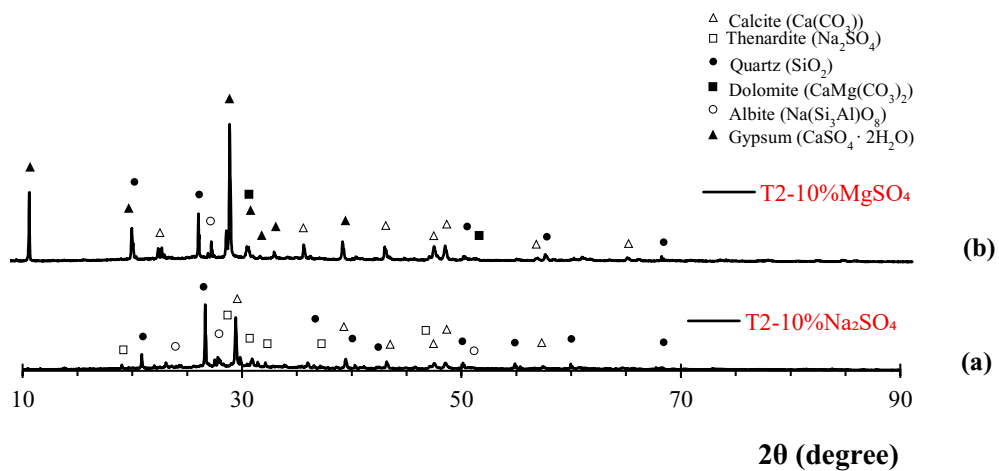


Fig. 76 – XRD spectra of ternary-2 AASCC specimens exposed to sulfate attack: (a) In 10% Na_2SO_4 solution; (b) In 10% MgSO_4 solution

6.5.1.3. Ion Chromatography

Table 23 shows the ion chromatography analysis of different AASCC systems in controlled 10% sulfate solutions after 182 days of exposure. Na^+ , Ca^{2+} , and Mg^{2+} concentrations in 10% MgSO_4 , 10% Na_2SO_4 , and 10% $\text{Na}_2\text{SO}_4 + 10\% \text{MgSO}_4$ sulfate solutions were significantly increased during the testing period. For single-precursor mixtures, concrete cylinders with 100% slag showed high concentration level of leached Ca when exposed to 10% MgSO_4 (756 mg/l) and 10% $\text{MgSO}_4 + 10\% \text{Na}_2\text{SO}_4$ (522 mg/l) than in 10% Na_2SO_4 (42 mg/l) sulfate solutions. In contrast, the concentrations of Na and Ca in all sulfate solutions were extremely high, especially in binary-1 mixtures with 10% SF replacing slag, indicating that these elements were leached from the mixtures into solutions, which was in line with the findings of a few previous studies (Bakharev, 2005; Ismail et al., 2013). The decrease in pH of sulfate solutions ≤ 9.8 resulted in the decalcification of C-(A)-S-H gel, which was revealed by the increased Ca concentration in the sulfate solutions. For example, in MgSO_4 and mixed sulfate solutions, the Ca concentration was 34,820 mg/l and 25,322 mg/l, respectively compared with 22,405 mg/l in Na_2SO_4 solutions.

Exposure of binary-2 silicon-rich mixtures to various sulfate solutions resulted in extensive leaching of Si, Na, and Ca into the solutions. For instance, in 10% MgSO_4 and 10% Na_2SO_4 solutions, the concentration of SiO_3 was about 396 and 320 mg/l, respectively. While in 10% mixed sulfate solution, the concentration of SiO_3 recorded was 638 mg/l after 182 days. This can be caused by the leaching of the unreacted sodium silicate content present in the pore solution or the gel structure. However, due to the continuous monitoring of pH and the depletion of silicon sources present in the AASCC binary FA-slag mixtures, the amount of leached Si decreased over time. The high pH value of the sulfate solutions used to make binary-2 mixtures has been identified as a contributing factor to the Si leaching, which was shown earlier (Bašcarević et al., 2015; Sindhunata et al., 2008; Temuujin et al., 2011).

Table 23 – Ion chromatography analysis and pH after 182 days in 10% sulfate solutions of the different AASCC systems

Sulfate solution	Mixture I.D.	pH	Element concentration in different sulfate solutions (mg/l)			
			Na	Ca	Mg	SiO_3
10% MgSO_4	Single	10.1	3515	756	87	26
	Binary-1	9.40	32485	34820	581	48
	Binary-2	10.1	6468	604	257	396
	Ternary-1	9.90	6920	836	999	25
	Ternary-2	10.1	3516	13679	1368	135
10% Na_2SO_4	Single	13.6	5739	42	247	22
	Binary-1	9.80	98134	25322	436	64
	Binary-2	11.3	4070	112	262	320
	Ternary-1	12.8	4439	202	25	16
	Ternary-2	12.8	5190	614	3	81
10% $\text{MgSO}_4 + 10\% \text{Na}_2\text{SO}_4$	Single	10.9	6299	522	145	20
	Binary-1	9.80	88184	22405	1266	53
	Binary-2	10.3	5886	460	794	638
	Ternary-1	10.2	5800	1348	1678	25
	Ternary-2	10.3	6783	5846	1109	84

The Na^+ , Ca^{2+} , and Mg^{2+} concentrations in ternary-precursor mixtures also increased over time, demonstrating a more pronounced impact of aggressive sulfate solutions on calcium-containing compounds like C-(N)-A-S-H gel in MgSO_4 and hybrid solutions. The test results of both ternary sets showed that higher pH values between 10 and 13 after 182 days of testing due to pore solution alkalis leaching or Ca release into the solutions due to the system's reaction with different sulfate compounds and ion exchange (Palomo et al., 1999; Bakharev, 2005, Ismail et al., 2013). Ternary-2 and ternary-1, for example, had Ca concentrations of 13,679 and 836 mg/l, 614 and 202 mg/l, and 5,846 and 1,348 mg/l in 10% MgSO_4 , 10% Na_2SO_4 , and mixed sulfate solutions, respectively.

6.5.2. Exposure II: NonControlled pH

6.5.2.1. Visual Appearance

Single-precursor mixtures. Fig. 77 (a–c) shows the visual appearance of AASCC single-precursor mixtures exposed partially to noncontrolled pH sulfate solutions revealed; (a) no signs of deterioration of the specimens of 100% AASCC single concrete in 10% MgSO_4 solution (Fig. 77a), (b) few spales of concrete at the exposed areas of specimens immersed in 10% Na_2SO_4 solution (Fig. 77b), (c) cracking and mass loss of concrete above the sulfate solution level of specimens immersed in 10% Na_2SO_4 + 10% MgSO_4 solution (Fig. 77c). All specimens were surrounded with whitish precipitates, which indicated that the concrete had been affected.

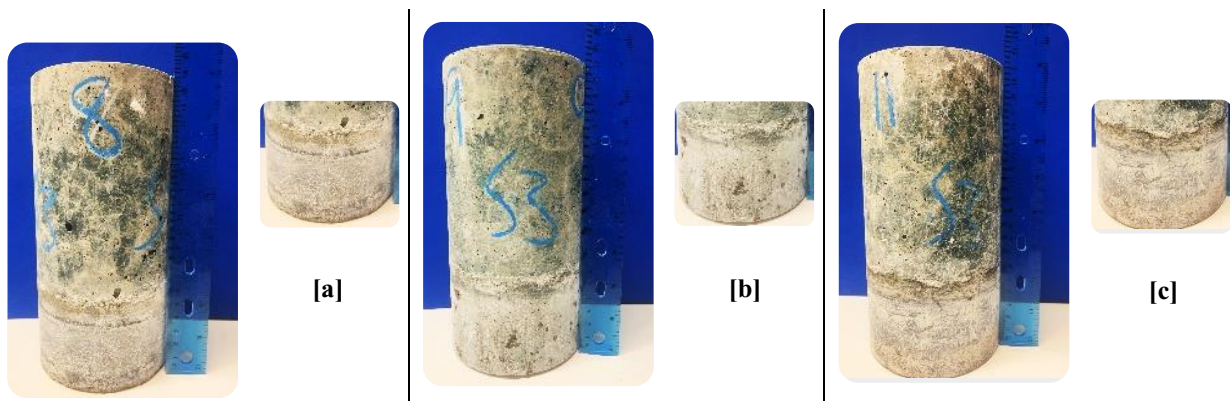


Fig. 77 – AASCC single-precursor mixtures exposed to a) 10% MgSO_4 b) 10% Na_2SO_4 and c) 10% mixed sulfate solutions at a noncontrolled pH environment

Binary-precursor mixtures. The noncontrolled pH exposure condition of binary-1 specimens to sulfate solutions for six months resulted in a higher level of deterioration, unexpectedly, as shown in Fig. 78(a–c). The severe loss of the concrete matrix at the bottom edge and above the exposed area was caused by the exposure to the MgSO_4 sulfate solution (Fig. 78a). In 10% Na_2SO_4 solution, broken portions above the partially exposed areas were noticeable (Fig. 78b), while white deposits were observed in 10% mixed solutions (Fig. 78c). For the binary-2 set of mixtures, in a noncontrolled pH sulfate environment, the surface erosion was minimal in all specimens above the exposed area; however, it was significantly greater in 10% MgSO_4 (Fig. 79a) and 10% MgSO_4 + 10% Na_2SO_4 (Fig. 79c) sulfate solutions.

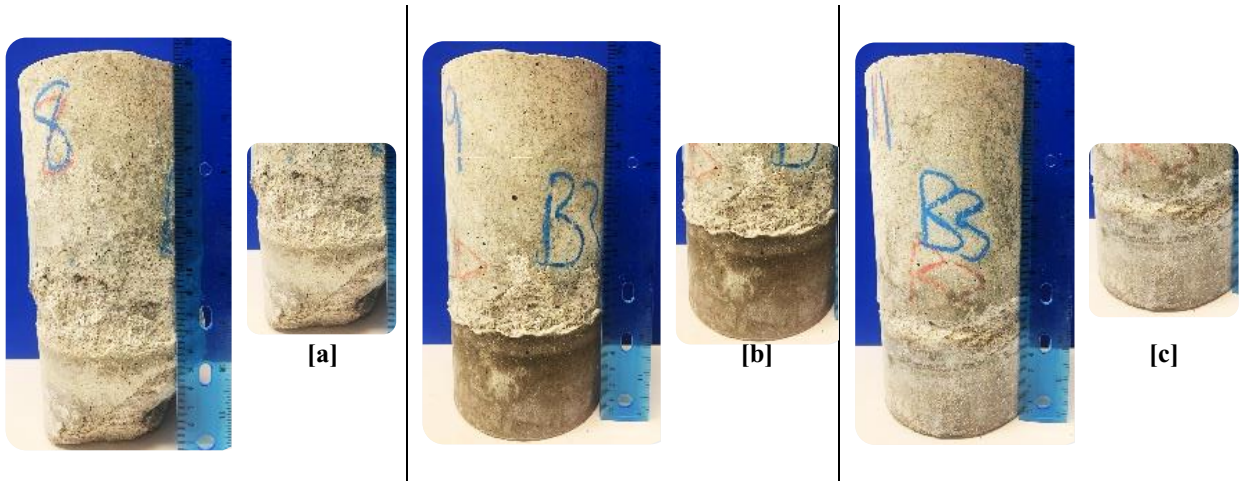


Fig. 78 – AASCC binary-1 mixtures exposed to a) 10% MgSO_4 b) 10% Na_2SO_4 and c) 10% mixed sulfate solutions at a noncontrolled pH environment

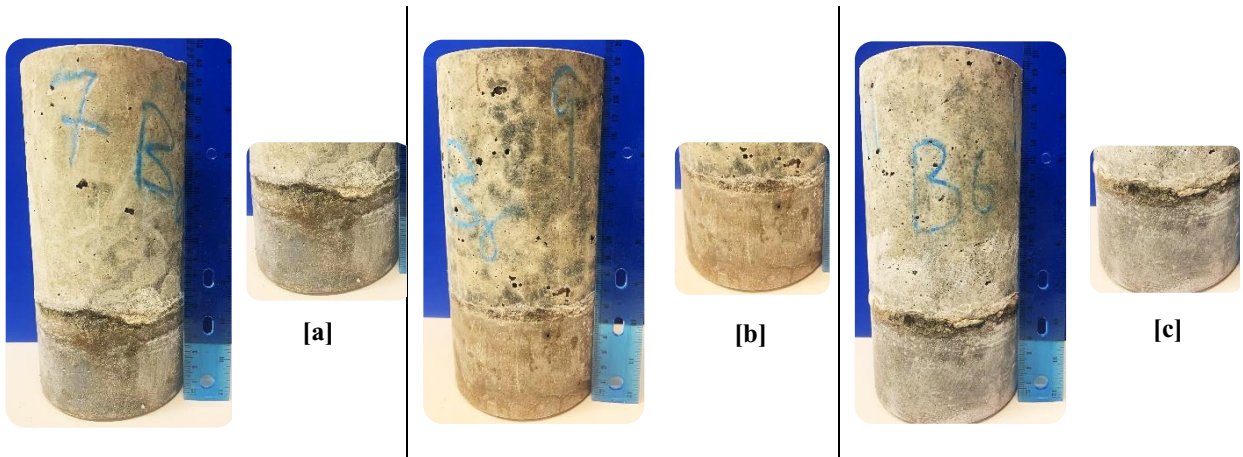


Fig. 79 – AASCC binary-2 mixtures exposed to a) 10% MgSO_4 b) 10% Na_2SO_4 and c) 10% mixed sulfate solutions at a noncontrolled pH environment

Ternary-precursor mixtures. After six months of exposure to sulfate solutions in a noncontrolled pH environment, the scaling of ternary-2 (**Fig. 81**) concrete surfaces appeared higher than that of ternary-1 mixtures (**Fig. 80**), which appeared above the sulfate solution level.

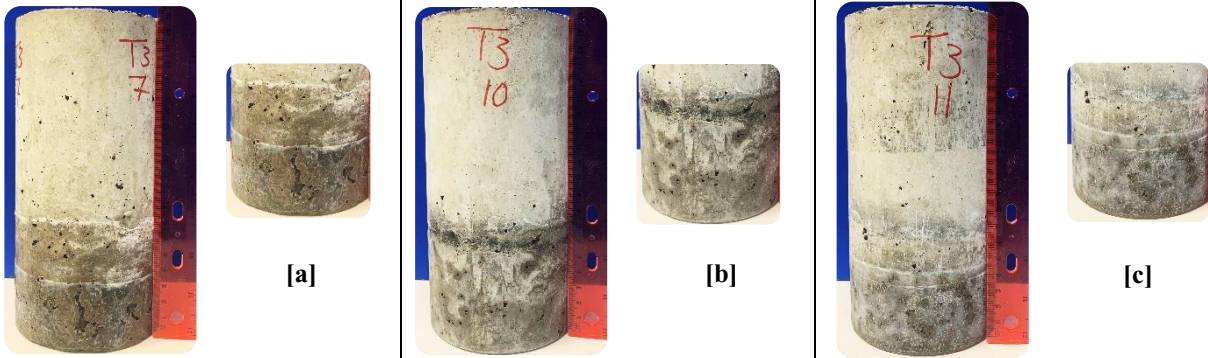


Fig. 80 – AASCC ternary-1 mixtures exposed to a) 10% MgSO_4 b) 10% Na_2SO_4 and c) 10% mixed sulfate solutions at a noncontrolled pH environment

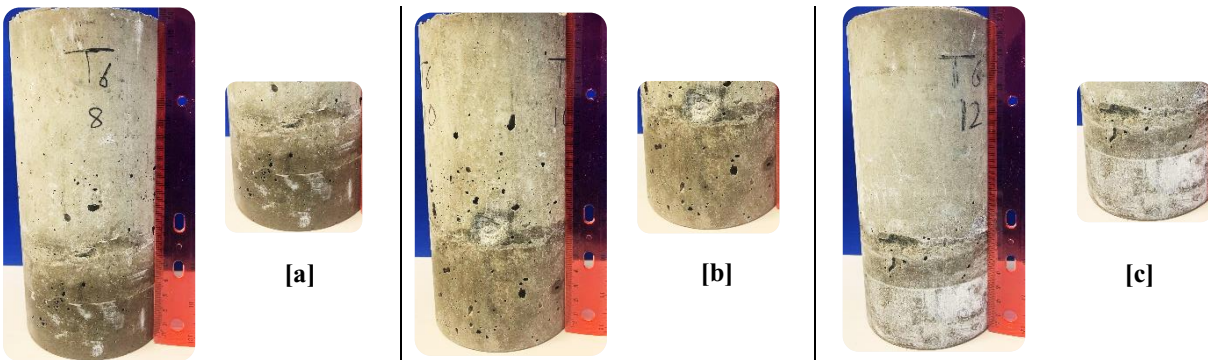


Fig. 81 – AASCC ternary-2 mixtures exposed to a) 10% MgSO_4 b) 10% Na_2SO_4 and c) 10% mixed sulfate solutions at a noncontrolled pH environment

6.5.2.2. Mass and Cross-Section Variations

Single-precursor mixtures. Fig. 82 and Fig. 83 show the time-dependent mass and cross-section variations of AASCC 100% slag specimens during the partial immersion in 10% MgSO_4 , 10% Na_2SO_4 and 10% MgSO_4 + 10% Na_2SO_4 non-controlled pH sulfate solutions. White deposits were observed for all mixtures when exposed to all sulfate solutions, although mass loss remained constant at less than 1%, most likely due to alkalis leaching in a near-neutral pH environment. On the other hand, the reaction between sulfates and AASCC slag mixtures caused a change in the cross-section of specimens, especially before the renewal of solutions ~100 days. Exposure to 10% MgSO_4 solutions for 30 days produced a 2% change in cross-section, which is about double the increase in the other sulfate solutions, yet the change was minimal till the end of the test. In 10% Na_2SO_4 and mixed sulfate solutions, a progressive increase in cross-section loss was noticed until the end of the testing period, indicating the little possible development of expansive ettringite or gypsum.

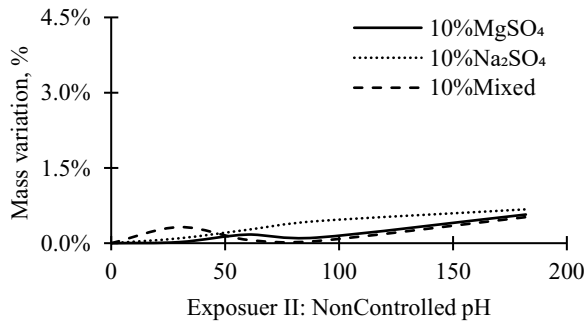


Fig. 82 – Time-dependent mass change of single-precursor AASCC mixtures exposed to a noncontrolled pH environment

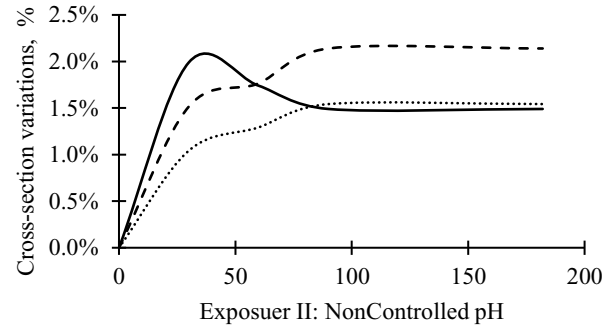


Fig. 83 – Time-dependent cross-section change of single-precursor AASCC mixtures exposed to a noncontrolled pH environment

Binary-precursor mixtures. The mass change of binary-precursor samples exposed to 10% MgSO_4 , 10% Na_2SO_4 , and 10% $\text{MgSO}_4 + 10\% \text{Na}_2\text{SO}_4$ solutions in an uncontrolled pH environment is shown in **Fig. 84 (a and b)**. While **Fig. 85 (a and b)** illustrates their corresponding cross-section variations after 182 days of partial immersion. The mass loss noted for binary-1 samples (**Fig. 84a**) subjected to MgSO_4 solution was 0.4% after 30 days of exposure, declining until the sulfate solution was renewed, yielding a mass gain of nearly 0.1% after 90 days. Samples continued to lose mass when the pH dropped between 6 - 8 at the end of the exposure period (2.1%) during solutions renewal. A different trend is observed for binary-2 samples in MgSO_4 solutions, where a marginal mass gain (0.1%) was noticed after 30 days, followed by a gradual mass loss reaching about 1%. However, neither binary set of samples exposed to Na_2SO_4 and mixed sulfate solutions was significantly affected, with mass losses of (0.8% and 0.7%) for binary-1 and (1.1% and 0.9%) for binary-2, respectively.

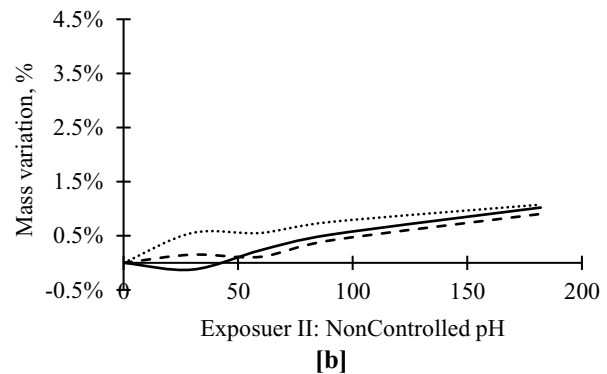
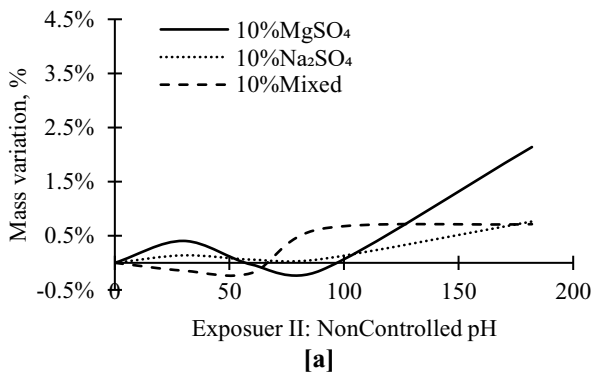


Fig. 84 – Time-dependent mass change of binary-precursor AASCC mixtures exposed to 10% sulfate solutions at a noncontrolled pH environment a) binary-1 and b) binary-2

Fig. 85 (a and b) shows the cross-section changes that occurred due to the degradation and surface scaling of the AASCC two binary-precursor sets. The highest cross-section change was observed in the MgSO_4 solution for the binary-1 specimens (4.4%) made with 10% SF replacing slag, followed by cylinders exposed to Na_2SO_4 and mixed sulfate solutions with up to 2.4%. On the other hand, the binary-2 AASCC portion immersed into all sulfate solutions was mostly

intact for all cylinders. Above the solution level, exposure to 10% MgSO₄ + 10% Na₂SO₄, 10% Na₂SO₄, and 10% MgSO₄ sulfate solutions for 182 days resulted in 2%, 1.7%, and 1.4% cross-section variation, respectively.

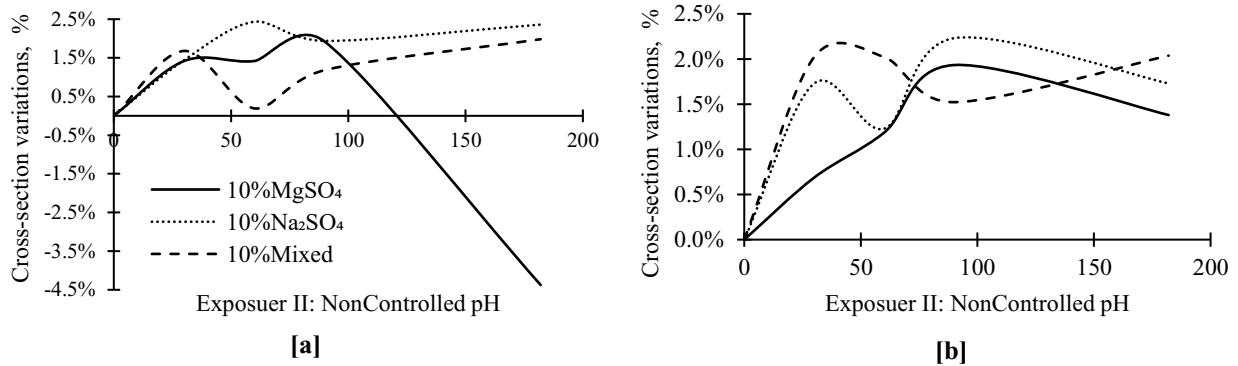


Fig. 85 – Time-dependent cross-section change of binary-precursor AASCC mixtures exposed to 10% sulfate solutions at a noncontrolled pH environment a) binary-1 and b) binary-2

Ternary-precursor mixtures. After 182 days of exposure to sulfate solutions, the exposed surface of the samples had no deposits and mostly showed no visible signs of deterioration in both sets of ternary mixtures. However, there were some mass changes in the samples of < 4% at the end of the testing period (**Fig. 86 a and b**). The ternary-1 samples prepared using a higher slag content lost a mass of 3.2% in the mixed sulfate, 2.5% in the Na₂SO₄, and 2.2% in the MgSO₄ sulfate solutions after 182 days of immersion. The extent of damage to ternary-1 specimens due to partial noncontrolled sulfate attack was not greatly associated with the cross-section changes.

Ternary-2 cylinders gained 0.1% in the magnesium sulfate solution after 90 days of exposure and lost 0.5% at the end of the test. However, ternary-2 mixtures exposed to mixed and sodium sulfate solutions lost 1.8% and 0.5% at a noncontrolled pH environment. In the solutions of Na₂SO₄+MgSO₄ and Na₂SO₄, ternary-2 samples had the most cross-section changes: 1.1% and 1.3% loss, while around 1.5% gain in the MgSO₄ solution (**Fig. 87b**).

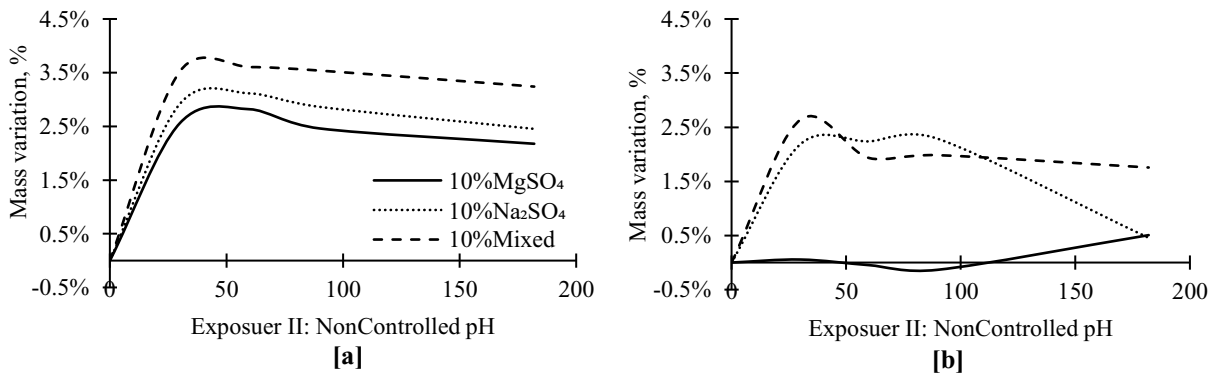


Fig. 86 – Time-dependent mass change of ternary-precursor AASCC mixtures exposed to 10% sulfate solutions at a noncontrolled pH environment a) ternary-1 and b) ternary-2

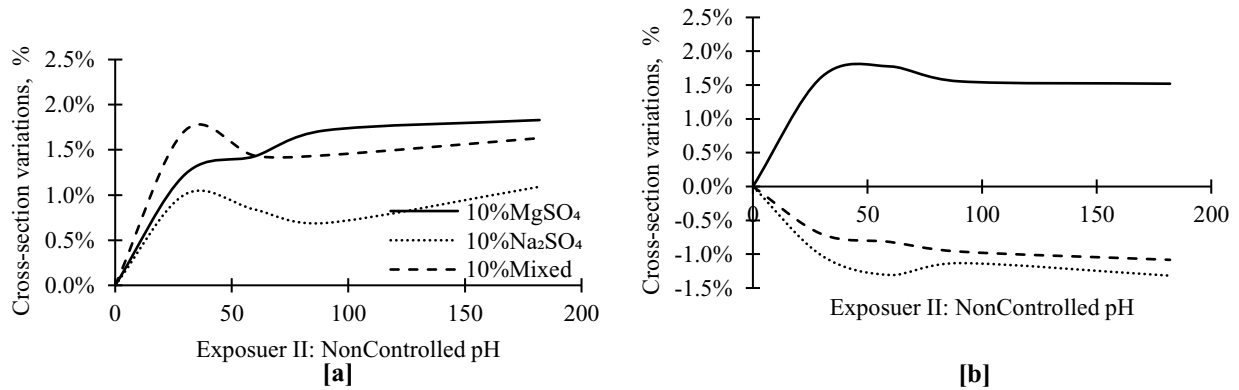


Fig. 87 – Time-dependent cross-section change of ternary-precursor AASCC mixtures exposed to 10% sulfate solutions at a noncontrolled pH environment a) ternary-1 and b) ternary-2

6.5.3. Exposure III: 5% Sulfate Solution - Controlled pH

6.5.3.1. Visual Appearance

Single-precursor mixtures. No signs of deterioration were detected after the exposure partially of single slag AASCC mixtures to 5% MgSO₄, 5% Na₂SO₄, and 5% MgSO₄ + 5% Na₂SO₄ sulfate solutions, as shown in **Fig. 88 (a-c)**. Overall, it can be observed that all single-precursor specimens remained visually intact with visual integrity, except the ones subjected to 5% MgSO₄ solution.

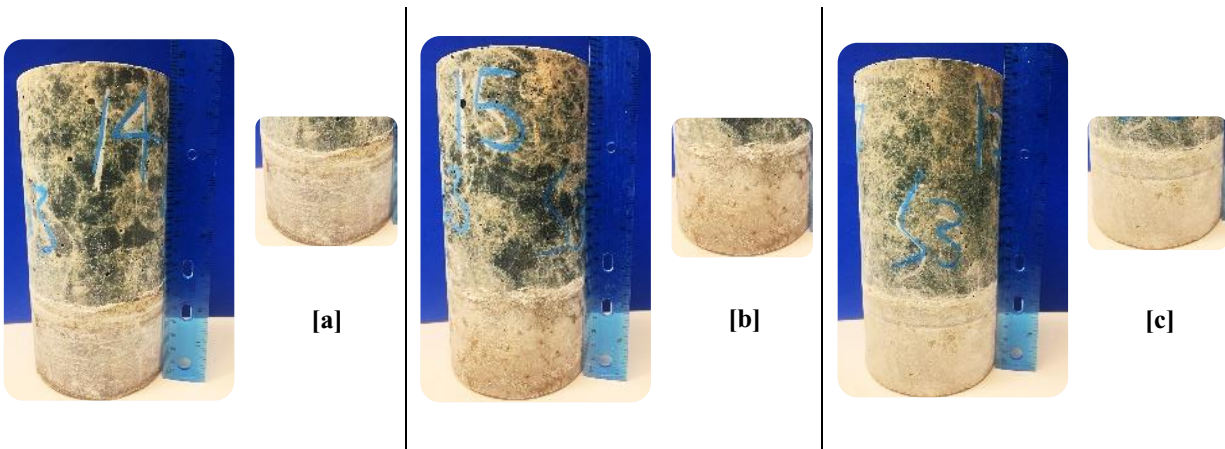


Fig. 88 – AASCC single-precursor mixtures exposed to a) 5% MgSO₄ b) 5% Na₂SO₄ and c) 5% mixed sulfate solutions at a controlled pH environment

Binary-precursor mixtures. For binary-1 mixtures using 10% SF replacing slag (**Fig. 89**) after six months of partial immersion in the 5% different sulfate solutions. The deteriorating conditions were most pronounced in 5% MgSO₄ (**Fig. 89a**) and 5% Na₂SO₄ (**Fig. 89b**) sulfate solutions. Cracks were detected along the length of the specimens in all sulfate solutions. The soft whitish material above the exposed area also showed signs of damage.

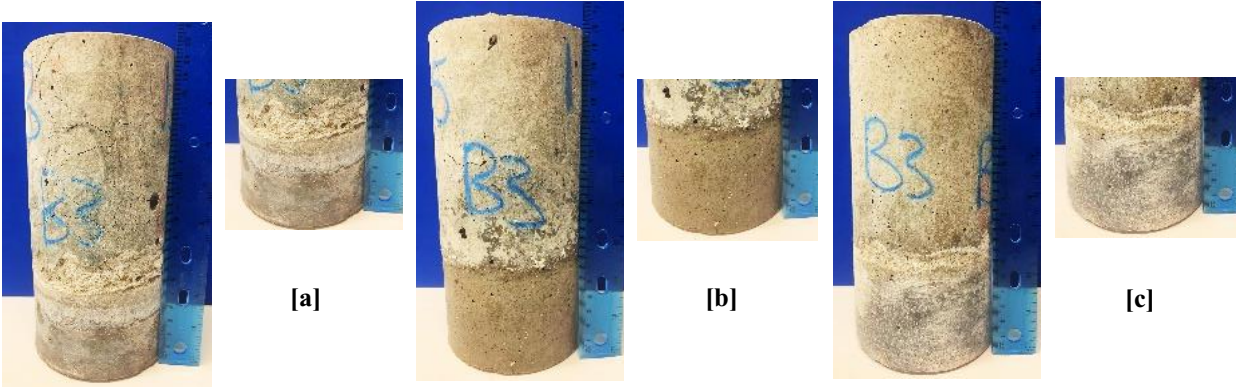


Fig. 89 – AASCC binary-1 mixtures exposed to a) 5% MgSO_4 b) 5% Na_2SO_4 and c) 5% mixed sulfate solutions at a controlled pH environment

Fig. 90 (a-c) shows binary-2 specimens after six months of partial immersion in the 5% different sulfate solutions. All binary-2 specimens were visually minimally intact, with some superficial cracks visible above the sulfates solutions level.

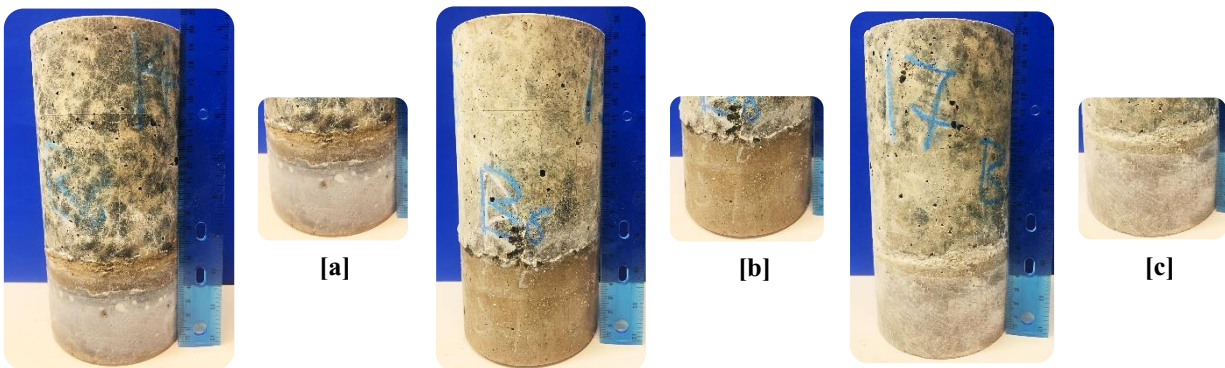


Fig. 90 – AASCC binary-2 mixtures exposed to a) 5% MgSO_4 b) 5% Na_2SO_4 and c) 5% mixed sulfate solutions at a controlled pH environment

Ternary-precursor mixtures. For both ternary-1 and ternary-2 AASCC mixtures using slag, FA, and SF, the immersed portions in the 5% sulfate solutions were mainly intact. Surface cracks and damage in the concrete's ternary-1 (**Fig. 91**) and ternary-2 (**Fig. 92**) were confined to the concrete segments above the sulfate solutions level, the maximum exposure level.

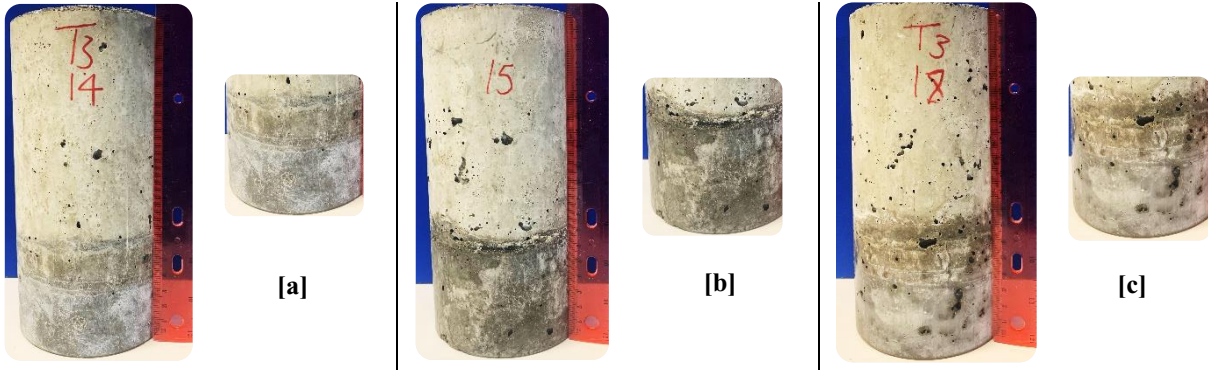


Fig. 91 – AASCC ternary-1 mixtures exposed to a) 5% MgSO_4 b) 5% Na_2SO_4 and c) 5% mixed sulfate solutions at a controlled pH environment

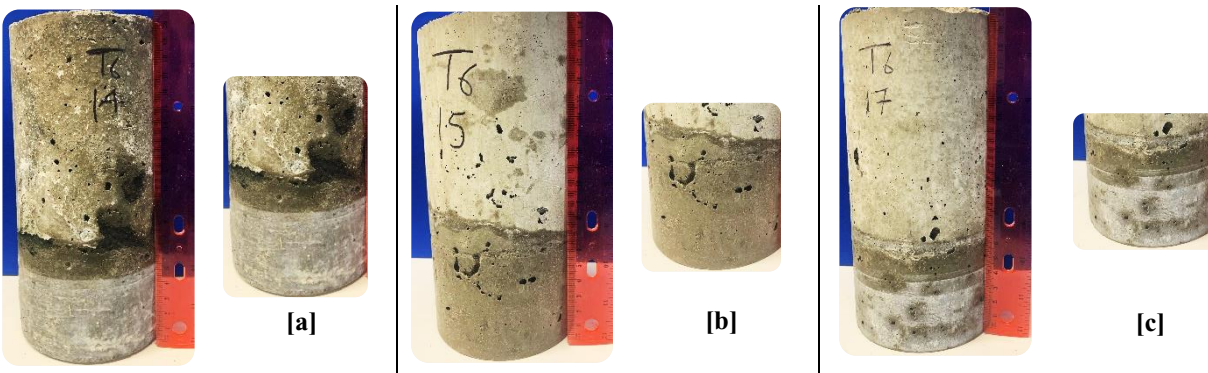


Fig. 92 – AASCC ternary-2 mixtures exposed to a) 5% MgSO_4 b) 5% Na_2SO_4 and c) 5% mixed sulfate solutions at a controlled pH environment

6.5.3.2. Mass and Cross-Section Variations

Single-precursor mixtures. The mass change of specimens made from 100% slag binder after 182 days of partial immersion in 5% various sulfate solutions is shown in **Fig. 93**. Exposing specimens to 5% MgSO_4 solution resulted in a 1% loss of mass, which is higher by 11%, and 67% than when exposed to 5% Na_2SO_4 and mixed sulfate solutions. However, the cross-section variation of the same set of samples immersed in 5% MgSO_4 solution was approximately 25% lower than that of the specimens exposed to 5% Na_2SO_4 and mixed sulfate solutions. The absence of significant deterioration in single-precursor slag specimens in 5% Na_2SO_4 and mixed solution could prove that expansive ettringite or gypsum formation is relatively low. On the other hand, specimen damage in MgSO_4 solutions could be due to the decalcification and transformation of C-(N)-A-S-H gels.

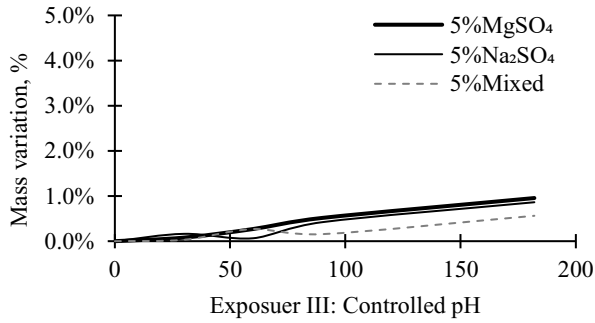


Fig. 93 – Time-dependent mass change of single-precursor AASCC mixtures exposed to 5% sulfate solutions at a controlled pH environment

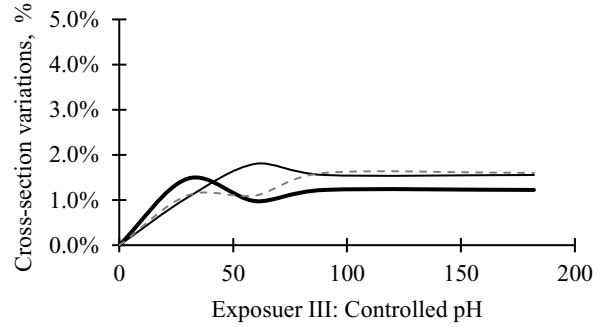
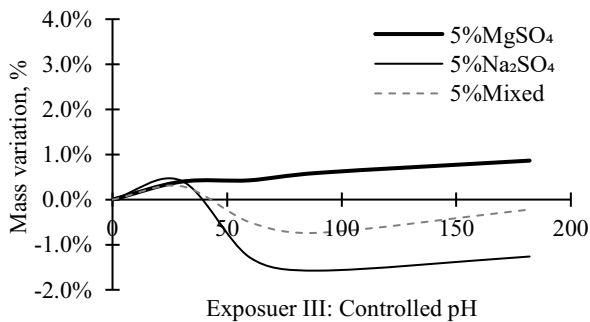
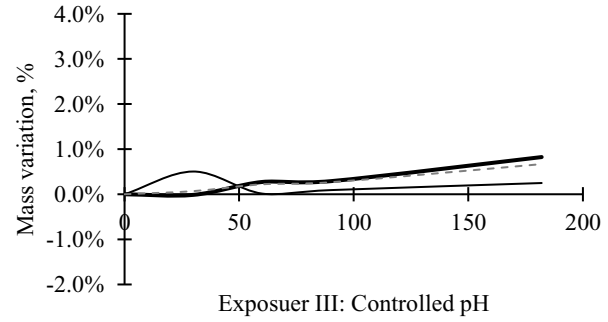


Fig. 94 – Time-dependent cross-section change of single-precursor AASCC mixtures exposed to 5% sulfate solutions at a controlled pH environment

Binary-precursor mixtures. Fig. 95 (a and b) shows the mass change of the binary-precursor cylinders in different 5% sulfate solutions. In the sodium sulfate solution, the binary-1 samples prepared using 10% SF replacing slag performed better than the binary-2 and had around 1.3% mass increase compared with 0.2% mass loss over the time of the experiment. Again, a similar trend was observed in the 5% mixed sulfate environment, with binary-1 gaining 0.2% mass after 182 days of exposure compared to losing 0.7% mass in binary-2. In contrast, in the binary-1 and binary-2 samples exposed to 5% $MgSO_4$ solutions, masses fluctuated and steadily increased from the initial value, i.e., 0.9% and 0.8%, respectively. The corresponding cross-section variations after 182 days of partial exposure are shown in Fig. 96 (a and b). Some fluctuation of the cross-section was observed in all binary-precursor specimens, especially in the magnesium and mixed sulfate solution. For example, the variations of the binary-precursor specimens finally equilibrated with a 5% and 1.2% decrease compared to the initial value in the binary-1 and binary-2 specimens, respectively. However, in the sodium sulfate solutions, 2.8% cross-section decline was measured in the binary-1 samples compared with about 1.7% in binary-2 samples. Almost similarly in the solution of sodium sulfate+magnesium sulfate, where 2.2% and 1.5% reduction were found in the binary-1 and binary-2 specimens, respectively.



[a]



[b]

Fig. 95 – Time-dependent mass change of binary-precursor AASCC mixtures exposed to 5% sulfate solutions at a controlled pH environment a) binary-1 and b) binary-2

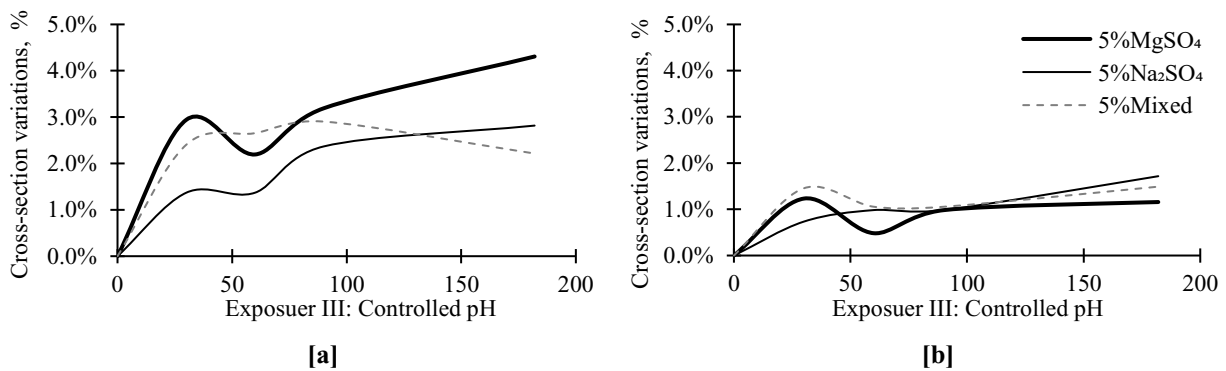


Fig. 96 – Time-dependent cross-section change of binary-precursor AASCC mixtures exposed to 5% sulfate solutions at a controlled pH environment a) binary-1 and b) binary-2

Overall, in binary mixtures exposed to 5% solution, the damage was only limited to the microstructural matrix in addition to few traces of damage above the embedded portion of cylinders, while the portion immersed in the solution was found in intact condition. The physical sulfate attack and leaching of ions were the proposed primary theories of damage. In contrast, a significant and steady paste transformation was observed after exposure to a 5% MgSO_4 solution, but little damage was observed in a 5% Na_2SO_4 solution. These findings are consistent with those of (Ismail et al., 2013), who discovered that when binary mixtures are exposed to MgSO_4 solution, the C-A(N)-S-H undergoes decalcification and silicate polymerization, but it remained essentially intact after exposure to Na_2SO_4 .

Ternary-precursor mixtures. For ternary-precursor mixtures exposed to different 5% sulfate solutions, the mass and cross-section variations are shown in **Fig. 97** and **Fig. 98**. After 182 days of immersion, ternary-1 cylinders with a higher Ca content showed slightly more damage than ternary-2 cylinders.

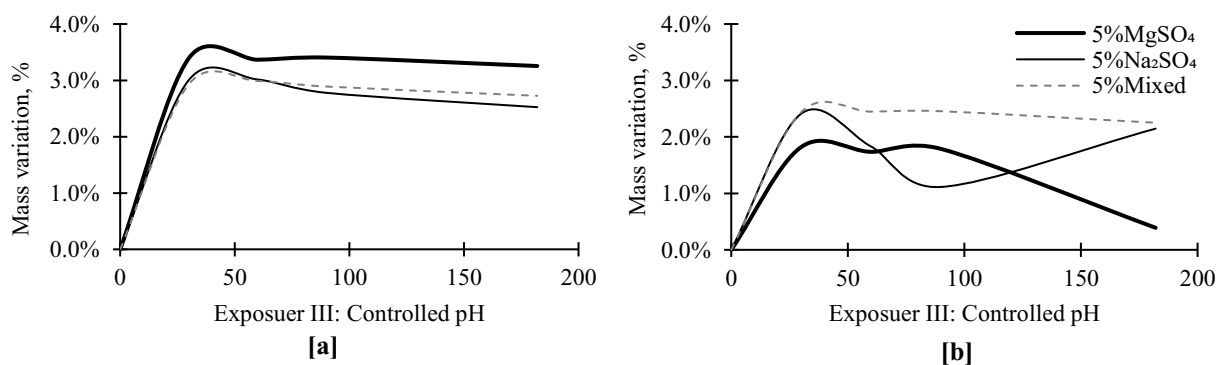


Fig. 97 – Time-dependent mass change of ternary-precursor AASCC mixtures exposed to 5% sulfate solutions at a controlled pH environment a) ternary-1 and b) ternary-2

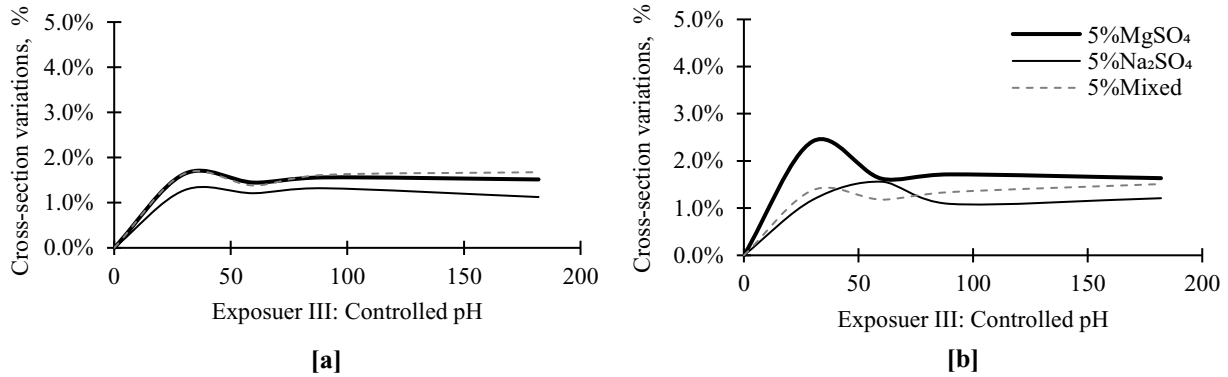


Fig. 98 – Time-dependent cross-section change of ternary-precursor AASCC mixtures exposed to 5% sulfate solutions at a controlled pH environment a) ternary-1 and b) ternary-2

For example, after immersing ternary-1 samples in MgSO_4 , Na_2SO_4 , and mixed sulfate solutions, mass losses of 3.3%, 2.5%, and 2.7% were reported, respectively. In contrast, the mass variation of all ternary-2 samples decreased as the CaO amount decreased, resulting in 0.4%, 2.1%, and 2.3% mass loss in MgSO_4 , Na_2SO_4 , and mixed sulfate solutions, respectively. Contrary to expectations and mass change results of ternary-1 samples, cross-section variation in Na_2SO_4 and mixed sulfate solutions for ternary-2 mixtures was high at about 2.1% and 2.3%, respectively, than in MgSO_4 solution at about 0.4%.

6.5.3.3. Ion Chromatography

Table 24 shows the variation in pH and element concentration of solutions containing the three different series of AASCC specimens, single-, binary-, and ternary-precursor specimens and subjected to 5% MgSO_4 , 5% Na_2SO_4 , and 5% $\text{MgSO}_4 + 5\% \text{Na}_2\text{SO}_4$ sulfate solutions. The pH of the solutions increased tremendously during the exposure to different sulfate solutions to maintain electroneutrality due to the migration and counter diffusion of alkalis ions from AASCC specimens to solutions. Prior to the immersion of specimens, the pH of all sulfate solutions was between 6 and 8, and after 182 days of exposure, the pH increased significantly, reaching the values shown in **Table 24**. The deterioration levels are quite related to the concentrations of the elements leached up to 182 days, after which the damage of the cylinders in 50 g/L solutions takes off, indicating the onset of significant cracking as found by Ye et al. (2019).

Despite the pH rise caused by interactions between sulfate solutions and AASCC various matrices, all elements were highly soluble at low sulfate concentrations, such as 5% solutions, as opposed to their status at higher sulfate concentrations as 10% solutions. In single-precursor systems, the extensive damage of the AASCC matrix was observed during immersion in 5% $\text{MgSO}_4 + 5\% \text{Na}_2\text{SO}_4$ solutions where the leached Ca concentration was 423 mg/l compared to 7719 mg/l in binary-1 and 238 mg/l in binary-2 systems. In contrast, extensive deterioration and Ca leaching were observed when low-calcium systems, such as ternary-precursor systems, were used, especially in ternary-1 samples (10,123 mg/l) in MgSO_4 sulfate solutions.

Table 24 – Ion chromatography analysis and pH after 182 days in 5% sulfate solutions of the different AASCC systems

Sulfate solution	Mixture I.D.	pH	Element concentration in different sulfate solutions (mg/l)			
			Na	Ca	Mg	SiO ₃
5% MgSO ₄	Single	12.1	4205	62	313	24
	Binary-1	9.80	51829	1103	120	72
	Binary-2	10.5	1900	62	26	4598
	Ternary-1	9.90	1426	876	1441	101
	Ternary-2	11.1	18826	10123	1271	127
5% Na ₂ SO ₄	Single	13.6	5081	38	193	23
	Binary-1	10.5	124089	1795	67	72
	Binary-2	12.9	6170	50	356	552
	Ternary-1	12.8	4730	876	1832	49
	Ternary-2	12.7	7769	4596	1111	81
5% MgSO ₄ + 5% Na ₂ SO ₄	Single	13.0	5617	423	105	28
	Binary-1	13.0	72134	7719	371	41
	Binary-2	10.9	5325	238	375	25
	Ternary-1	10.1	1950	588	933	16
	Ternary-2	10.5	8924	8322	4446	58

6.5.4. Exposure IV: Drying and Wetting Cycles

After 30 days of continuous exposure to daily wetting and drying cycles with drying for 8-h to a temperature of $40 \pm 2^\circ\text{C}$ [104°F] and RH of $35 \pm 5\%$, followed by a wetting cycle for 16-h to a temperature of $20 \pm 2^\circ\text{C}$ [68°F] and RH of $90 \pm 5\%$, efflorescence appeared on the concrete cylinders' drying surface above the solution level. In addition, salt precipitates were found on the immersed portion of the specimens in sulfate solutions. According to previous studies (Bassuoni and Rahman, 2016; Whittaker and Black, 2015; Nehdi et al., 2014; Haynes et al., 2008; Flatt, 2002; Thaulow and Sahu, 2004; Doehne et al., 2002), this exposure condition is favorable for the formation and precipitation of hydrous mirabilite from anhydrous thenardite and epsomite from kieserite, which can cause damage. In the Na₂SO₄ – H₂O system, thenardite (Na₂SO₄) transformation into mirabilite (Na₂SO₄·10H₂O) occurs at temperatures of 20°C and below 76% RH. This process generates an increase in the volume of 314% (Price and Brimblecombe, 1994). On the other hand, three stable crystalline phases exist in the MgSO₄ – H₂O system: epsomite (MgSO₄·7H₂O), hexahydrate (MgSO₄·6H₂O), and kieserite (MgSO₄·H₂O). When relative humidity reaches > 80% RH, kieserite transforms into hexahydrate and epsomite, with the latter produced by hydration of hexahydrate (Wang et al., 2009). The exposure lasted for six months (183 cycles of wetting and drying), and all AASCC cylinders were inspected to diagnose the level of damage. Higher surface scaling of concrete surfaces has appeared on some cylinders above the sulfate solution level due to the crystallization of salts. Other samples, in contrast, revealed that the portion of concrete immersed in the solution was relatively ruined as the leaching process's kinetics increased with temperature (Kamali et al., 2008). It should be noted that the reduced permeability of AASCC mixtures can be attributed to the denser structure of aluminosilicate gels, which reduced the manifestation of microcracking due to weathering effect. The schematic diagram (**Fig. 59**) illustrates the relevant sulfate efflorescence phenomena.

6.5.4.1. Visual Appearance

Single-precursor mixtures. After six months of exposure, i.e., 183 cycles of wetting and drying, the specimens exhibited signs of damage. Surface scaling appeared on the surfaces of single-precursor cylinders exposed to 10% MgSO_4 and 10% $\text{MgSO}_4 + 10\% \text{Na}_2\text{SO}_4$ mixed solutions (**Fig. 99c**). The concrete mass loss and surface spalling were most pronounced in the 10% MgSO_4 solution (**Fig. 99a**). However, no deterioration was observed on the cylinders exposed to 10% Na_2SO_4 solution, as shown in Fig. 36b. It should be noted that the cyclic conversion of sulfate crystals can generate stresses in concrete pores. This phenomenon can lead to surface scaling and substantial deterioration levels (Nehdi et al., 2014).

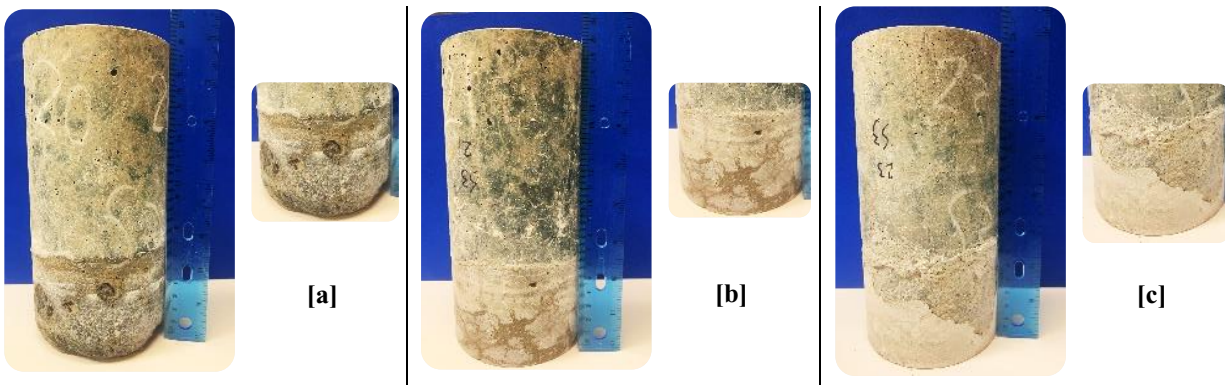


Fig. 99 – AASCC single-precursor mixtures exposed to a) 10% MgSO_4 b) 10% Na_2SO_4 , and c) 10% mixed sulfate solutions under drying and wetting cycles

Binary-precursor mixtures. For binary-1 mixtures, the mass loss due to the exposure to various sulfate solutions was caused in MgSO_4 and hybrid solutions. On the other hand, less degradation was observed with the Na_2SO_4 solution (**Fig. 100b**) with less surface scaling and concrete damage. A similar trend was observed in binary-2 mixtures (**Fig. 101**) but to a lesser extent. The binary-2 AASCC cylinders exhibit surface erosion and the manifestation of aggregates after the exposure to 10% MgSO_4 (**Fig. 101a**) and 10% $\text{MgSO}_4 + 10\% \text{Na}_2\text{SO}_4$ (**Fig. 101c**) sulfate solutions under drying and wetting cycles above the solution level.

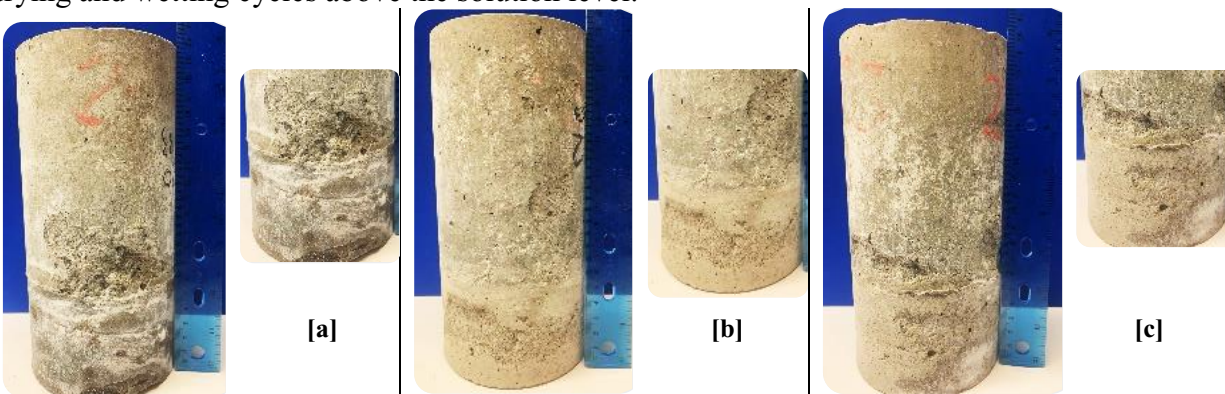


Fig. 100 – AASCC binary-1 mixtures exposed to a) 10% MgSO_4 b) 10% Na_2SO_4 , and c) 10% mixed sulfate solutions under drying and wetting cycles

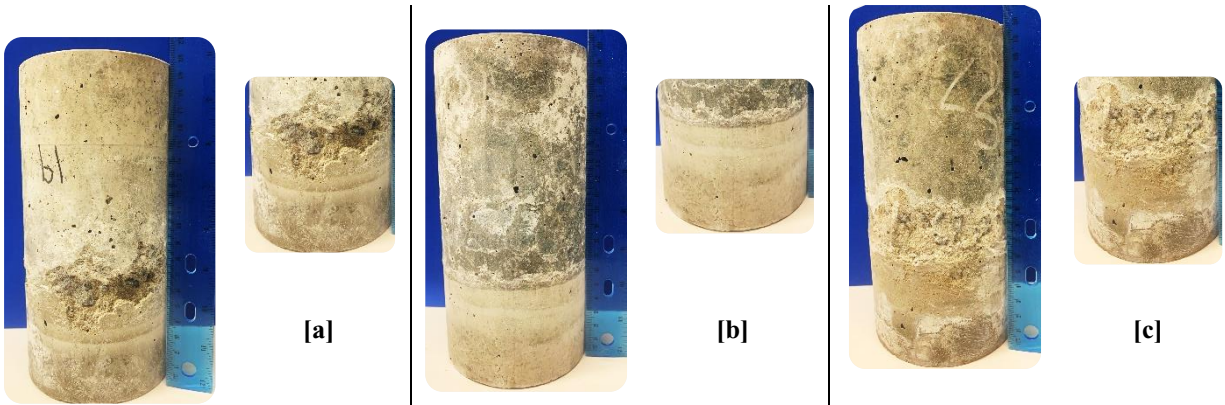


Fig. 101 – AASCC binary-2 mixtures exposed to a) 10% MgSO_4 b) 10% Na_2SO_4 , and c) 10% mixed sulfate solutions under drying and wetting cycles

Ternary-precursor mixtures. Ternary-1 and ternary-2 samples showed some changes in appearance, especially in the solution of 10% MgSO_4 under drying and wetting cycles. In the 10% Na_2SO_4 and 10% mixed sulfate solutions, samples were covered by a 1-mm-thick white cover, and a horizontal cracking in the ternary-2 specimens was found in the latter solution (**Fig. 103c**). Ternary-1 samples deteriorated less than ternary-2 samples that reported the most significant mass and cross-section variations. Significant deterioration tends to occur when magnesium cation is present in the sulfate solution. For instance, ternary-2 samples in 10% MgSO_4 and 10% $\text{MgSO}_4 + 10\% \text{Na}_2\text{SO}_4$ lost about 5.4% and 5% of their weights, respectively.

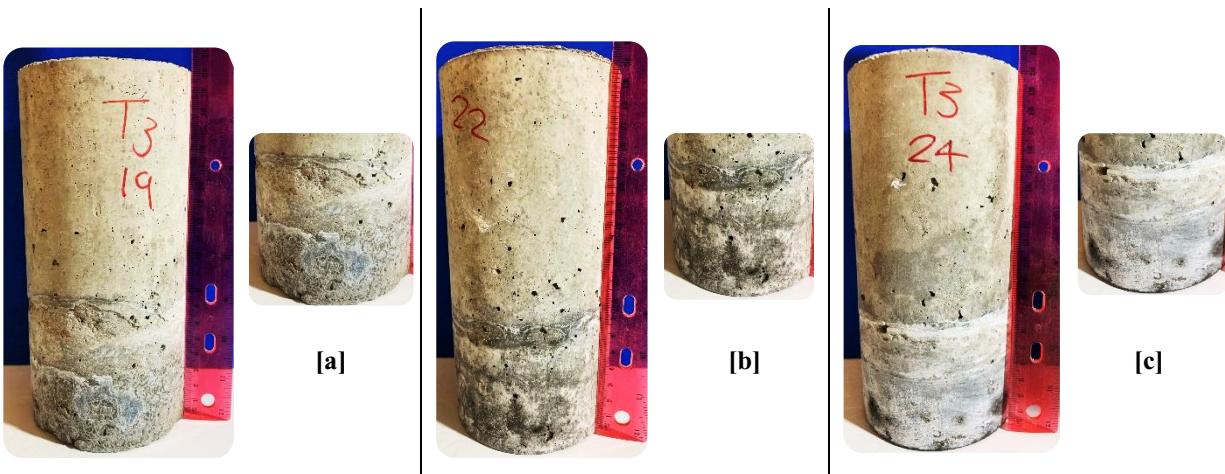


Fig. 102 – AASCC ternary-1 mixtures exposed to a) 10% MgSO_4 b) 10% Na_2SO_4 , and c) 10% mixed sulfate solutions under drying and wetting cycles

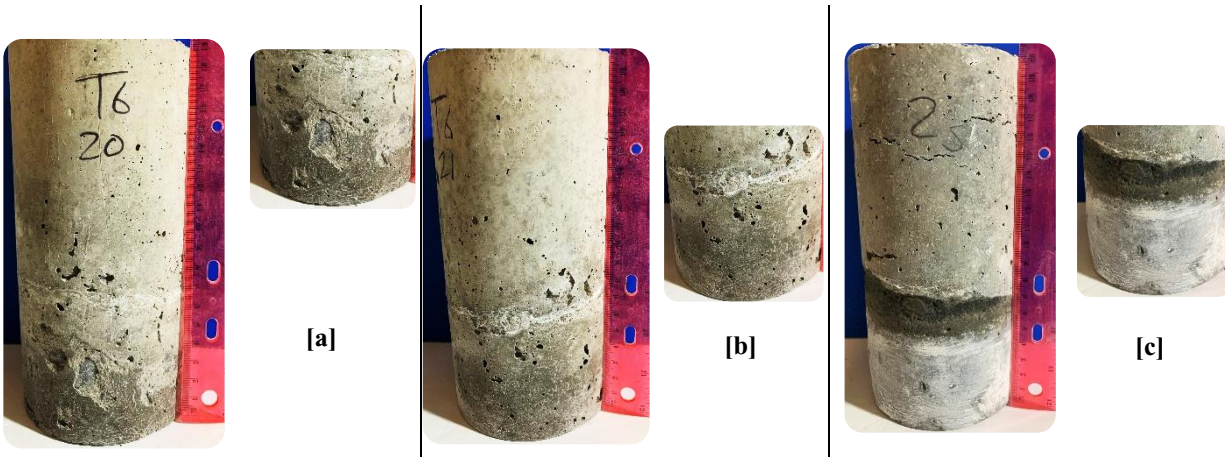


Fig. 103 – AASCC ternary-2 mixtures exposed to a) 10% MgSO_4 b) 10% Na_2SO_4 , and c) 10% mixed sulfate solutions under drying and wetting cycles

6.5.4.2. Mass and Cross-Section Variations

Single-precursor mixtures. **Fig. 104** and **Fig. 105** report the time-dependent mass and cross-section changes made from 100% slag after 182 days of exposure to sulfate solutions partially and under 183 drying and wetting cycles. In all sulfate solutions, atypical surface scaling of the immersed portion of concrete cylinders was observed (**Fig. 99 a-c**), in contrast to the expected damage in part above the level of the solution. After 60 days in MgSO_4 solution, single-precursor cylinders lost about 8% of their mass, which dropped sharply to 2.4% at the end of the exposure period. Single-precursor specimens exposed to 10% Na_2SO_4 solution lost 33% less mass than those exposed to 10% MgSO_4 solution, although the cross-section varied by roughly 2%. On the other hand, cylinders immersed in mixed sulfate solutions demonstrated an overall mass gain (0.8%) at 182 days, indicating that porosity decreased with immersion time. It should be noted that all single AASCC cylinders were intact above the solution level, indicating that the high sulfate concentration combined with drying and wetting cycles did not accelerate the damage mechanism.

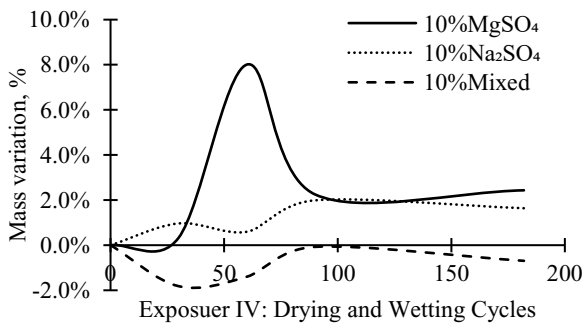


Fig. 104 – Time-dependent mass change of single-precursor AASCC mixtures exposed to 10% sulfate solutions under drying and wetting cycles

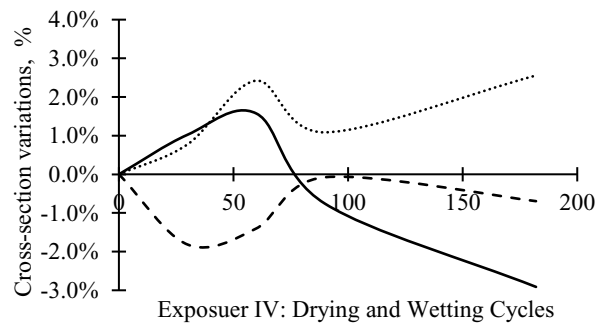


Fig. 105 – Time-dependent cross-section change of single-precursor AASCC mixtures exposed to 10% sulfate solutions under drying and wetting cycles

Binary-precursor mixtures. Fig. 107 and Fig. 108 show the mass and cross-section results of binary-precursor specimens immersed in various sulfate solutions and subjected to 183 drying-wetting cycles. For all binary samples exposed to different sulfate solutions, the mass loss and physical degradation occurred due to spalling of the concrete surface above the solution level. This could be attributed to the nucleation and growth of sulfate crystals in the supersaturated solution such as thenardite, which exerts stresses on the binary-precursor AASCC, causing damage and mass loss above the solution level and drying and wetting cycles. For instance, the mass variations of binary-1 mixtures immersed in $MgSO_4$ solutions resulted in roughly 2% mass loss and cross-section variations compared with 1.4% mass loss and 2.2% cross-section variations in mixed sulfate solutions after 182 days. After 6 months of drying and wetting cycles, thenardite and ettringite were detected in binary-1 samples exposed to 10% Na_2SO_4 solution (Fig. 106), while a significant amount of gypsum was found in samples subjected to 10% $MgSO_4$ solution. This suggests that the drying and wetting cycles had a significant impact on the rate of AASCC degradation.

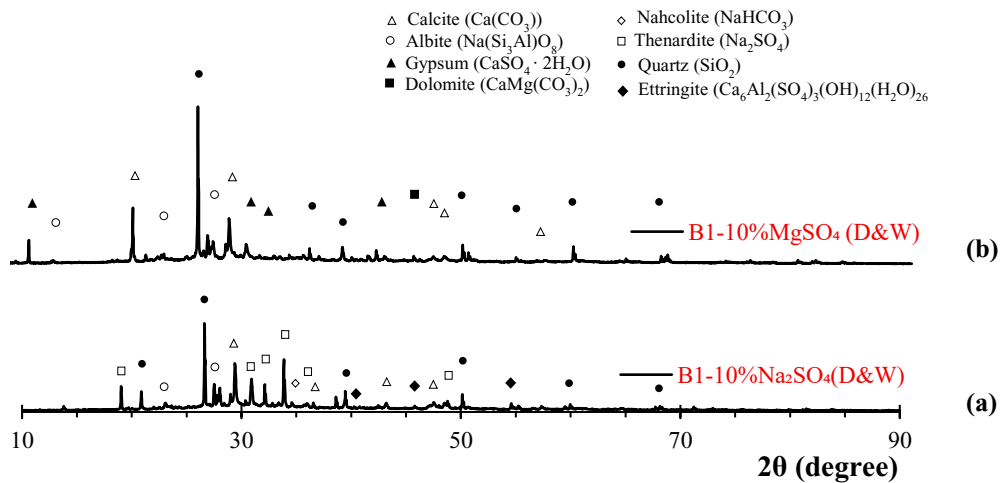


Fig. 106 – XRD spectra of binary-1 AASCC specimens exposed to sulfate attack under drying and wetting cycles: (a) In 10% Na_2SO_4 solution; (b) In 10% $MgSO_4$ solution

Similarly, surface scaling (Fig. 101) appeared on the drying surfaces of the binary-2 cylinders immersed in both $MgSO_4$ and mixed sulfate solutions, i.e., 1.2% and 0.7% mass loss, respectively. It should be noted that the crystalline phase of $MgSO_4$ (epsomite) would be stable close to room ambient temperature based on the thermodynamic data, but in dry conditions, epsomite would tend to dehydrate and produce the monohydrate kieserite phase; this process would develop a high crystallization pressure. However, after 60 days, binary-1 samples exposed to Na_2SO_4 showed a 1% mass gain, which reversed to a 1% mass loss at the end of the testing period. This can be attributed to the direct precipitation of thenardite (above ~ 32.4 °C) and the quick crystallization of mirabilite following thenardite dissolution, which causes a higher degradation level in porous mixtures mirabilite crystallization alone (Rodriguez-Navarro et al.,2002).

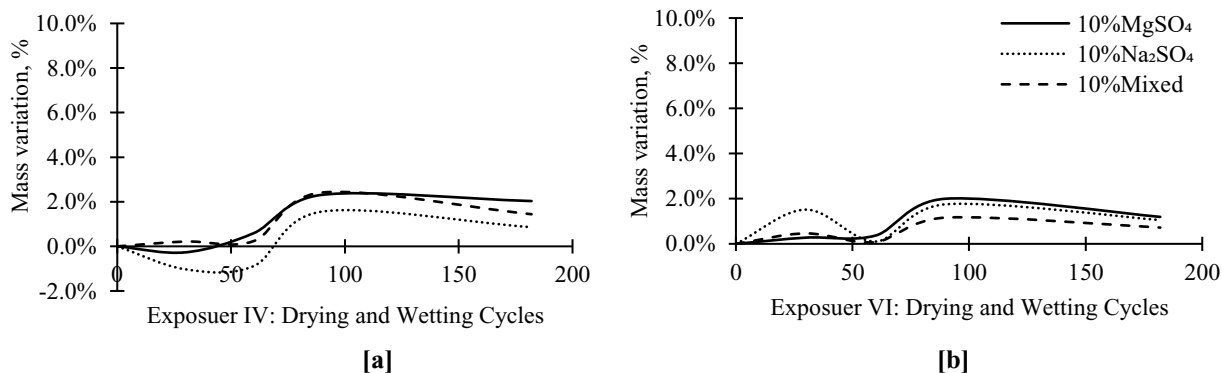


Fig. 107 – Time-dependent mass change of binary-precursor AASCC mixtures exposed to 10% sulfate solutions under drying and wetting cycles a) binary-1 and b) binary-2

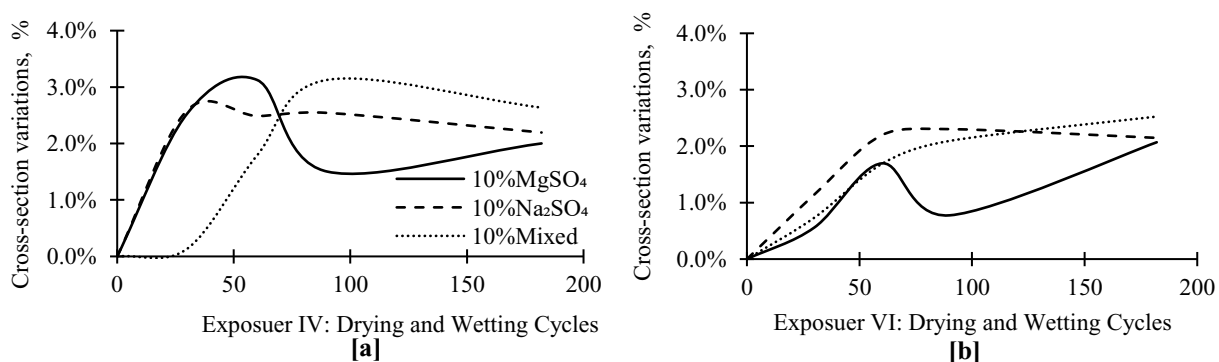


Fig. 108 – Time-dependent cross-section change of binary-precursor AASCC mixtures exposed to 10% sulfate solutions under drying and wetting cycles a) binary-1 and b) binary-2

Ternary-precursor mixtures. Figs. 109 and 110 (a and b) illustrate the ternary-precursor mixture mass fluctuations and their related specimens cross-section variations after six months of physical sulfate exposure. After one month of exposure, i.e., 30 cycles of drying and wetting, both ternary-precursor cylinders lost around 5% of their mass, while the exposure to all sulfate solutions was most probably due to the crystallization pressure on pores walls. These values continued to increase till the end of the testing period.

All ternary-1 samples with a higher CaO content had similar cross-section variations ranging from 1.4 to 1.9% when exposed to all sulfate solutions. However, cross-section results of low-calcium ternary-2 samples revealed higher variability in MgSO₄ (2%), Na₂SO₄ + MgSO₄ (1.2%) and Na₂SO₄ (0.3%) sulfate solutions. The dissolution and crystallization of soluble salts in porous materials like concrete due to the variations in temperature and relative humidity can cause phase changes between thenardite (Na₂SO₄) and mirabilite (Na₂SO₄ · 10H₂O) as well as kieserite (MgSO₄) and epsomite (MgSO₄ · 7H₂O).

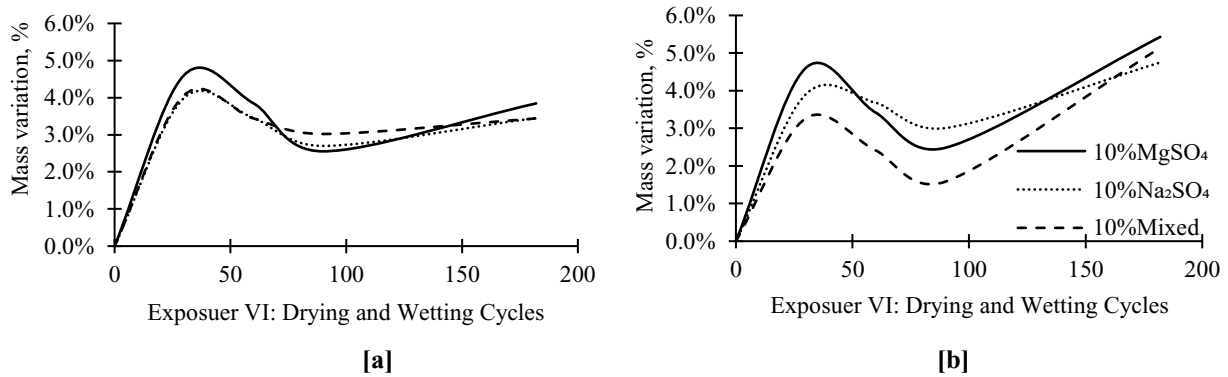


Fig. 109 – Time-dependent mass change of ternary-precursor AASCC mixtures exposed to 10% sulfate solutions under drying and wetting cycles a) Ternary-1 and b) Ternary-2

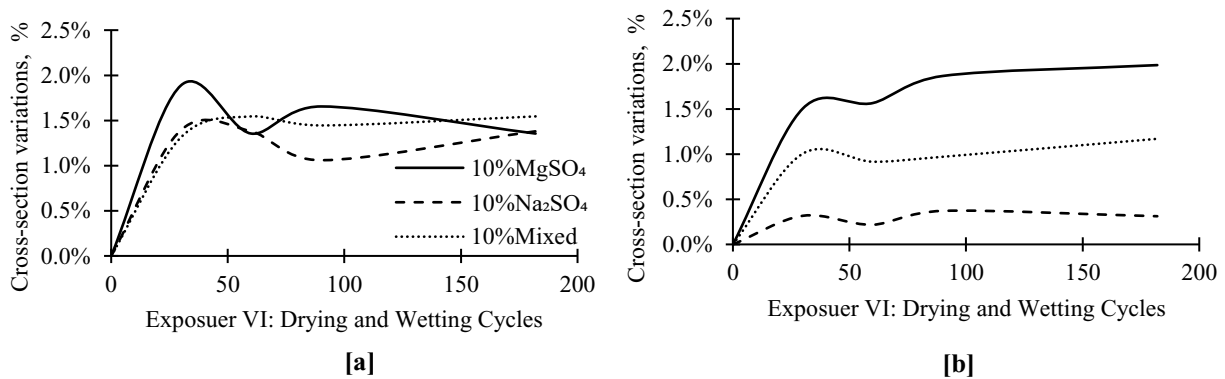
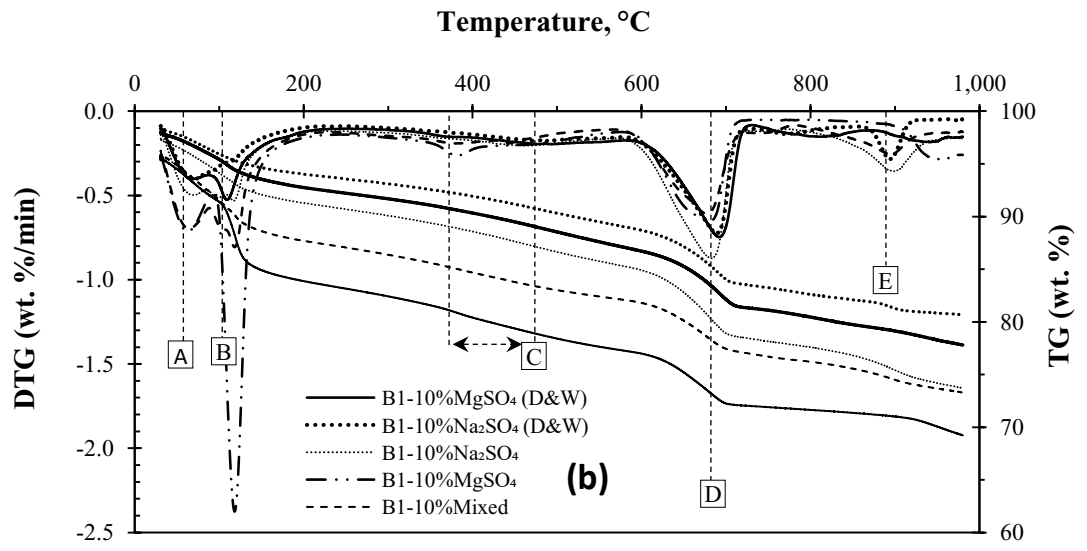
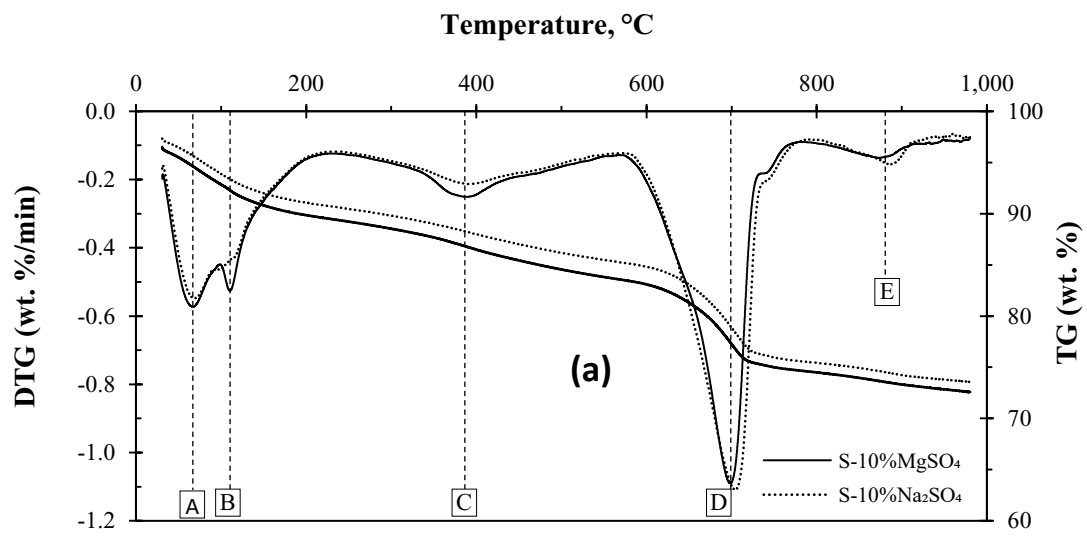


Fig. 110 – Time-dependent cross-section change of ternary-precursor mixtures exposed to 10% sulfate solutions under drying and wetting cycles a) Ternary-1 and b) Ternary-2

6.6. Thermogravimetry (TGA/DTG)

The TGA/DTG profiles for all AASCC mixtures are shown in **Fig. 111**, with mass loss ranging from 18 to 24% during the period of observation. The differential thermograms (DTG) of various mixtures exhibited peaks at various temperatures. Differential thermograms (DTG) of single-, binary-, and ternary-precursor mixtures showed distinct peaks at different temperatures, designated as A–C. The first two peaks (A and B) were observed at temperatures ranging from 70 °C to 120 °C for all AASCC mixtures exposed to various sulfate solutions due to the removal of free water in the pores and the dehydration of the C-A(N)-S-H, ettringite, or gypsum gel products, these phases were identified by XRD in all samples. Weak endothermic peaks between 375 °C and 485 °C were detected in all samples assigned to the dehydration of hydrotalcite at the spot labeled with C (Zuo et al., 2018). The decomposition of carbonate minerals, notable calcite, was explained with the weight loss observed in all samples within a temperature range of 675 °C to 735 °C (spot D). The presence of different structural forms of carbonates, particularly weakly crystalline or amorphous forms, in the matrix may be indicated by the higher decomposition temperature in the samples, which ranges from 820 °C to 930 °C (spot E).



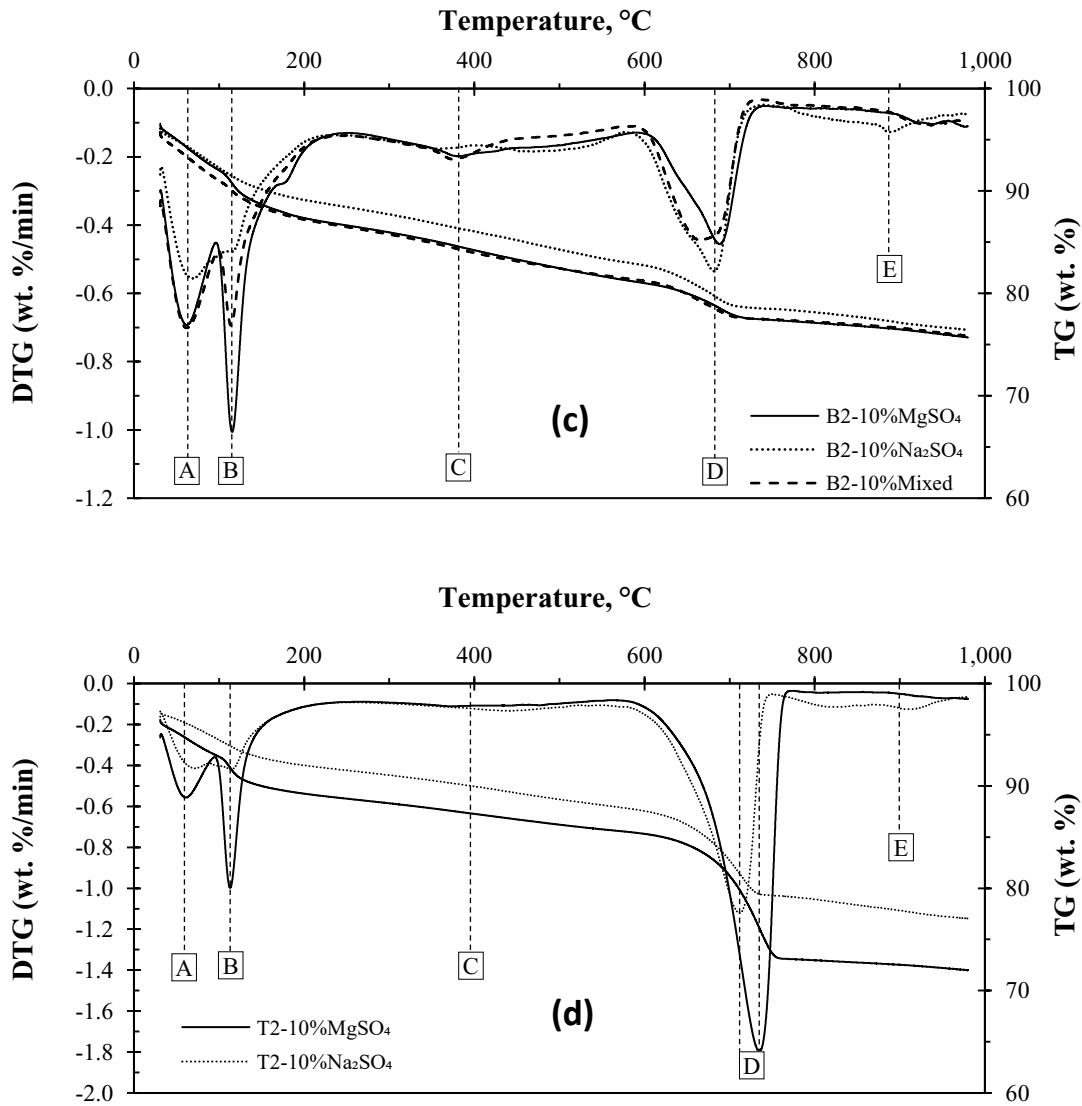


Fig. 111 – TGA/DTG data for AASCC exposed to different sulfate solutions a) single, b) binary-1, c) binary-2, and d) ternary-2 mixtures

6.7. Proposed Deterioration Mechanisms

The proposed mechanism for attack by magnesium sulfate, sodium sulfate, or a mixture of both sulfate solutions is shown in **Fig. 112**. Step 1 entails exposing AASCC specimens to different sulfate solutions: a) Na₂SO₄ and b) MgSO₄ with a pH range of 6–8. After one month of exposure to sulfate solutions, the pH of the surrounding solution changes to 11–12. Therefore, sulfate solutions were renewed, and the pH of the solution was kept low during Step 2 to maintain a consistent rate of attack; thus, the attack was expected to proceed. In Step 3, expansive gypsum and ettringite were expected to form in the surface regions of the AASCC cylinders near the sulfate solutions. However, the core beneath tries to resist the sulfate attack or decalcify the strength-giving products, resulting in a complete breakdown and disintegration of the specimen.

The reaction mechanisms between the AASCC matrix and different sulfate solutions differ depending on the sulfate type and hydration products in AASCC, as shown in **Fig. 112 a and b**. In Na_2SO_4 solution, ettringite formation, alkali leaching, slight decalcification, and dealumination from C-A-S-H phases (**Fig. 112a**) are assumed to occur in AASCC cylinders, as noticed from the analytical results. Nevertheless, it is believed that the presence of carbonate ions from the sodium carbonate activator inhibits ettringite formation due to the presence and competition mechanisms of carbonate ions and sulfate ions.

Experience with magnesium sulfates has frequently revealed that regular concrete can suffer from the formation of a layer of brucite $\text{Mg}(\text{OH})_2$ in the pore solution due to reactions between Mg^{2+} and OH^- ions. This can disrupt further attack since brucite precipitation is known to be rapid at $\text{pH} \sim 10.5$ (Pokrovsky and Schott, 2004). A direct decalcification of C-S-H may occur due to prolonged pH monitoring, which may later react with Mg^{2+} and SO_4^{2-} to form M-S-H. The potential degradation mechanisms of AASCC cylinders subjected to MgSO_4 sulfate solutions are shown in **Fig. 112b**. The anticipated attack by magnesium sulfate prompted the development of a "gypsum-layer". Gypsum precipitates may form as a result of the reaction between available Ca^{2+} in the pore solution and SO_4^{2-} , as well as carbonate-bearing phases as a result of the presence of carbonates in the pore solution.

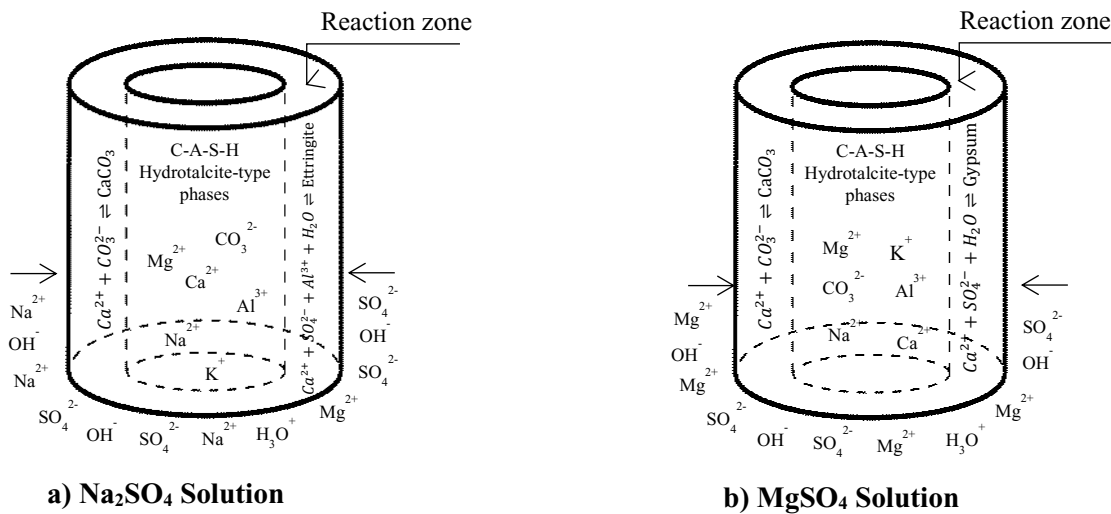


Fig. 112 – Proposed deterioration mechanism of AASCC cylinders in a) Na_2SO_4 and b) MgSO_4

Cross-section variations of AASCC specimens in all sulfate solutions followed a two-stage process. During Stage 1, the initial stage, the cross-section of the specimens gradually increased up to 60 days of exposure. A very modest increase followed this gradual change in the cross-section results (Stage 2), where the rate of change was nearly constant. On the other hand, cross-section variations fluctuated at a continuously increasing rate until the end of the testing period, considering the multi-damaging effect of a monitored pH environment, high sulfate concentration, and 183 cycles of drying and wetting.

6.8. Concluding Remarks

This chapter provided a thorough understanding of the resistance of various AASCC mixture designs as a result of the synergistic effect of various parameters in various sulfate solutions. The following conclusions can be drawn from the results of this study:

1. The results of continuous immersion in 10% sodium, 10% magnesium, and 10% mixed sulfate solutions indicate that, with the exception of binary-1 mixtures with SF replacing slag, all of the AASCC mixtures tested in this study were resistant to sulfates for up to 6 months. This could be due to these materials' impermeability when different precursor blend ratios and compositions are used.
2. In all AASCC cylinders, the main product of degradation in 10% MgSO_4 and 10% MgSO_4 + 10% Na_2SO_4 sulfate solutions is gypsum, whereas ettringite was produced in 10% Na_2SO_4 sulfate solutions.
3. The ion chromatography analysis of the sulfate solutions revealed that, during sample exposure, there was intensive leaching of Na, Ca, and Si from the structure of AASCC blends, particularly in MgSO_4 and mixed solutions.
4. The exposure of single, binary-2, and ternary-precursor mixtures resulted in pastes rich in C-(N)-A-S-H gels, other carbonate products, and mesopores rather than micropores, which delayed or inhibited the crystal growth of expansive products.
5. To increase the hostility of the exposure environment, high sulfate concentrations, pH control, partial immersion, and wetting-drying cycles were used; however, the synergistic action of all parameters increased the sulfate crystallization.
6. In comparison to the 10% continuous partial immersion (Exposure I), the continuous partial immersion with a noncontrolled pH condition (Exposure II), the 5% continuous partial immersion (Exposure III), and the 10% continuous partial immersion with wetting-drying cycles (Exposure IV). Exposures I and IV had nearly identical damage mechanisms, with the latter being the most severe.

Chapter 7 : Research Contributions and Recommendations

7.1. Research Contributions

The durability of alkali-activated self-consolidated concrete (AASCC) has been generally overlooked and confused when exposed to physical sulfate attack. Therefore, the behavior of these emerging materials subjected to sulfate-rich environments was investigated in this study under laboratory conditions and using various scenarios.

The current thesis's **Chapter 2** demonstrated that a lack of information about AASCC deterioration caused by external sulfate attacks has resulted in confusion and contradictory views. Furthermore, previous research has suggested that additional work should be conducted to understand better the attack processes and how they are affected by the different binder systems, activators, and other concrete mixture parameters.

Chapter 3 has shown that AAMs resistance requires a high level of effort to devote to relevant standards to recognize deterioration mechanisms where further validation is needed in laboratory and field studies. Particular attention should also be paid to the cations accompanying the salt and the concentration in sulfate-rich environments as this would alter the deterioration mechanism. There is a need to develop holistic assessment techniques to detect synergistic effects of sulfate attacks, single to multiple damages, under accelerated real field conditions to determine potential durability.

Chapter 4 – phase one showed that the workability of AASCC mixtures increased as the percentage of the alkali activator increased by up to 25% in the mortar mixtures due to Na_2CO_3 slow reaction and Na_2SiO_3 deflocculation behavior. Furthermore, Na_2CO_3 and $\text{MetaNa}_2\text{SiO}_3$ combinations have accelerated the hardening and strength development of dry-powder AASCC mixtures. Source materials and dry-powder activators should be milled to increase the amorphousness of the particles, which would improve the dissolution and reactivity of AASCC mixtures and address the issues associated with low early age strength. Finally, a mixture of 20% to 25% Na_2CO_3 and $\text{MetaNa}_2\text{SiO}_3$ activator is recommended for the best workability and strength performance.

In the absence of a clear methodology for designing AASCM mixtures, **Chapter 4 – phase two** demonstrated that the proper selection of precursor materials, proportions, activator type, and dosage plays a decisive role in the efficient development of AASCM mixtures. Calorimetric analysis has revealed that after adding water, a nearly instantaneous reaction corresponds to the initial dissolution and wetting of precursor materials, with the magnitude of the pre-induction peaks varying depending on the initial pH value activator content, type, and accompanying anion. Moreover, the chemical composition of the precursor materials affects the second exothermic peak of the post-induction stage the most. Lastly, the highest compressive strength values were achieved using a 25% activator dosage for all AASCM mixtures, except for single-precursor mixtures where up to 20% was appropriate for gels formation.

Chapter 5 demonstrated that the higher fraction of sodium carbonate/silicate activators, ranging from 20% to 25%, contributed to delayed reaction kinetics and satisfactory fresh and mechanical properties in all systems, single, binary, and ternary, due to their nature. Slag replacement with variable SF or FA class-F ratios, on the other hand, could indeed adjust the particle size distribution of the total binder material and improve the fresh concrete characteristics in binary and ternary systems. Finally, the formation of various reaction products and binding gels, i.e., C-(N)A-S-H, was found to have a significant impact on several transport mechanisms, including capillary sorptivity, permeable pores, and bulk electrical resistivity.

Chapter 6 demonstrated that single-, binary-, and ternary-precursor AASCC samples partially immersed in sodium, magnesium, and mixed sulfate solutions could experience a dual sulfate attack scheme. Chemical sulfate attack can occur in the immersed portion in sulfate solutions, while physical sulfate attack can occur in the portion above the solution level. The effect of physical sulfate attack on the concrete's properties was not significant since the damage was confined to the external surface. However, the damage was primarily controlled by the AASCC different systems' pore structure, which resulted in the leaching of ions from samples to solutions. It was found that maintaining the pH in the sulfate solutions had increased the rate of damage of AASCC mixtures. Furthermore, binary and ternary precursor blends partially replacing slag with SF, or FA resulted in decreased porosity, surface scaling, and AASCC deterioration due to an increase in the volume of very small diameter pores. Finally, in all AASCC systems, gypsum and ettringite were the primary degradation products of sulfate attack.

7.2. Recommendations

1. The current research showed the damage of the AASCC mixtures due to physical sulfate attack using a combination of carbonate/silicate dry-powder activators. This combination is assumed to improve the performance of AASCCs due to the synergistic effect of physical sulfate attack, controlled pH, and drying-wetting cycles. Therefore, the effect of using other types of dry-powder activators should be investigated.
2. Future research should consider the impact of freezing and thawing conditions while exposing AASCC with different precursor systems to physical sulfate attack to measure their durability performance in cold regions.
3. It is widely believed that physical sulfate attacks can only be truly simulated in-situ under various environmental conditions, such as temperature and humidity. Therefore, future studies must validate the study's findings in actual field-like exposure conditions.

Appendix I: Ion Chromatography Test

Table 1 – Ion chromatography analysis and pH after 182 days in 10%Na₂SO₄ solution

Mixture	Days	pH	Na ⁺	Ca ²⁺	Mg ²⁺	SiO ₃ ²⁻	SiO ₄ ²⁻
Single	30	13.6	5550	224	123	46	50459
	90	13.8	12767	279	57	54	80156
	182	13.6	5739	42	247	22	73866
Binary-01	30	10.8	40382	2050	442	59	40303
	90	11.5	159692	1878	261	117	37360
	182	9.8	98134	25322	436	64	36603
Binary-02	30	10.7	5313	53	322	28	43460
	90	12.2	7637	50	283	24	92951
	182	11.3	4070	11	262	32	64414
Ternary-01	30	10.5	11128	867	862	52	83711
	90	13.0	7368	2082	285	67	75548
	182	12.8	4439	202	25	16	54049
Ternary-02	30	13.1	4513	89	89	46	58954
	90	13.0	3355	40	322	68	39792
	182	12.8	5190	614	3	81	93930

Table 2 – Ion chromatography analysis and pH after 182 days in 10%MgSO₄ solution

Mixture	Days	pH	Na ⁺	Ca ²⁺	Mg ²⁺	SiO ₃ ²⁻	SiO ₄ ²⁻
Single	30	10.0	4376	1721	3	26	57292
	90	10.3	8660	116	228	57	43885
	182	10.1	3515	756	87	26	52960
Binary-01	30	8.4	35302	1357	274	42	13557
	90	11.0	140976	3077	239	108	48454
	182	9.4	32485	34820	581	48	36236
Binary-02	30	8.8	3214	2006	350	21	58644
	90	10.3	6569	378	122	116	62638
	182	10.1	6468	604	257	396	98357
Ternary-01	30	10.3	6416	155	141	46	63375
	90	10.0	4556	1645	270	67	50891
	182	9.9	6920	836	999	25	52044
Ternary-02	30	10.1	1835	1086	25	50	63396
	90	13.0	1597	1430	157	60	59357
	182	10.1	3516	13679	1368	135	53195

Table 3 – Ion chromatography analysis and pH after 182 days in 10% Mixed solution

Mixture	Days	pH	Na ⁺	Ca ²⁺	Mg ²⁺	SiO ₃ ²⁻	SiO ₄ ²⁻
Single	30	10.4	7550	1141	114	23	76887
	90	13.7	14744	197	75	71	70442
	182	10.9	6299	522	145	20	69119
Binary-01	30	9.1	88069	23177	1169	63	46119
	90	11.1	115125	4270	119	79	35995
	182	9.8	88184	22405	1266	53	38040
Binary-02	30	11.9	3952	1547	235	27	111976
	90	10.5	6801	237	142	26	69941
	182	10.3	5886	460	794	638	46852
Ternary-01	30	10.3	13192	3229	478	76	78552
	90	9.8	10473	3390	357	73	72072
	182	10.2	5800	1348	1678	25	74509
Ternary-02	30	10.4	3462	840	90	73	88601
	90	10.3	2423	780	49	69	48337
	182	10.3	6783	5846	1109	84	99538

Table 4 – Ion chromatography analysis and pH after 182 days in 5%Na₂SO₄ solution

Mixture	Days	pH	Na ⁺	Ca ²⁺	Mg ²⁺	SiO ₃ ²⁻	SiO ₄ ²⁻
Single	30	11.3	8754	45	511	26	51386
	90	13.7	8930	166	259	42	62938
	182	13.6	5081	38	193	23	54661
Binary-01	30	8.8	56333	20824	771	118	656921
	90	9.8	45774	27503	885	36	29733
	182	10.5	124089	1795	67	72	41030
Binary-02	30	10.6	7890	620	1245	36	43038
	90	10.3	5302	315	114	19	81884
	182	12.9	6170	50	356	552	105127
Ternary-01	30	10.4	4692	1951	761	104	44539
	90	13.0	4945	1945	217	47	76942
	182	12.8	4730	876	1832	49	47680
Ternary-02	30	13.0	2610	71	681	48	72750
	90	12.8	2584	615	82	43	68329
	182	12.7	7769	4596	1111	81	61403

Table 5 – Ion chromatography analysis and pH after 182 days in 5%MgSO₄ solution

Mixture	Days	pH	Na ⁺	Ca ²⁺	Mg ²⁺	SiO ₃ ²⁻	SiO ₄ ²⁻
Single	30	10.3	3502	234	82	82	65575
	90	13.5	8694	189	189	44	54097
	182	12.1	4205	62	313	24	58385
Binary-01	30	9.4	88550	13929	156	60	47321
	90	11.0	86194	2709	211	119	31586
	182	9.8	51829	1103	120	72	36494
Binary-02	30	9.8	4208	245	34	32	42111
	90	10.7	4937	162	104	25	54537
	182	10.5	1900	62	26	4598	64630
Ternary-01	30	10.1	22447	7301	2608	124	81368
	90	9.7	1524	2236	775	56	66687
	182	9.9	1426	876	1441	101	58816
Ternary-02	30	13.2	4260	2253	18	67	67223
	90	10.6	1766	269	126	56	53960
	182	11.1	18826	10123	1271	127	86801

Table 6 – Ion chromatography analysis and pH after 182 days in 5%MgSO₄ solution

Mixture	Days	pH	Na ⁺	Ca ²⁺	Mg ²⁺	SiO ₃ ²⁻	SiO ₄ ²⁻
Single	30	10.3	5995	3483	341	23	66063
	90	13.6	15000	943	94	72	75794
	182	13.0	5617	423	105	28	57855
Binary-01	30	10.2	93875	5040	542	207	157348
	90	12.2	209492	2544	301	222	38163
	182	13.0	72134	7719	371	41	29166
Binary-02	30	10.3	4420	188	289	19	118288
	90	12.6	6406	13	170	44	49638
	182	10.9	5325	238	375	25	55288
Ternary-01	30	10.2	5373	1817	920	64	68481
	90	11.5	2159	515	311	55	68873
	182	10.1	1950	588	933	16	70137
Ternary-02	30	11.0	2364	43	135	79	69002
	90	10.2	1025	300	103	73	59567
	182	10.5	8924	8322	4446	58	70521

Appendix II: Mass and Cross-Section Variations

Single-precursor mixture

Table 1 – Single-precursor samples mass change in different sulfate solutions

Initial Mass (g)	Mass (%)			
M_i (g)	30 (day)	60 (day)	90 (day)	182 (day)
3857.3	0.1%	0.2%	0.5%	0.7%
3831.85	0.2%	0.2%	0.5%	0.9%
3878.95	0.1%	0.1%	0.4%	0.8%
3837.35	0.0%	0.2%	0.1%	0.6%
3836.90	0.1%	0.3%	0.4%	0.7%
3871.05	0.3%	0.1%	0.0%	0.5%
3793.80	0.1%	0.3%	0.5%	1.0%
3902.25	0.2%	0.2%	0.4%	0.9%
3864.40	0.0%	-0.1%	0.2%	0.6%
3875.425	0.3%	8.0%	2.3%	2.4%
3882.56	1.0%	0.6%	2.0%	1.6%
3779.75	-1.8%	-1.4%	-0.1%	-0.7%

Table 2 – Single-precursor samples cross-section change in different sulfate solutions

$x=\Delta L/L_i$				$z=\Delta V/V_i$				$y=\Delta D/D_i$			
30 (day)	60 (day)	90 (day)	182 (day)	30 (day)	60 (day)	90 (day)	182 (day)	30 (day)	60 (day)	90 (day)	182 (day)
-0.06	-0.06	-0.06	-0.06	-0.05	-0.05	-0.05	-0.05	0.5%	0.5%	0.5%	0.5%
-0.11	-0.11	-0.11	-0.11	-0.10	-0.08	-0.08	-0.08	0.6%	1.6%	1.4%	1.4%
-0.11	-0.11	-0.11	-0.11	-0.09	-0.09	-0.09	-0.09	1.2%	1.2%	1.0%	1.0%
-0.07	-0.07	-0.07	-0.07	-0.04	-0.04	-0.04	-0.04	2.0%	1.7%	1.5%	1.5%
-0.08	-0.08	-0.08	-0.08	-0.06	-0.06	-0.05	-0.05	1.0%	1.3%	1.5%	1.5%
-0.11	-0.11	-0.11	-0.11	-0.08	-0.08	-0.07	-0.07	1.5%	1.8%	2.1%	2.1%
-0.13	-0.12	-0.13	-0.13	-0.10	-0.10	-0.10	-0.10	1.5%	1.0%	1.2%	1.2%
-0.12	-0.12	-0.12	-0.12	-0.10	-0.09	-0.09	-0.09	1.1%	1.8%	1.6%	1.6%
-0.09	-0.09	-0.09	-0.09	-0.07	-0.07	-0.06	-0.06	1.1%	1.1%	1.6%	1.6%
-0.09	-0.09	-0.11	-0.12	-0.07	-0.06	-0.12	-0.17	1.0%	1.6%	-0.8%	-2.9%
-0.10	-0.10	-0.10	-0.09	-0.07	-0.05	-0.06	-0.06	1.6%	2.4%	2.3%	2.0%
-0.11	-0.11	-0.12	-0.11	-0.09	-0.06	-0.10	-0.06	0.8%	2.4%	1.1%	2.6%

Binary-precursor mixture with SF

Table 3 – Binary-precursor (with SF) samples mass change in different sulfate solutions

Initial Mass (g)	Mass (%)				
	M_i (g)	30 (day)	60 (day)	90 (day)	182 (day)
3734.95		0.3%	0.0%	6.6%	1.9%
3817.45		0.4%	-0.8%	-1.5%	-1.0%
3784.20		0.1%	0.5%	0.9%	1.5%
3750.50		0.4%	0.0%	-0.1%	2.1%
3817.65		0.1%	0.1%	0.1%	0.8%
3794.45		-0.1%	-0.2%	0.6%	0.7%
3777.45		0.4%	0.4%	0.6%	0.9%
3823.95		0.4%	-1.3%	-1.6%	-1.3%
3753.55		0.3%	-0.5%	-0.7%	-0.2%
3791.05		-0.3%	0.6%	2.3%	2.0%
3827.00		-1.0%	-0.9%	1.6%	0.9%
3807.55		0.2%	0.2%	2.4%	1.4%

Table 4 – Binary-precursor (with SF) samples cross-section change in different sulfate solutions

$x=\Delta L/L_i$				$z=\Delta V/V_i$				$y=\Delta D/D_i$			
30 (day)	60 (day)	90 (day)	182 (day)	30 (day)	60 (day)	90 (day)	182 (day)	30 (day)	60 (day)	90 (day)	182 (day)
0.66	0.64	0.65	0.53	0.73	0.63	0.68	0.20	2.2%	-0.3%	0.7%	-11.5%
0.59	0.61	0.61	0.62	0.65	0.69	0.70	0.72	1.7%	2.7%	2.7%	3.0%
-0.05	-0.01	-0.01	-0.01	-0.05	0.03	0.03	0.04	0.2%	2.2%	1.9%	2.5%
-0.10	-0.09	-0.11	-0.14	-0.07	-0.05	-0.15	-0.21	1.4%	1.9%	-1.8%	-4.4%
-0.13	-0.13	-0.13	-0.13	-0.11	-0.09	-0.10	-0.09	1.4%	2.4%	1.9%	2.4%
-0.08	-0.07	-0.08	-0.08	-0.05	-0.07	-0.06	-0.04	1.7%	0.2%	1.2%	2.0%
-0.12	-0.12	-0.11	-0.12	-0.06	-0.08	-0.06	-0.04	2.9%	2.2%	3.2%	4.3%
-0.07	-0.07	-0.07	-0.07	-0.05	-0.04	-0.02	-0.02	1.4%	1.4%	2.4%	2.8%
-0.04	-0.04	-0.04	-0.03	0.00	0.01	0.02	0.01	2.4%	2.7%	2.9%	2.2%
-0.12	-0.12	-0.12	-0.12	-0.08	-0.06	-0.09	-0.08	2.5%	3.1%	1.5%	2.0%
-0.10	-0.10	-0.10	-0.09	-0.05	-0.05	-0.06	-0.05	2.6%	2.5%	2.5%	2.2%
-0.10	-0.10	-0.10	-0.10	-0.10	-0.07	-0.05	-0.05	0.1%	1.8%	3.1%	2.6%

Binary-precursor mixture with FA

Table 5 – Binary-precursor (with FA) samples mass change in different sulfate solutions

Initial Mass (g)	Mass (%)				
	M_i (g)	30 (day)	60 (day)	90 (day)	182 (day)
3789.80		0.2%	0.3%	0.6%	0.9%
3868.80		0.1%	0.2%	0.1%	0.6%
3808.45		0.0%	0.1%	0.4%	0.8%
3778.50		-0.1%	0.2%	0.5%	1.0%
3835.80		0.6%	0.6%	0.8%	1.1%
3803.35		0.2%	0.1%	0.4%	0.9%
3748.10		0.0%	0.3%	0.3%	0.8%
3818.85		0.5%	0.0%	0.1%	0.2%
3801.10		0.1%	0.2%	0.3%	0.7%
3813.47		0.3%	0.4%	2.0%	1.2%
3823.51		1.5%	0.1%	1.8%	1.1%
3828.61		0.5%	0.1%	1.2%	0.7%

Table 6 – Binary-precursor (with FA) samples cross-section change in different sulfate solutions

$x=\Delta L/L_i$				$z=\Delta V/V_i$				$y=\Delta D/D_i$			
30 (day)	60 (day)	90 (day)	182 (day)	30 (day)	60 (day)	90 (day)	182 (day)	30 (day)	60 (day)	90 (day)	182 (day)
-0.12	-0.12	-0.12	-0.12	-0.10	-0.10	-0.10	-0.08	1.0%	0.7%	1.0%	2.0%
-0.12	-0.11	-0.12	-0.12	-0.11	-0.09	-0.09	-0.09	0.5%	1.5%	1.5%	1.5%
-0.12	-0.12	-0.12	-0.12	-0.10	-0.11	-0.11	-0.08	1.3%	0.3%	0.8%	2.2%
-0.12	-0.12	-0.12	-0.12	-0.11	-0.10	-0.08	-0.10	0.7%	1.2%	1.9%	1.4%
-0.11	-0.11	-0.11	-0.11	-0.08	-0.09	-0.07	-0.08	1.7%	1.2%	2.2%	1.7%
-0.10	-0.10	-0.10	-0.10	-0.06	-0.06	-0.07	-0.06	2.0%	2.0%	1.5%	2.0%
-0.07	-0.07	-0.07	-0.07	-0.05	-0.06	-0.05	-0.05	1.2%	0.5%	1.0%	1.2%
-0.12	-0.12	-0.12	-0.12	-0.11	-0.10	-0.10	-0.09	0.7%	1.0%	1.0%	1.7%
-0.09	-0.09	-0.09	-0.09	-0.06	-0.07	-0.07	-0.06	1.5%	1.1%	1.1%	1.5%
-0.10	-0.10	-0.10	-0.10	-0.09	-0.07	-0.09	-0.06	0.6%	1.7%	0.8%	2.1%
-0.11	-0.11	-0.11	-0.11	-0.09	-0.07	-0.07	-0.07	1.1%	2.2%	2.3%	2.1%
-0.06	-0.06	-0.06	-0.06	-0.05	-0.03	-0.02	-0.01	0.7%	1.7%	2.1%	2.5%

Ternary-precursor mixture (T1)

Table 7 – Ternary1-precursor samples mass change in different sulfate solutions

Initial Mass (g)	Mass (%)				
	M_i (g)	30 (day)	60 (day)	90 (day)	182 (day)
3752.19		2.4%	2.5%	2.5%	2.3%
3662.30		2.7%	2.9%	2.5%	1.8%
3790.26		2.5%	2.5%	2.5%	2.3%
3736.77		2.6%	2.8%	2.5%	2.2%
3752.56		2.9%	3.1%	2.9%	2.5%
3728.47		3.5%	3.6%	3.5%	3.2%
3738.11		3.4%	3.4%	3.4%	3.3%
3759.48		3.0%	3.0%	2.8%	2.5%
3758.76		2.9%	3.0%	2.9%	2.7%
3730.16		4.6%	3.8%	2.6%	3.8%
3731.24		4.0%	3.5%	2.7%	3.5%
3721.90		4.1%	3.4%	3.0%	3.4%

Table 8 – Ternary1-precursor samples cross-section change in different sulfate solutions

$x=\Delta L/L_i$				$z=\Delta V/V_i$				$y=\Delta D/D_i$			
30 (day)	60 (day)	90 (day)	182 (day)	30 (day)	60 (day)	90 (day)	182 (day)	30 (day)	60 (day)	90 (day)	182 (day)
0.000	-0.002	0.002	0.000	0.036	0.028	0.031	0.026	1.8%	1.5%	1.4%	1.3%
-0.004	-0.004	0.001	-0.001	0.029	0.025	0.029	0.032	1.6%	1.5%	1.4%	1.6%
-0.005	0.000	0.000	-0.002	-0.031	0.026	0.031	0.031	-1.3%	1.3%	1.5%	1.7%
0.000	-0.001	0.000	-0.005	0.025	0.028	0.035	0.032	1.2%	1.4%	1.7%	1.8%
0.002	-0.001	0.000	0.002	0.023	0.016	0.014	0.024	1.0%	0.8%	0.7%	1.1%
0.001	-0.001	0.001	0.006	0.036	0.028	0.030	0.039	1.7%	1.4%	1.4%	1.6%
-0.006	-0.005	-0.001	0.001	0.027	0.024	0.030	0.032	1.6%	1.4%	1.6%	1.5%
-0.002	-0.002	0.000	0.000	0.023	0.022	0.027	0.023	1.3%	1.2%	1.3%	1.1%
-0.004	-0.001	-0.001	-0.001	0.029	0.027	0.031	0.032	1.6%	1.4%	1.6%	1.7%
0.002	0.000	0.001	0.000	0.041	0.027	0.035	0.027	1.9%	1.4%	1.7%	1.4%
-0.002	-0.002	0.000	-0.002	0.026	0.025	0.021	0.025	1.4%	1.4%	1.1%	1.4%
0.001	0.002	0.002	0.002	0.028	0.034	0.032	0.034	1.3%	1.5%	1.4%	1.5%

Ternary-precursor mixture (T2)

Table 9 – Ternary2-precursor samples mass change in different sulfate solutions

Initial Mass (g)	Mass (%)				
	M_i (g)	30 (day)	60 (day)	90 (day)	182 (day)
3675.65		2.7%	2.6%	2.6%	2.3%
3658.11		2.2%	2.3%	2.3%	2.2%
3706.31		2.3%	1.9%	1.9%	1.9%
3610.30		0.1%	0.0%	-0.1%	0.5%
3670.89		2.2%	2.2%	2.3%	0.5%
3700.37		2.6%	1.9%	2.0%	1.8%
3699.63		1.8%	1.7%	1.8%	0.4%
3672.76		2.4%	1.8%	1.1%	2.1%
3676.68		2.4%	2.4%	2.5%	2.3%
3621.55		4.6%	3.4%	2.5%	5.4%
3630.60		3.9%	3.7%	3.0%	4.7%
3679.15		3.3%	2.4%	1.6%	5.1%

Table 10 – Ternary2-precursor samples cross-section change in different sulfate solutions

$x=\Delta L/L_i$				$z=\Delta V/V_i$				$y=\Delta D/D_i$			
30 (day)	60 (day)	90 (day)	182 (day)	30 (day)	60 (day)	90 (day)	182 (day)	30 (day)	60 (day)	90 (day)	182 (day)
0.005	0.013	0.018	0.018	-0.009	-0.003	-0.004	-0.008	-0.8%	-1.1%	-1.0%	-1.1%
0.005	0.010	0.028	0.022	0.093	0.108	0.100	0.040	4.0%	4.0%	3.8%	3.8%
0.006	0.000	0.011	0.016	0.031	0.037	0.047	0.016	1.6%	1.5%	1.3%	1.5%
0.012	0.000	0.003	0.005	0.035	0.035	0.035	0.016	1.6%	1.8%	1.6%	1.5%
-0.007	-0.001	-0.004	0.001	-0.027	-0.026	-0.025	-0.010	-1.0%	-1.3%	-1.1%	-1.3%
0.000	-0.005	-0.002	0.005	-0.021	-0.022	-0.017	-0.007	-0.7%	-0.8%	-1.0%	-1.1%
-0.004	-0.002	0.001	0.004	0.030	0.036	0.037	0.024	2.4%	1.6%	1.7%	1.6%
0.013	0.001	0.019	0.021	0.033	0.041	0.046	0.012	1.2%	1.6%	1.1%	1.2%
0.008	0.005	-0.005	0.019	0.029	0.022	0.050	0.014	1.4%	1.2%	1.3%	1.5%
0.015	0.020	0.018	0.020	0.052	0.056	0.061	0.015	1.5%	1.6%	1.9%	2.0%
-0.006	0.022	0.010	0.004	0.027	0.017	0.010	0.003	0.3%	0.2%	0.4%	0.3%
-0.001	0.002	0.004	-0.004	0.020	0.024	0.019	0.010	1.0%	0.9%	1.0%	1.2%

References

- Abora, K., Beleña, I., Bernal, S. A., Dunster, A., Nixon, P. A., Provis, J. L., Tagnit-Hamou, A., and Winnefeld, F. (2014). Durability and Testing—Chemical Matrix Degradation Processes. *In Alkali activated materials*, Springer, Dordrecht, 177-221.
- ACI Committee 201, (2016). Guide to Durable Concrete (ACI-201.2R-16). *American Concrete Institute*, Farmington Hills, MI, USA.
- ACI Committee 222R, (2019). Guide to Protection of Reinforcing Steel in Concrete Against Corrosion (ACI 222R-19). *American Concrete Institute*, Farmington Hills, MI, USA, 60.
- ACI Committee 237, (2007). Self-Consolidating Concrete (ACI 237R-07). *American Concrete Institute*, Farmington Hills, MI, USA, 30.
- ACI Committee 318, (2014). Building Code Requirements for Structural Concrete and Commentary (ACI 318R-19). *American Concrete Institute*, Farmington Hills, MI, USA.
- Adam, A., Molyneaux, T., Patnaikuni, I., Law, D. (2009). Strength, Sorptivity and Carbonation of Geopolymer Concrete. *Challenges, Opportunities and Solutions in Structural Engineering and Construction*, Taylor and Francis, 563–568.
- Alanazi, H., Hu, J., and Kim, Y. R. (2019). Effect of Slag, Silica Fume, and Metakaolin on Properties and Performance of Alkali-Activated Fly Ash Cured at Ambient Temperature. *Construction and Building Materials*, 197, 747-756.
- Altan, E., and Erdoğan, S. T. (2012). Alkali Activation of a Slag at Ambient and Elevated Temperatures. *Cement and Concrete Composites*, 34(2), 131-139.
- Andersson, R., and Gram, H. E. (1987). Properties of Alkali Activated Slag Concrete. *Nordic concrete research*, (6), 7-18.
- Aragón, P., Robayo-Salazar, R. A., and Mejía de Gutiérrez, R. (2020). Alkali-Activated Concrete Based on Natural Volcanic Pozzolan: Chemical Resistance to Sulfate Attack. *Journal of Materials in Civil Engineering*, 32(5), 04020106.
- AS 2350 (2016). Methods of testing Portland, blended and masonry cements, Method 12: Preparation of a Standard Mortar and Moulding of Specimens. Committee BD/10. Australia.
- AS 3972 (2010). General Purpose and Blended cements. Committee BD/10. Australia.

ASTM C1012, (2004). Standard Test Method for Length Change of Hydraulic-Cement Mortars Exposed to a Sulfate Solution. *ASTM International*, PA, USA.

ASTM C1038 (2019). Standard Test Method for Expansion of Hydraulic Cement Mortar Bars Stored in Water. *ASTM International*, West Conshohocken, PA;USA.

ASTM C109 (2000). Standard Test Method for Compressive Strength of Hydraulic Cement Mortars. *ASTM International*, PA, USA.

ASTM C1585 (2020). Standard Test Method for Measurement of Rate of Absorption of Water by Hydraulic-Cement Concretes. *ASTM International*, PA, USA.

ASTM C1611 (2014). Standard Test Method for Slump Flow of Self-Consolidating Concrete. *ASTM International*, PA, USA.

ASTM C1760 (2012). Standard Test Method for Bulk Electrical Conductivity of Hardened Concrete. *ASTM International*, PA, USA.

ASTM C39 (2012). Standard Test Method for Compressive Strength of Cylindrical Concrete Specimens. *ASTM International*, PA, USA.

ASTM C452 (2019). Standard Test Method for Potential Expansion of Portland-Cement Mortars Exposed to Sulfate. *ASTM International*, PA, USA.

ASTM C642 (2006). Standard Test Method for Density, Absorption, and Voids in Hardened Concrete. *ASTM International*, PA, USA.

Atiş, C., Bilim, C., Çelik, Ö., and Karahan, O. (2009). Influence of Activator on the Strength and Drying Shrinkage of Alkali-Activated Slag Mortar. *Construction and Building Materials*, 23(1), 548-555.

Bakharev, T. (2005). Durability of Geopolymer Materials in Sodium and Magnesium Sulfate Solutions. *Cement and Concrete Research*, 35(6), 1233-1246.

Bakharev, T., Sanjayan, J. G., and Cheng, Y. B. (2000). Effect of Admixtures on Properties of Alkali-Activated Slag Concrete. *Cement and Concrete Research*, 30(9), 1367-1374.

Bakharev, T., Sanjayan, J. G., and Cheng, Y. B. (2002). Sulfate Attack on Alkali-Activated Slag Concrete. *Cement and Concrete research*, 32(2), 211-216.

Baldermann, C., Baldermann, A., Furat, O., Krüger, M., Nachtnebel, M., Schroettner, H., Juhart, J., Schmidt, V., and Tritthart, J. (2019). Mineralogical and Microstructural Response of Hydrated Cement Blends to Leaching. *Construction and Building Materials*, 229, 116902.

Barbosa, V., MacKenzie, K., and Thaumaturgo, C. (2000). Synthesis and Characterisation of Materials Based on Inorganic Polymers of Alumina and Silica:

Sodium Polysialate Polymers. *International Journal of Inorganic Materials*, 2(4), 309-317.

Barhoum, A., García-Betancourt, M. L., Rahier, H., and Van Assche, G. (2018). Physicochemical Characterization of Nanomaterials: Polymorph, Composition, Wettability, and Thermal Stability. In *Emerging Applications of Nanoparticles and Architecture Nanostructures*, 255-278.

Baščarević, Z., Komljenović, M., Miladinović, Z., Nikolić, V., Marjanović, N., and Petrović, R. (2015). Impact of Sodium Sulfate Solution on Mechanical Properties and Structure of Fly Ash based Geopolymers. *Materials and Structures*, 48(3), 683-697.

Bassuoni, M. T. F. (2008). Integrated Approach for Investigating the Durability of Self-Consolidating Concrete to Sulfate Attack, 69(11).

Bassuoni, M. T., and Nehdi, M. L. (2009). Durability of Self-Consolidating Concrete to Sulfate Attack under Combined Cyclic Environments and Flexural Loading. *Cement and Concrete Research*, 39(3), 206–226.

Bassuoni, M., and Rahman, M. (2016). Response of Concrete to Accelerated Physical Salt Attack Exposure. *Cement and Concrete Research*, 79, 395-408.

Bate, S. (1984). High Alumina Cement Concrete in Existing Building Structures. *Department of the Environment Building Research Establishment; Report BR235*.

Bellmann, F., Möser, B., and Stark, J. (2006). Influence of Sulfate Solution Concentration on the Formation of Gypsum in Sulfate Resistance Test Specimen. *Cement and Concrete Research*, 36(2), 358-363.

Beltrame, N. A. M., da Luz, C. A., Perardt, M., and Hooton, R. D. (2020). Alkali Activated Cement made from Blast Furnace Slag Generated by Charcoal: Resistance to Attack by Sodium and Magnesium Sulfates. *Construction and Building Materials*, 238, 117710.

Bernal, S. A., Mejía de Gutierrez, R., and Rodríguez, E. D. (2013). Alkali-Activated Materials: Cementing a Sustainable Future. *Ingeniería y competitividad*, 15(2), 211-223.

Bernal, S. A., Provis, J. L., Fernández-Jiménez, A., Krivenko, P. V., Kavalerova, E., Palacios, M., and Shi, C. (2014a). Binder Chemistry–High-Calcium Alkali-Activated Materials. In *Alkali Activated Materials*, Springer, Dordrecht, 59-91.

Bernal, S., de Gutierrez, R., Delvasto, S., Rodríguez, E. (2010). Performance of an Alkali-Activated Slag Concrete Reinforced with Steel Fibers. *Construction and Building Materials*, 24 (2), 208–214.

- Bernal, S., Krivenko, P., Provis, J., Puertas, F., Rickard, W., Shi, C., and van Riessen, A. (2014b). Other Potential Applications for Alkali-Activated Materials. *In Alkali Activated Materials, RILEM State-of-the-Art Reports*, 13 (2014): 339-379.
- Bernal, S., Mejía de Gutierrez, R., Pedraza, A., Provis, J., Rodríguez, E., Delvasto, S. (2011). Effect of Binder Content on the Performance of Alkali-Activated Slag Concretes. *Cement and Concrete Research*, 41 (1), 1–8.
- Bernal, S., Nicolas, R., van Deventer, J., and Provis, J. (2016). Alkali-Activated Slag Cements Produced with a blended Sodium Carbonate/Sodium Silicate Activator. *Advances in Cement Research*, 28(4), 262-273.
- Bernal, S., Provis, J., Myers, R., San Nicolas, R., and van Deventer, J. (2015). Role of Carbonates in the Chemical Evolution of Sodium Carbonate-Activated Slag Binders. *Materials and Structures*, 48(3), 517-529.
- Bernal, S., Rodríguez, E., de Gutiérrez, R., Gordillo, M., and Provis, J. (2011). Mechanical and Thermal Characterisation of Geopolymers Based on Silicate-Activated Metakaolin/Slag Blends. *Journal of Materials Science*, 46(16), 5477-5486.
- Bernal, S., Rodríguez, E., de Gutiérrez, R., Provis, J., and Delvasto, S. (2012). Activation of Metakaolin/Slag Blends Using Alkaline Solutions Based on Chemically Modified Silica Fume and Rice Husk Ash. *Waste and Biomass Valorization*, 3(1), 99-108.
- Bernal, S., San Nicolas, R., Myers, R., de Gutiérrez, R., Puertas, F., van Deventer, J., and Provis, J. (2015). MgO Content of Slag Controls Phase Evolution and Structural Changes Induced by Accelerated Carbonation in Alkali-Activated Binders. *Cement and Concrete Research*, 57, 33–43.
- Beushausen, H., and Luco, L. F. (2016). Performance-Based Specifications and Control of Concrete Durability. *RILEM TC*, 66-72.
- Bickley, J., Hooton, D., and Hover, C. (2006). Preparation of a Performance-Based Specification for Cast-In-Place Concrete. *RMC Research Foundation*, 1-36.
- Bijen, J. (1996). Benefits of Slag and Fly Ash. *Construction and Building Materials*, 10(5), 309-314.
- Bin, Q., Wu, X., and Tang, M. (1992). High Strength Alkali Steel–Iron Slag Binder. *In Proceeding of the 9th International Congress on the Chemistry of Cement*, New Delhi, 3, 291-297.
- Bonen, D. (1993). A Microstructural Study of the Effect Produced by Magnesium Sulfate on Plain and Silica Fume-Bearing Portland Cement Mortars. *Cement and Concrete Research*, 23(3), 541-553.

- Bonen, D. (1997). The Microstructure of Concrete Subjected to Highmagnesium and High-Magnesium Sulfate Brine Attack. *In Proceeding of the 10th International Congress on Chemistry of Cement*, Gothenberg, Sweden.
- Boyd, A. J., and Mindess, S. (2004). The Use of Tension Testing to Investigate the Effect of W/C Ratio and Cement Type on the Resistance of Concrete to Sulfate Attack. *Cement and Concrete Research*, 34(3), 373-377.
- Brough, A. R., Holloway, M., Sykes, J., and Atkinson, A. (2000). Sodium Silicate-Based Alkali-Activated Slag Mortars: Part II. The Retarding Effect of Additions of Sodium Chloride or Malic Acid. *Cement and Concrete Research*, 30(9), 1375-1379.
- Brown, P. W. (1981). An Evaluation of the Sulfate Resistance of Cements in a Controlled Environment. *Cement and Concrete Research*, 11(5-6), 719-727.
- Brylicki W., Malolepszy J. and Stryczek S. (1992). Alkali Activated Slag Cementitious Material for Drilling Operation. In Proceedings of the 9th International Congress on the Chemistry of Cement, New Delhi, 3, 312–318.
- Bui, P. T., Ogawa, Y., and Kawai, K. (2018). Long-Term Pozzolanic Reaction of Fly Ash in Hardened Cement-Based Paste Internally Activated by Natural Injection of Saturated Ca(OH)₂ Solution. *Materials and Structures*, 51(6), 1-14.
- Caijun, S., and Yinyu, L. (1989). Investigation on Some Factors Affecting the Characteristics of Alkali-Phosphorus Slag Cement. *Cement and Concrete Research*, 19(4), 527-533.
- Cao, H. T., Bucea, L., Ray, A., and Yozghatlian, S. (1997). The Effect of cement Composition and pH of Environment on Sulfate Resistance of Portland Cements and Blended Cements. *Cement and Concrete Composites*, 19(2), 161–171.
- Chabrelie, A. (2010). Mechanisms of Degradation of Concrete by External Sulfate Ions under Laboratory and Field Conditions (Doctoral dissertation, École Polytechnique Fédérale De Lausanne).
- Chareerat, T., Chindaprasirt, P., and Sirivivatnanon, V. (2007). Workability and Strength of Coarse High Calcium Fly Ash Geopolymers. *Cement and Concrete Composites*, 29, 224-229.
- Chatterji, S. (2005). Aspects of Generation of Destructive Crystal Growth Pressure. *Journal Of Crystal Growth*, 277(1-4), 566-577.
- Cheah, C., Tan, L., and Ramli, M. (2019). The Engineering Properties and Microstructure of Sodium Carbonate Activated Fly Ash/Slag Blended Mortars With Silica Fume. *Composites Part B: Engineering*, 160, 558-572.

Chen, S., Wu, M.Q. and Zhang, S.R. (2010). Mineral Phases and Properties of Alkali-Activated Metakaolin-Slag Hydroceramics for a Disposal of simulated Highly Alkaline Wastes. *Journal of Nuclear Materials*, 402(2–3),: 173–178.

Chithiraputhiran, S., and Neithalath, N. (2013). Isothermal Reaction Kinetics and Temperature Dependence of Alkali Activation of Slag, Fly Ash and their Blends. *Construction and Building Materials*, 45, 233-242.

Clifton, J., Frohnsdorff, G., and Ferraris, C. (1999). Standards for evaluating the susceptibility of cement-based materials to external sulfate attack. In J. Marchand and Skalny (eds). *Materials Science of Concrete Special Volume: Sulfate Attack Mechanisms*, American Ceramic Society, Westerville, OH, 337-355.

Cohen, M. D., and Mather, B. (1991). Sulfate Attack on Concrete: Research Needs. *Materials Journal*, 88(1), 62-69.

Collins, F. G., and Sanjayan, J. G. (1999). Workability and mechanical Properties of Alkali Activated Slag Concrete. *Cement and Concrete Research*, 29(3), 455-458.

Collins, F., and Sanjayan, J. (2010). Capillary Shape: Influence on Water Transport within Unsaturated Alkali Activated Slag Concrete. *Journal of Materials in Civil Engineering*, 22(3), 260-266.

Collins, F., and Sanjayan, J. G. (2000). Effect of Pore Size Distribution on Drying Shrinking of Alkali-Activated Slag Concrete. *Cement and Concrete Research*, 30(9), 1401-1406.

Costa, L., Escoqui, J., Oliveira, T., Fonseca, L., and Farage, M. (2018). Sodium Sulfate Attack on Portland Cement Structures: Experimental and Analytical Approach. *REM-International Engineering Journal*, 71(4), 531-542.

Criado, M., Walkley, B., Ke, X., Provis, J., and Bernal, S. (2018). Slag and Activator Chemistry Control the Reaction Kinetics of Sodium Metasilicate-Activated Slag Cements. *Sustainability*, 10(12), 4709.

CSA A3004 (2008). Test Method for Determination of Expansion of Blended Hydraulic Cement Mortar Bars due to External Sulphate Attack. Canadian Standards Association,

CSA-Group. (2018). Cementitious materials compendium A3000-18. Retrieved from https://store.csagroup.org/ccrz__ProductDetails?viewState=DetailView&cartID=&portalUser=&store=&cclcl=en_US&sku=A3000-18

Dave, N. G. (1981). Pozzolanic Wastes and their Activation to Produce Improved Lime Pozzolana Mixtures. In Proceedings of the 2nd Australian Conference on Engineering Materials, Sydney, Australia, 623–638.

Davidovits, J. (1982). *Alchemy and Pyramids*. Geopolymer Institute.

Davidovits, J. (1999). *Chemistry of Geopolymeric Systems Terminology: Proceedings of the 2nd International Conference on the Geopolymere'99*, Geopolymer Institute, Saint-Quentin, France.

Davidovits, J. (2012). Keynote Conference Video of State of Geopolymer R&D. Accessed em www.geopolymer.org/camp/gp-camp-2012.

Day, R. L. (2000). Development of Performance Tests for Sulfate Attack on Cementitious Systems. *Cement, Concrete and Aggregates*, 22(2), 169-176.

De Almeida, I. R. (1991). Resistance of High Strength Concrete to Sulfate Attack: Soaking and Drying Test. *Special Publication*, 126, 1073-1092.

De Schutter, G., Bartos, P., Domone, P., and Gibbs, J. (2008). *Self-Compacting Concrete (Vol. 288)*. Caithness: Whittles Publishing.

Deir, E., Gebregziabihier, B. S., and Peethamparan, S. (2014). Influence of Starting Material on the Early Age Hydration Kinetics, Microstructure and Composition of Binding Gel in Alkali Activated Binder Systems. *Cement and Concrete Composites*, 48, 108-117.

Demie, S., Nuruddin, M. F., and Shafiq, N. (2013). Effects of Micro-Structure Characteristics of Interfacial Transition Zone on the Compressive Strength of Self-Compacting Geopolymer Concrete. *Construction and Building Materials*, 41, 91-98.

DIN 1164: DIN Taschenbuch 73, Zement.

Ding, Y., Dai, J., and Shi, C. (2016). Mechanical Properties of Alkali-Activated Concrete: A State-Of-The-Art Review. *Construction and Building Materials*, 127, 68-79.

Djobo, J., Tchakoute, H., Ranjbar, N., Elimbi, A., Tchadjie, L., and Njopwouo, D. (2016). Gel Composition and Strength Properties of Alkali-Activated Oyster Shell-Volcanic Ash: Effect of Synthesis Conditions. *Journal of the American Ceramic Society*, 99(9), 3159-3166.

Doehne, E., Selwitz, C., and Carson, D. (2002). The Damage Mechanism of Sodium Sulfate in Porous Stone. *In Proceed. of the SALTeXPert Meeting*, 27-146.

Douglas, E., Bilodeau, A., Brandstetr, J., and Malhotra, V. (1991). Alkali Activated Ground Granulated Blast-Furnace Slag Concrete: Preliminary Investigation. *Cement and Concrete Research*, 21(1), 101-108.

Duxson, P., Mallicoat, S., Lukey, G., Kriven, W., and van Deventer, J. (2007). The Effect of Alkali and Si/Al Ratio on the Development of Mechanical Properties of

Metakaolin-Based Geopolymers. *Colloids and Surfaces A: Physicochemical and Engineering Aspects*, 292(1), 8-20.

EFNARC (2002). Guidelines for Self-Compacting Concrete, European Federation for Specialist Construction Chemicals and Concrete Systems, Norfolk, UK.

EFNARC (2005). Specification and Guidelines for Self-Compacting Concrete. European Federation of Producers and Applicators of Specialist Products for Structures, Norfolk, UK.

Eglinton, M. (1998). Lea's Chemistry of Cement and Concrete. Resistance of Concrete to Destructive Agencies, 299-342.

El-Sayed, H., Abo, E., Khater, H., and Hasanein, S. (2011). Resistance of Alkali Activated Water-Cooled Slag Geopolymer to Sulphate Attack. *Ceramics-Silikáty*, 55(2), 153-160.

Elyamany, H., Abd Elmoaty, M., and Elshaboury, A. (2018). Magnesium Sulfate Resistance of Geopolymer Mortar. *Construction and Building Materials*, 184, 111-127.

Faimon, J. (1996). Oscillatory Silicon and Aluminum Aqueous Concentrations During Experimental Aluminosilicate Weathering. *Geochimica et Cosmochimica Acta*, 60(15), 2901-2907.

Favier, A., Habert, G., de Lacaillerie, J., and Roussel, N. (2013). Mechanical Properties and Compositional Heterogeneities of Fresh Geopolymer Pastes. *Cement and Concrete Research*, 48, 9-16.

Fernandez-Altale, V. (2009). Availability of Al₂O₃ in Slag Blended Cements: Sulphate Attack Implications. *In the Proceedings of the Final Conference of the NANOCEM Marie Curie Research Training Network*, Villars-sur-Ollon, Switzerland, 1-3.

Fernández-Carrasco, L., Torrens-Martín, D., Morales, L., and Martínez-Ramírez, S. (2012). Infrared Spectroscopy in the Analysis of Building and Construction Materials. *Infrared Spectroscopy—Materials Science, Engineering and Technology*, 369-382.

Fernández-Jiménez, A., and Palomo, A. (2005). Composition and Microstructure of Alkali Activated Fly Ash Binder: Effect of the Activator. *Cement and Concrete Research*, 35(10), 1984-1992.

Fernández-Jiménez, A., and Puertas, F. (2003). Effect of Activator Mix on the Hydration and Strength Behaviour Of Alkali-Activated Slag Cements. *Advances in cement research*, 15(3), 129-136.

- Fernández-Jiménez, A., Palomo, J., and Puertas, F. (1999). Alkali-Activated Slag Mortars: Mechanical Strength Behaviour. *Cement and Concrete Research*, 29(8), 1313-1321.
- Ferraris, C., Stutzman, P., Peltz, M., and Winpigler, J. (2005). Developing a More Rapid Test to Assess Sulfate Resistance of Hydraulic Cements. *Journal of research of the National Institute of Standards and Technology*, 110(5), 529.
- Fixen, P. E. (2002). Soil test levels in North America. *Better Crops*, 86(1), 12-15.
- Flatt, R. J. (2002). Salt Damage in Porous Materials: How High Supersaturations are Generated. *Journal of Crystal Growth*, 242(3-4), 435-454.
- Frearson, J., and Higgins, D. (1995). Effect of Test Procedures on the Assessment of the Sulfate Resistance of Slag Cements. *Special Publication*, 153, 975-994.
- Galan, I., Baldermann, A., Kusterle, W., Dietzel, M., and Mittermayr, F. (2019). Durability of Shotcrete for Underground Support– Review and Update. *Construction and Building Materials*, 202, 465–493.
- Gao, X., Yu, Q., and Brouwers, H. (2015). Reaction Kinetics, Gel Character and Strength of Ambient Temperature Cured Alkali Activated Slag–Fly Ash Blends. *Construction and Building Materials*, 80, 105-115.
- Garcia-Loderio I, Fernandez A, and Palomo A. (2013). Variation in Hybrid Cements Over Time. Alkaline Activation of Fly Ash-Portland Cement Blends. *Cement and Concrete Research*, 52,112-22.
- GB/T 2420 (1981). Rapid Test for Sulphate Resistance of Cement. China Building Materials Federation, China.
- GB/T 749 (2008). Test Method for Determining Capability of Resisting Sulfate Corrode of Cement. China Building Materials Federation, Chine.
- Gebregziabihir, B., Thomas, R., and Peethamparan, S. (2015). Very Early-Age Reaction Kinetics and Microstructural Development in Alkali-Activated Slag. *Cement and concrete composites*, 55, 91-102.
- Giergiczny, Z. (1997). Sulphate Resistance of Cements with Mineral Admixtures. *In the Proceedings of the 10th International Congress on the Chemistry of Cement*, Gothenburg, Sweden.
- Gifford, P., and Gillott, J. (1997). Behaviour of Mortar and Concrete Made With Activated Blast Furnace Slag Cement. *Canadian Journal of Civil Engineering*, 24(2), 237-249.

Glasser, F. P. (2001). Mineralogical Aspects of Cement in Radioactive Waste Disposal. *Mineralogical Magazine*, 65(5), 621-633.

Glukhovskiy, V. D. (1959). Soil Silicates (Gruntosilikaty). *USSR Kiev: Budivelnik Publisher*.

Gonzalez, M., and Irassar, E. (1997). Ettringite Formation in Low C₃A Portland Cement Exposed to Sodium Sulfate Solution. *Cement and Concrete Research*, 27(7), 1061-1071.

Gruskovnjak, A., Lothenbach, B., Holzer, L., Figi, R., and Winnefeld, F. (2006). Hydration of Alkali-Activated Slag: Comparison with Ordinary Portland Cement. *Advances in Cement Research*, 18(3), 119-128.

Gülşan, M., Alzeebaree, R., Rasheed, A., Niş, A., and Kurtoğlu, A. (2019). Development of Fly Ash/Slag Based Self-Compacting Geopolymer Concrete using Nano-Silica and Steel Fiber. *Construction and Building Materials*, 211, 271-283.

Häkkinen, T. (1993). The Influence of Slag Content on the Microstructure, Permeability and Mechanical Properties of Concrete Part 1 Microstructural Studies and Basic Mechanical Properties. *Cement and concrete research*, 23(2), 407-421.

Hanehara, S., and Yamada, K. (1999). Interaction between Cement and Chemical Admixture from the Point of Cement Hydration, Absorption Behaviour of Admixture, and Paste Rheology. *Cement and Concrete Research*, 29(8), 1159-1165.

Hardjito, D., Wallah, S., Sumajouw, D., and Rangan, B. (2005). Fly Ash-Based Geopolymer Concrete. *Australian Journal of Structural Engineering*, 6(1), 77-86.

Haynes, H., O'Neill, R., and Mehta, P. (1996). Concrete Deterioration from Physical Attack by Salts. *Concrete International*, 18(1), 63-68.

Haynes, H., O'Neill, R., Neff, M., and Mehta, P. (2008). Salt Weathering Distress on Concrete Exposed to Sodium Sulfate Environment. *ACI Materials Journal*, 105(1), 35.

He, J., Bu, X., Bai, W., Zheng, W., Gao, Q., and Wang, Y. (2020). Preparation and Properties of Self-Compacting Alkali-Activated Slag Repair Mortar. *Construction and Building Materials*, 252, 119034.

He, J., Jie, Y., Zhang, J., Yu, Y., and Zhang, G. (2013). Synthesis and Characterization of Red Mud and Rice Husk Ash-Based Geopolymer Composites. *Cement and Concrete Composites*, 37, 108-118.

Hearn, N., and Young, F. (1999). W/C Ratio, Porosity and Sulfate Attack—A Review. *Materials Science of Concrete: Sulfate Attack Mechanisms*, Ed. J. Marchand and JP Skalny. *American Ceramic Society*, Westerbok, Ohio, 189-205.

- Heikal, M., Nassar, M., El-Sayed, G., and Ibrahim, S. (2014). Physico-Chemical, Mechanical, Microstructure and Durability Characteristics of Alkali Activated Egyptian Slag. *Construction and Building Materials*, 69, 60-72.
- Heikal, M., Zohdy, K. M., and Abdelkreem, M. (2013). Mechanical, Microstructure and Rheological Characteristics of High Performance Self-Compacting Cement Pastes and Concrete Containing Ground Clay Bricks. *Construction and Building Materials*, 38, 101-109.
- Hewlett, P., and Liska, M. (2019). *Lea's Chemistry of Cement and Concrete*: Butterworth-Heinemann.
- Hong, S., Kim, J., and Kim, J. (1993). Studies on the Hydration of Alkali Activated Slag. In *3rd Beijing International Symposium on Cement and Concrete*, 2, 1059-1063.
- Hooton, R. (2008). Bridging the Gap between Research and Standards. *Cement and Concrete Research*, 38(2), 247-258.
- Hooton, R., and Day, R. (2000). Development of Performance Tests for Sulfate Attack on Cementitious Systems. *Cement, Concrete and Aggregates*, 22(2), 169.
- Hooton, R., and Wafa, F. (1994). Accelerated Sulfate Attack on Concrete in a Hot Climate. *Cement, Concrete and Aggregates*, 16(1), 31.
- Huanhai, Z., Xuequan, W., Zhongzi, X., and Mingshu, T. (1993). Kinetic Study on Hydration of Alkali-Activated Slag. *Cement and Concrete Research*, 23(6), 1253-1258.
- Hubler, M., Thomas, J., and Jennings, H. (2011). Influence of Nucleation Seeding on the Hydration Kinetics and Compressive Strength of Alkali Activated Slag Paste. *Cement and Concrete Research*, 41(8), 842-846.
- Huseien, G. F., and Shah, K. W. (2020). Durability and Life Cycle Evaluation of Self-Compacting Concrete Containing Fly Ash as GBFS Replacement with Alkali Activation. *Construction and Building Materials*, 235, 117458.
- Huseien, G., Sam, A., and Alyousef, R. (2021). Texture, Morphology and Strength Performance of Self-Compacting Alkali-Activated Concrete: Role of Fly Ash as GBFS Replacement. *Construction and Building Materials*, 270, 121368.
- Huseien, G., Sam, A., Shah, K., and Mirza, J. (2020). Effects of Ceramic Tile Powder Waste on Properties of Self-Compacted Alkali-Activated Concrete. *Construction and Building Materials*, 236, 117574.
- Ionescu, D. V. (1999). *The Hydraulic Potential of High Iron Bearing Steel Slags*. Doctoral Dissertation, University of British Columbia, 181 p.

IS 456 (2000). Plain and Reinforced Concrete-Code of Practice. Bureau of Indian Standards, New Delhi, India.

Ismail, I., Bernal, S., Provis, J., Hamdan, S., and van Deventer, J. (2013). Microstructural Changes in Alkali Activated Fly Ash/Slag Geopolymers with Sulfate Exposure. *Materials and Structures*, 46(3), 361-373.

Ismail, I., Bernal, S., Provis, J., Hamdan, S., and van Deventer, J. (2013). Microstructural Changes in Alkali-Activated Fly Ash/Slag Geopolymers with Sulfate Exposure. *Materials and Structures*, 46(3), 361-373.

Ismail, I., Bernal, S., Provis, J., San Nicolas, R., Brice, D., Kilcullen, A., Hamdan, S., and van Deventer, J. (2013). Influence of Fly Ash on the Water and Chloride Permeability of Alkali-Activated Slag Mortars and Concretes. *Construction and Building Materials*, 48, 1187-1201.

Ismail, I., Bernal, S., Provis, J., San Nicolas, R., Hamdan, S., and van Deventer, J. (2014). Modification of Phase Evolution in Alkali-Activated Blast Furnace Slag by the Incorporation of Fly Ash. *Cement and Concrete Composites*, 45, 125-135.

Isozaki, K., Iwamoto, S., and Nakagawa, K. (1986). Some Properties of Alkali-Activated Slag Cements. *In the Proceedings of the 8th International Congress on Chemistry of Cements*, Rio de Janeiro, 6, 395-399.

Jansson, H., Bernin, D., and Ramser, K. (2015). Silicate Species of Water Glass and Insights for Alkali-Activated Green Cement. *Aip Advances*, 5(6), 067167.

Kalousek, G., Porter, L., and Benton, E. (1972). Concrete for Long-Time Service in Sulfate Environment. *Cement and Concrete Research*, 2(1), 79-89.

Kamali, S., Moranville, M., and Leclercq, S. (2008). Material and Environmental Parameter Effects on the Leaching of Cement Pastes: Experiments and Modelling. *Cement and Concrete Research*, 38, 575-585

Kashani, A., Provis, J., Qiao, G., and van Deventer, J. (2014). The Interrelationship between Surface Chemistry and Rheology in Alkali Activated Slag Paste. *Construction and Building Materials*. 65, 583-591.

Kashani, A., Provis, J., Qiao, G., and van Deventer, J. (2014). The Interrelationship Between Surface Chemistry and Rheology in Alkali Activated Slag Paste. *Construction and Building Materials*, 65, 583-591.

Khayat, K., Ghezal, A., and Hadriche, M. (2000). Utility of Statistical Models in Proportioning Self-Consolidating Concrete. *Materials and Structures*, 33(5), 338-344.

Khayat, K., Ghezal, A., and Hadriche, M. (2000). Utility of Statistical Models in Proportioning Self-Consolidating Concrete. *Materials and Structures*, 33(5), 338-344.

- Khayat, K., Vachon, M., and Lanctot, M. (1997). Use of blended Silica Fume Cement in Commercial Concrete Mixtures. *ACI Materials Journal*, 94, 183-192.
- Kim, T., and Kang, C. (2020). The Mechanical Properties of Alkali-Activated Slag-Silica Fume Cement Pastes by Mixing Method. *International Journal of Concrete Structures and Materials*, 14(1), 1-15.
- Komljenović, M., Baščarević, Z., Marjanović, N., and Nikolić, V. (2013). External Sulfate Attack on Alkali-Activated Slag. *Construction and Building Materials*, 49, 31–39.
- Komljenović, M., Baščarević, Z., Marjanović, N., and Nikolić, V. (2013). External sulfate attack on alkali-activated slag. *Construction and Building Materials*, 49, 31-39.
- Komljenović, M., Džunuzović, N. š., and Nikolić, V. (2018). Resistance to External Sulfate Attack - Comparison of Two Alkali-Activated Binders. *MATEC Web of Conferences*, 163, 06001.
- Kovtun, M., Kearsley, E. P., and Shekhovtsova, J. (2015). Dry Powder Alkali-Activated Slag Cements. *Advances in Cement Research*, 27(8), 447-456.
- Krivenko P.V. (1992). Alkaline cements. *In the Proceedings of the 9th International Congress on the Chemistry of Cement*, New Delhi, India, 4,482-488.
- Krivenko P.V. (1994). Alkaline cements. *In the Proceedings of the 1st International Conference on Alkaline Cements and Concretes*, Kiev, Ukraine, 11-129.
- Kuehl, H. (1908). U.S. Patent No. 900,939. Washington, DC: U.S. Patent and Trademark Office.
- Kumar, S., Kumar, R., and Mehrotra, S. (2010). Influence of Granulated Blast Furnace Slag on the Reaction, Structure and Properties of Fly Ash based Geopolymer. *Journal of Materials Science*, 45(3), 607-615.
- Landrou, G., Brumaud, C., Winnefeld, F., Flatt, R., and Habert, G. (2016). Lime as an Anti-Plasticizer for Self-Compacting Clay Concrete. *Materials*, 9(5), 330.
- Le Saoût G., Ben Haha M., Winnefeld F. and Lothenbach B. (2011). Hydration Degree of Alkali-Activated Slags: A ²⁹Si NMR Study. *Journal of the American Ceramic Society*, 94(12), 4541–4547.
- Lecomte, I., Liégeois, M., Rulmont, A., Cloots, R., and Maseri, F. (2003). Synthesis and Characterization of New Inorganic Polymeric Composites Based on Kaolin or White Clay and on Ground-Granulated Blast Furnace Slag. *Journal of materials research*, 18(11), 2571-2579.

- Li, C., Sun, H., and Li, L. (2010). A Review: The Comparison Between Alkali-Activated Slag (Si+ Ca) and Metakaolin (Si+ Al) Cements. *Cement and Concrete Research*, 40(9), 1341-1349.
- Li, N., Shi, C., and Zhang, Z. (2019). Understanding the Roles of Activators towards Setting and Hardening Control of Alkali-Activated Slag Cement. *Composites Part B: Engineering*, 171, 34-45.
- Li, P., Tang, J., Chen, X., Bai, Y., and Li, Q. (2019). Effect of Temperature and pH on Early Hydration Rate and Apparent Activation Energy of Alkali-Activated Slag. *Advances in Materials Science and Engineering*, 13 pp.
- Li, X. J., and Zhang, J. (2012). A Survey of Sulfate Resistance Test Methods. *Applied Mechanics and Materials*, 166, 1859–1862.
- Lindgård, J., Andiç-Çakır, Ö., Fernandes, I., Rønning, T., and Thomas, M. (2012). Alkali–Silica Reactions (ASR): Literature Review on parameters Influencing Laboratory Performance Testing. *Cement and Concrete research*, 42(2), 223-243.
- Ling, G., Shui, Z., Sun, T., Gao, X., Wang, Y., Sun, Y., and Li, Z. (2018). Rheological Behavior and Microstructure Characteristics of SCC Incorporating Metakaolin and Silica Fume. *Materials*, 11(12), 2576.
- Locher, F. (1966). The Problem of the Sulphate Resistance of Slag Cements. *Zement-Kalk-Gips*.
- Locher, F. W. (2013). *Cement: Principles of Production and Use*: Verlag Bau+ Technik.
- Long, W. J., Ye, T. H., Luo, Q. L., Wang, Y., and Mei, L. (2019). Reinforcing Mechanism of Reduced Graphene Oxide on Flexural Strength of Geopolymers: A Synergetic Analysis of Hydration and Chemical Composition. *Nanomaterials*, 9(12), 1723.
- Loser, R., and Leemann, A. (2015). An Accelerated Sulfate Resistance Test for Concrete. *Materials and Structures*, 49(8), 3445–3457.
- Lothenbach, B., and Gruskovnjak, A. (2007). Hydration of Alkali-Activated Slag: Thermodynamic Modelling. *Advances in Cement Research*, 19(2), 81-92.
- Lothenbach, B., Bary, B., Le Bescop, P., Schmidt, T., and Leterrier, N. (2010). Sulfate Ingress in Portland Cement. *Cement and Concrete Research*, 40(8), 1211–1225.
- Luukkonen, T., Abdollahnejad, Z., Yliniemi, J., Kinnunen, P., and Illikainen, M. (2018). One-Part Alkali-Activated Materials: A Review. *Cement and Concrete Research*, 103, 21-34.

- Ma, Q., Nanukuttan, S. V., Basheer, P. M., Bai, Y., and Yang, C. (2016). Chloride Transport and the Resulting Corrosion of Steel Bars in Alkali-Activated Slag Concretes. *Materials and Structures*, 49(9), 3663-3677.
- Malhotra, V., Carette, G., and Bremner, T. (1988). Current Status of CANMET's Studies on the Durability of Concrete Containing Supplementary Cementing Materials in Marine Environment. *Special Publication*, 109, 31-72.
- Malone, P. G., Randall Jr, C. A., and Kirkpatrick, T. (1985). Potential Applications of Alkali-Activated Alumino-Silicate Binders in Military Operations. Army Engineer Waterways Experiment Station Vicksburg Ms Geotechnical Lab.
- Manjunath, R., and Narasimhan, M. C. (2018). An Experimental Investigation on Self-Compacting Alkali Activated Slag Concrete Mixes. *Journal of Building Engineering*, 17, 1-12.
- Manjunath, R., Narasimhan, M., Umesh, K., Kumar, S., and Bharathi, U. (2019). Studies on Development of High Performance, Self-Compacting Alkali Activated Slag Concrete Mixes using Industrial Wastes. *Construction and Building Materials*, 198, 133-147.
- Marchand, J., Odler, I., and Skalny, J. P. (2003). Sulfate Attack on Concrete: CRC Press.
- Mehta, P. (1992). Sulfate Attack on Concrete-a Critical Review. In *Materials Science of Concrete III*. The American Ceramic Society, 105-130.
- Mehta, P. K. (1975). Evaluation of the Sulfate Resistance of Cements by a New Test Method. *American Concrete Institute*, 72(10), 573-575.
- Mehta, P. K. (1999). Concrete Technology for Sustainable Development. *Concrete International*, 21(11), 47-53.
- Mehta, P. K. (2000). Sulfate Attack on Concrete Separating Myths from Reality. *Concrete International*, 22(8), 57-61.
- Mehta, P., Pirtz, D., and Polivka, M. (1979). Properties of Alite Cements. *Cement and Concrete Research*, 9(4), 439-450.
- Memon, F., Nuruddin, F., and Shafiq, N. (2011). Compressive Strength and Workability Characteristics of Low-Calcium Fly Ash-Based Self-Compacting Geopolymer Concrete. *International journal of civil and environmental engineering*, 3(2), 72-78.

- Mithun, B., and Narasimhan, M. (2016). Performance of Alkali Activated Slag Concrete Mixes Incorporating Copper Slag as Fine Aggregate. *Journal of Cleaner Production*, 112, 837–844.
- Mittermayr, F., Baldermann, A., Kurta, C., Rinder, T., Klammer, D., Leis, A., Tritthart, J., and Dietzel, M. (2013). Evaporation — A Key Mechanism for the Thaumassite form of Sulfate Attack. *Cement and Concrete Research*, 49, 55–64.
- Muntingh, Y. (2006). Durability and Diffusive Behaviour Evaluation of Geopolymeric Material (Doctoral Dissertation, Stellenbosch: University of Stellenbosch).
- Muroga, Y., Ohsuga, T., Date, S., and Hirata, A. (1999). A Flow Analysis for Self-Compacting Concrete. *In the 1st International RILEM Symposium on Self-Compacting Concrete*, Stockholm, 13-14 September, 71-82.
- Muttashar, H., Ariffin, M., Hussein, M., Hussin, M., and Ishaq, S. (2018). Self-Compacting Geopolymer Concrete with Spinel Garnet as Sand Replacement. *Journal of Building Engineering*, 15, 85-94.
- Myers, R., Bernal, S., Nicolas, R., and Provis, J. (2013). Generalized Structural Description of Calcium–Sodium Aluminosilicate Hydrate Gels: the Cross-Linked Substituted Tobermorite Model. *Langmuir* 29(17), 5294–5306.
- Myers, R., Lothenbach, B., Bernal, S., and Provis, J. (2016). Corrigendum to Thermodynamic Modelling of Alkali-Activated Slag-Based Cements. *Applied Geochemistry*, 100(67), 186, 233–247.
- Nagaraj V., Babu D. (2018). Assessing the Performance of Molarity and Alkaline Activator Ratio on Engineering Properties of Self-Compacting Alkaline Activated Concrete at Ambient Temperature. *Journal of Building Engineering*, 20, 137-155.
- Najim, K., Al-Jumaily, I., and Atea, A. (2016). Characterization of Sustainable High Performance/Self-Compacting Concrete Produced using CKD as a Cement Replacement Material. *Construction and Building Materials*, 103, 123-129.
- Najimi, M., Sobhani, J., and Pourkhorshidi, A. (2011). Durability of Copper Slag Contained Concrete Exposed to Sulfate Attack. *Construction and Building materials*, 25(4), 1895-1905.
- Nath, P., Sarker, P., and Rangan, V. (2015). Early Age Properties of Low-Calcium Fly Ash Geopolymer Concrete Suitable for Ambient Curing. *Procedia Engineering*, 125, 601-607.
- NBR 13583 (2014). Determination of Dimensional Variation of Portland Cement Mortar Bars Exposed to Sodium Sulfate Solution. Brazilian Association of Technical Standards, Rio de Janeiro, Brazil.

- Nehdi, M., and Hayek, M. (2005). Behavior of Blended Cement Mortars Exposed to Sulfate Solutions Cycling in Relative Humidity. *Cement and Concrete Research*, 35(4), 731-742.
- Nehdi, M., Suleiman, A., and Soliman, A. (2014). Investigation of Concrete Exposed to Dual Sulfate Attack. *Cement and Concrete Research*, 64, 42-53.
- Nehdi, M., Suleiman, A., and Soliman, A. (2014). Investigation of Concrete Exposed to Dual Sulfate Attack. *Cement and Concrete Research*, 64, 42-53.
- Nematollahi, B., and Sanjayan, J. (2015). Effect of Different Superplasticizers and Activator Combinations on Workability and Strength of Fly Ash Based Geopolymer. *Materials and Design*, 57, 667-672.
- Nematollahi, B., Sanjayan, J., and Shaikh, F. (2015b). Synthesis of Heat and Ambient Cured One-Part Geopolymer Mixes with Different Grades of Sodium Silicate. *Ceramics International*, 41(4), 5696-5704.
- Neupane, K., Kidd, P., Chalmers, D., Baweja, D., and Shrestha, R. (2016). Investigation on Compressive Strength Development and Drying Shrinkage of Ambient Cured Powder-Activated Geopolymer Concretes. *Australian Journal of Civil Engineering*, 14(1), 72-83.
- Neville, A. (2004). The Confused World of Sulfate Attack on Concrete. *Cement and Concrete Research*, 34(8), 1275-1296.
- Nijland, T., and Larbi, J. (2010). Microscopic Examination of Deteriorated Concrete. *In Non-destructive Evaluation of Reinforced Concrete Structures*, Woodhead Publishing, 137-179.
- Okamura, H.M. and Ouchi, M. (2003) Self-Compacting Concrete. *Journal of Advances Concrete Technology*, 1, 5-15.
- Ouyang, X., Ma, Y., Liu, Z., Liang, J., and Ye, G. (2020). Effect of the sodium Silicate Modulus and Slag Content on Fresh and Hardened Properties of Alkali-Activated Fly Ash/Slag. *Minerals*, 10(1), 15.
- Palacios, M., and Puertas, F. (2004). Stability of Superplasticizer and Shrinkage-Reducing Admixtures Stability of Superplasticizer and Shrinkage-Reducing Admixtures in High Basic Media. *Materiales de Construcción*, 54(276), 65-86.
- Palomo, A., Blanco-Varela, M., Granizo, M., Puertas, F., Vazquez, T., and Grutzeck, M. (1999). Chemical Stability of Cementitious Materials based on Metakaolin. *Cement and Concrete Research*, 29(7), 997-1004.

- Palomo, Á., Fernández-Jiménez, A., López-Hombrados, C., and Lleyda, J. L. (2011). Railway Sleepers Made of Alkali Activated Fly Ash Concrete. *Revista Ingeniería de Construcción*, 22(2), 75-80.
- Palomo, A., Grutzeck, M., and Blanco, M. (1999). Alkali-Activated Fly Ashes: A Cement for the Future. *Cement and Concrete Research*, 29(8), 1323-1329.
- Pan, Z., Li, D., Yu, J., and Yang, N. (2003). Properties and Microstructure of the Hardened Alkali-Activated Red Mud–Slag Cementitious Material. *Cement and Concrete Research*, 33(9), 1437-1441.
- Park, S., Park, H., Yoon, H., Seo, J., Yang, C., Provis, J., and Yang, B. (2020). Hydration Kinetics and Products of MgO-Activated Blast Furnace Slag. *Construction and Building Materials*, 249, 118700.
- Pasupathy, K., Berndt, M., Sanjayan, J., Rajeev, P., and Cheema, D. (2017). Durability of Low-Calcium Fly Ash Based Geopolymer Concrete Culvert in a Saline Environment. *Cement and Concrete Research*, 100, 297-310.
- Patel, Y. J., and Shah, N. (2018). Study on Workability and Hardened Properties of Self Compacted Geopolymer Concrete Cured at Ambient Temperature. *Indian Journal of Science and Technology*, 11(1), 1-12.
- Peng, Z., Vance, K., Dakhane, A., Marzke, R., and Neithalath, N. (2015). Microstructural and ²⁹Si MAS NMR Spectroscopic Evaluations of Alkali Cationic Effects on Fly Ash Activation. *Cement and Concrete Composites*, 57, 34-43.
- Planel, D., Sercombe, J., Le Bescop, P., Adenot, F., and Torrenti, J. (2006). Long-term Performance of Cement Paste during Combined Calcium Leaching–Sulfate Attack: Kinetics and Size Effect. *Cement and Concrete Research*, 36(1), 137–143.
- Pokrovsky, O., and Schott, J. (2004). Experimental Study of Brucite Dissolution and Precipitation in Aqueous Solutions: Surface Speciation and Chemical Affinity Control. *Geochimica et Cosmochimica Acta*, 68(1), 31-45.
- Price, C., and Brimblecombe, P. (1994). Preventing Salt Damage in Porous Materials. *Studies in Conservation*, 39(sup2), 90-93.
- Provis, J. L. (2018). Alkali-Activated Materials. *Cement and Concrete Research*, 114, 40-48.
- Provis, J. L., and Van Deventer, J. S. (Eds.). (2013). Alkali activated Materials: State-Of-The-Art Report, *RILEM TC 224-AAM (Vol. 13)*. Springer Science and Business Media.

Provis, J., and Bernal, S. (2014). Geopolymers and Related Alkali-Activated Materials. *Annual Review of Materials Research*, 44, 299-327.

Provis, J., and Van Deventer, J. (2009). Introduction to Geopolymers. *In Geopolymers*. Woodhead Publishing and CRC Press, Cambridge and Boca Raton, 1-11.

Provis, J., and Van Deventer, J. (2013). Alkali Activated Materials: State-of-the-Art Report, *RILEM TC 224-AAM*, Springer Science and Business Media, Vol. 13.

Provis, J., Myers, R., White, C., Rose, V., and Van Deventer, J. (2012). X-ray Microtomography Shows Pore Structure and Tortuosity in Alkali-Activated Binders. *Cement and Concrete Research*, 42(6), 855-864.

Pu X., Gan C., Wang S. and Yang C. (1988). Summary Reports of Research on alkali-Activated Slag Cement and Concrete. *Chongqing Institute of Architecture and Engineering*, 6 vols. (In Chinese)

Puertas, F., Amat, T., Fernández-Jiménez, A., and Vázquez, T. (2003). Mechanical and Durable Behaviour of alkaline Cement Mortars Reinforced with Polypropylene Fibres. *Cement and Concrete Research*, 33(12), 2031-2036.

Puertas, F., González-Fonteboa, B., González-Taboada, I., Alonso, M., Torres-Carrasco, M., Rojo, G., and Martínez-Abella, F. (2018). Alkali-activated Slag Concrete: Fresh and Hardened Behaviour. *Cement and Concrete Composites*, 85, 22-31.

Puertas, F., Gutierrez, R., Fernández-Jiménez, A., Delvasto, S., and Maldonado, J. (2002). Alkaline Cement Mortars. Chemical Resistance to Sulfate and Seawater Attack. *Materiales de Construcción*, 52(267), 55-71.

Puertas, F., Martínez-Ramírez, S., Alonso, S., and Vázquez, T. (2000). Alkali-Activated Fly Ash/Slag Cement Strength Behavior And Hydration Products. *Cement and Concrete Research*, 30, 1625-1632.

Purdon, A. O. (1940). The Action of Alkalis on Blast-Furnace Slag. *Journal of the Society of Chemical Industry*, 59(9), 191-202.

Qing-Hua, C., Tagnit-Hamou, A., and Sarkar, S. (1991). Strength and Microstructural Properties of Water Glass Activated Slag. *MRS Online Proceedings Library*, 245(1), 49-54.

Qiu, J., Zhao, Y., Xing, J., and Sun, X. (2019). Fly Ash/Blast Furnace Slag-Based Geopolymer as a Potential Binder for Mine Backfilling: Effect of Binder Type and Activator Concentration. *Advances in Materials Science and Engineering*, 12pp.

- Ramezaniapour, A., and Moeini, M. (2018). Mechanical and Durability Properties of Alkali Activated Slag Coating Mortars Containing Nanosilica and Silica Fume. *Construction and Building Materials*, 163, 611-621.
- Rebel, B., Detwiler, R., Gebler, S., and Hooton, R. (2005). The Right Sulfate Test Makes a Difference. *Concrete International*, 27(2), 49-52.
- Rodríguez, E., Bernal, S., de Gutiérrez, R., and Puertas, F. (2008). Alternative Concrete Based on Alkali-Activated Slag. *Materiales de Construcción*, 58(291), 53-67.
- Rodriguez-Navarro, C., Linares-Fernandez, L., Doehne, E., and Sebastian, E. (2002). Effects of Ferrocyanide Ions on NaCl Crystallization in Porous Stone. *Journal of Crystal Growth*, 243(3-4), 503-516.
- Rowles, M., Hanna, J., Pike, K., Smith, M., and O'connor, B. (2007). ^{29}Si , ^{27}Al , ^1H and ^{23}Na MAS NMR Study of the Bonding Character in Aluminosilicate Inorganic Polymers. *Applied Magnetic Resonance*, 32(4), 663.
- Roy, D. M. (1999). Alkali-Activated Cements Opportunities and Challenges. *Cement and Concrete Research*, 29(2), 249-254.
- Royak, S., P'yachev, V., and Shkolnik, Y. (1978). A Structure of Blast Furnace Slags and Activity. *Tsement* (in Russian).
- Sadek, D, Amin, S., and Youssef, N. (2014). Blended Cement Utilizing Ceramic Wall Tiles Waste. *In proceeding of the 1st International Conference on Construction Materials and Structures (ICCMATS)*, Johannesburg, South Africa, 152-161.
- Sahmaran, M., Erdem, T., and Yaman, I. (2007). Sulfate Resistance of Plain and Blended Cements Exposed to Wetting–Drying and Heating–Cooling Environments. *Construction and Building Materials*, 21(8), 1771-1778.
- Saini, G., and Vattipalli, U. (2020). Assessing Properties of Alkali Activated GGBS Based Self-Compacting Geopolymer Concrete using Nano-Silica. *Case Studies in Construction Materials*, 12.
- Salami, B., Johari, M., Ahmad, Z., and Maslehuddin, M. (2017). Durability Performance of Palm Oil Fuel Ash-Based Engineered Alkaline-Activated Cementitious Composite (POFA-EACC) Mortar in Sulfate Environment. *Construction and Building materials*, 131, 229-244.
- Santana, H., Neto, J., Júnior, N., Ribeiro, D., Cilla, M., and Dias, C. (2020). Self-Compacting Geopolymer Mixture: Dosing Based on Statistical Mixture Design and Simultaneous Optimization. *Construction and Building Materials*, 249, 118677.

Santhanam, M., Cohen, M., and Olek, J. (2002). Mechanism of Sulfate Attack: A Fresh Look: Part 1: Summary of Experimental Results. *Cement and Concrete Research*, 32(6), 915-921.

Santhanam, M., Cohen, M., and Olek, J. (2003). Effects of Gypsum Formation on the Performance of Cement Mortars during External Sulfate Attack. *Cement and Concrete Research*, 33(3), 325-332.

Sashidhar, C., Jawahar, J., Neelima, C., and Kumar, D. (2015). Fresh and Strength Properties of Self compacting Geopolymer Concrete Using Manufactured Sand. *International Journal of ChemTech Research (IJCRGG)*, 8, 183-190.

Scherer, G. W. (2004). Factors Affecting Crystallization Pressure. *In the Proceedings of the International RILEM TC 186-ISA Workshop on Internal Sulfate Attack and Delayed Ettringite Formation*, Rilem Publications SARL, 139-154.

Shafiq, I., Azreen, M., and Hussin, M. (2017). Sulphuric Acid Resistant of Self Compacted Geopolymer Concrete Containing Slag and Ceramic Waste. *In MATEC Web of Conferences*, 97, 01102.

Shi, C. and Day, R. (1996). Alkali-slag Cements for The Solidification of Radioactive Wastes. *In Gilliam and Wiles (eds) Stabilization and Solidification of Hazardous, Radioactive, and Mixed Wastes*, American Society for Testing and Materials (ASTM STP 1240), Philadelphia, USA, 163–173.

Shi, C., and Day, R. (1995). A Calorimetric Study of Early Hydration of Alkali-Slag Cements. *Cement and Concrete Research*, 25(6), 1333-1346.

Shi, C., and Day, R. (1996). Selectivity of Alkaline Activators for the Activation of Slags. *Cement, Concrete and Aggregates*, 18(1), 8-14.

Shi, C., Roy, D., and Krivenko, P. (2003). *Alkali-Activated Cements and Concretes*: CRC press, 392 pp.

Shi, C., Tang, X., and Li, Y. (1989). Studies on the activation of phosphorus slag. *In the Proceedings of the 3rd International Conference on the Use of Fly Ash, Silica Fume, Slag and Natural Pozzolans in Concrete*, ACI SP-114, Trondheim, Norway, 657-666.

Shi, C., Wu, Z., Lv, K., and Wu, L. (2015). A Review on Mixture Design Methods for Self-Compacting Concrete. *Construction and Building Materials*, 84, 387-398.

Shi, D., Ye, J., and Zhang, W. (2020). Effects of Activator Content on Properties, Mineralogy, Hydration and Microstructure of Alkali-Activated Materials Synthesized from Calcium Silicate Slag and Ground Granulated Blast Furnace Slag. *Journal of Building Engineering*, 32, 101791.

Shunsuke, H., and Kazuo, Y. (1999). Interaction Between Cement and Chemical Admixture from the Point of Cement Hydration, Absorption Behaviour of Admixture, and Paste Rheology. *Cement and Concrete Research*, 29(8), 1159-1165.

Sindhunata, Provis, J. L., Lukey, G. C., Xu, H., and van Deventer, J. (2008). Structural evolution of fly ash based geopolymers in alkaline environments. *Industrial and Engineering Chemistry Research*, 47(9), 2991-2999.

Skalny, J., and Pierce, J. (1999). Sulfate Attack: an Overview. *Materials Science of Concrete: Sulfate Attack Mechanisms*, J. Marchand and JP Skalny, eds., *The American Ceramic Society*, 49-64.

Skalny, J., and Thaulow, N. (2002). Sulfate Attack in North America. *In Proceedings of the 1st International Conference on Thaumasite in Cementitious Materials*, Garston, UK, 63–70.

Škvára, F. (2007). Alkali Activated Materials or Geopolymers. *Ceramics-Silikáty*, 51(3), 173-177.

Slavik, R., Bednarik, V., Vondruska, M., and Nemeč, A. (2008). Preparation of Geopolymer from Fluidized Bed Combustion Bottom Ash. *Journal of Materials Processing Technology*, 200(1-3), 265-270.

Sobolev, K., Flores, I., Hermosillo, R., and Torres-Martínez, L. (2006). Nanomaterials and Nanotechnology for High-Performance Cement Composites. *In the Proceedings of ACI session on Nanotechnology of Concrete: Recent Developments and Future Perspectives*, 91-118.

Song, S., and Jennings, H. (1999). Pore Solution Chemistry of Alkali-Activated Ground Granulated Blast-Furnace Slag. *Cement and Concrete Research*, 29(2), 159-170.

Song, S., Sohn, D., Jennings, H., and Mason, T. (2000). Hydration of Alkali-Activated Ground Granulated Blast Furnace Slag. *Journal of Materials Science*, 35, 249-257. 21.

Steiger, M., Linnow, K., Ehrhardt, D., and Rohde, M. (2011). Decomposition Reactions of Magnesium Sulfate Hydrates and Phase Equilibria in the $\text{MgSO}_4\text{-H}_2\text{O}$ and $\text{Na}^+\text{-Mg}^{2+}\text{-Cl}^-\text{-SO}_4^{2-}\text{-H}_2\text{O}$ Systems with Implications for Mars. *Geochimica et Cosmochimica Acta*, 75(12), 3600-3626.

Sugama, T., Brothers, L., and Van de Putte, T. (2005). Acid-Resistant Cements for Geothermal Wells: Sodium Silicate Activated Slag/Fly Ash Blends. *Advances in Cement Research*, 17(2), 65-75.

Suleiman, A. R. (2014). Physical Sulphate Attack on Concrete (Doctoral dissertation, University of Western Ontario).

- Sun, G., Young, J., and Kirkpatrick, R. (2006). The Role of Al in C–S–H: NMR, XRD, and Compositional Results for Precipitated Samples. *Cement and Concrete Research*, 36(1), 18-29.
- Sun, Z., and Vollpracht, A. (2018). Isothermal Calorimetry and In-Situ XRD Study of the NaOH Activated Fly Ash, Metakaolin and Slag. *Cement and Concrete Research*, 103, 110-122.
- Talling, B. (1989). Effect of Curing Conditions on Alkali-Activated Slags. Special Publication In 3rd International Conference Proceedings: Fly Ash, Silica Fume, Slag and Natural Pozzolans in Concrete, *American Concrete Institute (ACI)*, 114, 1485-1500.
- Tanada, S., Kabayama, M., Kawasaki, N., Sakiyama, T., Nakamura, T., Araki, M., and Tamura, T. (2003). Removal of Phosphate by Aluminum Oxide Hydroxide. *Journal of colloid and interface science*, 257(1), 135-140.
- Taylor, H. F. (1997). *Cement Chemistry (Vol. 2)*. London: Thomas Telford.
- Taylor, R., Richardson, I., and Brydson, R. (2010). Composition and Microstructure of 20-Year-Old Ordinary Portland Cement–Ground Granulated Blast-Furnace Slag Blends Containing 0 to 100% slag. *Cement and Concrete Research*, 40(7), 971–983.
- Temuujin, J., Minjigmaa, A., Lee, M., Chen-Tan, N., and Van Riessen, A. (2011). Characterization of Class F Fly Ash Geopolymer Pastes Immersed in Acid and Alkaline Solutions. *Cement and Concrete Composites*, 33(10), 1086-1091.
- Teoreanu, I. (1991). The Interaction Mechanism of Blast-Furnace Slags with Water. The Role of the Activating Agents. *IL cemento*, 8(2), 91-7.
- Thaulow, N., and Sahu, S. (2004). Mechanism of Concrete Deterioration due to Salt Crystallization. *Materials Characterization*, 53(2-4), 123-127.
- Thokchom, S., Ghosh, P., and Ghosh, S. (2010). Performance of Fly ash Based Geopolymer Mortars in Sulphate Solution. *Journal of Engineering Science and Technology Review*, 3(1), 36–40.
- Thomas, M. (2011). The Effect of Supplementary Cementing Materials on Alkali-Silica Reaction: A Review. *Cement and Concrete Research*, 41(12), 1224-1231.
- Tian, B., and Cohen, M. (2000). Does Gypsum Formation During Sulfate Attack on Concrete Lead to Expansion?, *Cement and Concrete Research*, 30(1), 117-123.
- Turner, L., and Collins, F. (2013). Carbon Dioxide Equivalent (CO₂-e) Emissions: A Comparison between Geopolymer and OPC Cement Concrete. *Construction and Building Materials*, 43, 125-130.

- Ushaa, T., Anuradha, R., and Venkatasubramani, G. (2015). Performance of Self-compacting Geopolymer Concrete Containing Different Mineral Admixtures. *Indian Journal of Engineering and Materials Sciences (IJEMS)*, 22(4), 473-481.
- Valencia Saavedra, W., Angulo, D., and Mejía de Gutiérrez, R. (2016). Fly ash Slag Geopolymer Concrete: Resistance to Sodium and Magnesium Sulfate Attack. *Journal of Materials in Civil Engineering*, 28(12), 04016148.
- Van Deventer, J., Provis, J., and Duxson, P. (2012). Technical and Commercial Progress in the Adoption of Geopolymer Cement. *Minerals Engineering*, 29, 89-104.
- Van Deventer, J., Provis, J., Duxson, P., and Brice, D. (2010). Chemical Research and Climate Change as Drivers in the Commercial Adoption of Alkali Activated Materials. *Waste and Biomass Valorization*, 1(1), 145-155.
- Van Eijk, R., and Brouwers, H. (1998). Study of the Relation between Hydrated Portland Cement Composition and Leaching Resistance. *Cement and Concrete Research*, 28(6), 815-828.
- Van Jaarsveld, J., Van Deventer, J., Lorenzen, L. (1997). The Potential Use of Geopolymeric Materials to Immobilise Toxic Metals: Part I. Theory and Applications. *Minerals Engineering*, 10(7), 659-669.
- Van Tittelboom, K., and De Belie, N. (2009). A critical Review on Test Methods for Evaluating the Resistance of Concrete Against Sulfate Attack. In *International RILEM TC211-PAE Final Conference on Concrete in Aggressive Aqueous Environments, Performance, Testing and Modeling*, Rilem Publications, 298-306.
- Vijai, K., Kumutha, R., and Vishnuram, B. (2010). Effect of Types of Curing on Strength of Geopolymer Concrete. *International Journal of Physical Sciences*, 5(9), 1419-1423.
- Vikan, H., Justnes, H., Winnefeld, F., and Figi, R. (2007). Correlating Cement Characteristics with Rheology of Paste. *Cement and Concrete Research*, 37(11), 1502-1511.
- Wafa, F. (1994). Accelerated Sulfate Attack on Concrete in a Hot Climate. *Cement, Concrete and Aggregates*, 16(1), 31-35.
- Walkley, B., San Nicolas, R., Sani, M., Rees, G., Hanna, J., van Deventer, J., and Provis, J. (2016). Phase Evolution of C-(N)-ASH/NASH Gel Blends Investigated Via Alkali-Activation of Synthetic Calcium Aluminosilicate Precursors. *Cement and Concrete Research*, 89, 120-135.

- Wang, A., Freeman, J., and Jolliff, B. (2009). Phase Transition Pathways of the Hydrates of Magnesium Sulfate in the Temperature Range 50 C to 5 C: Implication for Sulfates on Mars. *Journal of Geophysical Research: Planets*, 114(E4).
- Wang, J. G. (1994). Sulfate Attack on Hardened Cement Paste. *Cement and Concrete Research*, 24(4), 735-742.
- Wang, K., Du, L., Lv, X., He, Y., and Cui, X. (2017). Preparation of Drying Powder Inorganic Polymer Cement Based on Alkali-Activated Slag Technology. *Powder Technology*, 312, 204-209.
- Wang, S., and Scrivener, K. (1995). Hydration Products of Alkali Activated Slag Cement. *Cement and Concrete Research*, 25(3), 561-571.
- Wang, S., Scrivener, K., and Pratt, P. (1994). Factors Affecting the Strength of Alkali-Activated Slag. *Cement and Concrete Research*, 24(6), 1033-1043.
- Wardhono, A., Law, D., and Molyneaux, T. (2015). Long-Term Performance of Alkali-Activated Slag Concrete. *Journal of Advanced Concrete Technology*, 13(3), 187-192.
- Weng, L., and Sagoe-Crentsil, K. (2007). Dissolution Processes, Hydrolysis and Condensation Reactions during Geopolymer Synthesis: Part I—Low Si/Al Ratio Systems. *Journal of Materials Science*, 42(9), 2997-3006.
- Wetzel, A., and Middendorf, B. (2019). Influence of Silica Fume on Properties of Fresh and Hardened Ultra-High Performance Concrete based on Alkali-Activated Slag. *Cement and Concrete composites*, 100, 53-59.
- Whittaker, M., and Black, L. (2015). Current Knowledge of External Sulfate Attack. *Advances in Cement Research*, 27(9), 532-545.
- Xu, A., Shayan, A., and Baburamani, P. (1998). Test Methods for Sulfate Resistance of Concrete and Mechanism of Sulfate Attack: A State-of-the-Art Review. ARRB Transport Research, Ltd., & National Interest Service, Vermont South, Australia.
- Yan, Z., Sun, Z., Yang, J., Yang, H., Ji, Y., and Hu, K. (2021). Mechanical Performance and Reaction Mechanism of Copper Slag Activated with Sodium Silicate or Sodium Hydroxide. *Construction and Building Materials*, 266, 120900.
- Yang, D., Sun, W., and Tan, Y. (2005). Performance Evaluation of Binary Blends of Portland Cement and Fly Ash with Complex Admixture for Durable Concrete Structures. *Computers and Concrete*, 2(5), 381-388.
- Yang, K., and Song, J. (2009). Workability Loss and Compressive Strength Development of Cementless Mortars Activated by Combination of Sodium Silicate and Sodium Hydroxide. *Journal of Materials in Civil Engineering*, 21(3), 119-127.

- Yang, K., Song, J., Ashour, A., and Lee, E. (2008). Properties of Cementless Mortars Activated by Sodium Silicate. *Construction and Building Materials*, 22(9), 1981-1989.
- Yang, M., Wu, Q., Chen, Z., Zhang, B., Tang, B., Yao, J., Drevensek-Olenik, I., and Xu, J. (2014). Generation and Erasure of Femtosecond Laser-Induced Periodic Surface Structures on Nanoparticle-Covered Silicon by a Single Laser Pulse. *Optics Letters*, 39(2), 343-346.
- Ye, H., Chen, Z., and Huang, L. (2019). Mechanism of Sulfate Attack on Alkali-Activated Slag: The Role of Activator Composition. *Cement and Concrete Research*, 125, 105868.
- Yeginobali, A., and Dilek, F. (1995). Sulfate resistance of mortars containing silica fumes as evaluated by different methods. *Special Publication*, 153, 795-814.
- Yogendran, V., Langan, B., Haque, M., and Ward, M. (1987). Silica Fume in High-Strength Concrete. *Materials Journal*, 84(2), 124-129.
- Yu, C., Sun, W., and Scrivener, K. (2013). Mechanism of Expansion of Mortars Immersed in Sodium Sulfate Solutions. *Cement and Concrete Research*, 43, 105-111.
- Yuan, B. (2017). Sodium Carbonate Activated Slag: Reaction Analysis, Microstructural Modification and Engineering Application. *Doctoral Dissertation: Technische Universiteit Eindhoven*.
- Yusuf, M. O. (2015). Performance of Slag Blended Alkaline Activated Palm Oil Fuel Ash Mortar in Sulfate Environments. *Construction and Building Materials*, 98, 417-424.
- Zhang, J., Shi, C., Zhang, Z., and Ou, Z. (2017). Durability of Alkali-Activated Materials in Aggressive Environments: A Review on Recent Studies. *Construction and Building Materials*, 152, 598-613.
- Zhang, Z., Provis, J., Zou, J., Reid, A., and Wang, H. (2016). Toward an Indexing Approach to Evaluate Fly Ashes for Geopolymer Manufacture. *Cement and Concrete Research*, 85, 163-173.
- Zhang, Z., Yao, X., and Zhu, H. (2010). Potential Application of Geopolymers as Protection Coatings for Marine Concrete: I. Basic Properties. *Applied Clay Science*, 49(1-2), 1-6.
- Zuo, Y., Nedeljković, M., and Ye, G. (2018). Coupled Thermodynamic Modelling and Experimental Study of Sodium Hydroxide Activated Slag. *Construction and Building Materials*, 188, 262-279.
- Zuo, Y., Nedeljković, M., and Ye, G. (2019). Pore Solution Composition of Alkali-Activated Slag/Fly Ash Pastes. *Cement and Concrete Research*, 115, 230-250.